Site U1334[1]

Expedition 320/321 Scientists[2]

Chapter contents

Background and objectives 1
Science summary 2
Operations 6
Lithostratigraphy 7
Biostratigraphy 10
Paleomagnetism 14
Geochemistry 16
Physical properties 18
Stratigraphic correlation and composite section 19
Downhole measurements 21
References 21
Figures 24
Tables 78

Background and objectives

Integrated Ocean Drilling Program (IODP) Site U1334 (7°59.998′N, 131°58.408′W; 4799 meters below sea level [mbsl]) (Fig. F1; Table T1) is located ~380 km southeast of previously drilled Ocean Drilling Program (ODP) Site 1218 (~42 Ma crust) in the central area drilled during the Pacific Equatorial Age Transect (PEAT) program (IODP Expedition 320/321). Site U1334 (~38 Ma crust) is situated ~100 km north of the Clipperton Fracture Zone on abyssal hill topography draped with ~280 m sediment (Fig. F2). The fabric of the abyssal hills within the sites is oriented either due north or slightly east of due north.

Water depth in the vicinity of Site U1334 ranges between 5.0 and 5.1 km for the depressions between the abyssal hills. The abyssal hills range between 4.70 and 4.85 km water depth and generally show a thicker and more consistent sediment cover than the basins. In fact, a significant amount of the bathymetric difference between hills and basins is controlled by the amount of sediment cover. The comparison of sediment thickness and clarity of seismic sections led us to select a location on the middle elevation of one of the abyssal plateaus.

Site U1334 sediments were estimated to have been deposited on top of late middle Eocene crust with an age of ~38 Ma and target the events bracketing the Eocene–Oligocene transition with the specific aim of recovering carbonate-bearing sediments of latest Eocene age prior to a large deepening of the calcium carbonate compensation depth (CCD) that occurred during this greenhouse to icehouse transition (Kennett and Shackleton, 1976; Miller et al., 1991; Zachos et al., 1996; Coxall et al., 2005). The Eocene–Oligocene transition experienced the most dramatic deepening of the Pacific CCD during the Paleogene (van Andel, 1975), which has now been shown by Coxall et al. (2005) to coincide with a rapid stepwise increase in benthic oxygen stable isotope ratios, interpreted to reflect a combination of growth of the Antarctic ice sheet and decrease in deepwater temperatures (DeConto et al., 2008; Liu et al., 2009).

So far the most complete Eocene/Oligocene boundary section recovered from the equatorial Pacific has been at Site 1218 on 42 Ma crust; however, it is far from exceptionally preserved. Carbonate weight percentages drop markedly below the boundary and reach 0 wt% near 34 Ma during a time of apparent global shoaling of the CCD just prior to the Eocene–Oligocene transition and CCD deepening

[1] Expedition 320/321 Scientists, 2010. Site U1334. *In* Pälike, H., Lyle, M., Nishi, H., Raffi, I., Gamage, K., Klaus, A., and the Expedition 320/321 Scientists, *Proc. IODP,* 320/321: Tokyo (Integrated Ocean Drilling Program Management International, Inc.).
doi:10.2204/iodp.proc.320321.106.2010
[2] Expedition 320/321 Scientists' addresses.

(Bohaty et al., 2008). This prevented the recovery of information about paleoceanographic conditions prior to the Eocene–Oligocene transition and also has implications for the interpretation of paleotemperature proxies such as Mg/Ca ratios in foraminifer shells that were bathed in waters with very low carbonate ion concentrations (Lear et al., 2008). The integrated stratigraphy from Site 1218 has been correlated to the planktonic foraminifer marker extinction of *Hantkenina* in exceptionally well preserved shallow clay-rich sediments from Tanzania described by Pearson et al. (2008), who demonstrated that the Eocene/Oligocene boundary falls within the middle plateau of the stable isotope double-step described by Coxall et al. (2005), just prior to the base of magnetochron C13n (Fig. **F3**).

Data from Site 1218 allowed the astronomical time calibration of the entire Oligocene (Coxall et al., 2005; Wade and Pälike, 2004; Pälike et al., 2006b), but the lack of carbonate in the uppermost Eocene at this site made the detailed time control now available for the Oligocene much less certain for the late Eocene. Site U1334 is located on crustal basement age of ~38 Ma and crossed the paleoequator shortly thereafter. It was located to provide the missing information about the crucial chain of events prior to and during the Eocene–Oligocene transition. We positioned Site U1334 and the other PEAT sites south of the estimated paleoequatorial position at their target ages in order to maximize the time that drill sites remain within the equatorial zone (i.e., ±2° of the equator), to allow for some southward bias of the equatorial sediment mound relative to the hotspot frame of reference (Knappenberger, 2000), and to place the interval of maximum interest above the basal hydrothermal sediments. We located Site U1334 using the seafloor digital age grid from Müller et al. (1997), heavily modified and improved with additional magnetic anomaly picks from Petronotis (1991), Petronotis et al. (1994), and Deep Sea Drilling Project (DSDP)/ODP basement ages. For this grid, each point is then backrotated in time to zero age using the fixed-hotspot stage-poles from Koppers et al. (2001) and Engebretson et al. (1985) and the paleopole data from Sager and Pringle (1988). From the backtracked latitudes for each grid point we then obtained the paleoequator at the crustal age by contouring. The nearest older drill locations in this plate segment bounded by the Clipperton Fracture Zone nearby to the south and the Clarion Fracture Zone to the north are DSDP Site 160 (with a crustal age of ~35 Ma) to the east and Site 1218 (with a crustal age of 42 Ma) to the west, lending support to our backrotation modeling.

One of the common objectives of the PEAT program for all sites is to provide a limited depth transect for several Cenozoic key horizons, such as the Eocene–Oligocene transition (Coxall et al., 2005). For this objective, Site U1334 will form the youngest and shallowest paleodepth constraint, with an estimated crustal paleodepth of ~3.5 km during the Eocene–Oligocene transition. Site U1334 also targets the Oligocene/Miocene boundary and the Mi-1 event (Zachos et al., 2001; Pälike et al., 2006a), again as part of a limited depth transect. Site U1334 is estimated to have been ~4.2 km below sea level at that time (~23 Ma).

All Expedition 320/321 drill sites have in common the objective to improve and extend the extensive intercalibrated bio-, magneto-, chemo-, and astronomical stratigraphies for the Cenozoic (e.g., Shackleton et al., 2000; Pälike et al., 2006b).

The 48-channel stacked and migrated data (Fig. **F2**) (Pälike et al., 2008; Lyle et al., 2006) allowed us to optimize the Site U1334 position on the intersection of seismic Lines 1 and 6 from the AMAT-03 survey. Site U1334 was located at the crossing position because the sediment and basement are well imaged. Any additional thickness away from the cross of Lines 1 and 6 was primarily caused by additional Miocene sediment on top and not by the section of primary interest below. We estimated sediment thickness using interval velocities published for ODP Site 574 by Mayer et al. (1985). The subbottom profiler sections image ~20 m of transparent surface sediment and ~100 m of layered sediments in the upper sediment column (Pälike et al., 2008).

Site survey piston Core RR0603-8JC was taken west of Site U1334 (Fig. **F1B**). The survey piston core lithology consists of a surface layer of siliceous clay over upper Miocene to upper middle Miocene radiolarian oozes, devoid of carbonate. The age at the base of this core is ~12.4 Ma based on radiolarian assemblages. An interpretation of the site survey seismic data (Fig. **F2**) indicated that Site U1334 might penetrate seismic reflectors Orange (O), P5, and P4 of Lyle et al., (2002). The predicted ages for the latter two can be confirmed by coring (see **"Science summary"**).

Science summary

Three holes were cored at Site U1334 (7°59.998′N, 131°58.408′W; 4799 mbsl) (Fig. **F1;** Table **T1**), targeting the events bracketing the Eocene–Oligocene transition as part of an investigation of the wider Cenozoic climatic evolution (e.g., Zachos et al., 2001) and providing data toward a depth transect across the Oligocene (see **"Eocene/Oligocene Boundary**

[Site U1334; 38 Ma crust]" in the "Expedition summary" chapter) that will allow exploitation and verification of a previous astronomical age calibration from Site 1218 (Pälike et al., 2006a).

Site U1334 is in the center of the PEAT program transect, ~100 km north of the Clipperton Fracture Zone and ~380 km southeast of the previously drilled Site 1218. At Site U1334, seafloor basalt is overlain by ~285 m of pelagic sediment. The oldest sediment is of late middle Eocene age (38 Ma).

The topmost ~47 m thick lithologic Unit I contains a 15 m thick interval of brown radiolarian clay overlying ~32 m of alternating radiolarian clay and nannofossil ooze. The uppermost section (320-U1334A-1H-CC) is of late Miocene age (radiolarian Zone RN7; ~8.5 Ma). Below, Unit II comprises a ~200 m thick succession of upper Miocene to Oligocene nannofossil ooze and chalk above a ~35 m thick sequence of upper Eocene nannofossil chalk, radiolarite, and claystone (Unit III). Basal lithologic Unit IV (~1 m thick) consists of middle Eocene intercalated micritic chalk and limestone on basalt (Figs. **F4, F5**).

Holes U1334A–U1334C provided high-quality APC-cored sediments from the mudline to ~210 m core depth below seafloor (CSF) (Cores 320-U1334A-22H, 320-U1334B-22H, and 320-U1334C-22H). Below this depth we encountered increasingly stiffer and harder sediment, after which we switched to the extended core barrel (XCB) cutting shoe. XCB coring advanced to 288.5 m drilling depth below seafloor (DSF) through lower Oligocene and Eocene sediments with high recovery. At the base of the holes, an intercalated unit of basalt and hard micritic chalk and limestone occurs below a 10–20 m thick section of nannofossil ooze and chalk. For detailed coring activities, see **"Operations."**

Carbonate content exceeds 92 wt% in the upper lower Miocene below Section 320-U1334A-5H-3 and remains high throughout the Oligocene. Eocene sediments still contain considerable amounts of carbonate, and nannofossil ooze and chalk are dominant lithologies apart from several short less carbonate rich intervals (e.g., Section 320-U1334A-28X-3). In the middle Eocene, carbonate content cycles between ~40 and 85 wt% (see **"Geochemistry"**) (Fig. **F6**), with higher values encountered toward the basal part of the Eocene section. Two short intervals in the upper Eocene (~249 to ~257 m CSF) exhibit carbonate content of <20 wt%.

A series of middle Oligocene cores (Cores 320-U1334A-16H through 21H) were recovered that had very distinct colors ranging from light grayish green to light blue (see **"Lithostratigraphy"**). These uniquely colored carbonate oozes exhibit extremely low magnetic susceptibilities that complicated stratigraphic correlation. These oozes have lost almost their entire magnetic susceptibility signal from ~145 to ~215 m CSF (Figs. **F5, F7**). Similar colored cores have previously been described for DSDP Sites 78 and 79 (Hays et al., 1972).

The Eocene–Oligocene transition at Site U1334 is much more expanded than at IODP Sites U1331–U1333 and even Site 1218. The transition was encountered at ~250 m CSF and fully recovered in Cores 320-U1334A-27X and 320-U1334B-26X; Hole U1334C was used to fill small stratigraphic gaps. The Oligocene–Miocene transition was fully recovered in all three holes in Cores 320-U1334A-10H (based on magnetostratigraphy, the boundary is at Sample 320-U1334A-10H-6, 98 cm), 320-U1334B-10H (top of Section 2), and 320-U1334C-10H.

All major microfossil groups occur in sediments from Site U1334 and provide a consistent, coherent, and high-resolution biostratigraphic succession spanning a near-continuous sequence from the middle Miocene to the uppermost middle Eocene. The uppermost 12 m of radiolarian clay is barren of calcareous microfossils but contains radiolarians of middle Miocene age, similar to the site survey piston Core RR0306-08JC (Lyle et al., 2006). Nannofossil ooze and radiolarian clays are present in the Miocene and Eocene parts of the section, with nannofossil ooze dominant in the thick Oligocene section. Radiolarians are present through most of the section, apart from the lowermost cores, and are well preserved in the Eocene. They provide a coherent high-resolution biochronology and indicate a complete sequence of radiolarian zones from RN7 (upper Miocene) to RP17 (uppermost middle Eocene). Calcareous nannofossils are present and moderately to well preserved through most of the succession, and there appears to be a complete sequence of nannofossil zones from NN6 (middle Miocene) to NP17 (uppermost middle Eocene), providing a minimum age estimate for basaltic basement of 38 Ma. In the Eocene, the base of *Chiasmolithus oamaruensis* is determined in Sample 320-U1334A-30X-1, 66 cm, and the top of *Chiasmolithus grandis* in Sample 320-U1334-30X-2, 74 cm. Intriguingly, both species are mid- to high-latitude taxa (Wei and Wise, 1989) and are present only rarely and sporadically at Site U1334. Planktonic foraminifers are present through most of the succession and are relatively abundant and well preserved from the lower Miocene to the lower Oligocene. The lower Miocene is characterized by the presence of *Dentoglobigerina* spp., *Paragloborotalia siakensis–mayeri, Paragloborotalia kugleri,* and *Paragloborotalia pseudokugleri.* Oligocene sediments contain *Catapsydrax* spp., *Paragloborotalia opima-nana,* and characteristic *Dento-*

globigerina spp. Preservation and abundance of planktonic foraminifers is more variable in the middle Miocene and upper Eocene/lowermost Oligocene. No Eocene/Oligocene boundary marker hantkeninids were identified. Benthic foraminifers are present through most of the section and indicate lower bathyal to abyssal paleodepths.

Sedimentation rates, as derived from magneto- and biostratigraphic age determinations, vary throughout the section and are ~4 m/m.y. in the topmost sediment cover, vary between ~12 and 14 m/m.y. in the lower Miocene through upper lower Oligocene section, increase to ~24 m/m.y. in the lower Oligocene, and are ~8 m/m.y. in the upper Eocene. There is no obvious hiatus in the shipboard biostratigraphic sequence. The presence of all major fossil groups as well as a detailed and well-resolved magnetostratigraphy will allow us to achieve one of the main PEAT objectives of arriving at an integrated Cenozoic stratigraphy and age calibration for major parts of the Miocene, Oligocene, and Eocene.

A full physical property program was run on cores from Site U1334. This program comprises Whole-Round Multisensor Logger (WRMSL) measurements of magnetic susceptibility, bulk density, and *P*-wave velocity, along with natural gamma radiation (NGR) and measurements of color reflectance, followed by discrete measurements of moisture and density (MAD) properties, sound velocities, and thermal conductivity in Hole U1334A. All track data are variable throughout the section, allowing a detailed correlation between different holes, with the exception of a very low magnetic susceptibility signal within an interval extending slightly above and below the light greenish gray tinted cores of Unit II (see **"Lithostratigraphy"** for exact color definitions), between ~140 and 205 m CSF. Magnetic susceptibility varies between 10×10^{-5} and 40×10^{-5} SI in Unit I, oscillates around 5×10^{-5} to 10×10^{-5} SI above the colored sediments, and then drops to near zero and negative values, returning to values around 10×10^{-5} SI in the lower part of Unit II and Subunit IIIa. NGR increases slightly at the Eocene/Oligocene boundary at ~246 m CSF (from 4 to 7 counts per second [cps]). *P*-wave velocity remains uniform through the upper 150 m of sediment (varying around 1500 m/s) but increases rapidly below the ooze/chalk boundary to ~1600 m/s. This explains the slightly thicker sediment section than was expected from seismic data prior to coring (~20 m thicker). For Hole U1334B, no *P*-wave velocity WRMSL data were collected between ~125 and 240 m CSF to allow for a more timely stratigraphic correlation of cores within the iron reduction–dominated colored cores with the gamma ray attenuation (GRA) instrument. Bulk density and grain density increase gradually with carbonate content to ~204 m CSF to a maximum of ~1.8 g/cm^3 and then show stepped decreases in the lower part of this succession. Ephemeral whole-round samples were collected at ~50 and ~165 m for shore-based studies of sediment permeability.

WRMSL data were used to achieve stratigraphic correlation among holes at Site U1334. Magnetic susceptibility was initially the main parameter used for real-time correlation, as a second loop of the susceptibility meter is mounted on the Special Task Multisensor Logger (STMSL); the second bulk density instrument on this track was not working. In the very low (sometimes negative) magnetic susceptibility interval between ~140 and ~205 m CSF (Cores 320-U1334A-16H through 21H), the signal was not useful for correlation, and we measured the corresponding cores from Hole U1334B out of sequence to establish the amount of core overlap using bulk density. The coring effort in Hole U1334C was successful at covering gaps between cores at this site to ~111 m core composite depth below seafloor (CCSF-A; see **"Core composite depth scale"** in the "Methods" chapter), as well as from 250 to 335 m CCSF-A, almost to the bottom of the section. The correlation was challenging between the three holes at Site U1334 in the greenish–light gray interval (Cores 320-U1334A-15H through 22H, 320-U1334B-14B through 22H, and 320-U1334C-14H through 22H) and in the bottom 80 m of the section, where XCB coring compromised the GRA density variations that would otherwise help stratigraphic correlation. Visual inspection, comparison with core imagery, and biostratigraphic datums were used to establish and verify hole to hole correlation where track data lacked clearly identifiable features. Stratigraphic correlation between individual holes indicates a growth factor (ratio between the CCSF-A and CSF depth scales) of ~16%. Stratigraphic correlation resulted in a complete splice through the Eocene–Oligocene transition almost to basement (~38 Ma).

A full range of paleomagnetic analyses was conducted on 66 advanced piston corer (APC) cores and 188 discrete samples from Site U1334 for the APC-cored section of Site U1334 (upper ~209 m). Unlike Sites U1331 and U1332, the drilling overprint was generally weak for Site U1334 cores, but only for those collected with nonmagnetic core barrels (Cores 320-U1334A-1H through 16H, 320-U1334B-1H through 15H, and 320-U1334C-1H through 15H). In contrast, those cores collected with steel core barrels are highly overprinted. The overprint is so severe that even demagnetization at 20 mT only partially removes it. This extreme overprint notably degrades the paleomagnetic declination data, as can be noted by their higher variability, which makes polarity determination much more difficult in the intervals collected with steel core barrels. The problem is exacerbated by the decay in the intensity (and magnetic susceptibility) that occurs at ~135 m CSF in all three holes as a result of reduction diagenesis. Even within the highly reduced interval, an interpretable signal was present prior to switching to steel core barrels. Magnetic susceptibility in the upper 45 m of Hole U1334A averages ~18 × 10^{-5} SI (volume normalized) and decreases to a mean of 6 × 10^{-5} SI from 45 to 135 m CSF. A notable low occurs from ~140 to 204 m CSF, where the average susceptibility is 0.6 × 10^{-5} SI. This low interval is associated with a change in sediment color from yellowish tan to very light green, blue, and gray at ~143 m CSF and another abrupt change to reddish brown tones at ~192 m CSF, which corresponds to middle early Oligocene (~30 Ma). Just below 205 m, magnetic susceptibility steps up to an average of 5 × 10^{-5} SI and then increases again across the Eocene/Oligocene boundary (~245 m) to an average of 18 × 10^{-5} SI. The magnetostratigraphy in Hole U1334A has been interpreted from the top of Chron 11r (29.957 Ma), which occurs ~55 cm below the top of Section 320-U1334C-21H-4 (~195 m CSF) through the base of Chron C3n.4n (5.235 Ma) in Core 320-U1334A-1H (~4 m CSF). The youngest sediments recovered are in the upper ~2 m of Core 320-U1334A-1H, which record Chrons C1n through C2r.1r.

A standard shipboard suite of geochemical analyses of pore water and organic and inorganic sediment properties was undertaken on samples from Site U1334. We also conducted a high-resolution (one per section) Rhizon pore water investigation across the interval's middle Oligocene cores (320-U1334C-16H through 21H) that exhibited colored sediments. Site U1334A is marked by alkalinities between 3 and 4 mM throughout. The most striking features in the interstitial water geochemistry are a dissolved manganese peak from ~20 to ~240 m CSF with a maximum of ~6 µM at ~110 m CSF and a dissolved iron peak as high as >15 µM centered at 165 m CSF. The depth range of the dissolved iron peak, indicative of iron oxide reduction, coincides with the colorful interval seen in the lithology and with the interval of low magnetic susceptibilities (~140–205 m CSF). Sulfate results indicate limited sulfate reduction. Calcium carbonate contents are low in the uppermost ~35 m of Site U1334, and calcium carbonate contents are generally high (~80 wt%) below the uppermost clay layer.

Wireline logging was attempted in Hole U1334C with a redesigned tool string configuration after the loss of equipment at Site U1332. However, this attempt had to be abandoned after the logging winch failed when the tool was on its way down the drill pipe.

Five downhole temperature measurements were conducted in Hole U1334B with the advanced piston corer temperature tool (APCT-3) tool and reveal a thermal gradient of 33°C/km. Seafloor temperature is ~1.5°C. Temperature data combined with whole-round core temperature conductivity measurements indicate the heat flow is 31.6 mW/m² at this site. This is somewhat lower than values obtained for the nearest site (1218).

Highlights

Eocene–Oligocene and Oligocene–Miocene transitions and depth transects

Site U1334 was planned as the youngest and shallowest component of the PEAT Eocene–Oligocene depth transect component, which will allow the study of critical intervals (such as the Eocene–Oligocene transition; see Coxall et al., 2005) and variations of the equatorial CCD. Site U1334 is estimated to have been ~3.5 km deep during the Eocene–Oligocene transition, ~1.3 km shallower than today and 800 m shallower at that time than Site U1333. Unlike previously drilled sites, the dominant lithology below the Eocene–Oligocene transition is still nannofossil ooze and chalk, with significant amounts of carbonate present. These carbonate amounts will allow us to achieve the prime objective for this site. The Eocene–Oligocene transition, which was cored multiple times at Site U1334, has higher sedimentation rates than previously cored examples. The overlying Oligocene is also much more expanded than at Site 1218, with better preservation of planktonic foraminifers over a longer time interval, permitting a more detailed study of the Oligocene climate system. Site U1334 contains carbonate-bearing sediments across the Oligocene–Miocene transition. Physical property data from Site U1334 can be correlated cycle by cycle to Site 1218, allowing correlation to a previously astronomically calibrated site for the Oligocene.

Geochemical front

At Site U1334 we recovered a ~50 m thick interval of light greenish gray carbonates that show a distinct peak in dissolved Fe concentrations, characteristic of a geochemical alteration front. A similar but much thicker alteration zone is also observed at IODP Site U1335 and provides the opportunity to study organic matter degradation while these sites migrate from south to north through the equatorial belts of high productivity.

Age transect of seafloor basalt

At Site U1334 we recovered what appear to be fresh fragments of seafloor basalt, aged ~38 Ma as estimated from biostratigraphic results. This material will, when combined with other PEAT basalt samples, provide important sample material for the study of seawater alteration of basalt.

Operations

Transit to Site U1334

The 410 nmi voyage from Site U1333 to Site U1334 took 40.8 h and was accomplished at an average speed of 10.1 kt. During the transit the ship's clocks were advanced 1 h, resetting local ship time to more closely follow the earlier rising sun as we migrated eastward to each site. Times for Site U1334 are given in ship local time (UTC – 9 h).

Site U1334

Hole U1334A

Once the vessel approached the coordinates of the new location, the captain slowed the vessel and maneuvered the vessel over the site. We were positioning over the new location by 1222 h on 6 April 2009. After assembling the drill string and lowering it to the seafloor, we attempted to spud the new site with the bit positioned 10 m shallower than the corrected depth of 4798.4 m drilling depth below rig floor (DRF) (4787.0 mbsl) from the precision depth recorder (PDR). We recovered only water, so the bit was lowered to 4798 m DRF for a second attempt. This was successful, and Hole U1334A was spudded with the APC at 0030 h on 7 April. The mudline recovered in Core 1H was used to establish the seafloor depth as 4799.3 m DRF (4787.9 mbsl) (Table T1). This depth was within 1 m of the corrected PDR depth.

APC Cores 1H through 22H were taken from 0 to 206.9 m DSF, and we recovered 212.39 m (103%) (Table T1). APC coring was terminated when Core 22H did not stroke fully and required 80,000 lb to release it from the formation. Nonmagnetic core barrels were used on Cores 1H through 16H; standard steel core barrels were used on Cores 17H through 22H.

XCB Cores 23X through 32X were taken from 206.9 to 285.5 m DSF, and we recovered 77.99 m (99%). Coring was terminated when we recovered basalt in Core 32X. The total cored interval for Hole U1334A was 285.5 m, and we recovered 288.83 m (102%). The drill string was pulled out of the hole and cleared the seafloor at 2150 h on 8 April.

Hole U1334B

The ship was offset 25 m west of Hole U1334A, and we spudded Hole U1334B at 2330 h on 8 April 2009 with the bit 5 m deeper than at the first hole. APC Cores 1H through 22H were taken from 3.7 to 210.7 m DSF, and we recovered 218.43 m (105%). Nonmagnetic core barrels were used on Cores 1H through 15H, and standard steel barrels were used on Cores 16H through 22H. Downhole temperature measurements were obtained at 32.2, 49.2, 68.2, 87.2, and 106.2 m DSF (Cores 3H, 5H, 7H, 9H, and 11H, respectively). Core 5H was advanced 7.5 m to maintain an ~5 m vertical offset with Hole U1334A.

XCB Cores 23X through 31X were taken from 207.0 to 281.7 m DSF, and we recovered 76.84 m (103%). We stopped coring when we recovered basalt in Core 31X. We pulled the drill string out of the hole and the bit cleared the seafloor at 1840 h on 10 April.

Hole U1334C

After the ship was offset 25 m west of Hole U1334B, Hole U1334C was spudded at 2020 h on 10 April 2009 with the bit 3 m deeper than Hole U1334A. APC Cores 1H through 22H penetrated from 0 to 209.0 m DSF, and we recovered 213.0 m (102%). Nonmagnetic core barrels were used on Cores 1H through 15H; Cores 16H through 22H used standard steel barrels. We had to drillover Cores 19H, 21H, and 22H to release them from the formation. We then switched to XCB coring. Cores 23X through 33X were taken from 209.0 to 280.7 m DSF, and we recovered 72.9 m (102%). Core 26X was advanced by 6 m to maintain stratigraphic overlap with the first two holes. Coring finished when limestone including basalt clasts was recovered in the last core. Cores from Hole U1334C successfully covered the stratigraphic gaps in the first two holes.

Our final operations planned for Hole U1334C were to conduct two downhole logging runs. We circulated the hole with 50 bbl of attapulgite mud and then displaced the hole with 100 bbl of attapulgite mud. We raised the bit up to 95 m DSF and rigged up for logging. The first tool string was assembled and deployed into the pipe at 1930 h on 12 April. While lowering the logging tool string into the hole, the transmission on the logging winch failed when the tool was ~1700 m below the rig floor. We started to manually retrieve the tool string using T-bar clamps, air tuggers, and the starboard crane. After recovering ~550 m of wireline and spooling it back onto the logging winch drum, we decided to retrieve the remaining logging wireline by spooling the logging wireline onto the core winch drum. The logging tool was back on the rig floor at ~1200 h on 13 April. No more logging could be conducted during Expedition 320.

We started pulling the drill string out of the hole and the bit cleared the seafloor at 1225 h on 13 April. After the drill string was recovered and the thrusters retracted, we began the transit for Site U1335 at 2200 h on 13 April.

Lithostratigraphy

Drilling at Site U1334 recovered an ~285 m thick section of pelagic sediments overlying seafloor basalt (Fig. F5). The sedimentary sequence at Site U1334 is divided into four major lithologic units (Fig. F5; Table T2). The top of the section (0–47 m CSF) is an early to middle Miocene clay intercalated with nannofossil and radiolarian oozes (Unit I). The topmost 15 m interval of Unit I consists predominantly of radiolarian clay with varying amounts (<15%) of micronodules and zeolite. These sediments overlie alternations of radiolarian clay and nannofossil ooze. Unit II consists of ~200 m of early Miocene to Oligocene nannofossil ooze and chalk overlying a ~35 m thick alternating sequence of late Eocene nannofossil chalk, radiolarite, and claystone (Unit III). A thin layer (~1 m thick) of middle Eocene micritic chalk and limestone was recovered at the base of the sedimentary sequence (Unit IV) above basement basalt.

Lithologic units and boundaries are defined by differences in lithology, physical property data series, and calcium carbonate ($CaCO_3$) content as measured by coulometry. Lithologic differences, based on both visual core description and smear slide analysis, are primarily attributable to varying distributions of biogenic components such as nannofossils, radiolarians, and diatoms and clay-sized lithogenic material (Fig. F5; see "Site U1334 smear slides" in "Core descriptions"). Lithologic descriptions are based primarily on sediments recovered in Hole U1334A, supplemented with observations from Holes U1334B and U1334C.

Unit I

Intervals: 320-U1334A-1H-1, 0 cm, through 5H-CC, 25 cm; 320-U1334B-1H-1, 0 cm, through 5H-3, 55 cm; 320-U1334C-1H-1, 0 cm, through 5H-1, 65 cm

Depths: Hole U1334A = 0.0–46.76 m CSF; Hole U1334B = 0.0–45.25 m CSF; Hole U1334C = 0.0–38.7 m CSF

Age: early to middle Miocene

Lithology: clay, radiolarian clay, clayey radiolarian ooze, and nannofossil ooze

The major lithologies in Unit I are light yellowish brown (10YR 6/4) to very dark brown (10YR 3/2) to very dark gray (10YR 3/1) clay, dark grayish brown (10YR 4/2) to very dark grayish brown (10YR 3/2) radiolarian clay, brown (10YR 4/3) radiolarian ooze, and very pale brown to brown (10YR 8/2 to 10YR 5/3) nannofossil ooze. Clay occurs with minor amounts of zeolites and micronodules, as well as radiolarians and nannofossils. Radiolarian ooze occurs with minor amounts of clay or nannofossils. Nannofossil ooze sometimes occurs with radiolarians or clay. The uppermost 2 to 5 m of the unit is composed of clay with significant amounts of zeolites and micronodules (up to 15%). Radiolarian clay dominates to 15 m CSF, below which radiolarian clay and clayey radiolarian ooze alternate with nannofossil ooze. The transition from the topmost interval of clayey sediments to the underlying clay/nannofossil ooze alternations is characterized by an increase in the amplitude of variations and absolute values in magnetic susceptibility, gamma ray attenuation (GRA) bulk density and color reflectance (b* and L* shown) (Fig. F5; see "Physical properties" for discussion of reflectance, including a*). $CaCO_3$ contents are near zero at the top of Unit I and highly variable where clays and nannofossil oozes alternate. The transition to Unit II is indicated by the increased importance of biogenic oozes relative to clay and a marked shift in physical properties, including a decrease in magnetic susceptibility, an increase in GRA bulk density, and an increase in L* (Fig. F5).

Unit II

Intervals: 320-U1334A-6H-1, 0 cm, through 27X-2, 26 cm; 320-U1334B-5H-3, 55 cm, through 26X-4, 124 cm; 320-U1334C-5H-1, 65 cm, through 27X-6, 96 cm

Depths: Hole U1334A = 46.76–244.96 m CSF; Hole U1334B = 45.25–243.94 m CSF; Hole U1334C = 38.7–247.66 m CSF

Age: early Miocene to late Eocene

Lithology: nannofossil ooze, nannofossil ooze with radiolarians, and nannofossil chalk

The dominant lithology in Unit II is white (10YR 8/1) to very pale brown (10YR 8/2, 10YR 8/3, 10YR 7/3, and 10YR 7/4) nannofossil ooze with an exceptional 65 m thick interval of greenish and yellowish nannofossil ooze (Figs. F5, F7). Between 141 and 206 m CSF (Hole U1334A) sediment color undergoes a downhole transition from pale yellow (5Y 8/2) to several shades of light greenish gray (10Y 8/1, 10G 8/1, and 5 BG 8/1), light gray (N7), and back again through pale yellow (2.5Y 8/2) before returning to very pale brown (10YR 8/3). Bioturbation is generally minor throughout the unit. Nannofossil ooze sometimes includes radiolarians and clay as minor lithologic components. The alteration of relatively pure nannofossil oozes and nannofossil ooze with radiolarians or with clay creates subtle color banding on scales 20 to 80 cm thick (Fig. F8). Unit II sediments have $CaCO_3$ contents that are typically near 90 wt% (Fig. F5; see "Geochemistry"). L* and GRA bulk densities are elevated throughout Unit II (~90 and <1.6 g/cm^3, respectively), whereas magnetic susceptibility remains low (typically <15 × 10^{-6} SI). The interval of light greenish gray nannofossil ooze between 143 and 191 m CSF (Hole U1334A) is associated with a pronounced decrease in b* but little change in L* (Figs. F5, F7). Magnetic susceptibility is exceptionally low, approaching zero and sometimes below zero, throughout the greenish and yellowish intervals between 141 and 206 m CSF (Figs. F5, F7; see "Physical properties" and "Geochemistry").

Unit III

Intervals: 320-U1334A-27X-2, 26 cm, through 31X-2, 25 cm; 320-U1334B-26X-4, 124 cm, through 31X-5, 30 cm; 320-U1334C-27X-6, 96 cm, through 31X-2, 40 cm
Depths: Hole U1334A = 244.96–283.55 m CSF; Hole U1334B = 243.94–282.90 m CSF; Hole U1334C = 247.66–279.41 m
Age: middle to late Eocene
Lithology: nannofossil chalk, clayey nannofossil chalk, and clayey radiolarite

The dominant lithologies in Unit III are very pale brown (10YR 8/1 and 10YR 7/3) to light gray (10YR 7/2) to light yellowish brown (10YR 6/4) nannofossil chalk with lesser amounts of very dark brown (10YR 2/2) and very dark grayish brown (10YR 3/2) clayey nannofossil chalk and brown (10YR 5/3 and 10YR 4/3) nannofossil chalk with clay and very dark grayish brown (10YR 3/2) clayey radiolarite. Within the major lithologies, nannofossil chalk occurs with radiolarians and clay as minor lithologic components. The Unit II–III transition is identified by an increase in clay and radiolarian contents relative to nannofossils, an increase in magnetic susceptibility, and a decrease in GRA bulk density, L* and b* reflectance, and $CaCO_3$ contents (Fig. F5).

Unit IV

Intervals: 320-U1334A-31X-2, 25 cm, through at least 32X-CC, 40 cm; 320-U1334B-31X-5, 30 cm, through at least 31X-CC, 9 cm; 320-U1334C-31X-2, 40 cm, through at least 32X-CC, 43 cm
Depths: Hole U1334A = 283.55–285.40 m CSF; Hole U1334B = 282.90–283.99 m CSF; Hole U1334C = 279.41–280.13 m CSF
Age: middle Eocene
Lithology: micritic nannofossil chalk and limestone

The major lithologies in Unit IV are very pale brown (10YR 8/2) micritic nannofossil chalk and very pale brown (10YR 7/4) to brown (10YR 5/4) nannofossil chalk and white limestone. Unit IV is distinguished from Unit III by the presence of micrite as a major component in nannofossil chalk and of limestone.

Unit V

Intervals: 320-U1334A-32X-CC, 40 cm, to at least 32X-CC, 43 cm; 320-U1334B-31X-CC, 9 cm, to at least 31X-CC, 11 cm; 320-U1334C-32X-CC, 43 cm, to at least 32X-CC, 49 cm
Depths: Hole U1334A = 285.40 to at least 285.43 m CSF; Hole U1334B = 283.99 to at least 284.01 m CSF; Hole U1334C = 280.13 to at least 280.19 m CSF

Several broken pieces of basalt up to 10 cm in length were recovered at the base of each hole at Site U1334. Basalt is either intercalated with or overlain by the micritic chalks and limestone of Unit IV.

Redox related color changes

The relatively homogeneous lithology of Unit II is marked by vivid color changes that are made obvious against the backdrop of relatively white nannofossil oozes. Sediment color shifts downhole from white (10YR 8/1) to very pale brown (10YR 8/2) to pale yellow (2.5Y 8/1) to light greenish gray (10GY 8/1) over a 65 m thick interval and persists as light greenish gray for ~40 m before returning back through pale yellow to very pale brown and white (Fig. F7). Reflectance parameters a* and b*, which measure green–red and blue–yellow portions of the spectrum, respectively, shift in a steplike manner to lower values or toward green (a*) and blue (b*) with these observed color changes (Fig. F7). Magnetic susceptibility drops to near zero throughout the light greenish gray interval. Dissolved Fe and Mn concentrations in pore fluids increase 5 to 6 µM/L within these sediments from background concentration of close to zero (see "Geochemistry"). Together with the loss of magnetic signal (see "Paleomagnetism"), the increase in dissolved Fe concentrations and changes in sediment color indicate intensified microbial Fe reduction, perhaps fueled by higher organic carbon accumulation rates across this interval relative to the under- and overlying nannofossil ooze at Site U1334.

Light–dark color cycles within Oligocene nannofossil oozes

Readily observable but subtle color variations are common within the very pale brown nannofossil oozes of Unit II. These meter-scale light–dark cycles are associated with minor variations in the relative amounts of minor lithologic components, including clay, radiolarians, and diatoms (Fig. F8), and also in physical properties including L*, b*, magnetic susceptibility, and GRA bulk density (Fig. F5; see "Physical properties"). Nannofossils dominate the sediments, making up >95% of the fine fraction observed in smear slides. The remaining 5% is dominated by clay, radiolarians, and diatoms. The lithology name remains nannofossil ooze across these slight but apparent variations. The seemingly small shifts in nannofossil contributions, however, often between 95% and 99%, are necessarily associated with an approximately two-fold increase in clay or radiolarian content.

Sediments across the Oligocene–Miocene transition

The Oligocene/Miocene boundary was recovered in all three holes drilled at Site U1334 (Fig. F9). The Oligocene/Miocene boundary is defined by the appearance of the planktonic foraminifer *P. kugleri* (23.0 Ma) and approximated well by the short-lived (~100 k.y.) calcareous nannofossil *Sphenolithus delphix* (23.1–23.2 Ma), just below C6Cn.2n. *P. kugleri* is present in Sample 320-U1334A-10H-2, 38–40 cm, but not in Sample 10H-5, 38–40 cm, placing the midpoint of this datum in Core 320-U1334A-10H-3 (Fig. F9; see "Biostratigraphy"). The base of Chron C6Cn.2n, the magnetostratigraphic Oligocene/Miocene marker, however, locates the boundary 2 to 6 m lower, around interval 320-U1334A-10H-6, 100 cm. *S. delphix* is identified between intervals 320-U1334A-10H-7, 30 cm, and 11H-2, 20 cm, consistent with the magnetostratigraphic data.

The Oligocene–Miocene transition in Hole U1334A occurs in very pale brown nannofossil ooze with subtle light (10YR 8/2) and dark (10YR 7/4) color alternations. Four darker (10YR 7/4) layers alternating with lighter ones are evident upsection of the Oligocene/Miocene boundary in Hole U1334A (Fig. F9). The same alternating sequence is also observed above the Oligocene–Miocene transition in Cores 320-U1334B-9H and 320-U1334C-9H (Fig. F9). Smear slide observations do not show significant differences in constituents between dark and light layers, but compositional variations are indicated by variations of GRA bulk density, L*, and magnetic susceptibility that accompany the color changes (Fig. F9). A similar pattern in magnetic susceptibility is identified in Holes U1334B and U1334C (Fig. F9) and at Site 1218 (Shipboard Scientific Party, 2002b; Pälike et al., 2005).

Sediments across the Eocene–Oligocene transition

An Eocene–Oligocene transition section was recovered in all three holes drilled at Site U1334 (Holes U1334A–U1334C) (Figs. F5, F10). The Eocene/Oligocene boundary marker, *Hantkenina* species, has not been found at Site U1334 (see "Biostratigraphy"). However, radiolarian and nannofossil biostratigraphy provide excellent age control, indicating that the Eocene/Oligocene boundary falls near the middle of Biozone NP21 and just above the Zone RP20/RP19 boundary (near the base of Core 320-U1334A-27X, in the upper part of Core 320-U1334B-26X, and toward the lower part of Core 320-U1334C-27X) (Fig. F10).

The lithostratigraphy of the Eocene–Oligocene transition is well captured in all three holes drilled at Site U1334. In Hole U1334B, starting in Core 320-U1334B-26X, a downhole transition takes place from light gray (10YR 7/2) nannofossil ooze to dark brown (10YR 3/3) clayey nannofossil chalk (Figs. F10, F11), and these sediments overlie an alternating sequence of grayish brown (10YR 5/2) nannofossil chalk and very dark grayish brown (10YR 3/2) clayey nannofossil chalk with an underlying prominent (~60 cm thick) bed of very dark brown (10YR 2/2) radiolarian clay in Section 320-U1334B-27X-5 (Figs. F10, F11). Similar downhole lithologic transitions are seen in Holes U1334A and U1334C (Fig. F10). Thus, the Eocene–Oligocene transition at Site U1334 is marked by a distinct stepwise downhole color change from pale nannofossil ooze through dark clayey nannofossil chalk to alternations of dark nannofossil chalk and even darker clayey nannofossil chalk. Magnetic susceptibility, a*, and b* display pronounced downhole stepwise increases with pronounced downhole deceases in GRA bulk density, L*, and $CaCO_3$ content (Figs. F5, F10; see "Physical properties").

The lithostratigraphic results for the Eocene–Oligocene transition at Site U1334 are broadly consistent with those at Sites U1331–U1333 and multiple sites drilled during ODP Leg 199, in particular, Site 1218 (see the "Site U1331," "Site U1332," and "Site U1333" chapters) (Shipboard Scientific Party, 2002a). The most obvious lithostratigraphic difference between the Eocene–Oligocene transition at Sites U1334 and U1333 is that the transition at Site U1334 takes place within sediments that are significantly darker in color (L* values up to 60% at Site U1334 and up to 80% at Site U1333) (Fig. F12). The darker sediments at Site U1334 correspond to a more calcareous lithologic sequence and higher $CaCO_3$ contents than the darker Eocene sediments at Site U1333 (compare Fig. F5 in this chapter with Fig. F4 in the "Site U1333" chapter) (Fig. **F12**). The darker Eocene–Oligocene transition at Site U1334 is therefore attributed to higher clay content than at Site U1333, as indicated by magnetic susceptibility records for the two sites (Site U1334 = up to 60 × 10^{-5} SI units; Site U1333 = up to 40 × 10^{-5} units) (Fig. **F12**).

Summary

At Site U1334, Eocene seafloor basalt is overlain by about 285 m of pelagic sediments that are divided into four major lithologic units. Sediments are dominated by nannofossil oozes and nannofossil chalks. The early Miocene sedimentary sequence contains more clay and radiolarians relative to the Oligocene and Eocene sediments. The near-white Oligocene nannofossil oozes are characterized by both subtle meter-scale dark–light color cycles and vivid color variations that take place over 60 m. The subtle color cycles are the manifestation of small changes in the relative proportions of lithologic components, namely radiolarians, clay, and diatoms. The more vivid color cycles are related to changes in the oxidation state of Fe in the sediments and sedimentary pore waters. The oxidation-reduction reactions responsible for the observed color and pore water chemistry changes are likely fueled by enhanced availability of organic carbon relative to overlying and underlying sediments. The Oligocene–Miocene transition at Site U1334 is characterized by four subtle light–dark color alternations in very pale brown nannofossil ooze. The Eocene–Oligocene transition at Site U1334 is marked by a distinct stepwise color change from pale nannofossil ooze to dark clayey nannofossil chalk to alternations of dark nannofossil chalk and even darker clayey nannofossil chalk. Compared to Site U1333, the Eocene–Oligocene transition at Site U1334 takes place in significantly darker sediments. This observation is attributed to higher clay content, indicated by the higher values in the magnetic susceptibility record for Site U1334.

Biostratigraphy

At Site U1334, we recovered a 285 m thick succession of middle Miocene to uppermost middle Eocene nannofossil ooze and radiolarian clays with nannofossils. The uppermost 12 m of brown clay is barren of calcareous microfossils but contains radiolarians of middle Miocene age. Nannofossil ooze and radiolarian clays occur in the Miocene and Eocene parts of the section, with nannofossil ooze dominant in the thick Oligocene sequence. Radiolarians are present through most of the section, apart from the lowermost cores, and are well preserved in the Eocene. They provide a coherent high-resolution biochronology, and there appears to be a complete sequence of radiolarian zones from Zones RN7 (middle Miocene) to RP17 (uppermost middle Eocene). Calcareous nannofossils are present and moderately to well preserved through most of the succession, and there appears to be a complete sequence of nannofossil zones from Zone NN6 (middle Miocene) to upper Zone NP17 (uppermost middle Eocene). Nannofossil zonal determinations agree well with the radiolarian biostratigraphy; an integrated calcareous and siliceous microfossil biozonation is shown in Figure **F13.** A detailed age-depth plot including biostratigraphic and paleomagnetic datums is shown in Figure **F14.** Planktonic foraminifers are present through most of the succession and are relatively abundant and well preserved from the lower Miocene to the lower Oligocene. The preservation and abundance of planktonic foraminifers is more variable in the middle Miocene and upper Eocene to lowermost Oligocene. Benthic foraminifers are present through most of the section and indicate lower bathyal to abyssal paleodepths.

Calcareous nannofossils

Calcareous nannofossil biostratigraphy is based on analysis of core catcher samples from all three holes and from samples from most core sections of Hole U1334A. Depth positions and age estimates of biostratigraphic marker events are shown in Table **T3.** Nannofossils are generally abundant and moderately to well preserved throughout. Distinct intervals of poor nannofossil preservation are associated with dark lithologies within light–dark cycles around the early/middle Miocene boundary (Cores 320-U1334A-4H through 6H) and the Oligocene/Miocene boundary (Cores 320-U1334A-9H through 12H). Nannofossils are also less abundant and less well preserved in the low carbonate interval immediately below the Eocene/Oligocene boundary (Cores 320-U1334A-27H and 28H).

The uppermost interval of the succession, from Samples 320-U1334A-1H-1, 100 cm, to 2H-3, 70 cm, is barren of nannofossils. The first moderately well preserved nannofossil assemblages, between Samples 320-U1334A-2H-6, 120 cm, and 3H-4, 50 cm, are assigned to the mid to lower part of Neogene Zone NN6 (middle Miocene) based on the presence of *Coronocyclus nitescens* and *Calcidiscus premacintyrei* and the absence of *Sphenolithus heteromorphus.* The top common occurrence of *Cyclicargolithus floridanus* (lowermost Zone NN6) is recognized in Sample 320-U1334A-3H-3, 50 cm, followed by the top of *S. heteromorphus* (top of Zone NN5) in Sample 320-U1334A-3H-5, 50 cm, which suggests continuous deposition through this interval. Nannofossil Zones NN4 and NN5 cannot be differentiated in this succession because of the absence of the zonal marker *Helicosphaera ampliaperta;* however, the presence of *Discoaster petaliformis* between Samples 320-U1334A-3H-5, 50 cm, and 3H-CC indicates an age of upper Zone NN4 to NN5 (Young, 1999; Raffi et al., 2006). The base of *D. petaliformis* has been calibrated at 15.70 Ma at ODP Sites 925 and 926 (*Discoaster signus* in Raffi et al., 2006) and at this site occurs in Sample 320-U1334A-3H-CC. This is followed by the intra–Zone NN4 datum top common *Discoaster deflandrei* in Sample 320-U1334A-4H-2, 70 cm.

Calcareous nannofossils are generally poor to moderately well preserved within Cores 320-U1334A-4H and 5H, and because of the absence of *Sphenolithus belemnos,* probably due to poor preservation, the base of Zone NN4 cannot be distinguished. Nannofossil preservation improves and abundance increases just below the top of *Triquetrorhabdulus carinatus* in Sample 320-U1334A-5H-4, 120 cm, which marks the base of Zone NN3. The base of *Discoaster druggii* occurs in Sample 320-U1334A-9H-CC, marking the base of Zone NN2, but this species is only sporadically distributed in Cores 320-U1334A-5H through 9H. Supplementary biostratigraphic events in this Zone NN1–NN2 interval are the top of the *T. carinatus* acme event (Raffi et al., 2006) in Sample 320-U1334A-9H-CC, the base of *Sphenolithus disbelemnos* in Sample 320-U1334A-8H-CC, and the top and base of *S. delphix,* which are present in Samples 320-U1334A-10H-CC and 11H-1, 20 cm, respectively. The top of *S. delphix* occurs just prior to the Oligocene/Miocene boundary.

The Oligocene succession is dominated by white nannofossil oozes with abundant nannofossils that are moderately to well preserved. Initial nannofossil biostratigraphy indicates that this is a complete Oligocene sequence with consistently high sedimentation rates (~15 m/m.y.). The top of Zone NP25 is recognized by the top of *Sphenolithus ciperoensis* in Sample 320-U1334A-12H-CC. The intra–Zone NP24 abundance crossover from *Triquetrorhabdulus longus* to *T. carinatus* occurs between Samples 320-U1334A-12H-CC and 12H-7, 30 cm, and the top of *Cyclicargolithus abisectus* in Sample 320-U1334A-13H-1, 45 cm. The presence of all three sphenolith species, *S. ciperoensis, Sphenolithus distentus,* and *Sphenolithus predistentus,* in Sample 320-U1334A-16H-CC indicates Zone NP24 age and is also the base of consistent and common *S. ciperoensis* and the top of *S. distentus* and *S. predistentus*. Zones NP24–NP21 are recognized using the base of *S. ciperoensis* in Sample 320-U1334A-18H-CC; the top of *Reticulofenestra umbilicus* in Sample 320-U1334A-25X-1, 80 cm; and the top of *Coccolithus formosus* in Sample 320-U1334A-26X-3, 100 cm. The base of *S. distentus* is an intra–Zone NP23 datum and occurs in Sample 320-U1334A-21H-CC.

The age-depth plot for Site U1334 (Fig. **F14**) suggests that there is a calibration problem with the *S. ciperoensis* datums. The base of *S. ciperoensis* is difficult to locate because of rare and sporadic occurrences through its lower range followed by a distinct but short abundance peak near the tops of *S. distentus* and *S. predistentus*. The calibration of 27.1 Ma (Blaj et al., 2009) appears to be coincident with the base of the abundance peak and not its full range, which appears to be ~1 m.y. older and closer to the calibration used during Leg 199 (28.1 Ma) (Lyle, Wilson, Janecek, et al., 2002; see discussion in Wei and Wise, 1989).

The Eocene/Oligocene boundary interval lies between the top of *C. formosus* and the top of *Discoaster saipanensis,* which occurs in Sample 320-U1334A-27X-CC. The boundary interval yields nannofossils throughout and is apparently complete at the resolution provided by the nannofossil biostratigraphy. Eocene nannofossil Zones NP19–NP20 through NP17 are recognized using the base of *Isthmolithus recurvus* in Sample 320-U1334A-29X-CC, base of *C. oamaruensis* in Sample 320-U1334A-30X-1, 66 cm, and top of *C. grandis* in Sample 320-U1334A-30X-2, 74 cm. Both *I. recurvus* and *C. oamaruensis* are mid- to high-latitude taxa (Wei and Wise, 1989) and are present only rarely and sporadically at Site U1334. The presence of *Dictyococcites bisectus* to the base of the section indicates that the oldest sediment is between 37.1 and 38.0 Ma (upper Zone NP17).

Radiolarians

The radiolarian stratigraphy at Site U1334 (Fig. **F14;** Table **T4**) spans the interval from Zone RN7 (upper Miocene) in the base of Core 320-U1334-1H to the uppermost part of Zone RP17 (middle Eocene) in Sample 320-U1334-30X-2, 120–122 cm (Tables **T5, T6, T7**). The upper part of the first core (Samples 320-U1334A-1H-2, 105–107 cm, and 1H-4, 105–107 cm) recovered poorly preserved, reworked older radiolarians of Oligocene through early Miocene age. No reliable age determination could be made for these samples; however, the youngest species identified was *Calocycletta costata* (last occurrence at 14.23 Ma). In the Miocene through Oligocene interval, the radiolarian assemblage contains traces of reworked older microfossils, particularly in the upper Oligocene sediments (Zone RP21; Cores 320-U1334-10H, 11H, and 16H through 21H). Reworked older radiolarians are also found in the uppermost Eocene interval (Zone RP19; Cores 320-U1334A-27X and 28X). Radiolarians are usually moderately well preserved, but intervals of poor preservation are found in the uppermost part of the section (Zones RP5–RP7; Cores 320-U1334A-1H through 3H), as well as in parts of the upper Oligocene (Zone RP21; Cores 320-U1334A-17H through 20H). As in all other sites, the lowermost Oligocene (lower part of Zone RP20; Cores 320-U1334A-23X through 26X) contain common to abundant diatom frustules in the >63 µm, acid-treated fraction.

The Eocene section is indurated and the contained radiolarians are encrusted with clay and reprecipitated silica. Cleaning with a strong base solution (45% KOH) removed most of the encrustation and allowed the reliable identification of species, even for samples in which the microfossils were fragmented and poorly preserved (Samples 320-U1334A-27X-CC, 28X-2, 126–127 cm, 28X-CC, 29X-2, 50–52 cm, and 30X-2, 120–122 cm). Below Sample 320-U1334A-30X-2, 120–122 cm, sediments are barren of radiolarians.

Diatoms

Diatoms were examined in core catcher samples, as well as other samples obtained from Holes U1334A and U1334B. The interval examined represents the *Craspedodiscus coscinodiscus* Zone and the *Rossiella fennerae* through *Coscinodiscus excavatus* Zones of Barron (1985, 2006) and Barron et al. (2004). Diatoms range in abundance from rare to abundant depending on the specific sample. Diatom preservation is variable but generally moderate. Diatoms are typically absent or are rare in the core catcher samples from the upper eight cores. The exceptions are Samples 320-U1334A-1H-CC and 320-U1334B-1H-CC, which contain a middle Miocene diatom assemblage consisting of *Cavitatus jouseanus, Rossiella paleacea, Thalassiosira yabei, C. coscinodiscus,* and *Denticulopsis simonsenii.* Several of these species are suggestive of placement in the lower portion of the *C. coscinodiscus* Zone. Note that reworking of older specimens, such as *Rocella vigilans,* is recognized in this sample. No zonal assignment is possible for Samples 320-U1334A-2H-CC through 8H-CC.

The interval from Samples 320-U1334A-9H-2, 110–111 cm, through 10H-4, 110–111 cm, is assigned to the *R. fennerae* Zone based on the occurrence of *Bogorovia veniamini* and *Craspedodiscus barronii* without *Rocella gelida* or *R. vigilans.* Also characteristic of this interval are *C. jouseanus, Azpeitia oligocenica, R. paleacea,* and *Cestodiscus pulchellus.*

The interval from Samples 320-U1334A-10H-CC through 13H-2, 115–116 cm, is assigned to the *R. gelida* Zone based on the occurrence of *R. gelida* and *C. baronii* in this interval. This zonal assignment is supported by the occurrence of *Rocella schraderi* in Sample 320-U1334A-12H-2, 115–116 cm.

Diatoms are rare and typically have poor preservation in the interval from Samples 320-U1334A-13H-CC through 16H-2, 110–111 cm. The zonal assignment for this interval is tentative. *Rozellea vigilans* occurs in most samples examined in this interval. The occurrence of *B. veniamini* in Section 320-U1334A-15H-2 and Sample 320-U1334A-15H-4, 110–111 cm, suggests placement of these samples in the *B. veniamini* Zone. Such a zonal placement is supported by the occurrence of *Cestodiscus kugleri* in Sample 320-U1334A-14H-2, 110–111 cm.

The interval from Samples 320-U1334A-16H-4, 110–111 cm, through 20H-2, 115–116 cm, is assigned to the *R. vigilans* Zone based on the occurrence of *R. vigilans* without *B. veniamini.* The occurrence of *Kozloviella minor* in Sample 320-U1334A-17H-2, 110–111 cm, suggests placement of this sample in Subzone C of the *R. vigilans* Zone. The occurrence of *Rossiella symmetrica* in Sample 320-U1334A-17H-4, 110–111 cm, suggests placement of this sample in Subzone B of the *R. vigilans* Zone. Samples examined immediately below this interval (Samples 320-U1334A-20H-4, 115–116 cm, through 22H-CC) contain rare diatoms or poor preservation and are not zoned.

Section 320-U1334A-23X-2 is assigned to the *Cestodiscus trochus* Zone based on the occurrence of *C. trochus* without *R. vigilans* or *C. excavatus.* The interval from Samples 320-U1334A-23X-4, 90–91 cm, through 26X-4, 111–112 cm, is assigned to the *C. excavatus* Zone based on the occurrence of *C. excavatus.* Samples examined in Cores 320-U1334A-27X and below are unzoned because of the paucity of diatoms and/or the state of diatom preservation. One sample of note in this interval is Sample 320-U1334A-29X-1, 129–130 cm, which contains common diatom fragments including *Hemiaulus.*

Planktonic foraminifers

Core catchers were sampled from all three holes at Site U1334, and additional samples were taken in Hole U1334A (two per core) to develop a high-resolution biostratigraphy. Preservation and abundance is variable in the middle Miocene but improves downcore with good preservation recorded in the early Miocene and for much of the Oligocene. As found at previous Sites U1331–U1333, both preservation and abundance decreases across the Eocene/Oligocene boundary. Planktonic foraminifer biostratigraphy at this site indicates a middle Eocene through middle Miocene from Zone E13 or higher to Zone M9b/N12, which agrees well with calcareous nannofossil and radiolarian zonal determinations (Fig. F13). Depth positions and age estimates of biostratigraphic marker events identified are shown in Table T8. Taxon abundance and planktonic foraminifer preservation are shown in Table T9.

The topmost planktonic foraminifer zone recognized is Zone M9b/N12 in the middle Miocene defined by the base of *Globorotalia (Fohsella) fohsi robusta* in Sample 320-U1334A-2H-CC (18.11 m CSF). This sample is well preserved and contains a diverse fauna including *Globorotalia (Fohsella) fohsi lobata, Sphaeroidinellopsis disjuncta, Dentoglobigerina altispira,* and *Paragloborotalia mayeri*. Zones M5–M9a/N8–N12 are undifferentiated between Samples 320-U1334A-2H-CC and 4H-2, 38–40 cm (29.08 m CSF). *Praeorbulina sicana* was identified in Sample 320-U1334A-4H-2, 38–40 cm, but the base of Zone M5 was undefined because underlying Samples 320-U1334A-4H-CC, 320-U1334B-4H-CC, and 320-U1334C-4H-CC are barren or contain only very rare planktonic foraminifers. Zones M2–M4 were determined between the last occurrences of *P. kugleri* and *P. pseudokugleri* and the barren interval above which Zone M5 is identified. *P. sicana* was not found, indicating sediments younger than Zone M5. The absence of *Globigerinatella insueta* prevented further subdivision of Zones M2–M3, and Zones M3 and M4 were not differentiated because the last occurrence of *Catapsydrax dissimilis* was not reliable. The overlapping ranges of *Globoquadrina dehiscens, P. kugleri,* and *P. pseudokugleri* defines Zone M1b between Samples 320-U1334A-5H-6, 39–41 cm (44.59 m CSF), and 8H-CC (75.06 m CSF). Zone M1a occurs between the base of *G. dehiscens* in Sample 320-U1334A-8H-CC (75.06 m CSF) and the base of *P. kugleri* in Sample 320-U1334A-10H-2, 38–40 cm (86.08 m CSF).

The Oligocene/Miocene boundary is constrained at Site U1334 between Samples 320-U1334A-10H-2, 38–40 cm (86.08 m CSF), and 10H-5, 38–40 cm (90.58 m CSF), by the base of *P. kugleri,* which is present throughout its stratigraphic range in low abundance. Zone O6 is determined between the base of *P. kugleri* and the top of *Paragloborotalia opima*. The top and base of *P. opima* between Samples 320-U1334A-17X-2, 10–12 cm (152.58 m CSF), and 22X-4, 38–40 cm (203.80 m CSF), respectively, indicates Zones O2–O5. The lowest occurrence or base of *Globigerina angulisuturalis* falls within the range of *P. opima* in Sample 320-U1334A-19X-2, 38–40 cm (172.18 m CSF), and enables the distinction of Zones O4 and O5. The paucity of *Chiloguembelina cubensis* prevents Zones O4 and O5 from being differentiated. The top of *Turborotalia ampliapertura* is defined in both Holes U1334B and U1334C between Samples 320-U1334B-22H-CC and 23X-CC and Samples 320-U1334C-22H-CC and 23X-CC, respectively (Table T8). At Site U1334A, *T. ampliapertura* occurs sporadically and the datum is found at a lower stratigraphic level. It is not possible to divide planktonic foraminifer Zones O1 and O2 because of the absence of *Pseudohastigerina naguewichensis* from the assemblage.

As noted at previous sites, definition of the Eocene/Oligocene boundary is hindered by the absence of *Hantkenina,* which may at least in part be attributed to enhanced dissolution during this time interval and, thus, reduced foraminifer abundances and preservation but also related to the paleoecological preferences of the late Eocene hantkeninids (Coxall et al., 2003). In the absence of *Hantkenina* sp., the Eocene/Oligocene boundary is approximated at Site U1334 using the first occurrence of *Globoquadrina venezuelana* in Sample 320-U1334C-25X-CC (233.32 m CSF) and the first consistent presence of *Catapsydrax unicavus* in Sample 320-U1334C-26X-CC (240.51 m CSF). This approximation agrees well with the placement of the Eocene/Oligocene boundary in Tanzania (Wade and Pearson, 2008) and the radiolarian and nannofossil biostratigraphy.

Middle–late Eocene sediments contain a moderately preserved assemblage indicative of Zones E13–E16. The assemblage is dominated by small parasubbotinids, paragloborotaliids, and subbotinids. Taxa identified include *Dentoglobigerina tripartita, Paragloborotalia griffinoides, Parasubbotina griffinae, Paragloborotalia nana, Subbotina angiporoides, Subbotina eocaena, Turborotalia increbescens,* and *Turborotalia pomeroli*. The lack of *Globigerinatheka, Acarinina,* and *Morozovelloides* prevents differentiation of individual zones within the middle–late Eocene. The presence of *Subbotina linaperta* in Sample 320-U1334A-30X-6, 48–50 cm (280.08 m CSF), indicates a basement age older than 37.7 Ma (Berggren et al., 1995). This is consistent with the age of basement estimated using calcareous nannofossils between 37.1 and 38.0 Ma.

Benthic foraminifers

Benthic foraminifers were examined semiquantitatively from the three holes of Site U1334. Benthic foraminifers are almost continuously present in samples from Site U1334. The distribution of benthic foraminifers at this site is shown in Table T10.

The uppermost sample in Hole U1334A (Sample 320-U1331A-1H-CC; 8.22 m CSF) contains only rare benthic foraminifers and preservation varies from poor to moderate. In Samples 320-U1334A-2H-CC and 3H-CC (18.14 and 27.68 m CSF, respectively), *Oridorsalis umbonatus, Nuttallides umbonifer, Cibicidoides mundulus,* and *Globocassidulina subglobosa* are common and *Pullenia bulloides, Spheroidina bulloides, Melonis pomplioides,* and *Melonis barleeanum* are subordinate. A similar fauna is found in Samples 320-U1334B-1H-CC through 3H-CC (13.71–32.65 m CSF) and 320-U1334C-1H-CC through 3H-CC (9.84–28.10 m CSF). Middle Miocene taxa identified here indicate lower bathyal and abyssal paleodepths (van Morkhoven et al., 1986).

In Samples 320-U1334A-4H-CC through 25X-CC (37.21–233.98 m CSF), *O. umbonatus, N. umbonifer, C. mundulus, G. subglobosa,* and *Gyroidinoides* spp. are common and *P. bulloides, Astrononion echolsi,* and *Cibicidoides grimsdalei* are subordinate. Samples 320-U1334A-4H-CC and 9H-CC (37.21 and 84.77 m CSF, respectively) contain rare benthic foraminifers, but agglutinated forms are common. Preservation of foraminifer tests is good to moderate, except in Samples 320-U1334A-4H-CC and 9H-CC. Similar benthic foraminifer taxa are also recognized in Holes U1334B (Samples 320-U1334B-4H-CC through 26X-CC; 41.95–247.89 m CSF) and U1334C (Samples 320-U1334C-4H-CC through 26X-CC; 38.30–240.73 m CSF). There is no marked difference in faunal composition or preservation of benthic foraminifers between the green-colored sediments (e.g., Samples U1334A-16H-CC through 20H-CC) and other white-colored sediments in the Oligocene. Faunal compositions recorded here indicate lower bathyal and abyssal paleodepths during the Oligocene and the early Miocene, similar to those of Sites U1332 and U1333 and previous studies in the eastern equatorial Pacific (ODP Site 573, Thomas, 1985; ODP Sites 1218 and 1219, Takata and Nomura, 2005). *N. umbonifer* and *C. mundulus* occur in high abundances in the Oligocene of Site U1334, but they show a more sporadic stratigraphic distribution than at Sites U1332 and U1333 (Fig. **F15**). Other minor species—*C. grimsdalei, P. bulloides, S. bulloides, A. echolsi,* and *Gyroidinoides* spp.—have more variable abundances than observed at Sites U1332 and U1333. These subtle differences in Oligocene benthic foraminifer fauna may arise from variations in water mass properties with depth. For example, the discontinuous abundance of *N. umbonifer,* a species tolerant to carbonate undersaturation and/or low food supply (e.g., Mackensen et al., 1990; Schmiedl et al., 1997), at Site U1334 in the Oligocene could be interpreted as a reduced influence of Southern Component Water and/or carbonate undersaturation of deep water compared to other sites.

Benthic foraminifers are present in Samples 320-U1334A-26X-CC through 31X-CC (243.39–283.92 m CSF), including common *O. umbonatus, Nuttallides truempyi, C. grimsdalei,* and *G. subglobosa*. Similar occurrences are also recognized in Samples 320-U1334B-27X-CC through 29X-CC (257.73–276.92 m CSF) and 320-U1334C-27X-CC through 30X-CC (248.17–277.95 m CSF). In addition, various taxa, such as *Abyssamina quadrata, Abyssamina poagi, Alabamina dissonata, Anomalinoides* sp. A, and *Gyroidinoides* spp., are subordinate in Sample 320-U1334C-30X-CC. Preservation of these calcareous foraminifers is generally poor. These faunal assemblages suggest lower bathyal to abyssal paleodepths in the middle to late Eocene. Faunal associations of these calcareous taxa in the middle to late Eocene are basically similar to those of Sites U1331–U1333 and previous preliminary studies in the eastern equatorial Pacific (Site 1218, Wilson, Lyle, and Firth, 2006).

Paleomagnetism

We studied the paleomagnetism of sediments from Site U1334 with a primary focus on determining a preliminary magnetostratigraphy, which can be used to assist in dating the stratigraphic section. To accomplish this, we measured the natural remanent magnetization (NRM) of archive-half sections from 66 APC cores recovered from Holes U1334A–U1334C. Measurements were made along each section at 5 cm intervals before and after alternating-field (AF) demagnetization of 20 mT. When time permitted, some sections were measured at 1 or 2.5 cm intervals. We found the higher resolution data to be more useful than measuring the 5, 10, or 15 mT demagnetization steps as had been done at the previous sites. We also did not measure archive-half sections of any XCB cores at this site because the shallow paleomagnetic inclination of the sediments along with the relative azimuthal rotation that occurs between adjacent pieces of XCB core (referred to as “drilling biscuits”) results in neither useful intensity nor direction data.

We processed the paleomagnetic data by removing measurements made within 5 cm of section ends and data from disturbed intervals (Table **T11**). Cleaned data are presented in Tables **T12, T13, T14, T15, T16,** and **T17** and Figures **F16, F17,** and **F18.**

Azimuthal core orientation was determined solely by correlating distinct reversal patterns as recorded by paleomagnetic declinations in each hole with the geomagnetic polarity timescale (GPTS) (See **“Paleomagnetism”** in the “Methods” chapter and **“Paleomagnetism”** in the “Site U1331” chapter). This process is aided by rather detailed age constraints, which significantly limit the range of possible correlations with the GPTS (see **“Biostratigraphy”**). Once we had confidently identified a unique, unambiguous reversal pattern, the mean paleomagnetic directions for each core were calculated using Fisher statistics (Table **T18**). Subsequently, data were reoriented so that normal and reversed polarity magnetozones had declinations of ~0° and ~180°, respectively (see

"Paleomagnetism" in the "Site U1331" chapter). Reoriented declinations are provided for Holes U1334A–U1334C in Tables T13, T15, and T17, respectively, for data collected after AF demagnetization at 20 mT.

We measured magnetic properties of 188 discrete paleomagnetic samples, with one sample collected from nearly every section in Hole U1334A. Of these, 87 samples were subjected to progressive AF demagnetization up to 60 mT. Remanence measurements and characteristic remanent magnetization (ChRM) directions computed using principal component analysis (PCA) are given in Tables T19 and T20, respectively. Magnetic susceptibilities and masses, along with volumes estimated using MAD data (see "Physical properties"), are given in Table T21. This table also includes magnetic susceptibilities from whole-core data for the intervals corresponding to where the discrete samples were taken, which is useful for checking the scale factor, 0.68×10^{-5} (see "Paleomagnetism" in the "Methods" chapter), for converting the whole-core raw susceptibility meter measurements into true volume-normalized susceptibility values.

Results

Downhole variations in paleomagnetic data from split-core and discrete samples and susceptibility data from whole-core and discrete samples are shown in Figures F16, F17, and F18. The most prominent features of the records are

1. The clear 180° alternations in declination for the upper ~140–150 m CSF of the section, reflecting the magnetic polarity zones (magnetozones);
2. The remanent magnetic intensity and magnetic susceptibility low that occurs between ~135 and 210 m CSF, referred to as the magnetic-low zone; and
3. The general degradation of the paleomagnetic direction within the magnetic-low zone with further degradation at the depth where coring switched from using nonmagnetic to steel core barrels (compare the results above and below the dashed line in Figs. F16, F17, and F18).

The magnetic-low zone can be attributed to reduction diagenesis, whereby oxygen from fine-grained iron oxides (titanomagnetite and magnetite) is used by bacteria to break down organic matter. This mobilizes iron and converts some of the iron oxides into various iron sulfides, most of which have very low magnetic susceptibilities and retain little or no remanent magnetization.

Unlike Sites U1331 and U1332, where the drilling overprint was present regardless of which type of core barrel was used, the drilling overprint was generally weak for Site U1334 cores when nonmagnetic core barrels were used (Cores 320-U1334A-1H through 16H, 320-U1334B-1H through 15H, and 320-U1334C-1H through 15H). In contrast, those cores collected with steel core barrels are highly overprinted, similar to what was observed at Site U1333 (Fig. F19). At Site U1334, the overprint appears more severe than at any of the other sites, which might be related to mineralogy (replacement of the primary iron oxides with iron sulfides). Whatever the cause, even demagnetization at 20 mT fails to remove the overprint fully. As a result, paleomagnetic declination data have notably higher variability, which makes polarity determination much more difficult in the intervals collected with steel core barrels.

Discrete sample demagnetization data from cores collected above ~130 m CSF (those collected with nonmagnetic core barrels and that are above the magnetic-low zone) indicate that the ChRM of the sediments can be resolved by AF demagnetization above ~10 mT (Fig. F20). We interpret this ChRM to be the primary depositional remanent magnetization. Unlike most of the samples from Sites U1331–U1333, most Site U1334 samples have more poorly resolved ChRM directions (more scattered directions along a linear demagnetization path in the orthogonal demagnetization plot). We attribute this mainly to the weaker magnetization of Site U1334 sediments. For example, within the magnetic-low zone, magnetizations are very close to the noise level of the magnetometer. Even more strongly magnetized intervals are only about an order of magnitude above the noise level. Generally, those samples that are sufficiently strongly magnetized yield linear demagnetization paths that decay toward but do not terminate at the origin of the orthogonal demagnetization diagrams (Fig. F20). This offset from the origin most likely reflects measurement artifacts (a small anhysteretic magnetization imparted to samples as they are demagnetized). Even with this artifact, ChRM directions for the more strongly magnetized samples are well constrained. These ChRMs, estimated from the linear demagnetization paths using PCA, agree well with those of coeval intervals of the archive-half measurements (Fig. F16), indicating that magnetic directions from the split cores after 20 mT demagnetization step provide a reliable indicator of the ChRM of the sediments.

Magnetostratigraphy

Cleaned paleomagnetic data provide a series of distinct ~180° alternations in declination and subtle changes in inclination, which, when combined with biostratigraphic age constraints, allow a continuous magnetostratigraphy to be constructed that correlates well with the GPTS. The magnetostratigraphic record extends from the top of Chron C1n (0 Ma) at the mudline of Hole U1334A (0 m CSF) to the top of Chron C11r (29.957 Ma) at 195.06 m CSF in Hole U1334C (Figs. F19, F21, F22; Table T22). The interpretation is complicated in only two intervals. The first complication occurs for the thin Pliocene and Pleistocene section, which was cored only once (in the upper 5 m CSF of Hole U1334A) (Fig. F21A). Either coring deformation or hiatuses make it difficult to connect what appear to be Chrons C1n through C2n in the upper 2 m of Core 320-U1334A-1H to a clear continuous sequence of magnetozones that correlate well from the base of Chron C3r at 5.3 and 1.8 m CSF in Holes U1334A and U1334C, respectively, to the top of Chron C9n (26.508 Ma) at 139.5, 136.2, and 131.9 m CSF in Holes U1334A–U1334C, respectively. Below this, correlation of the magnetozones to Chrons C9r–C12n is more speculative as a result of the more variable declinations in the magnetic-low zone and the larger drilling overprint, as discussed above. We consider it too speculative to correlate the highly variable declinations from Cores 320-U1334A-22H, 320-U1334B-22H, or 320-U1334C-22H with the GPTS. Below these cores, only XCB cores were collected, from which polarity determination is improbable.

Some highlights of the magnetostratigraphy at Site U1334 include resolving a clear sequence of magnetozones corresponding to Chrons C3r–C9n, which yield a total of 250 dated reversals from the three holes and provide detailed chronostratigraphic and sedimentation rate constraints (see **"Stratigraphic correlation and composite section"**), the identification of a previously observed cryptochron (C5Dr-1n) in all three holes, and the identification of eight possible excursions, seven of which are recorded in at least two of the holes (Table T22; Figs. F19, F21, F22).

Geochemistry

Sediment gases sampling and analysis

Headspace gas samples were taken at a frequency of one sample per core in Hole U1334A as part of the routine environmental protection and safety monitoring program. All headspace sample analyses resulted in nondetectable levels of methane (C_1; <1 ppmv), with no higher hydrocarbons, consistent with the low organic carbon content of these sediments.

Interstitial water sampling and chemistry

Thirty-four interstitial water samples were collected using the whole-round squeezing approach (Table T23; Fig. F23). In addition, 61 samples were taken using Rhizon samplers from Sections 320-U1334B-13H-5 and 13H-6 and 320-U1334C-13H-5 through 23X-3 with a sampling frequency of one sample per section, resulting in a stratigraphic resolution of ~1.5 m (Table T24; Fig. F24). This depth interval was selected for Rhizon sampling to study the profiles of dissolved Mn and Fe of the interstitial water geochemistry revealed by the whole-round samples (Fig. F23) in more detail. Chemical constituents were determined according to the procedures outlined in **"Geochemistry"** in the "Methods" chapter. In this section, we first describe the overall site geochemistry based on the whole-round samples and then present a more detailed comparison of elements analyzed by squeezed and Rhizon samples in the depth interval of their overlap.

Chlorinity shows relatively little variability with depth, with values ranging mainly from 553 to 566 mM (Fig. F23; Table T23). However, chlorinity values reveal a distinct increase from 553 to 565 mM in the uppermost 30 m CSF, potentially reflecting the change from the more saline ocean at the Last Glacial Maximum to the present (Adkins and Schrag, 2003). Alkalinity shows little variability with values ranging from 2.7 to 4.0 mM. Sulfate concentrations vary between 24 and 29 mM, with decreasing values in the upper 60 m CSF and higher values below 250 m CSF. Dissolved phosphate concentrations are ~2 µM in the shallowest sample, decreasing to ~0.5 µM in the uppermost ~15 m CSF. Dissolved manganese peaks with concentrations of up to 6 µM between ~50 and 150 m CSF, with peak manganese values (at ~110 m CSF) shallower than the peak dissolved iron value of 6 µM between 150 and 180 m CSF. Because of the relatively high sulfate concentrations, dissolved Ba concentrations are low and relatively homogeneous, with values between 0.8 and 1.5 µM. Concentrations of dissolved silicate increase with depth from ~400 to ~850 µM.

Calcium and magnesium concentrations are relatively uniform, with values ranging from 10.2 to 11.5 and from 50 to 53 mM, respectively (Fig. F23).

Lithium concentrations decrease from ~26 µM at the surface to 15 µM at ~100 m CSF, with the strongest decrease apparent between 10 and 20 m CSF. Lithium strongly increases below 220 m CSF toward basement. Strontium concentrations range between 78 and 107 µM. Values show an increase from the top toward 110 m CSF, followed by a decrease toward basement. Boron concentrations range between 400 and 500 µM, showing a relatively constant decrease from top to basement.

Interstitial water samples derived from Rhizon and whole-round squeezing show good agreement for some elements (Fig. F25). Because these two data sets were collected in different holes, data are plotted in CCSF-A depths to facilitate comparison. In the depth range of overlap, the more frequently sampled Rhizon profiles and the squeezed profiles give comparable absolute values and profile shapes for some elements (Fig. F25), especially when considering the analytical reproducibility of shipboard techniques (see the "Methods" chapter). This includes elements with relatively constant depth profiles (e.g., sulfate and silicate) and those with relatively large concentration changes (e.g., manganese).

The deepest three Rhizon samples were taken in the first three sections of the first core at this hole to be cored with the XCB. The more fragmented nature of the recovered sediments led to Rhizon samples that very rapidly filled with water and to results that appear more contaminated with seawater drilling fluid. Rhizon profiles are noisier, partially because of the greater depth resolution of sampling and the limits of analytical reproducibility. However, some of this variability appears related to actual sampling variability between Rhizons in a single depth profile and between holes regardless of sampling technique. For example, one Rhizon sample shows clear signs of drill fluid contamination as excursions toward seawater values are observed for several elements (alkalinity, silicate, lithium, and strontium in Sample 320-U1334C-15H-1, 75 cm; 161.98 m CCSF-A) (Fig. F25), but this sample was taken in an area of clear drilling disturbance.

We were particularly interested in the iron and manganese profiles, indicative of suboxic oxidation of organic carbon by manganese oxide and iron oxide reduction. The depth zone with high dissolved iron concentrations corresponds to the depth zone of low magnetic susceptibility (Fig. F25) and the tail of the dissolved manganese peak (Figs. F23, F25). We reran the squeezed samples with the Rhizon samples for dissolved manganese and iron, finding generally excellent analytical reproducibility on the replicate runs. The Rhizon and squeezed profiles agree well for dissolved manganese, with some occasional excursions in the Rhizon samples to higher manganese concentrations. The iron profiles also generally agree well. The exceptions are two substantially higher iron values in the squeezed samples in the 160–180 m CCSF-A range, the depth interval of the color change from yellowish gray to greenish gray. This may represent true interhole variability or a sampling artifact.

Bulk sediment geochemistry: major and minor elements

At Site U1334, bulk sediment samples for minor and major element analyses were distributed over the core depth to characterize the major lithologic units (0–280 m CSF; Hole U1334A). We analyzed concentrations of silicon, aluminum, iron, manganese, magnesium, calcium, sodium, potassium, titanium, phosphorus, barium, copper, chromium, scandium, strontium, vanadium, yttrium, and zirconium in the sediments by inductively coupled plasma–atomic emission spectroscopy (ICP-AES) (Table T25).

SiO_2 ranges between 7 and 54 wt%, with values decreasing from 50 wt% at the surface to values <10 wt% between 50 and 220 m CSF. Below 220 m CSF, SiO_2 concentrations vary between 7 and 54 wt%, with concentrations below 10 wt% near the basement. Concentrations of Al_2O_3 range from 0.2 to 12 wt%, with values decreasing in the upper 50 m CSF from 12 to <1 wt%. Between 50 and 250 m CSF, Al_2O_3 concentrations are mainly below 1 wt%. Around 250–260 m CSF, Al_2O_3 concentrations slightly increase to 2 wt%. A distribution with depth similar to that of Al is shown by TiO_2 (0.006–0.6 wt%), K_2O (0.1–2.2 wt%), Zr (18–240 ppm), and Sc (0.5–40 ppm).

Concentrations of Fe_2O_3 vary between 0.5 and 10 wt%, following the general pattern of SiO_2. Similar trends are also shown by MnO (0.07 to >0.2 wt%), MgO (0.4–4 wt%), copper (45 to >140 ppm), and vanadium (up to 115 ppm). The peak concentrations of Mn and Cu could not be quantified because they exceeded the calibrated range (Table T24).

Calcium (CaO) ranges from 1 to 42 wt%, with high values corresponding to minima in SiO_2 and Al_2O_3. Strontium concentrations range from 345 to >700 ppm, showing a similar pattern to CaO. Barium and P_2O_5 values range from below detection limit to >566 ppm and 1 wt%, respectively, showing minima at high CaO concentrations.

Bulk sediment geochemistry: sedimentary inorganic and organic carbon

$CaCO_3$, inorganic carbon (IC), and total carbon (TC) concentrations were determined on sediment samples from Hole U1334A (Table T26; Fig. F6). $CaCO_3$ concentrations ranged between <1 and 95 wt%. In the uppermost ~16 m CSF, $CaCO_3$ concentrations are very low (<1 wt%) and then, from 16 to 46 m CSF, vary greatly between <1 and 74 wt%. Carbonate concentrations are consistently high (74–95 wt%), from 46 to 247 m CSF, with a few relatively low concentrations at 57.9, 87.9, 103, and 116.9 m CSF. From 247 to 260 m CSF, $CaCO_3$ concentrations are low (<1–56 wt%). Below 260 m CSF, $CaCO_3$ concentrations are variable, ranging between 37 and 86 wt%. Variations in $CaCO_3$ concentrations correspond to lithostratigraphic changes (see "Lithostratigraphy").

Total organic carbon (TOC) concentrations were determined by acidification (see **"Geochemistry"** in the "Methods" chapter) (Table **T26;** Fig. **F6**) and are very low throughout the sediment column, with a range from below the detection limit to 0.15 wt% (Fig. **F24**).

Physical properties

Physical properties at Site U1334 were measured on whole cores, split cores, and discrete samples. WRMSL (GRA bulk density, magnetic susceptibility, and *P*-wave velocity), thermal conductivity, and NGR measurements comprised the whole-core measurements. Compressional wave velocity measurements on split cores and MAD analyses on discrete core samples were made at a frequency of one per undisturbed section in Cores 320-U1334A-1H through 31X (Table **T27**). Compressional wave velocities were measured toward the bottom of sections. MAD analyses were located 10 cm downsection from carbonate analyses (see **"Geochemistry"**). Lastly, the Section Half Multisensor Logger (SHMSL) was used to measure spectral reflectance on archive-half sections.

Density and porosity

Two methods were used to evaluate wet bulk density at Site U1334. GRA provided an estimate from whole cores (Fig. **F26**). MAD samples gave a second, independent measure of wet bulk density, along with providing dry bulk density, grain density, water content, and porosity from discrete samples (Table **T28**). MAD and GRA bulk density measurements display the same trends and are also similar in absolute values through the entire section (Fig. **F27B**). Cross-plots of wet and dry bulk density versus interpolated GRA density (Fig. **F28**) show good correlation between MAD and GRA data.

Generally, wet bulk density corresponds with changes in lithology. Bulk density is very uniform for the first 15 m within Unit I, corresponding to a clay-rich interval at the top of the section (see **"Lithostratigraphy"**). An increase toward higher and less uniform bulk density values occurs in the lower part of Unit I. In Unit II, bulk density increases to values of ~1.6 g/cm^3, reflecting the major lithology of this lithostratigraphic unit, nannofossil ooze. In Hole U1334A, bulk density decreases from 1.7 to 1.5 g/cm^3 at 205 m CSF. A similar decrease occurs at 210 m CSF in Hole U1334B. A very slight trend toward higher bulk density begins at the ooze–chalk transition between Unit II and Subunit IIIa. Subunit IIIb is marked by a prominent decrease in bulk density. Within Subunit IIIb, bulk density begins to increase toward the base of the section.

Variation in grain density in Hole U1334A generally matches changes in lithology (Fig. **F27C**). Grain density is highly variable with values between 2.1 and 2.9 g/cm^3 in Unit I and the top of Unit II. Within Unit II, below 90 m CSF, grain densities are more uniform (2.7 g/cm^3), reflecting the character of the major lithology, nannofossil ooze. Grain density is slightly less uniform in Subunits IIIa and IIIb, with lower values (2.2 g/cm^3).

Porosity averages 85% in the top of Unit I and decreases to 75% in the lower section of Unit I (Fig. **F27**). Porosity becomes uniform in the upper 80 m of Unit II, with values of ~65% to 75%. Below 130 m CSF, porosity becomes more uniform and shows a slight downhole decrease to between 60% and 70%. Porosity increases slightly in Subunit IIIa and shows little change in Subunit IIIb.

Magnetic susceptibility

Whole-core magnetic susceptibility measurements correlate well with major differences in lithology and changes in bulk physical properties (Fig. **F26**). Magnetic susceptibility values are high and variable (10×10^{-5} to 40×10^{-5} SI) in Unit I. A sharp drop in magnetic susceptibility occurs at the top of Unit II, owing to decreased concentration of ferromagnetic minerals in the nannofossil ooze–dominated lithology. The low values of this lithologic unit (~5×10^{-5} to 10×10^{-5} SI) are punctuated in several places with small jumps in magnetic susceptibility to values as high as 30×10^{-5} SI (e.g., 55 m CSF). These jumps can generally be correlated from hole to hole. At 140 m CSF the magnetic susceptibility signal is lost because of iron reduction in the sediments (see **"Geochemistry"**). The magnetic susceptibility signal returns at 205 m CSF in Hole U1334A and at 210 m CSF in Hole U1334B. Magnetic susceptibility values are 10×10^{-5} SI and relatively uniform for the remainder of Unit II and Subunit IIIa. A sharp increase in magnetic susceptibility occurs at the base of Subunit IIIb.

Compressional wave velocity

Shipboard results

Whole-core *P*-wave logger (PWL) and discrete velocity measurements made on split cores follow similar trends. The velocity record of Site U1334 is unremarkable in Units I and II, with very uniform velocity values of 1500 m/s (Fig. **F26**). A small increase in velocity to ~1540 m/s occurs in the middle of Unit II at ~150 m CSF; this may be linked to the color change toward green sediments observed here (See **"Lithostratigraphy"**). A key transition in velocity occurs at the ooze/chalk boundary between Unit II and Subunit IIIa. Below this lithologic unit boundary, velocity values increase steadily to 1600 m/s at the base of the section. Discrete velocity measurements along the *x*-, *y*-, and *z*-axis are in excellent agreement with the PWL for most of the section (Fig. F29). However, below the sonic discontinuity at 150 m CSF, velocity measurements in the *y*-axis become higher by ~50 m/s compared to PWL velocity measurements. Measuring discrete velocity became impossible below the ooze–chalk transition between Unit II and Subunit IIIa; large cracks formed during insertion of the transducers because of poor cohesion of the radiolarian-dominated sediments. Discrete *x*-axis velocity measurements closely track the PWL measurements throughout the section.

Postcruise correction

During the analysis of Site U1334 cores, it was decided that the consistently high *x*-direction values are the result of using an incorrect liner thickness. Based on a limited number of liner thickness measurements, it was decided that the liner correction should use 3.2 mm for the liner thickness. However, during the analysis of Hole U1337A cores, it was determined that high *x*-direction velocities do not result from thicker than expected core liner but instead are the result of using an incorrect value for the system delay associated with the contact probe (see **"Physical properties"** in the "Site U1337" chapter). Critical parameters used in this correction are system delay = 19.811 µs, liner thickness = 2.7 mm, and liner delay = 1.26 µs. During the analysis of Hole U1337A cores, it was also determined that consistently low PWL velocities required the addition of a constant value that would produce a reasonable velocity of water (~1495 m/s) for the quality assurance/quality control (QA/QC) liner (see **"Physical properties"** in the "Site U1337" chapter). These corrections have not been applied to the velocity data presented in this chapter.

Natural gamma radiation

Natural gamma radiation was measured on all whole cores at Site U1334 (Fig. F26). The highest NGR values are present at the seafloor (~15 cps). NGR values decrease to the base of Unit I. NGR is uniform throughout Unit II and Subunit IIIa. A slight increase by ~3 cps accompanies the lithologic boundary between Subunits IIIa and IIIb.

Thermal conductivity

Thermal conductivity was measured on the third section of each core from Hole U1334A (Table T29). Thermal conductivity shows a strong dependence on porosity and lithology downhole through the succession (Figs. F30, F31). Decreased conductivity occurs with increasing porosity as increased interstitial spacing attenuates the applied current from the probe. Thermal conductivity is 0.8 W/(m·K) in Unit I and increases to a maximum value of 1.2–1.3 W/(m·K) in Unit II. Values decrease to 0.9 W/(m·K) in Subunits IIIa and IIIb.

Reflectance spectroscopy

Spectral reflectance was measured on split archive section halves from all three holes using the SHMSL (Fig. F32). The parameters L* (black–white), a* (green–red), and b* (blue–yellow) follow changes in lithology, with variations in L*, a*, and b* correlating very well to carbonate content, density, and magnetic susceptibility measurements (Figs. F5, F32). L* has relatively low amplitude variations around 80 in the carbonate section of Unit II, whereas in more radiolarian-dominated intervals, L* has lower values, with higher amplitude variation, ranging from 25 to 75. Except for the light greenish gray interval discussed later, a* and b* generally show high values (~5 and 13, respectively) with high-amplitude and high-frequency variation in the more carbonate dominated Unit II. The light greenish gray carbonate interval, between 144 and 190 m CSF, is clearly seen in the a* data as values shift to around –3; negative a* values are indicative of green colors. The b* values decrease sharply to ~4 in this interval before rapidly increasing back to 13 at its base. L*, a*, and b* values all decrease at the boundary between Subunits IIIa and IIIb, correlating with the sudden increase in radiolarian content, which subsequently decreases toward the bottom of Subunit IIIb (whereas luminance values increase). The limestone present in Unit IV is represented by high values of L*, a*, and b* (around 60, 6, and 15, respectively) corresponding to its extremely light, almost white color.

Stratigraphic correlation and composite section

STMSL data were collected at 5 cm intervals from Holes U1334B and U1334C and compared to the WRMSL data obtained at 2.5 cm resolution from Hole U1334A. In this way we monitored drilling in Holes U1334B and U1334C in real time to recover and construct a stratigraphically complete composite section. Several intervals between Holes U1334A and U1334B did not overlap sufficiently to cover gaps between cores. Thus, coring of Hole U1334C was designed to recover the missing intervals, as well as to provide additional material for high-resolution studies. The coring effort in Hole U1334C was successful at covering gaps between cores in Holes U1334A and U1334B to ~222 m CCSF-A (Figs. F33, F34) and from 250 to 336 m CCSF-A, almost to the bottom of the section. Stratigraphic correlation between the three holes at Site U1334 was challenging in the light greenish gray interval (Cores 320-U1334A-15H through 22H, 320-U1334B-14H through 22H, and 320-U1334C-14H through 22H), which is characterized by very low magnetic susceptibilities, and in the bottom ~80 m, where coring with the XCB compromised core quality. The correlation between the three holes for the chosen parameters was adequate to good and, in some depth intervals, excellent. The gaps between successive cores in any of the holes are on the order of 1 to 2 m, with a maximum of ~4 m between Cores 320-U1334C-3H and 4H and ~14 m between Cores 320-U1334A-21H and 22H (see discussion below).

The correlation was refined once magnetic susceptibility and GRA density data were available at 2.5 cm resolution from the WRMSL, and NGR and color reflectance data were available from the NGR track and the SHMSL (see "Physical properties"). Visual inspection, comparison with core imagery, and biostratigraphic datums were used to establish and verify hole to hole correlation where track data lacked clearly identifiable features. Magnetic susceptibility and GRA density proved most useful for correlating between holes at Site U1334 (Figs. F33, F34). Features in the magnetic susceptibility and GRA density are well aligned between Holes U1334A–U1334C to ~155 m CCSF-A. From ~155 to ~222 m CCSF-A, GRA density data allow confident alignment of cores despite very low magnetic susceptibility values. In the interval from ~222 to ~250 m CCSF-A (Cores 320-U1334A-21H through 22H, 320-U1334B-20H through 22H, and 320-U1334C-20H through 22H), no features in any of the measurements available could be correlated. Several attempts to match the records did not provide convincing results. We suggest that this interval has to undergo detailed shore-based investigation to attempt the construction of a complete stratigraphic sequence. It cannot be ruled out that the apparent intensive geochemical alteration (see "Geochemistry" for discussion) in this interval has canceled out any signal detectable with the shipboard instrumentation. It is interesting to note that Cores 320-U1334A-22H, 320-U1334B-22H, and 320-U1334C-22H are the last APC cores in each hole and had to be recovered by overdrilling. The following cores (320-U1334A-23X, 320-U1334B-23X, and 320-U1334C-23X) are the first XCB cores and are therefore very likely to be affected by severe coring disturbance. In addition to switching to the XCB, a geochemical transition occurs in Cores 320-U1334A-23X and 320-U1334B-23X and between Cores 320-U1334C-22H and 23X (see "Geochemistry" for discussion). It is characterized by a color change and the reappearance of a good-quality magnetic susceptibility signal. This color transition occurs at substantially different CSF depths in the three holes cored at Site U1334 (onset at 204.7 m CSF in Hole U1334A, 211.8 m CSF in Hole U1334B, and between 208 and 209 m CSF in Hole U1334C). Aligning the color transition leads to a ~14 m core gap in Hole U1334A from 229 to 243 m CCSF-A (Figs. F33E, F34E). The top of Core 320-U1334A-22H exhibits unusually strong coring disturbance in the first two sections, suggesting that drilling conditions might have contributed to the coring gap. Biostratigraphic datum levels imply that the bottom of Core 320-U1334A-22H aligns with the middle of Cores 320-U1334B-22H and 320-U1334C-22H (compare Figs. F33E, F34E), suggesting that the geochemical transition does not occur at the same depth in the Site U1334 holes. A tentative comparison to the Site 1218 GRA record (Shipboard Scientific Party, 2002b) reveals no apparent correlation to Cores 320-U1334B-22H and 320-U1334C-22H and thus suggests disturbance or interruption of the stratigraphic sequence by undetected or unidentifiable causes. Low-amplitude variations of all track data, caused presumably by geochemical alteration, hinders construction of a complete stratigraphic section throughout this interval with the shipboard data available. We decided to append the splice in the interval between ~222 and ~250 m CCSF-A. Below this depth, magnetic susceptibility and GRA data correlate well and have been used to construct a robust composite section (cf. Figs. F33, F34).

Offsets and composite depths are listed in Table T30. Following construction of the composite depth section for Site U1334, a single spliced record was assembled for the aligned cores to Section 320-U1334B-30X-2 at 336.45 m CCSF-A (Fig. F33). The sections of core used for the splice are identified in Table T31 and displayed in Figures F33 and F34. The spliced composite section consists of almost equal proportions from all three holes.

We avoided intervals with significant disturbance or distortion and intervals where whole-round samples for interstitial water chemistry were taken (see "Paleomagnetism;" Table T11). The Site U1334 splice can be used as a sampling guide to recover a single sedimentary sequence from 0 to 336 m CCSF-A with gaps between 222 and 250 m CCSF-A, although it is advisable to overlap a few decimeters from different holes when sampling to accommodate anticipated ongoing development of the depth scale. Stretching and compression of sedimentary features in aligned cores indicates distortion of the cored sequence. Because much of the distortion occurs within individual cores on depth scales of <9 m, it was not possible to align every single feature in the magnetic susceptibility, GRA, NGR, and color reflectance records. However, at crossover points along the splice (Table **T31**), care was taken to align highly identifiable features from cores in each hole.

A growth factor of 1.16 is calculated by linear regression for all holes at Site U1334, indicating a 16% increase in CCSF-A relative to CSF depth (Fig. **F35**). We used this value to calculate the CCSF-B depth (see **"Corrected core composite depth scale"** in the "Methods" chapter) presented in Table **T30** to calculate sedimentation rates and aid in the calculation of mass accumulation rates.

Sedimentation rates

All the principal biostratigraphic datums and a set of 61 paleomagnetic reversals (restricted to the APC-cored section of the site) are defined in Holes U1334A–U1334C (Table **T32;** see **"Biostratigraphy"** and **"Paleomagnetism"**) and were used in establishing age control (Fig. **F14**). Only the paleomagnetic reversals were used to calculate the average linear sedimentation rates (LSRs) for the APC section of Site U1334 from the CCSF-B depth scale, as depicted in Figure **F14.** In XCB cores, all available biostratigraphic datums were used to calculate the average LSRs.

The LSR at Site U1334 in the nannofossil oozes and chalks of lithologic Units II and III between the basement and the lower Oligocene section are ~8 m/m.y., increase in the lower Oligocene to 24 m/m.y., and then decrease throughout the Oligocene and Miocene to 4 m/m.y. (Fig. **F14**).

Downhole measurements

Heat flow

Five APCT-3 downhole temperature measurements in Hole U1334B ranged from 2.82°C at 32.2 m to 5.09°C at 106.2 m (Table **T33**), giving a geothermal gradient of 33.0°C/km (Fig. **F36**). The bottom water temperature was 1.457°C, based on the average of the minimum temperature in the five APCT-3 temperature profiles. Thermal conductivity under in situ conditions was estimated from laboratory-determined thermal conductivity using the method of Hyndman et al. (1974) (see **"Physical properties"** in the "Methods" chapter). The calculated in situ values are up to 2.2% below the measured laboratory values. Thermal resistance was then calculated by cumulatively adding the inverse of the in situ thermal conductivity values over depth intervals downhole (Fig. **F36**). A heat flow of 31.6 mW/m^2 was obtained from the linear fit between temperature and thermal resistance (Fig. **F36**) (Pribnow et al., 2000), which is an intermediate value compared to nearby sites in the global heatflow database.

References

Adkins, J.F., and Schrag, D.P., 2003. Reconstructing Last Glacial Maximum bottom water salinities from deep-sea sediment pore fluid profiles. *Earth Planet Sci. Lett.,* 216:109–123. **doi:10.1016/S0012-821X(03)00502-8**

Amante, C., and Eakins, B.W., 2008. *ETOPO1 1 Arc-Minute Global Relief Model: Procedures, Data Sources and Analysis:* Washington, DC (DOC/NOAA/NESDIS/NGDC).

Barron, J.A., 1985. Late Eocene to Holocene diatom biostratigraphy of the equatorial Pacific Ocean, Deep Sea Drilling Project Leg 85. *In* Mayer, L., Theyer, F., Thomas, E., et al., *Init. Repts. DSDP,* 85: Washington, DC (U.S. Govt. Printing Office), 413–456. **doi:10.2973/dsdp.proc.85.108.1985**

Barron, J.A. 2006. Diatom biochronology for the early Miocene of the equatorial Pacific. *Stratigraphy,* 2(4):281–30.

Barron, J.A., Fourtanier, E., and Bohaty, S.M., 2004. Oligocene and earliest Miocene diatom biostratigraphy of ODP Leg 199 Site 1220, equatorial Pacific. *In* Wilson, P.A., Lyle, M., Janecek, T.R., and Firth, J.V. (Eds.), *Proc. ODP, Sci. Results,* 199: College Station (Ocean Drilling Program), 1–25. **doi:10.2973/odp.proc.sr.199.204.2004**

Berggren, W.A., Kent, D.V., Swisher, C.C., III, and Aubry, M.-P., 1995. A revised Cenozoic geochronology and chronostratigraphy. *In* Berggren, W.A., Kent, D.V., Aubry, M.-P., and Hardenbol, J. (Eds.), *Geochronology, Time Scales and Global Stratigraphic Correlation.* Spec. Publ.—SEPM (Soc. Sediment. Geol.), 54:129–212.

Blaj, T., Backman, J., and Raffi, I., 2009. Late Eocene to Oligocene preservation history and biochronology of calcareous nannofossils from paleo-equatorial Pacific Ocean sediments. *Rivista Italiana Paleontologia e Stratigrafia,* 115(1):67–84.

Bohaty, S.M., Pälike, H., Ridgwell, A., Zachos, J.C., and Lear, C.H., 2008. Timing and significance of a global deep-sea dissolution event during the Eocene–Oligocene transition. *Eos Trans. AGU,* Fall Meet. Suppl., Abstract PP41D-1487. **http://adsabs.harvard.edu/abs/2008AGUFMPP41D1487B**

Busch, W.H., Vanden Berg, M.D., and Masau, P.E., 2006. Velocity and density of Paleogene equatorial sediments: variation with sediment composition. *In* Wilson, P.A., Lyle, M., and Firth, J.V. (Eds.), *Proc. ODP, Sci. Results,* 199: College Station, TX (Ocean Drilling Program), 1–31. **doi:10.2973/odp.proc.sr.199.226.2006**

Coxall, H.K., Huber, B.T., and Pearson, P.N., 2003. Origin and morphology of the Eocene planktonic foraminifer *Hantkenina.* Journal of Foraminiferal Research, 33(3):237–261. **doi:10.2113/33.3.237**

Coxall, H.K., Wilson, P.A., Pälike, H., Lear, C.H., and Backman, J., 2005. Rapid stepwise onset of Antarctic glaciation and deeper calcite compensation in the Pacific Ocean. *Nature (London, U. K.),* 433(7021):53–57. **doi:10.1038/nature03135**

DeConto, R.M., Pollard, D., Wilson, P.A., Palike, H., Lear, C.H., and Pagani, M., 2008. Thresholds for Cenozoic bipolar glaciation. *Nature (London, U. K.),* 455(7213):652–656. **doi:10.1038/nature07337**

Engebretson, D.C., Cox, A., and Gordon, R.G., 1985. *Relative Motions between Oceanic and Continental Plates in the Pacific Basin.* Spec. Pap.—Geol. Soc. Am., 206.

Hays, J.D., et al., 1972. *Init. Repts. DSDP,* 9: Washington, DC (U.S. Govt. Printing Office). **doi:10.2973/dsdp.proc.9.1972**

Hyndman, R.D., Erickson, A.J., and Von Herzen, R.P., 1974. Geothermal measurements on DSDP Leg 26. *In* Davies, T.A., Luyendyk, B.P., et al., *Init. Repts. DSDP,* 26: Washington, DC (U.S. Govt. Printing Office), 451–463. **doi:10.2973/dsdp.proc.26.113.1974**

Kennett, J.P., and Shackleton, N.J., 1976. Oxygen isotopic evidence for the development of the psychrosphere 38 Myr ago. *Nature (London, U. K.),* 260(5551):513–515. **doi:10.1038/260513a0**

Knappenberger, M., 2000. Sedimentation rates and Pacific plate motion calculated using seismic cross sections of the Neogene equatorial sediment bulge [M.Sc. thesis]. Boise State Univ., Idaho.

Koppers, A.A.P., Phipps Morgan, J., Morgan, J.W., and Staudigel, H., 2001. Testing the fixed hotspot hypothesis using $^{40}Ar/^{39}Ar$ age progressions along seamount trails. *Earth Planet. Sci. Lett.,* 185(3–4):237–252. **doi:10.1016/S0012-821X(00)00387-3**

Lear, C.H., Bailey, T.R., Pearson, P.N., Coxall, H.K., and Rosenthal, Y., 2008. Cooling and ice growth across the Eocene–Oligocene transition. *Geology,* 36(3):251–254. **doi:10.1130/G24584A.1**

Liu, Z., Pagani, M., Zinniker, D., DeConto, R., Huber, M., Brinkhuis, H., Shah, S.R., Leckie, R.M., and Pearson, A., 2009. Global cooling during the Eocene–Oligocene climate transition. *Science,* 323(5918):1187–1190. **doi:10.1126/science.1166368**

Lyle, M., Liberty, L., Moore, T.C., Jr., and Rea, D.K., 2002. Development of a seismic stratigraphy for the Paleogene sedimentary section, central tropical Pacific Ocean. *In* Lyle, M., Wilson, P.A., Janecek, T.R., et al., *Proc. ODP, Init. Repts.,* 199: College Station, TX (Ocean Drilling Program), 1–21. **doi:10.2973/odp.proc.ir.199.104.2002**

Lyle, M.W., Pälike, H., Moore, T.C., Mitchell, N., and Backman, J., 2006. *Summary Report of R/V Roger Revelle Site Survey AMAT03 to the IODP Environmental Protection and Safety Panel (EPSP) in Support for Proposal IODP626:* Southampton, U.K. (Univ. Southampton). **http://eprints.soton.ac.uk/45921/**

Lyle, M., Wilson, P.A., Janecek, T.R., et al., 2002. *Proc. ODP, Init. Repts.,* 199: College Station, TX (Ocean Drilling Program). **doi:10.2973/odp.proc.ir.199.2002**

Mackensen, A., Grobe, H., Kuhn, G., and Fütterer, D.K., 1990. Benthic foraminiferal assemblages from the eastern Weddell Sea between 68° and 73°S: distribution, ecology and fossilization potential. *Mar. Micropaleontol.,* 16(3–4):241–283. **doi:10.1016/0377-8398(90)90006-8**

Mayer, L.A., Shipley, T.H., Theyer, F., Wilkens, R.H., and Winterer, E.L., 1985. Seismic modeling and paleoceanography at Deep Sea Drilling Project Site 574. *In* Mayer, L., Theyer, F., Thomas, E., et al., *Init. Repts. DSDP,* 85: Washington, DC (U.S. Govt. Printing Office), 947–970. **doi:10.2973/dsdp.proc.85.132.1985**

Miller, K.G., Wright, J.D., and Fairbanks, R.G., 1991. Unlocking the ice house: Oligocene–Miocene oxygen isotopes, eustasy, and margin erosion. *J. Geophys. Res.,* 96(B4):6829–6848. **doi:10.1029/90JB02015**

Müller, R.D., Roest, W.R., Royer, J.-Y., Gahagan, L.M., and Sclater, J.G., 1997. Digital isochrons of the world's ocean floor. *J. Geophys. Res.,* 102(B2):3211–3214. **doi:10.1029/96JB01781**

Pälike, H., Moore, T., Backman, J., Raffi, I., Lanci, L., Parés, J.M., and Janecek, T., 2005. Integrated stratigraphic correlation and improved composite depth scales for ODP Sites 1218 and 1219. *In* Wilson, P.A., Lyle, M., and Firth, J.V. (Eds.), *Proc. ODP, Sci. Results,* 199: College Station, TX (Ocean Drilling Program), 1–41. **doi:10.2973/odp.proc.sr.199.213.2005**

Pälike, H., Lyle, M.W., Ahagon, N., Raffi, I., Gamage, K., and Zarikian, C.A., 2008. Pacific equatorial age transect. *IODP Sci. Prosp.,* 320/321. **doi:10.2204/iodp.sp.320321.2008**

Pälike, H., Frazier, J., and Zachos, J.C., 2006a. Extended orbitally forced palaeoclimatic records from the equatorial Atlantic Ceara Rise. *Quat. Sci. Rev.,* 25(23–24):3138–3149. **doi:10.1016/j.quascirev.2006.02.011**

Pälike, H., Norris, R.D., Herrle, J.O., Wilson, P.A., Coxall, H.K., Lear, C.H., Shackleton, N.J., Tripati, A.K., and Wade, B.S., 2006b. The heartbeat of the Oligocene climate system. *Science,* 314(5807):1894–1898. **doi:10.1126/science.1133822**

Pearson, P.N., McMillan, I.K., Wade, B.S., Dunkley Jones, T., Coxall, H.K., Bown, P.R., and Lear, C.H., 2008. Extinction and environmental change across the Eocene–Oligocene boundary in Tanzania. *Geology,* 36(2):179–182. **doi:10.1130/G24308A.1**

Petronotis, K.E., 1991. Paleomagnetic studies of the skewness of Pacific plate marine magnetic anomalies 25–32R: implications for anomalous skewness and the motion of the Pacific plate and hotspots [Ph.D. thesis]. Northwestern Univ., Evanston, IL.

Petronotis, K.E., Gordon, R.G., and Acton, G.D., 1994. A 57 Ma Pacific plate paleomagnetic pole determined from a skewness analysis of crossings of marine magnetic anomaly 25r. *Geophys. J. Int.,* 118(3):529–554. **doi:10.1111/j.1365-246X.1994.tb03983.x**

Pribnow, D.F.C., Kinoshita, M., and Stein, C.A., 2000. *Thermal Data Collection and Heat Flow Recalculations for ODP Legs 101–180:* Hanover, Germany (Inst. Joint Geosci. Res., Inst. Geowiss. Gemeinschaftsauf. [GGA]). **http://www-odp.tamu.edu/publications/heatflow/ODPReprt.pdf**

Raffi, I., Backman, J., Fornaciari, E., Pälike, H., Rio, D., Lourens, L., and Hilgen, F., 2006. A review of calcareous nannofossil astrobiochronology encompassing the past 25 million years. *Quat. Sci. Rev.,* 25(23–24):3113–3137. **doi:10.1016/j.quascirev.2006.07.007**

Sager, W.W., and Pringle, M.S., 1988. Mid-Cretaceous to early Tertiary apparent polar wander path of the Pacific plate. *J. Geophys. Res., [Solid Earth],* 93(B10):11753–11771. **doi:10.1029/JB093iB10p11753**

Schmiedl, G., Mackensen, A., and Müller, P.J., 1997. Recent benthic foraminifera from the eastern South Atlantic Ocean: dependence on food supply and water masses. *Mar. Micropaleontol.,* 32(3–4):249–287. **doi:10.1016/S0377-8398(97)00023-6**

Shackleton, N.J., Hall, M.A., Raffi, I., Tauxe, L., and Zachos, J., 2000. Astronomical calibration age for the Oligocene–Miocene boundary. *Geology,* 28(5):447–450. **doi:10.1130/0091-7613(2000)28<447:ACAFTO>2.0.CO;2**

Shipboard Scientific Party, 2002a. Leg 199 summary. *In* Lyle, M., Wilson, P.A., Janecek, T.R., et al., *Proc. ODP, Init. Repts.,* 199: College Station, TX (Ocean Drilling Program), 1–87. **doi:10.2973/odp.proc.ir.199.101.2002**

Shipboard Scientific Party, 2002b. Site 1218. *In* Lyle, M., Wilson, P.A., Janecek, T.R., et al., *Proc. ODP, Init. Repts.,* 199: College Station, TX (Ocean Drilling Program), 1–125. **doi:10.2973/odp.proc.ir.199.111.2002**

Takata, H., and Nomura, R., 2005. Data report: Oligocene benthic foraminifers from the eastern equatorial Pacific, Sites 1218 and 1219, ODP Leg 199. *In* Wilson, P.A., Lyle, M., and Firth, J.V. (Eds.), *Proc. ODP, Sci. Results,* 199: College Station, TX (Ocean Drilling Program), 1–26. **doi:10.2973/odp.proc.sr.199.224.2005**

Thomas, E., 1985. Late Eocene to recent deep-sea benthic foraminifers from the central equatorial Pacific Ocean. *In* Mayer, L., Theyer, F., et al., *Init. Repts. DSDP,* 85: Washington (U.S. Govt. Printing Office). **doi:10.2973/dsdp.proc.85.117.1985**

van Andel, T.H., 1975. Mesozoic/Cenozoic calcite compensation depth and the global distribution of calcareous sediments. *Earth Planet. Sci. Lett.,* 26(2):187–194. **doi:10.1016/0012-821X(75)90086-2**

van Morkhoven, F.P.C.M., Berggren, W.A., and Edwards, A.S., 1986. *Cenozoic Cosmopolitan Deep-Water Benthic Foraminifera.* Bull. Cent. Rech. Explor.—Prod. Elf-Aquitaine, Mem. 11.

Wade, B.S., and Pälike, H., 2004. Oligocene climate dynamics. *Paleoceanography,* 19(4)PA4019. **doi:10.1029/2004PA001042**

Wade, B.S., and Pearson, P.N., 2008. Planktonic foraminiferal turnover, diversity fluctuations and geochemical signals across the Eocene/Oligocene boundary in Tanzania. *Mar. Micropaleontol.,* 68(3–4):244–255. **doi:10.1016/j.marmicro.2008.04.002**

Wei, W., and Wise, S.W., Jr., 1989. Paleogene calcareous nannofossil magnetobiochronology: results from South Atlantic DSDP Site 516. *Mar. Micropaleontol.,* 14(1–3):119–152. **doi:10.1016/0377-8398(89)90034-0**

Wilson, P.A., Lyle, M., and Firth, J.V. (Eds.), 2006. *Proc. ODP, Sci. Results,* 199: College Station, TX (Ocean Drilling Program). **doi:10.2973/odp.proc.sr.199.2006**

Young, J.R., 1999. Neogene. *In* Bown, P.R. (Ed.), *Calcareous Nannofossil Biostratigraphy:* Dordrecht, The Netherlands (Kluwer Academic Publ.), 225–265.

Zachos, J.C., Quinn, T.M., and Salamy, K.A., 1996. High-resolution (10^4 years) deep-sea foraminiferal stable isotope records of the Eocene–Oligocene climate transition. *Paleoceanography,* 11(3):251–266. **doi:10.1029/96PA00571**

Zachos, J.C., Shackleton, N.J., Revenaugh, J.S., Pälike, H., and Flower, B.P., 2001. Climate response to orbital forcing across the Oligocene–Miocene boundary. *Science,* 292(5515):274–278. **doi:10.1126/science.1058288**

Publication: 30 October 2010
MS 320321-106

Figure F1. A. ETOPO1 (Amante and Eakins, 2008) bathymetric overview map of Site U1334 and PEAT drilling locations, with previous ODP and DSDP sites. **B.** Swath map bathymetry for Site U1334 region from the AMAT-03 site survey. Black labels = seismic shotpoints, white labels = bathymetric contours. White line = survey Line 1, purple line = survey Line 6. F.Z. = fracture zone.

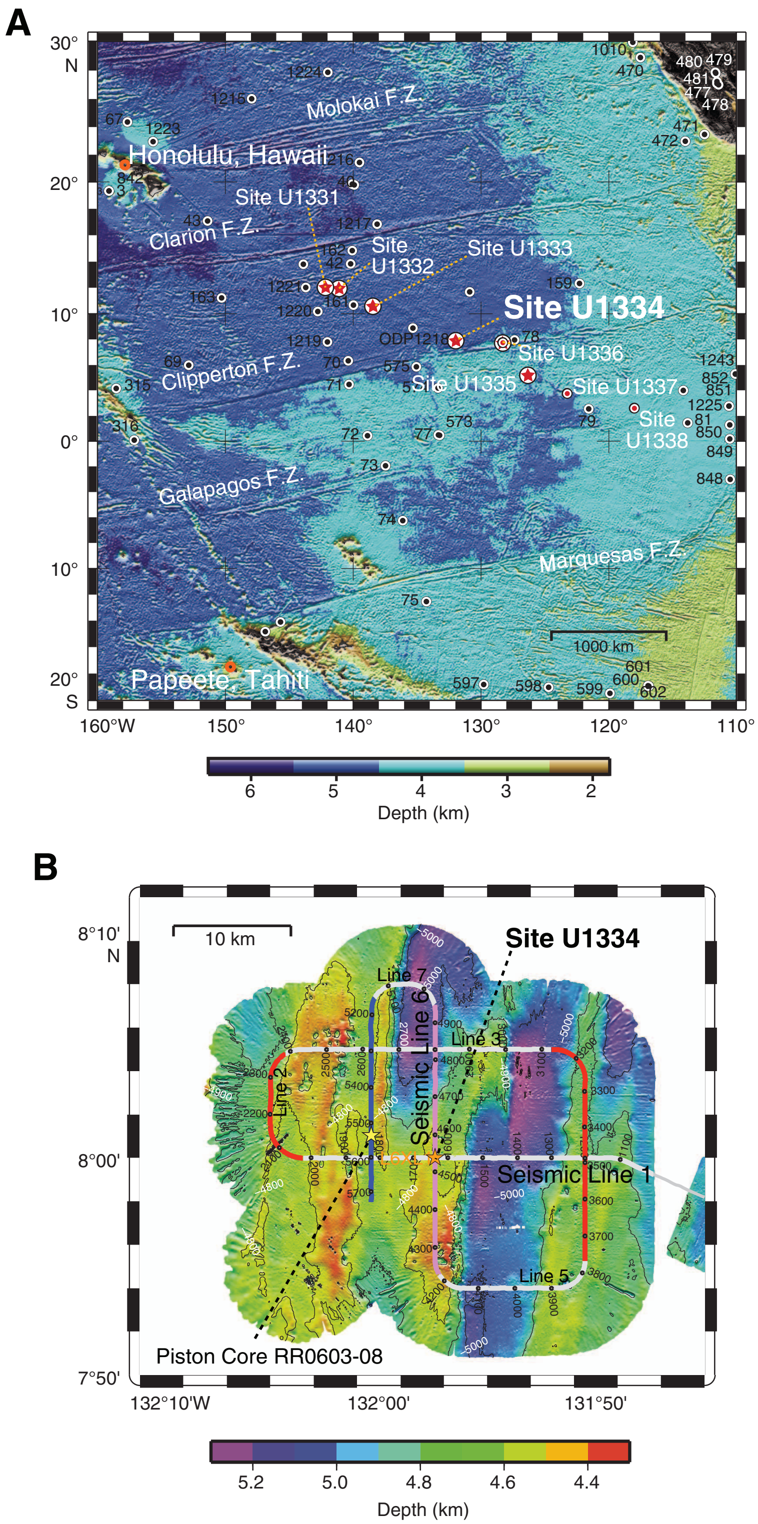

Figure F2. Seismic reflection profile PEAT-4C (Site U1334) Line 1 from the 48-channel seismic reflection survey, annotated in shotpoints (Lyle et al., 2006). Data are filtered, stacked, and migrated. Site was located where basal reflections appeared less strong to minimize possible cherts. Tentative conversion from two-way traveltime to depth uses velocity model of Busch et al. (2006). All times are Universal Time Coordinated (UTC). TD = total depth.

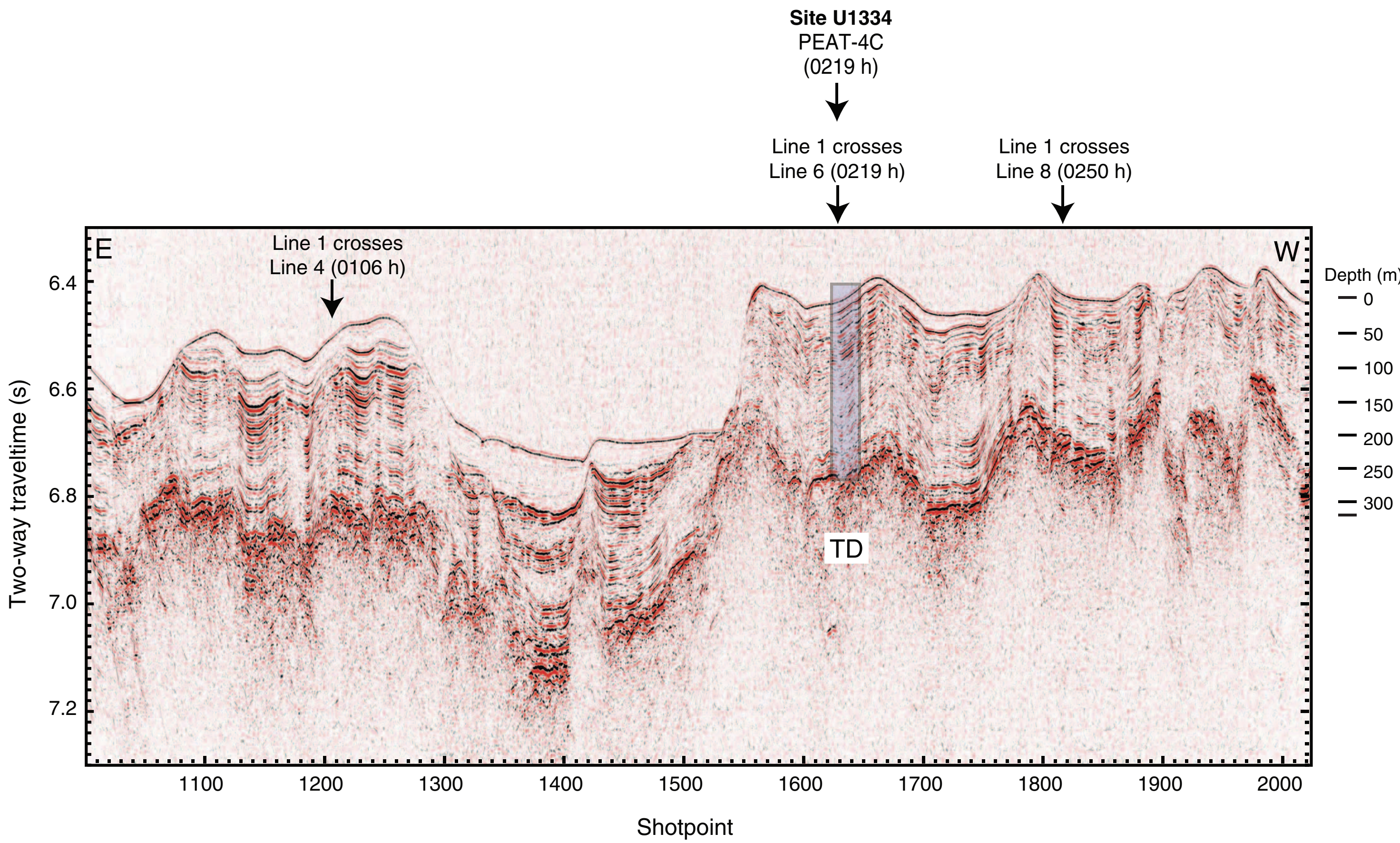

Figure F3. Correlation of Eocene/Oligocene (E/O) boundary from Pearson et al. (2008) with Site 1218 data (Coxall et al., 2005; Pälike et al., 2006b) and astronomical parameters. Amplitude min = 1.2 m.y. orbital amplitude minimum and 400 k.y. eccentricity minimum (green bar). MAR = mass accumulation rate, ETP = Eccentricity-Tilt-Precession mix.

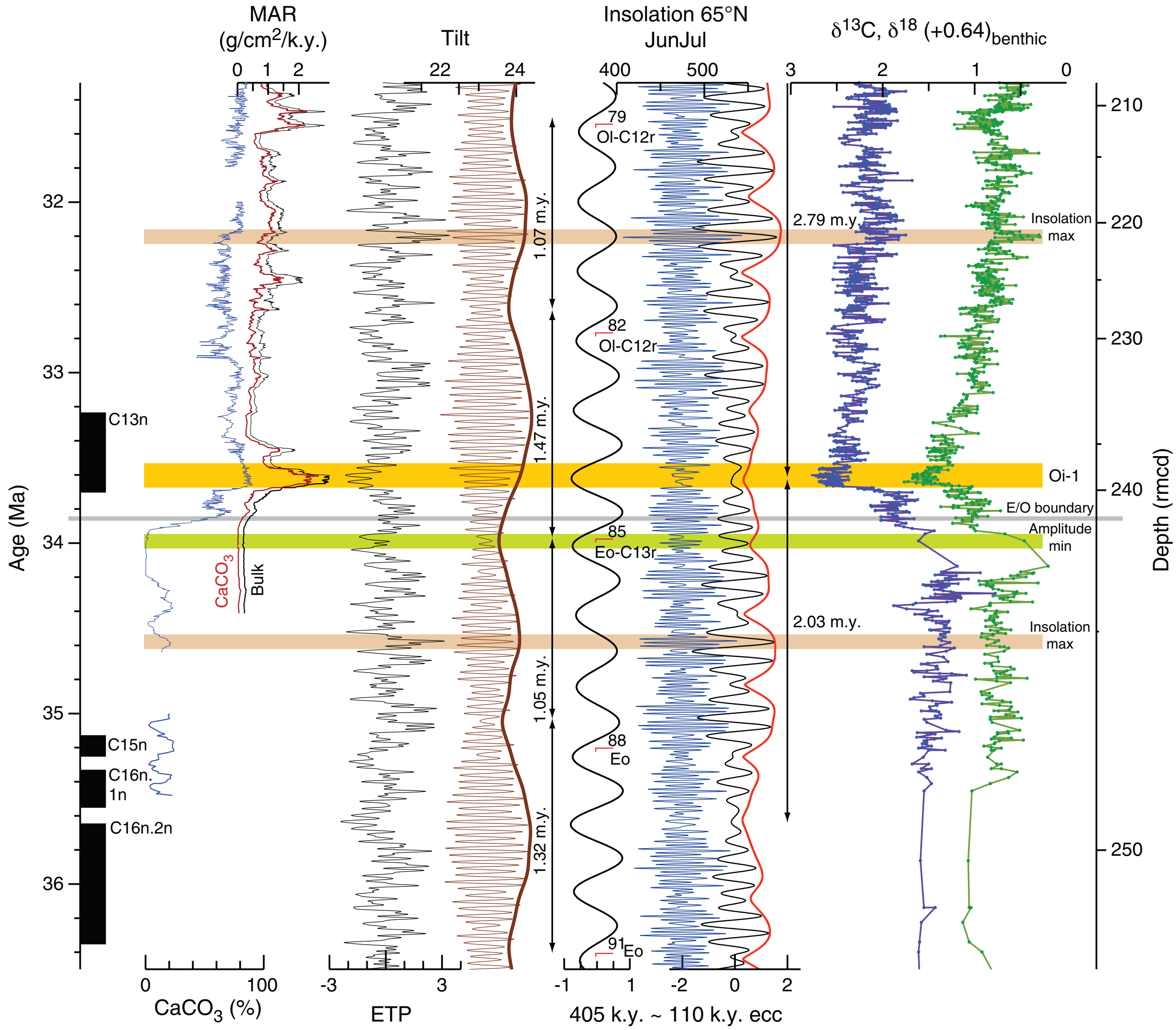

Figure F4. Site U1334 summary. At Site U1334, planktonic foraminifer Zones O2, O3, and O6 are informally divided into an upper and lower part using the base of *Paragloborotalia opima* and top of *Subbotina angiporoides* and the base of *Paragloborotalia pseudokugleri,* respectively.

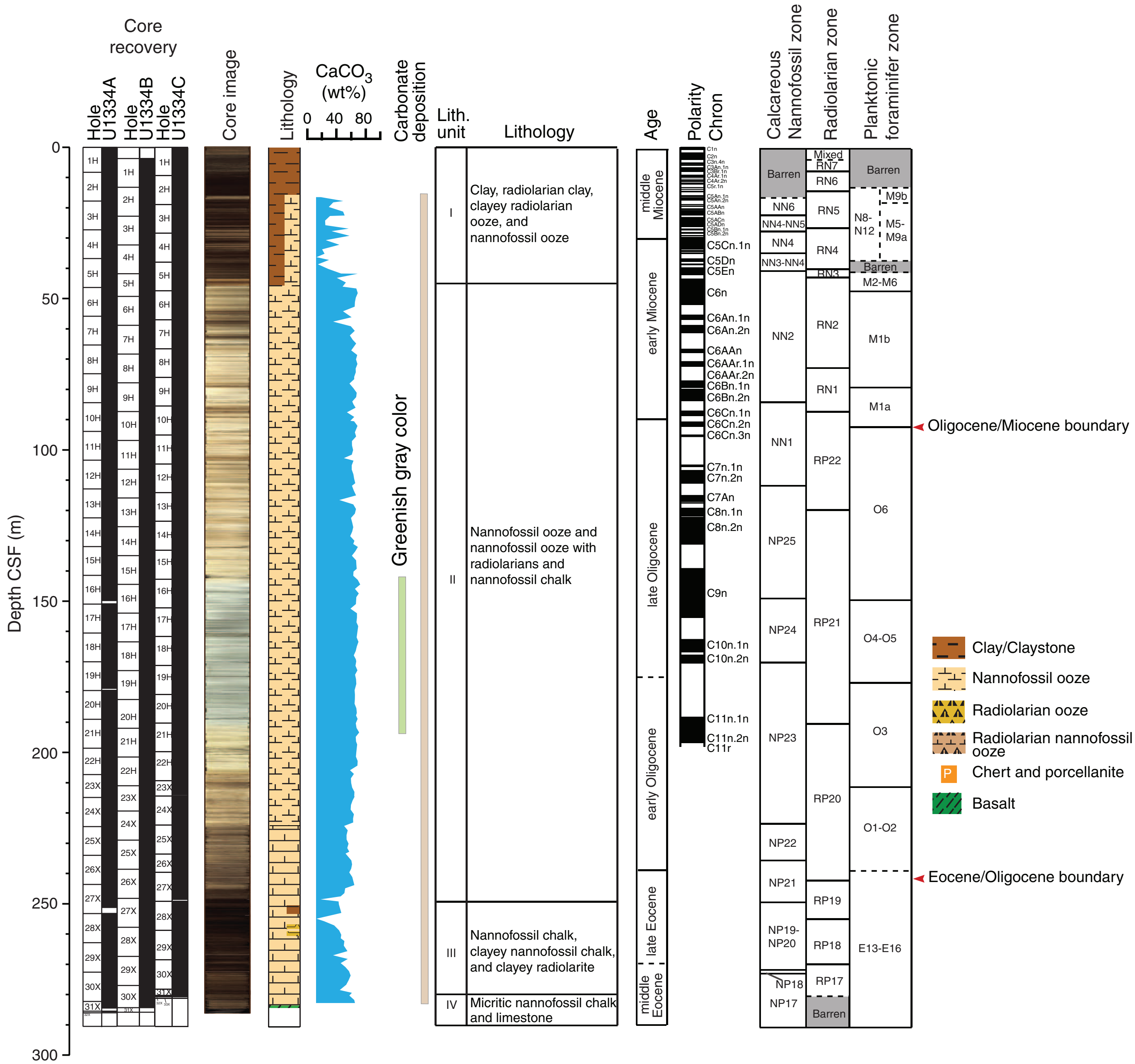

Figure F5. Lithologic summary, Site U1334. L*, b* = reflectance value of sediment as defined in the LAB color model.

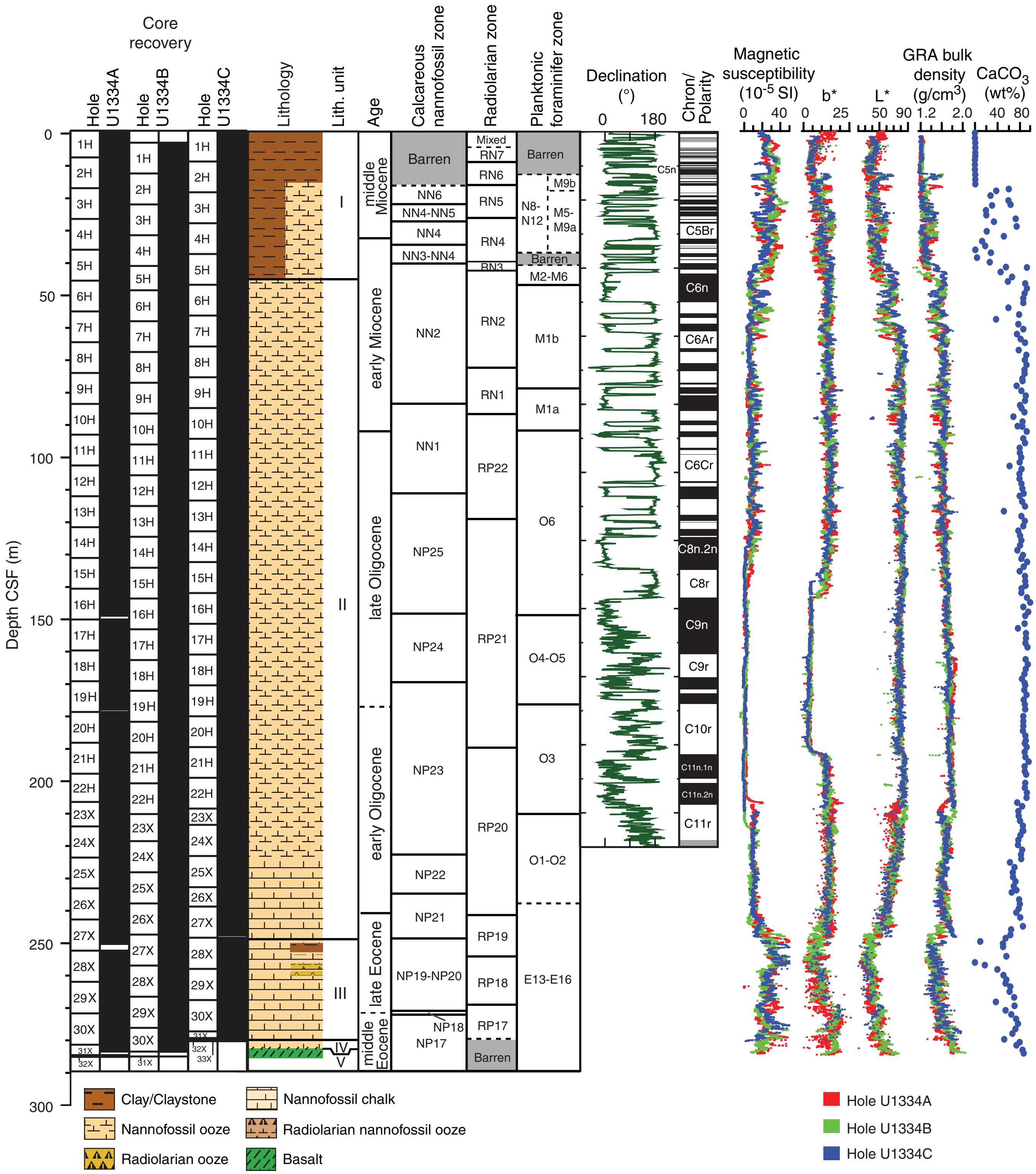

Figure F6. Calcium carbonate ($CaCO_3$), total carbon (TC), inorganic carbon (IC), and total organic carbon (TOC) determined by normal and acidification methods in sediments from Hole U1334A. (See **"Lithostratigraphy"** for information on unit boundaries.)

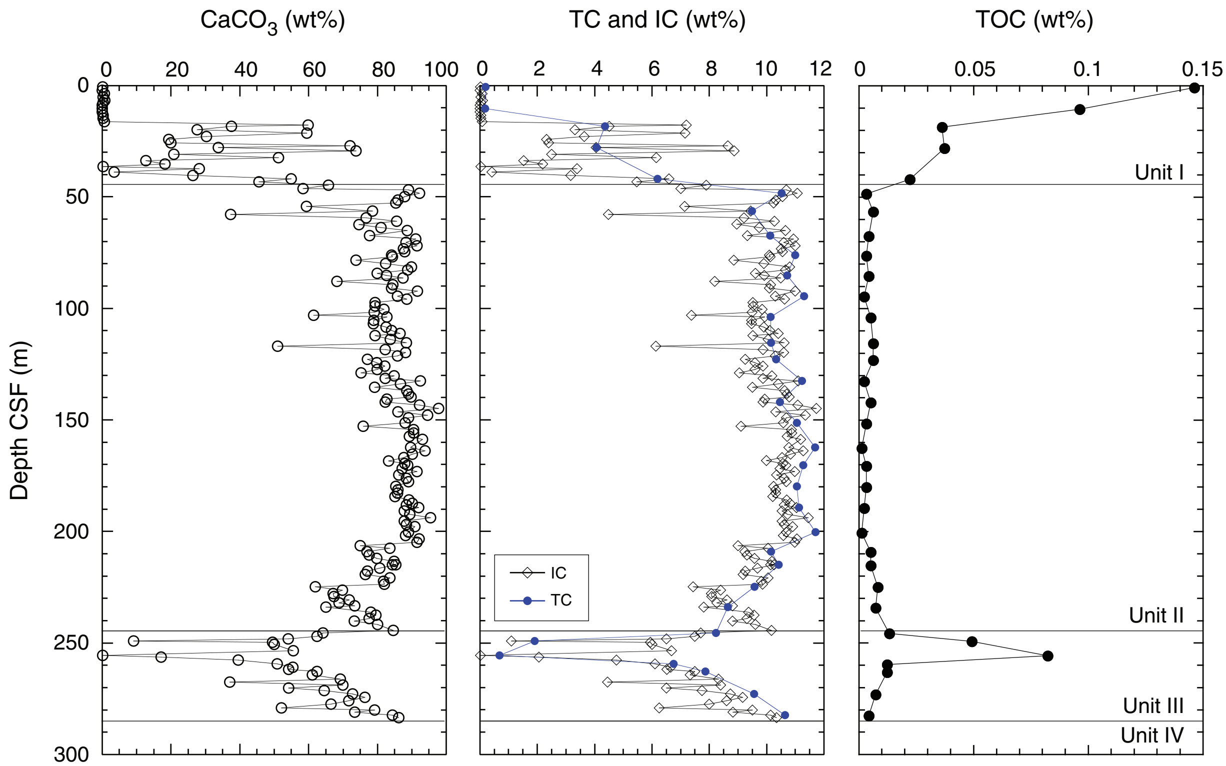

Figure F7. Color reflectance and magnetic susceptibility, Hole U1334A. Line scan images from Cores 320-U1334A-15H through 16H and 21H through 23X highlight observed color changes. L*, a*, b* = reflectance value of sediment as defined in the LAB color model.

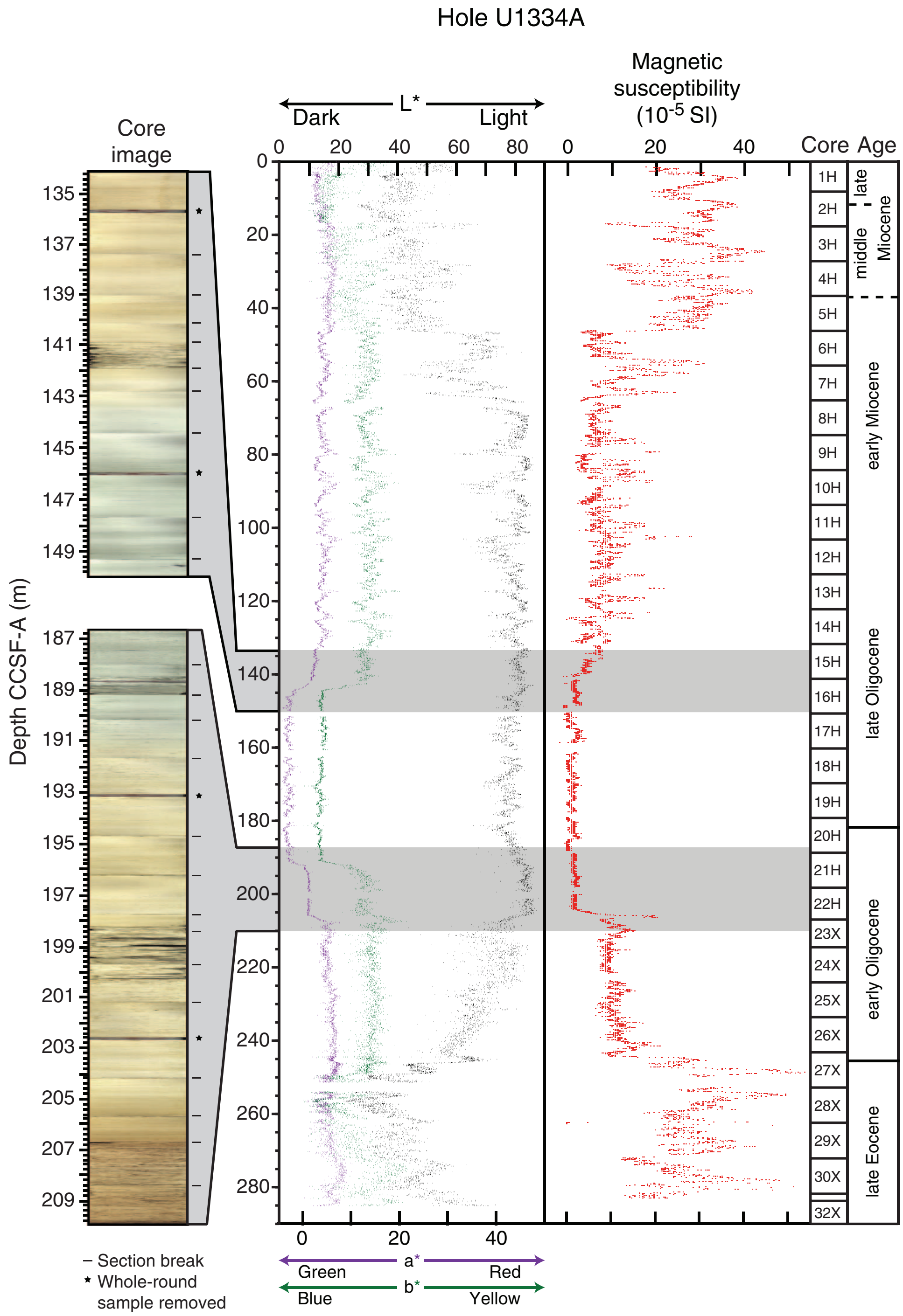

Figure F8. Subtle color variations in Sections 320-U1334B-8H-3 through 8H-5 and 11H-2 and 11H-3. Pie charts show the compositions of sediments based on smear slide descriptions.

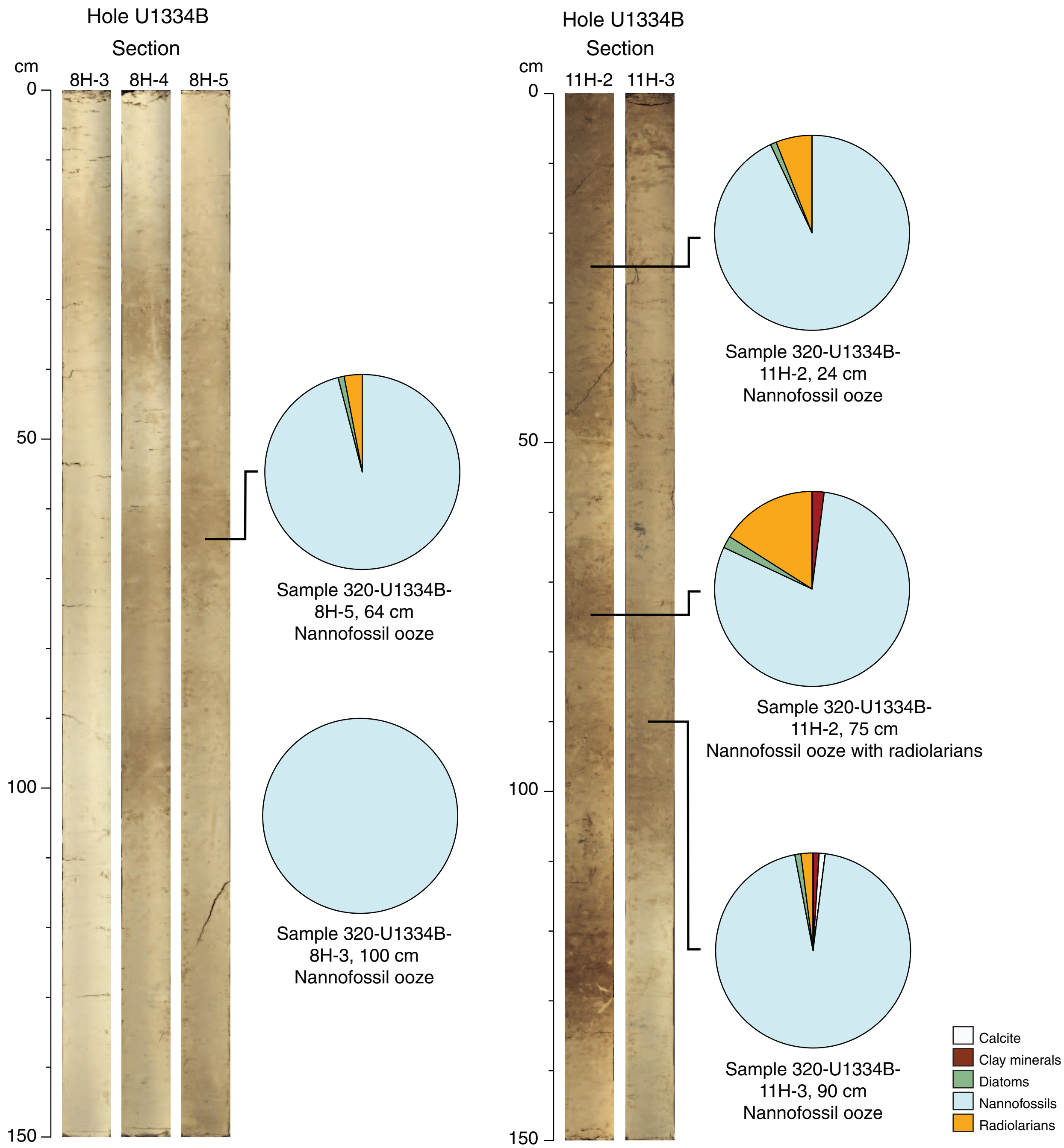

Figure F9. Line scan images of Oligocene–Miocene transition. **A.** Hole U1334A. **B.** Hole U1334B. **C.** Hole U1334C. L* = reflectance value of sediment as defined in the LAB color model. FO = first occurrence, LO = last occurrence.

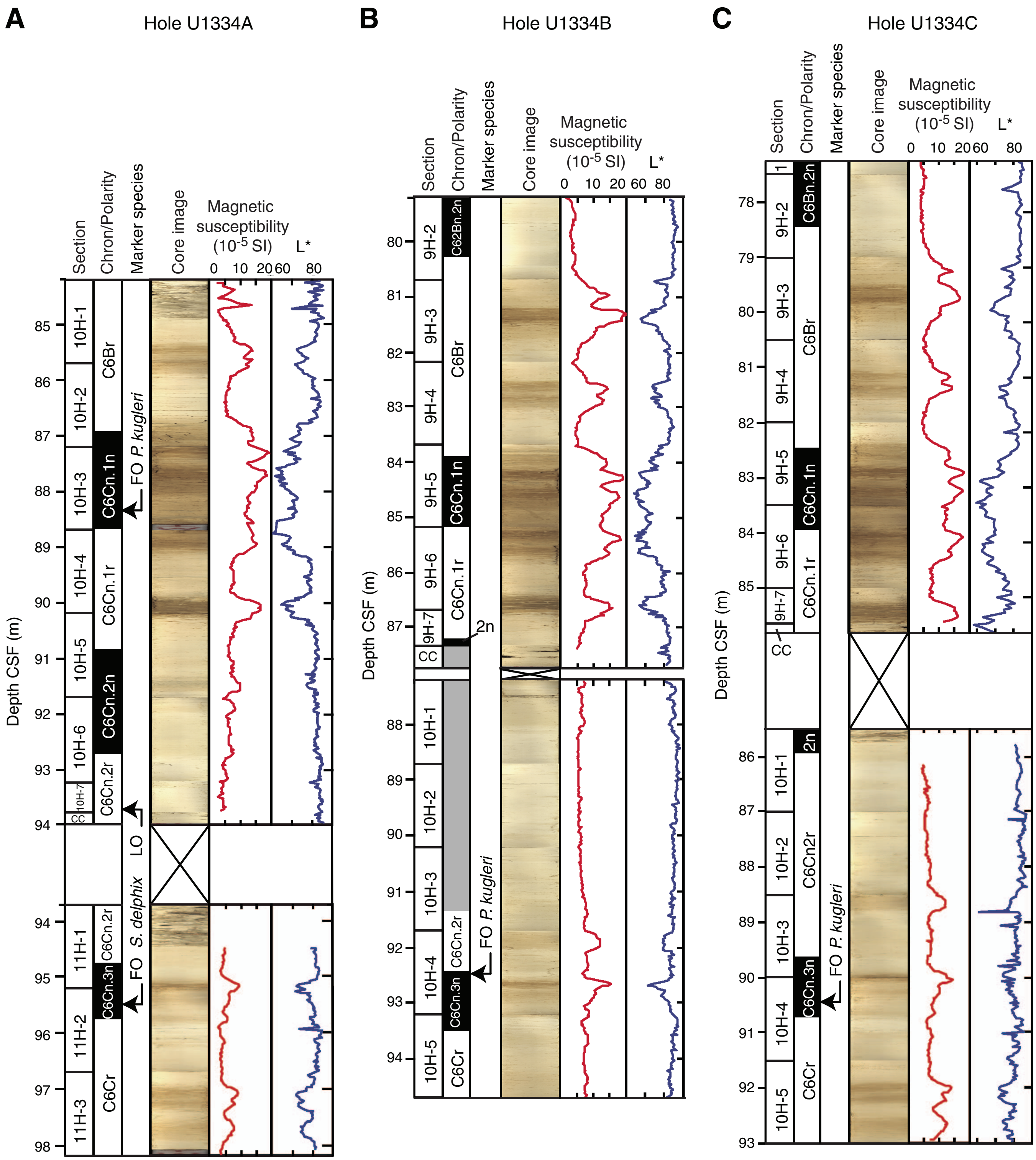

Figure F10. Line scan images of Eocene–Oligocene transition. **A.** Hole U1334A. **B.** Hole U1334B. **C.** Hole U1334C. Images were manipulated by applying a shadow-highlight adjustment to the whole image for better visual inspection of the darker strata. Nonmanipulated images are shown in Figure F12. L* = reflectance value of sediment as defined in the LAB color model.

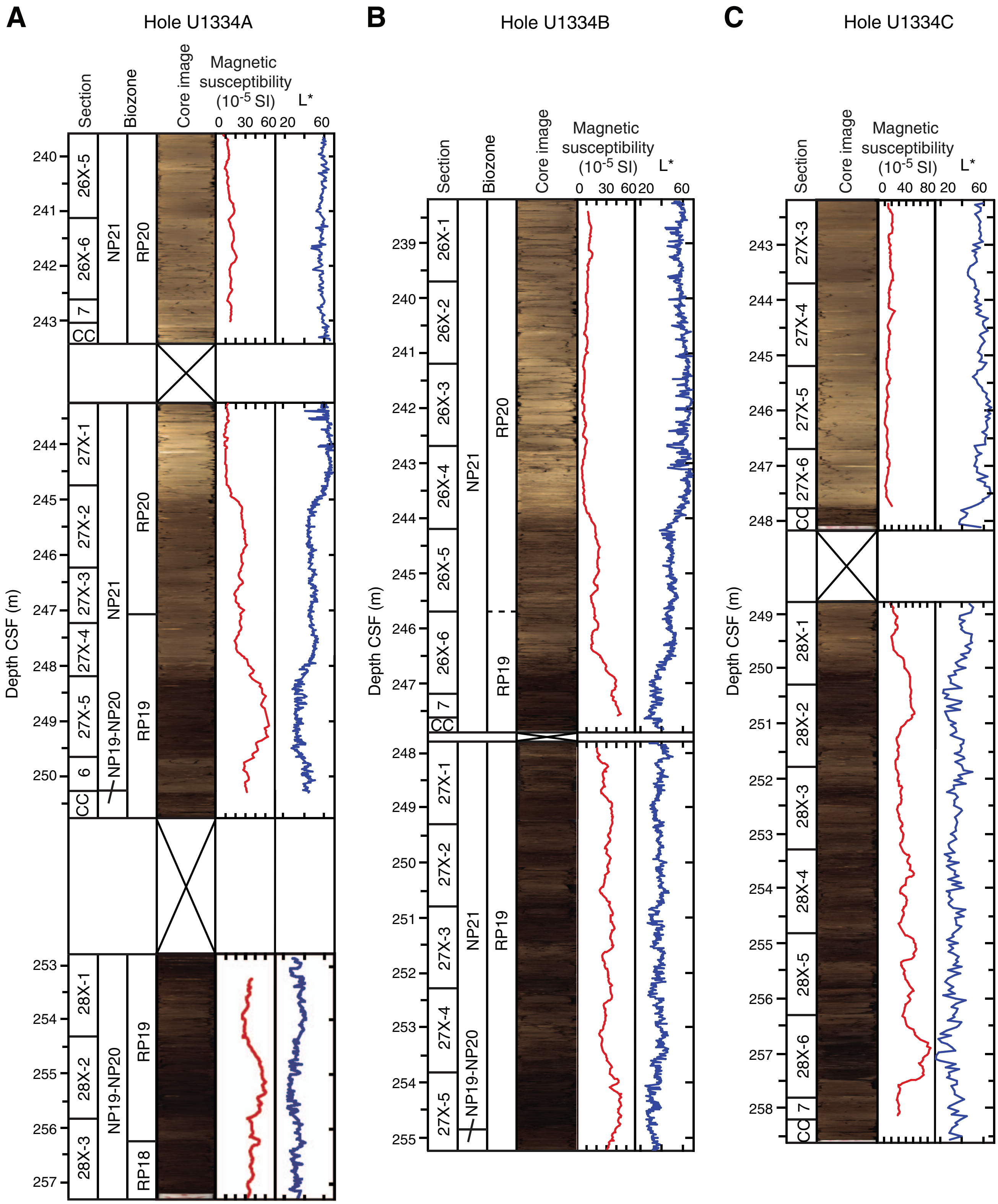

Figure F11. Photomicrographs of smear slides taken across the Eocene–Oligocene transition, Site U1334. Panels are arranged in stratigraphic order (increasing age top to bottom). See "**Site U1334 smear slides**" in "Core descriptions" for full descriptions. Left image = plane-polarized light, right image = cross-polarized light. **A.** Nannofossil ooze (Sample 320-U1334B-26X-5, 41 cm). **B.** Clayey nannofossil ooze with radiolarians (Sample 320-U1334B-26X-6, 141 cm). **C.** Nannofossil ooze with clay (Sample 320-U1334B-27X-4, 26 cm). **D.** Radiolarian claystone (Sample 320-U1334B-27X-5, 77 cm).

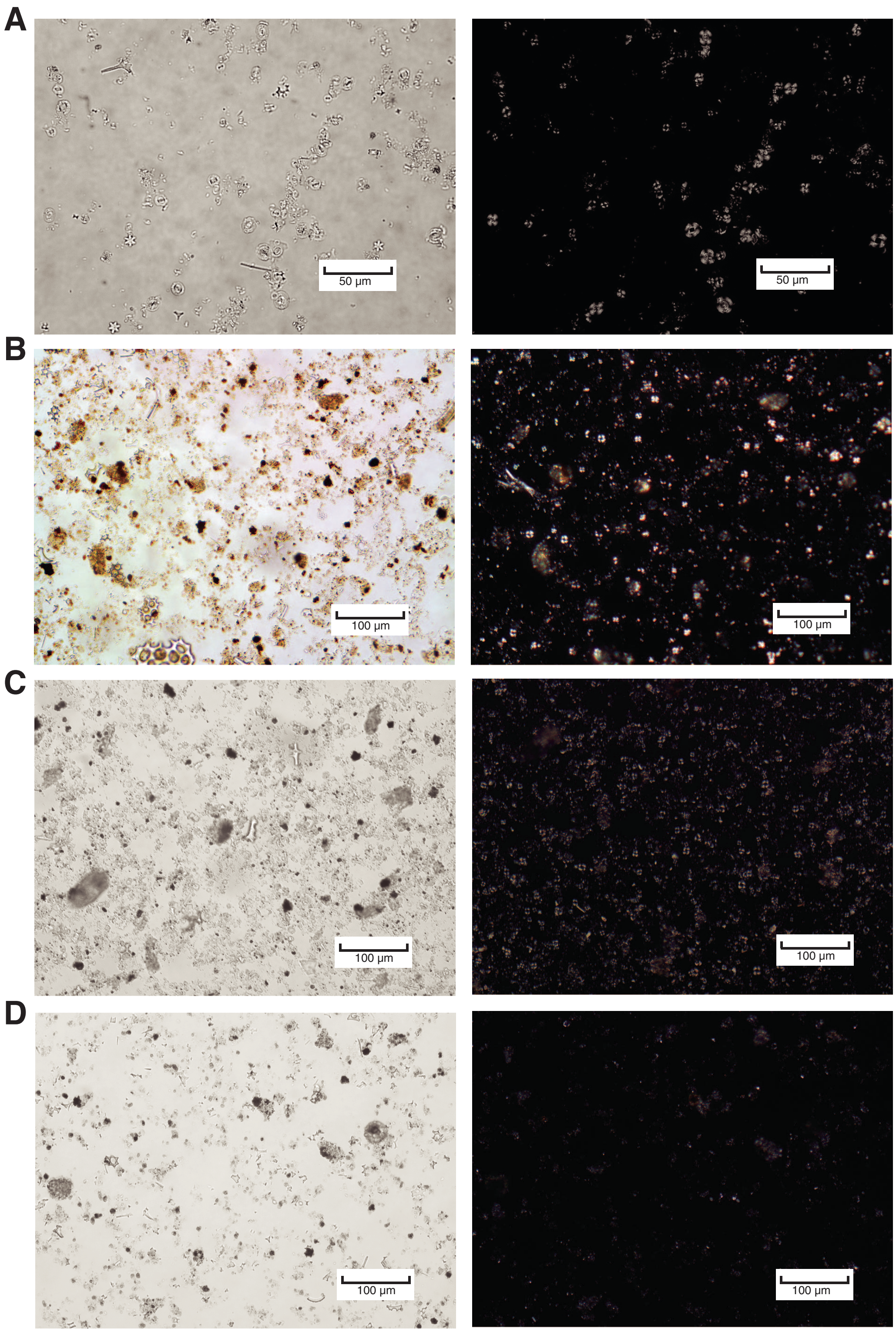

Figure F12. Line scan images of Eocene–Oligocene transition. Images are not adjusted to allow for direct comparison between the two sites. **A.** Hole U1334A. **B.** Hole U1334B. L* = reflectance value of sediment as defined in the LAB color model.

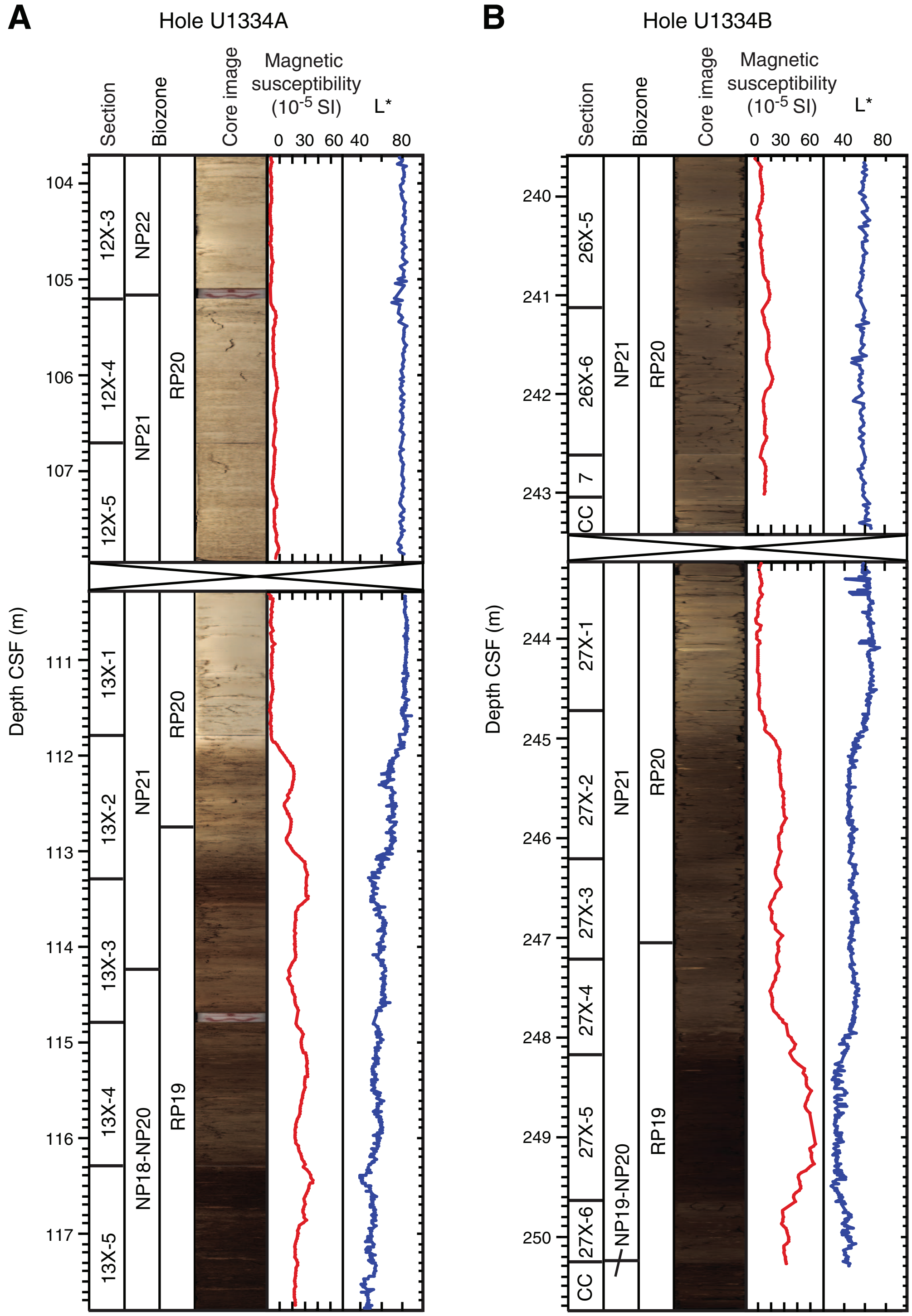

Figure F13. Integrated calcareous and siliceous microfossil biozonation, Site U1334. Calcareous microfossil zonation was limited by the presence of extensive barren intervals; dashed zonal boundaries indicate stratigraphic extent of calcareous microfossil assemblages consistent with a particular zonal assignment.

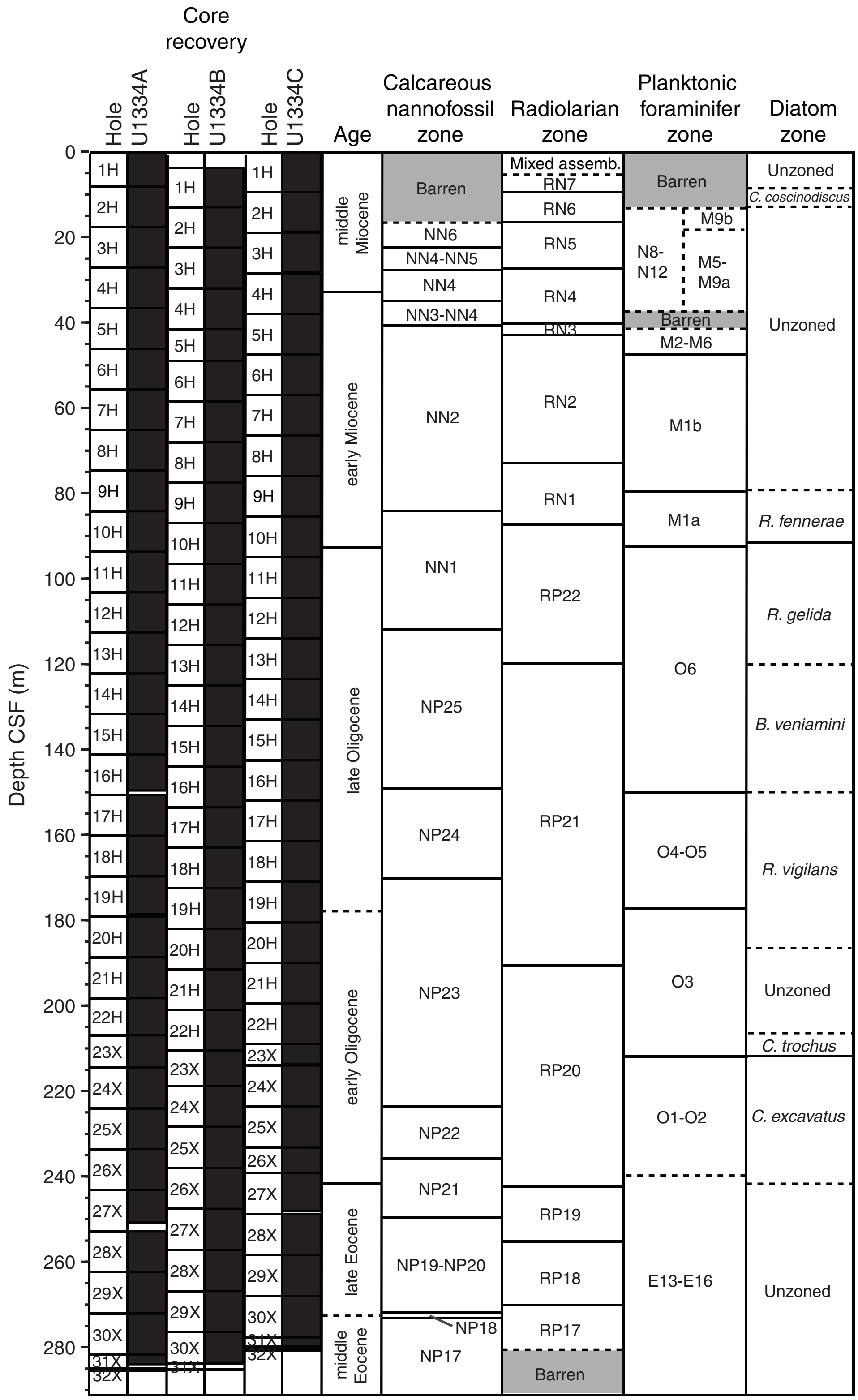

Figure F14. Linear sedimentation rates and chronostratigraphic markers, Site U1334.

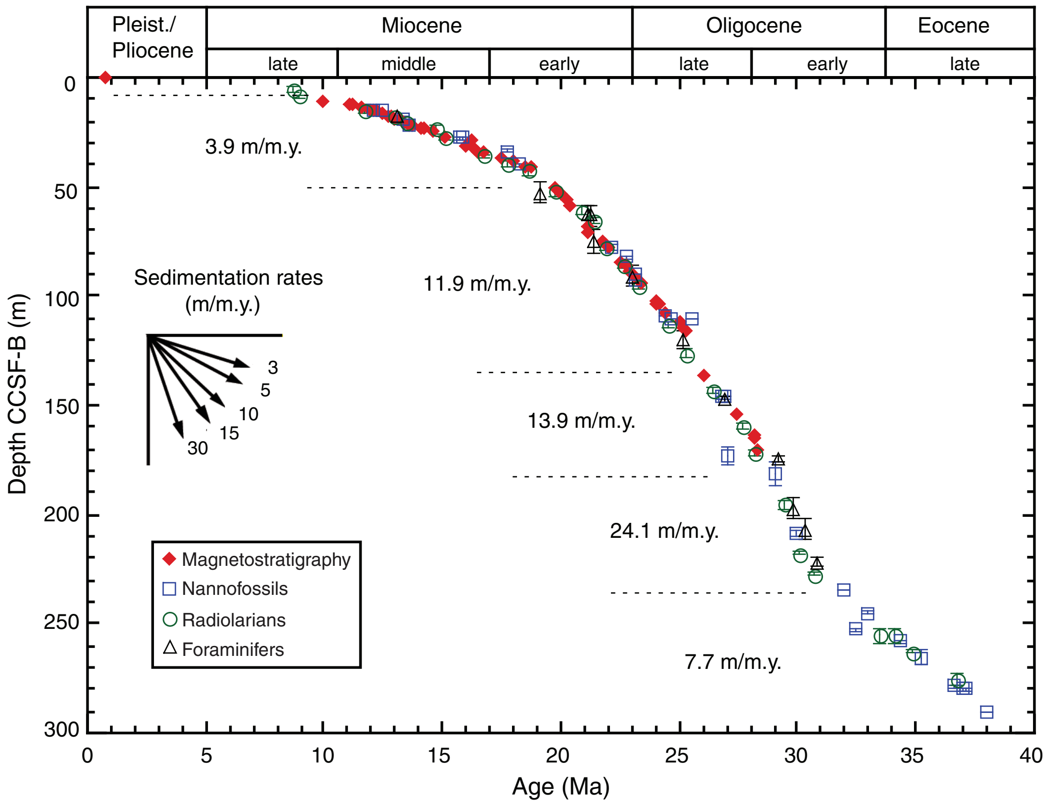

Figure F15. Stratigraphic distributions of abundance of *Nuttallides umbonifer* and *Cibicidoides mundulus* during the Oligocene. **A.** Site U1334. **B.** Site U1333. **C.** Site U1332.

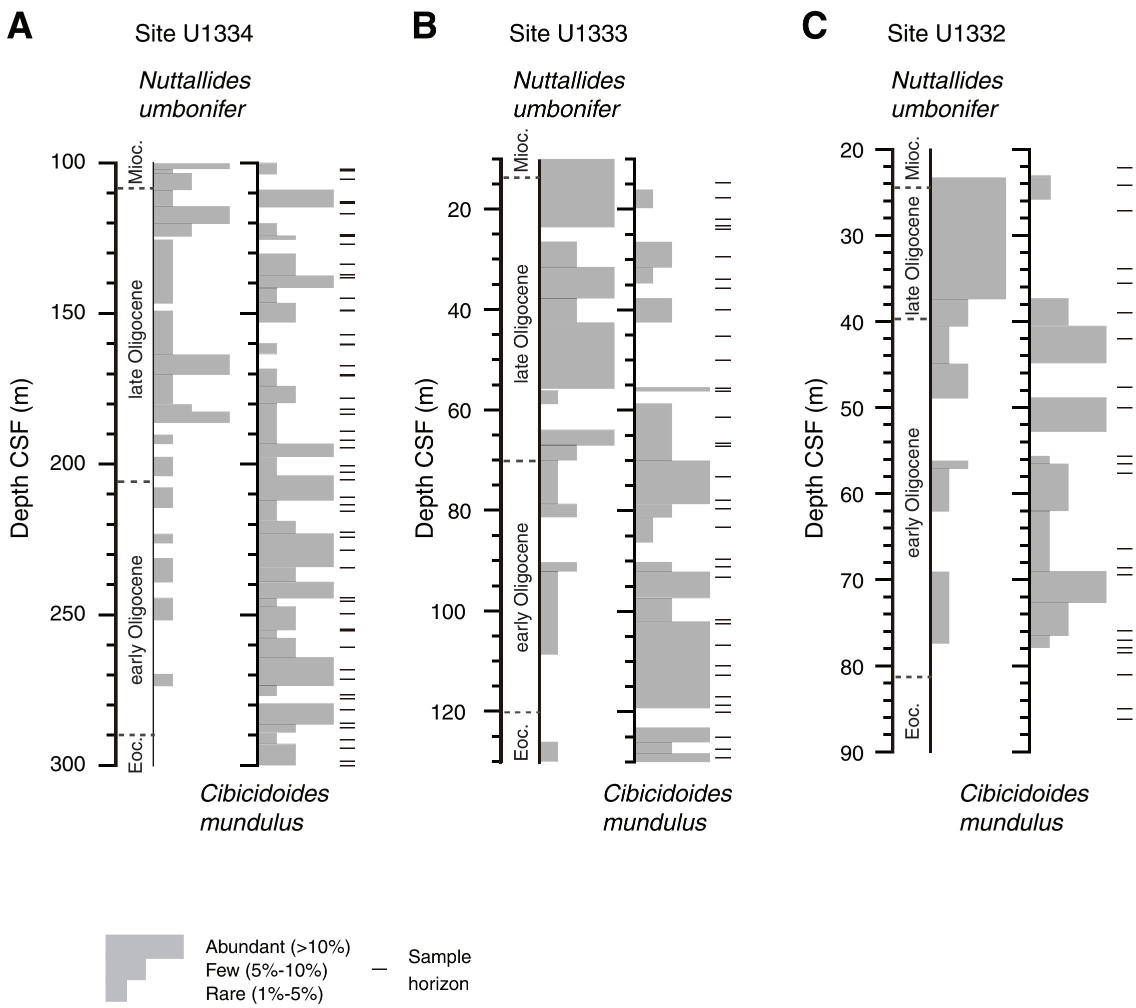

Figure F16. Summary of magnetic susceptibility and paleomagnetic results, Hole U1334A. Susceptibility measurements were on whole cores. ChRM directions for discrete samples were estimated using principal component analysis (PCA).

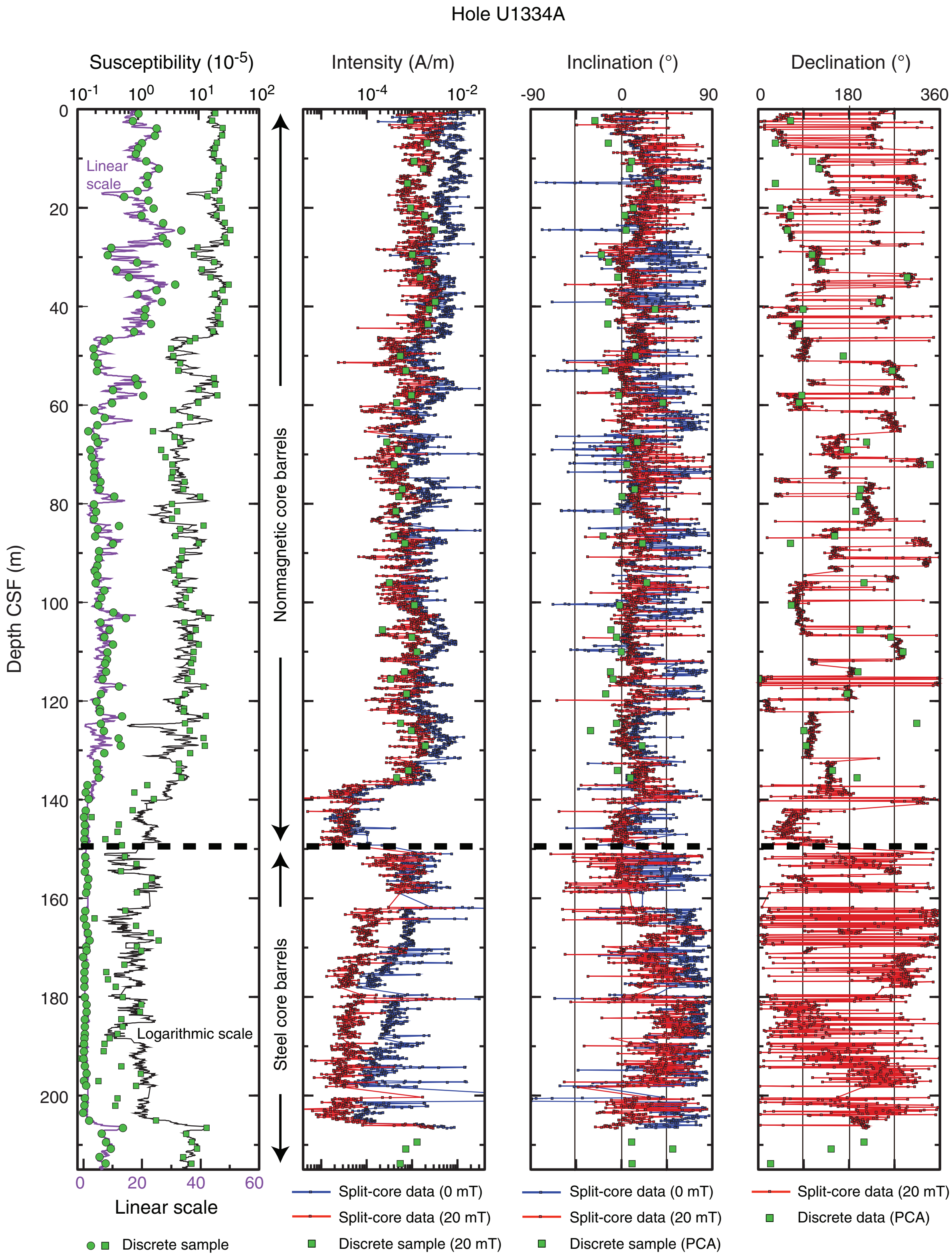

Figure F17. Summary of magnetic susceptibility and paleomagnetic results, Hole U1334B. Susceptibility measurements were on whole cores. ChRM directions for discrete samples were estimated using principal component analysis.

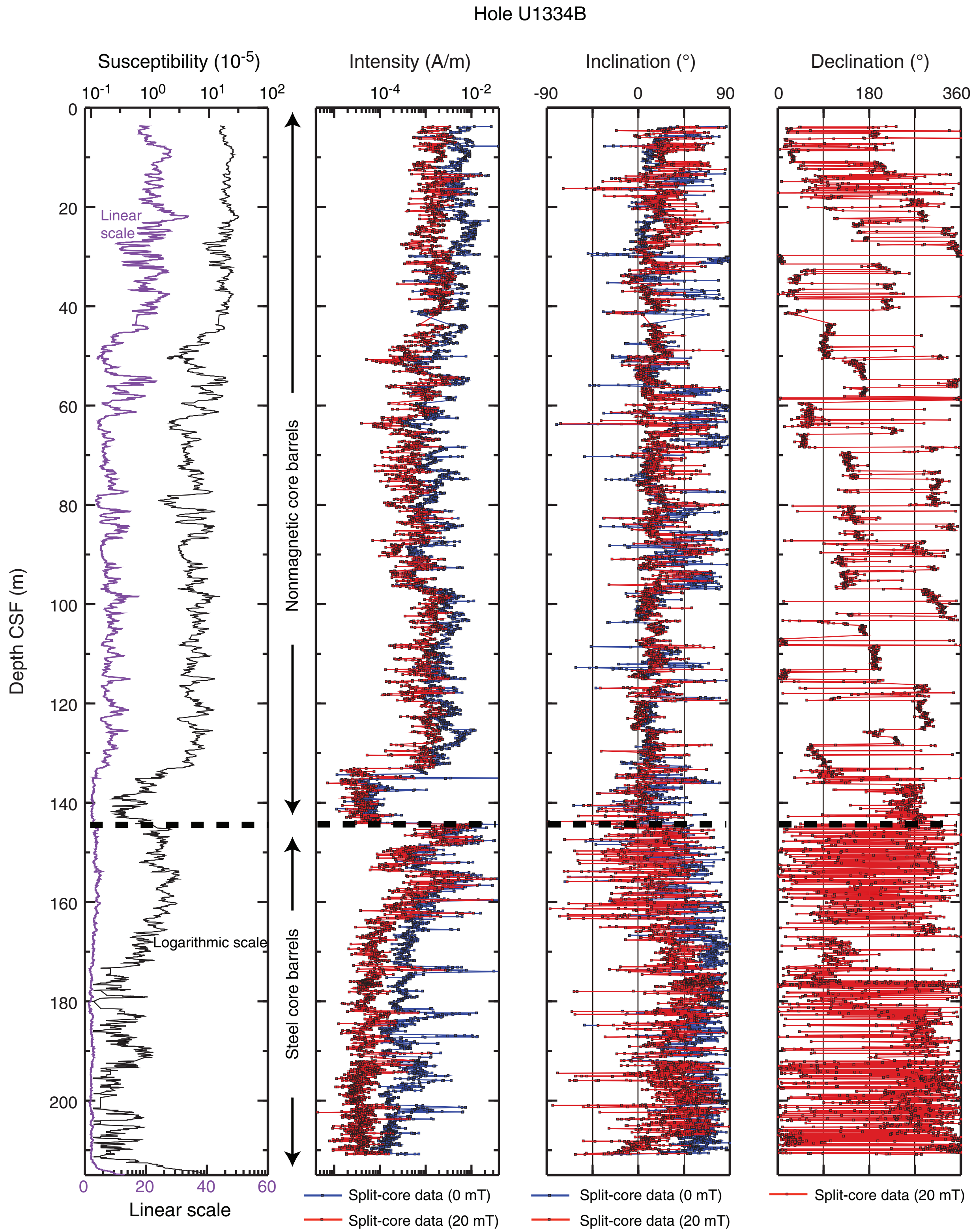

Figure F18. Summary of magnetic susceptibility and paleomagnetic results, Hole U1334C. Susceptibility measurements were on whole cores. ChRM directions for discrete samples were estimated using principal component analysis.

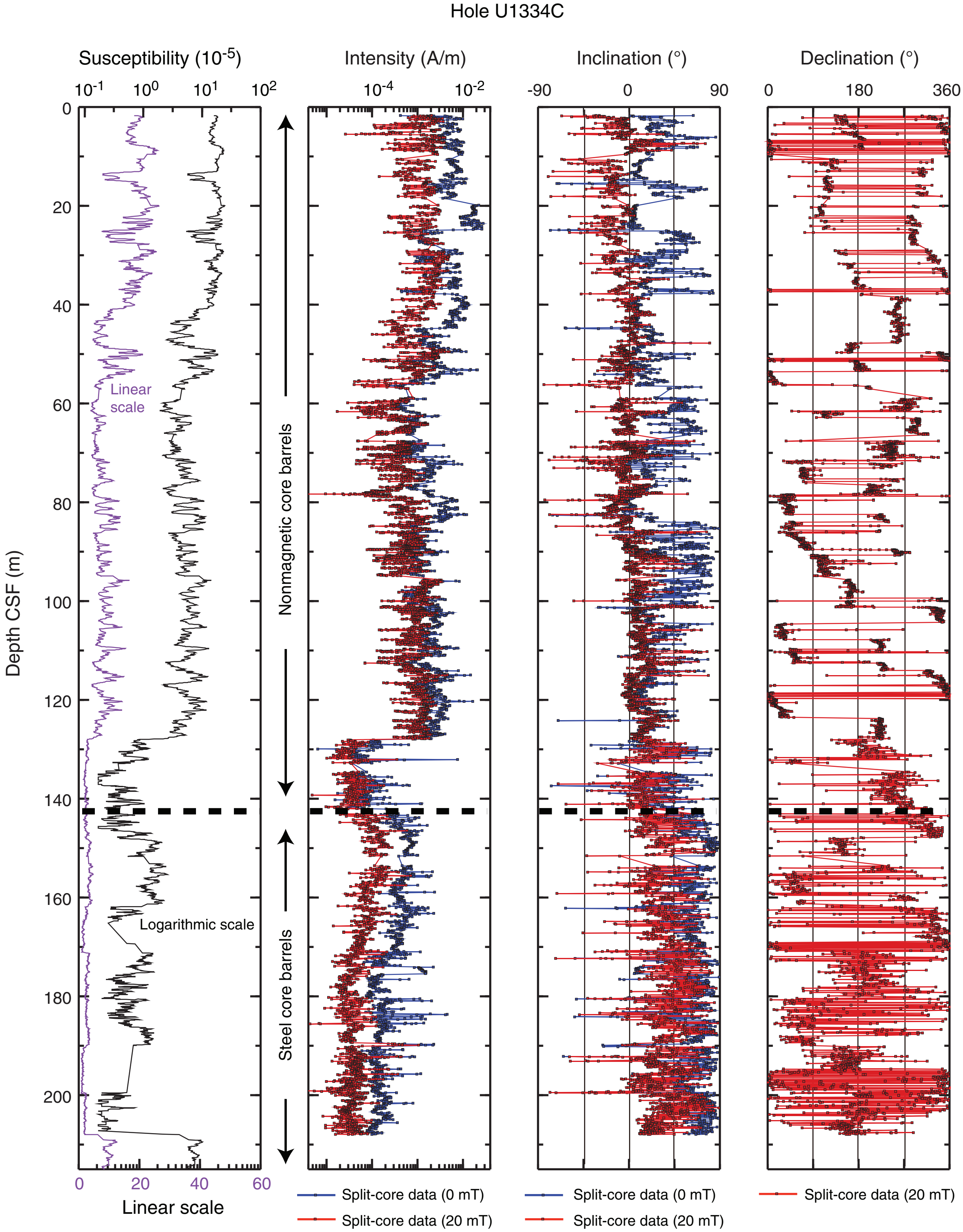

Figure F19. Latitude of the virtual geomagnetic pole (VGP), as determined from paleomagnetic directions, Hole U1334B. * = locations of possible geomagnetic excursions. North latitudes = normal polarity, south latitudes = reversed polarity. Those intervals of indeterminate polarity are shaded gray. **A.** 0–30 m CSF. (**Continued on next two pages.**)

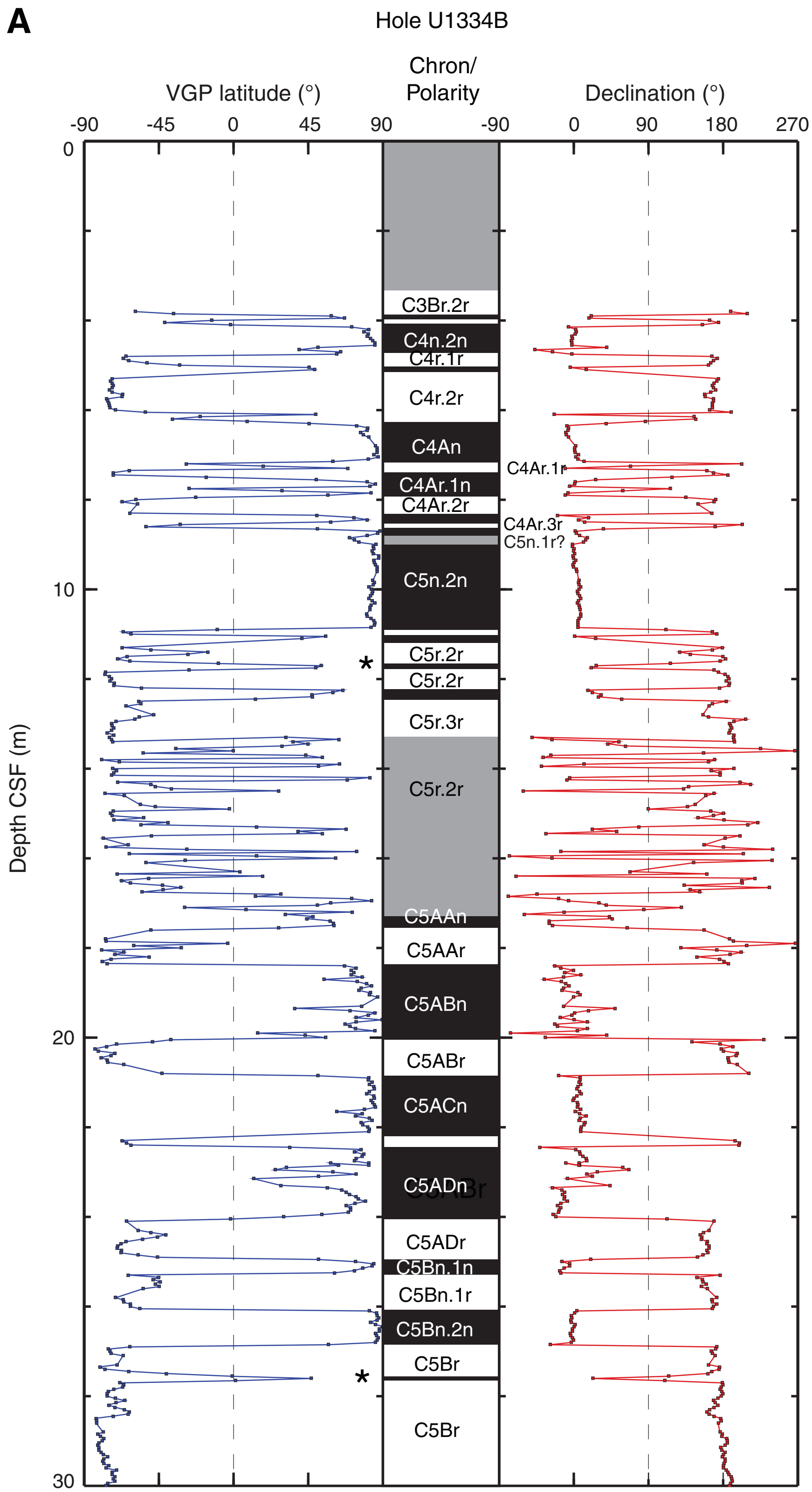

Figure F19 (continued). **B.** 25–105 m CSF. (**Continued on next page.**)

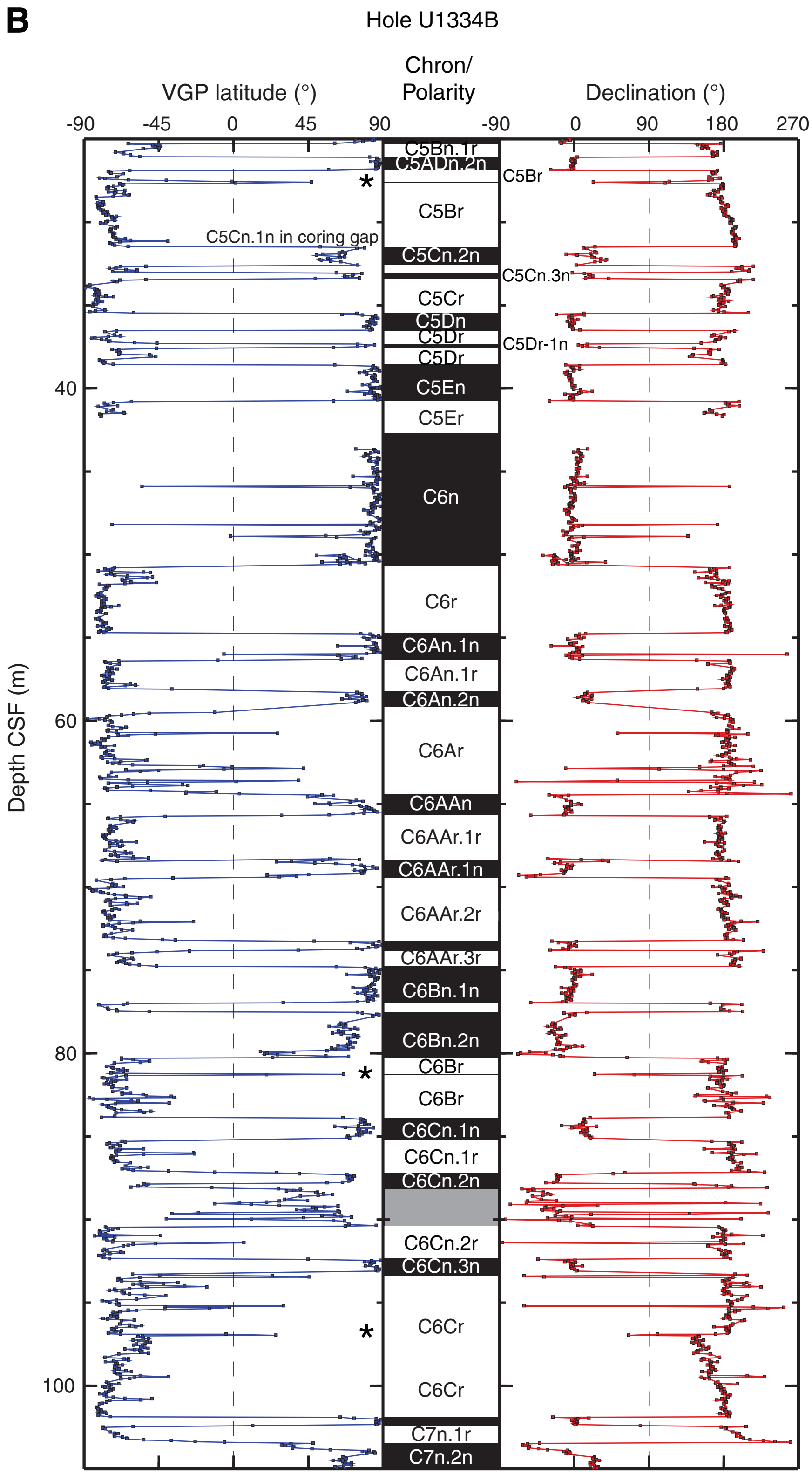

Figure F19 (continued). C. 100–215 m CSF.

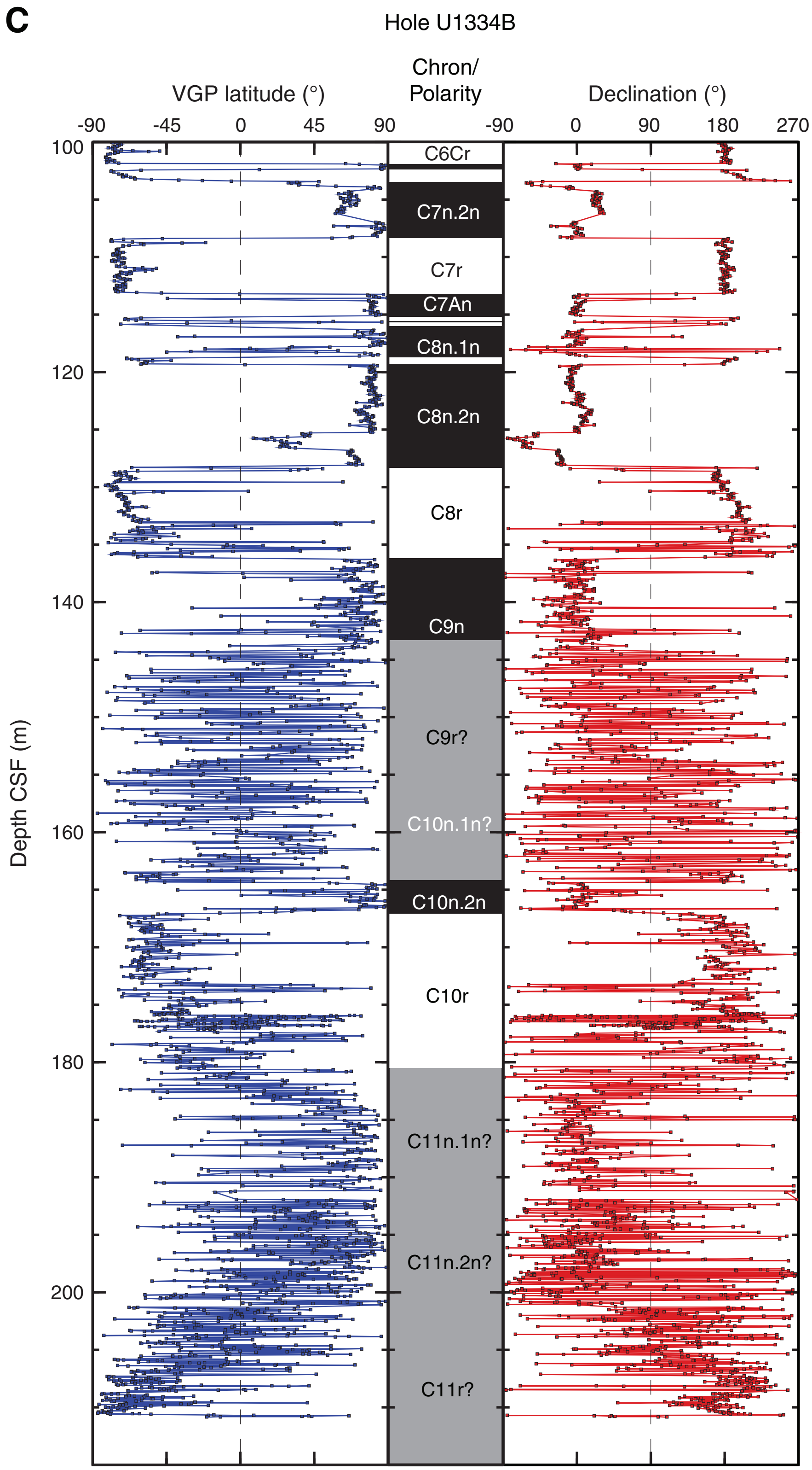

Figure F20. Alternating-field demagnetization (demag) results representative of some of the best samples from Site U1334. Top plot shows vector endpoints of paleomagnetic directions on vector demagnetization diagrams or modified Zijderveld plots (squares = inclinations, circles = declinations), middle plot = intensity variation with progressive demagnetization, bottom plot = directions plotted on an equal-angle stereonet (Wulff projection). Data illustrate the removal of a steep drilling overprint by ~10 mT, with the remaining magnetization providing a relatively well resolved characteristic remanent magnetization. **A.** Sample 320-U1334A-4H-5, 85 cm (34.05 m CSF). **B.** Sample 320-U1334A-5H-2, 85 cm (39.05 m CSF). NRM = natural remanent magnetization.

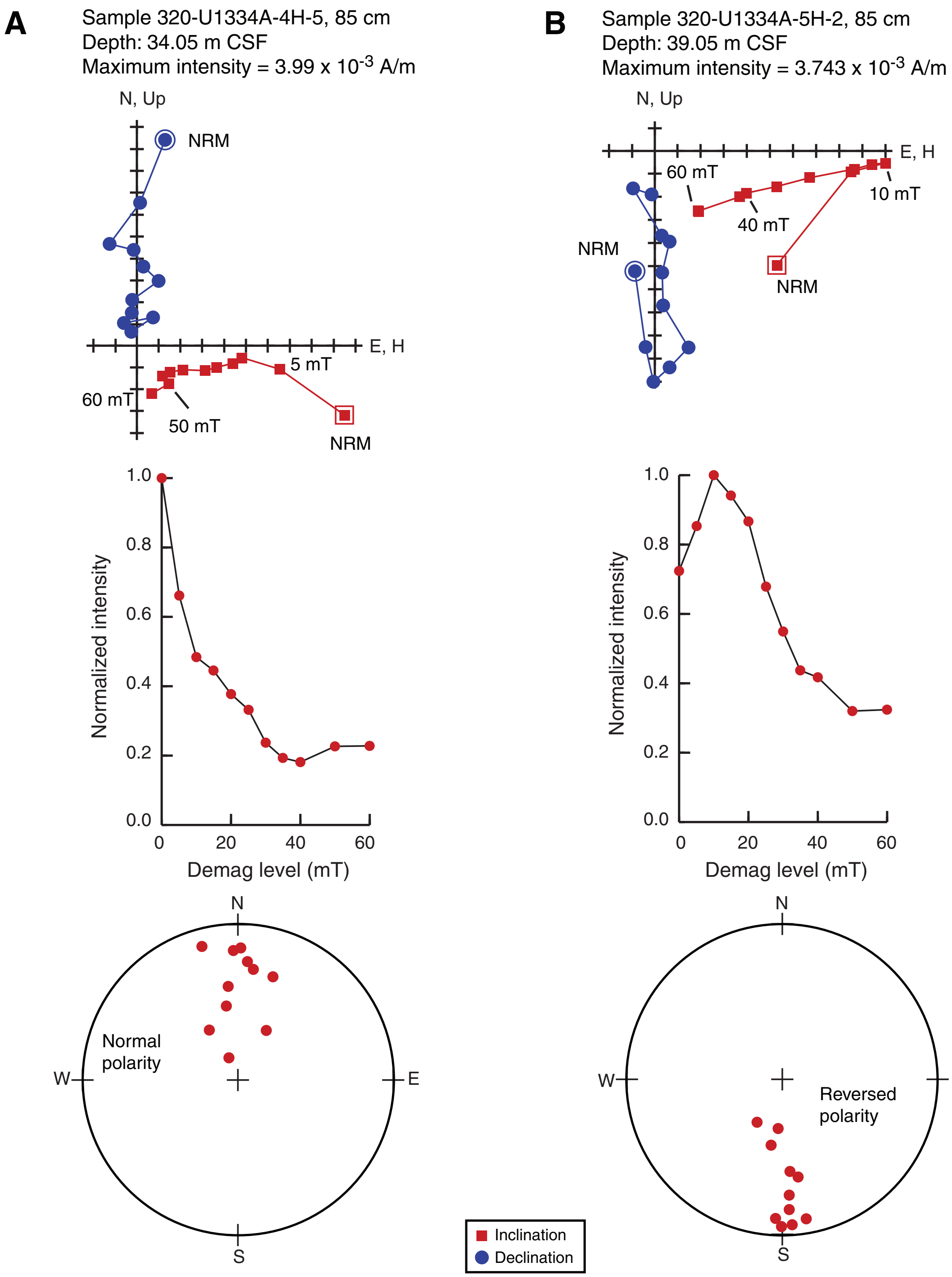

Figure F21. Latitude of the virtual geomagnetic pole (VGP), Hole U1334A. * = locations of possible geomagnetic excursions. North latitudes = normal polarity, south latitudes = reversed polarity. Those intervals of indeterminate polarity are shaded gray. **A.** 0–30 m CSF. (**Continued on next two pages.**)

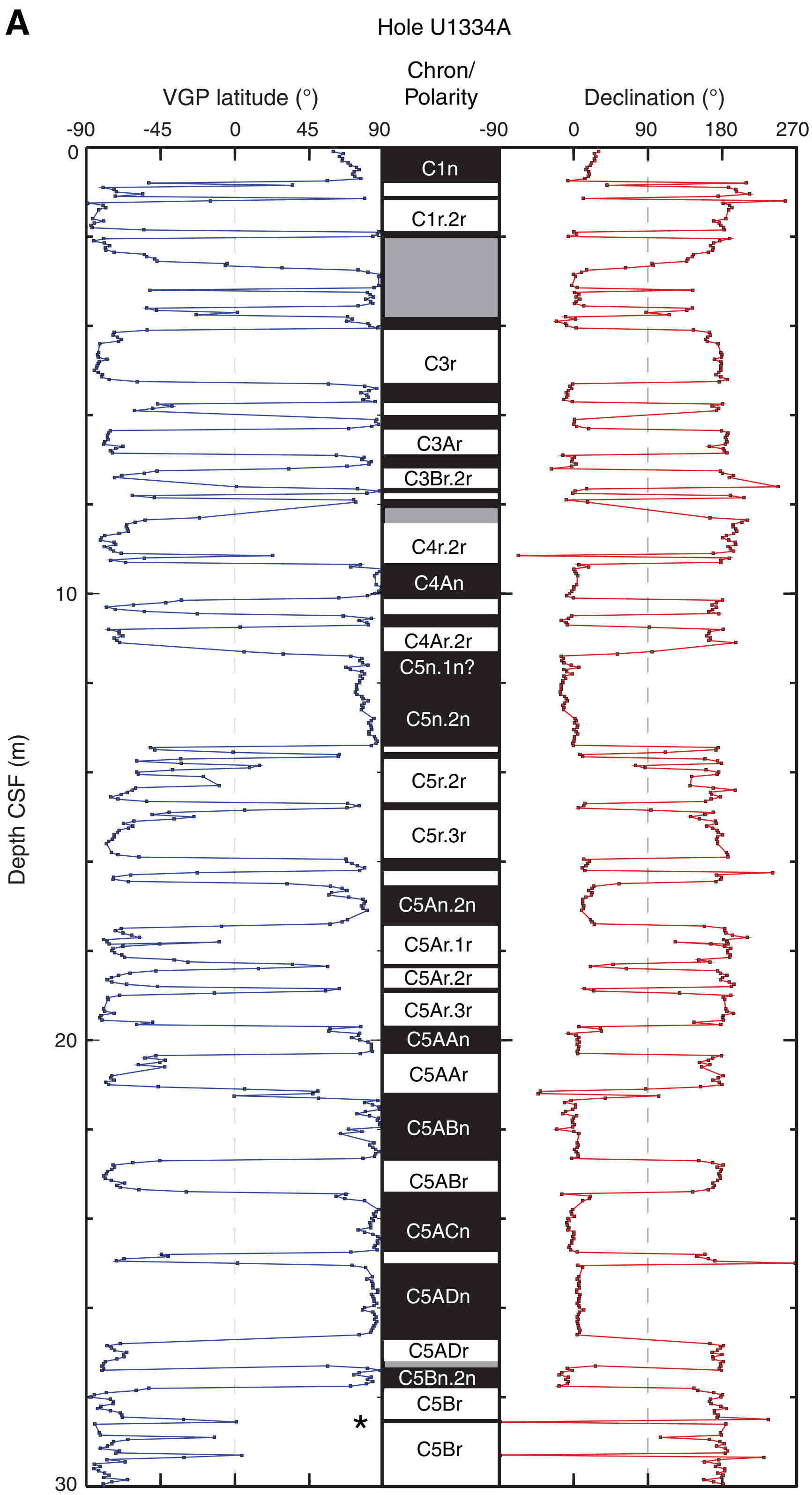

Figure F21 (continued). B. 25–105 m CSF. (Continued on next page.)

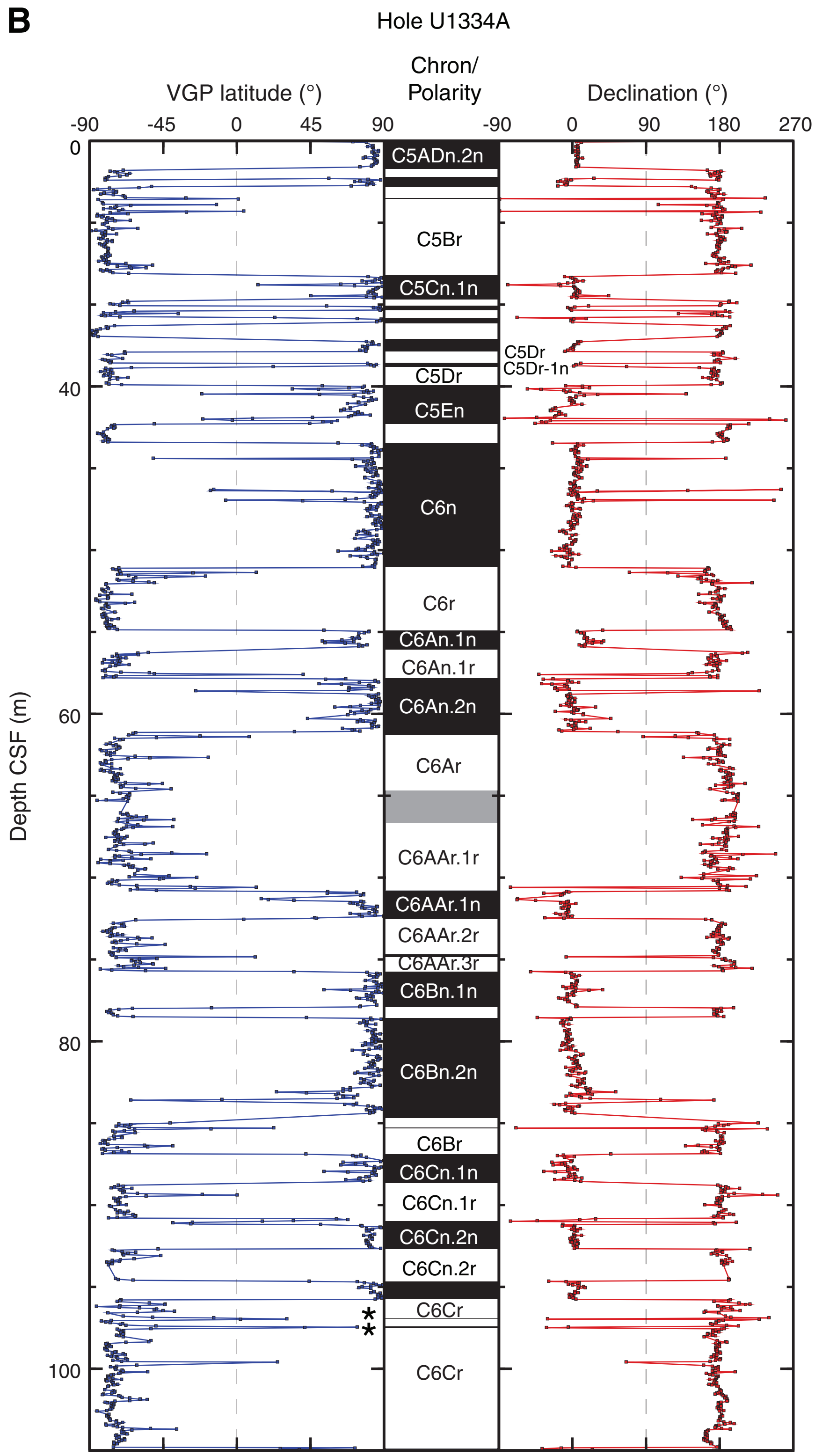

Figure F21 (continued). C. 100–215 m CSF.

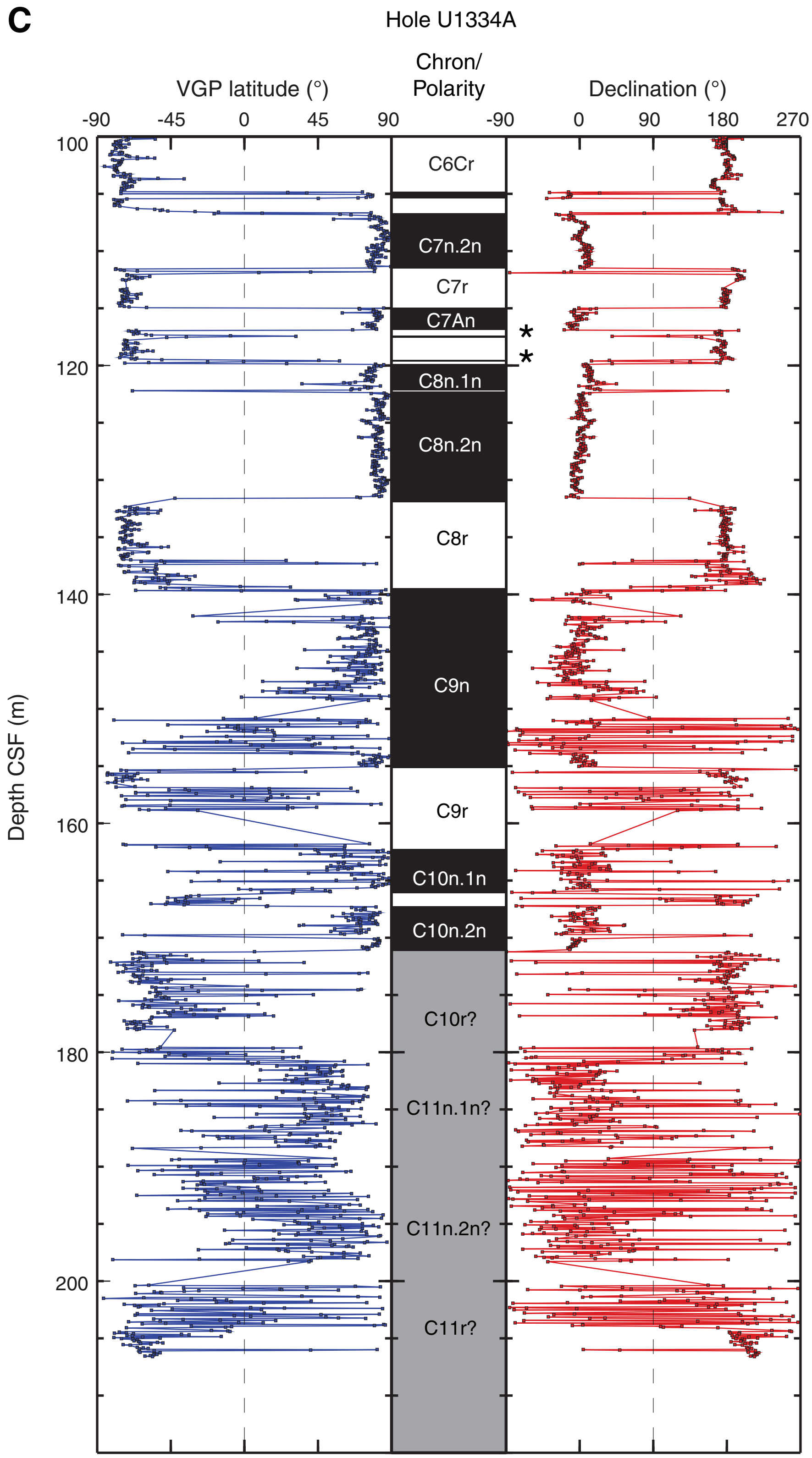

Figure F22. Latitude of the virtual geomagnetic pole (VGP), as determined from paleomagnetic directions, Hole U1334C. * = locations of possible geomagnetic excursions. North latitudes = normal polarity, south latitudes = reversed polarity. Those intervals of indeterminate polarity are shaded gray. **A.** 0–30 m CSF. (**Continued on next two pages.**)

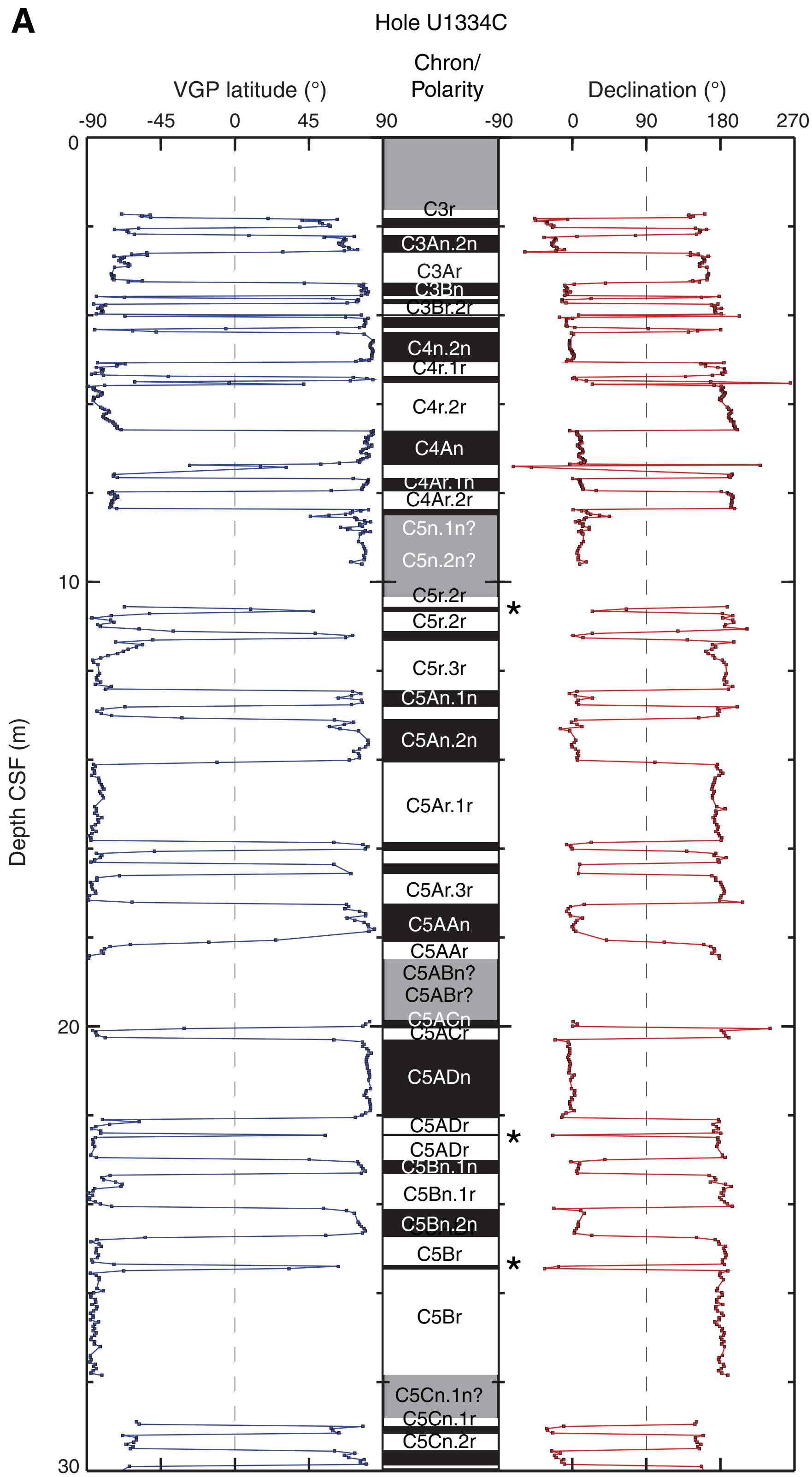

Figure F22 (continued). B. 25–105 m CSF. (Continued on next page.)

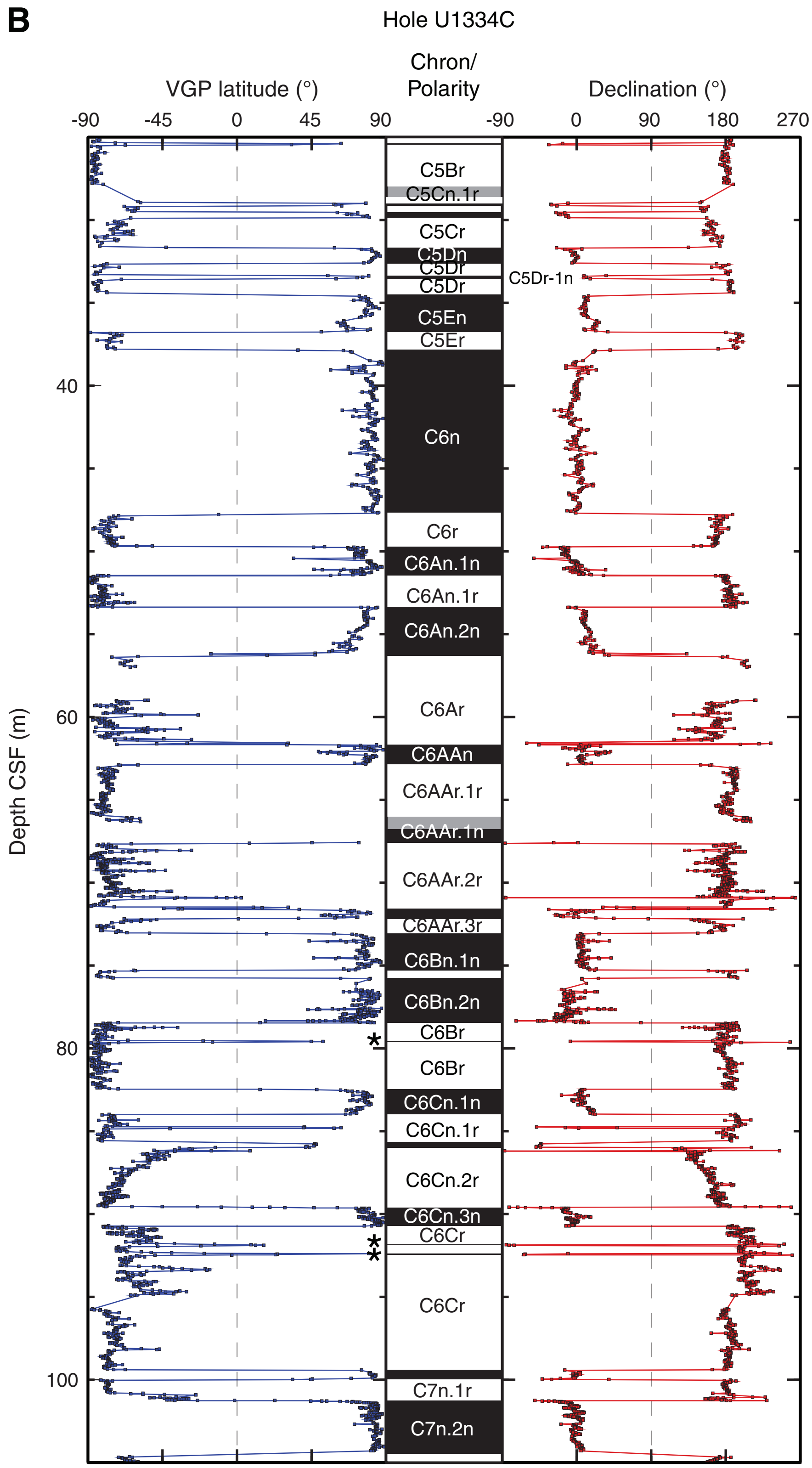

Figure F22 (continued). C. 100–215 m CSF.

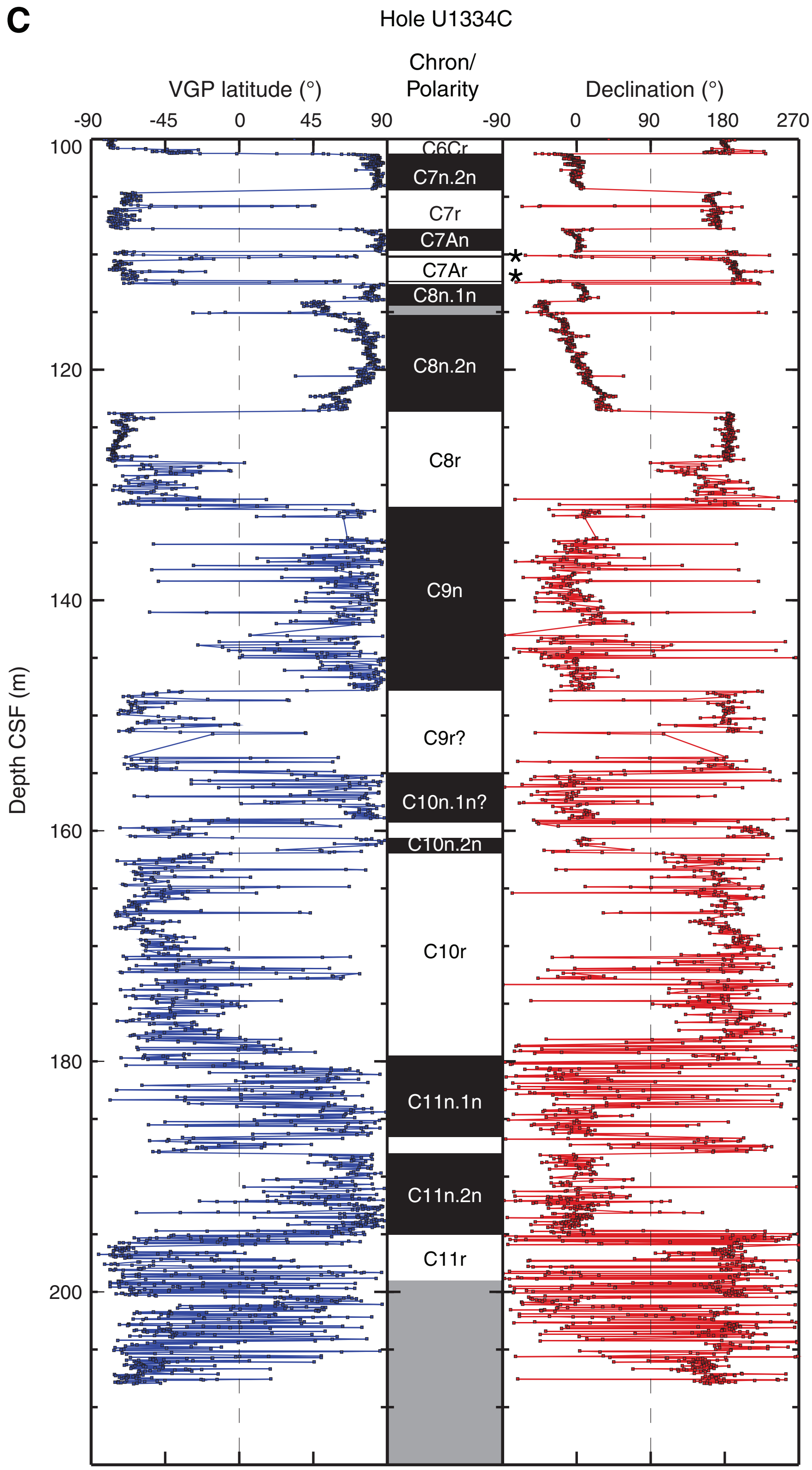

Figure F23. Interstitial water chemistry, Hole U1334A. Values below the detection limit (see Table **T23**) are plotted as zero. (See **"Lithostratigraphy"** for information on unit boundaries.)

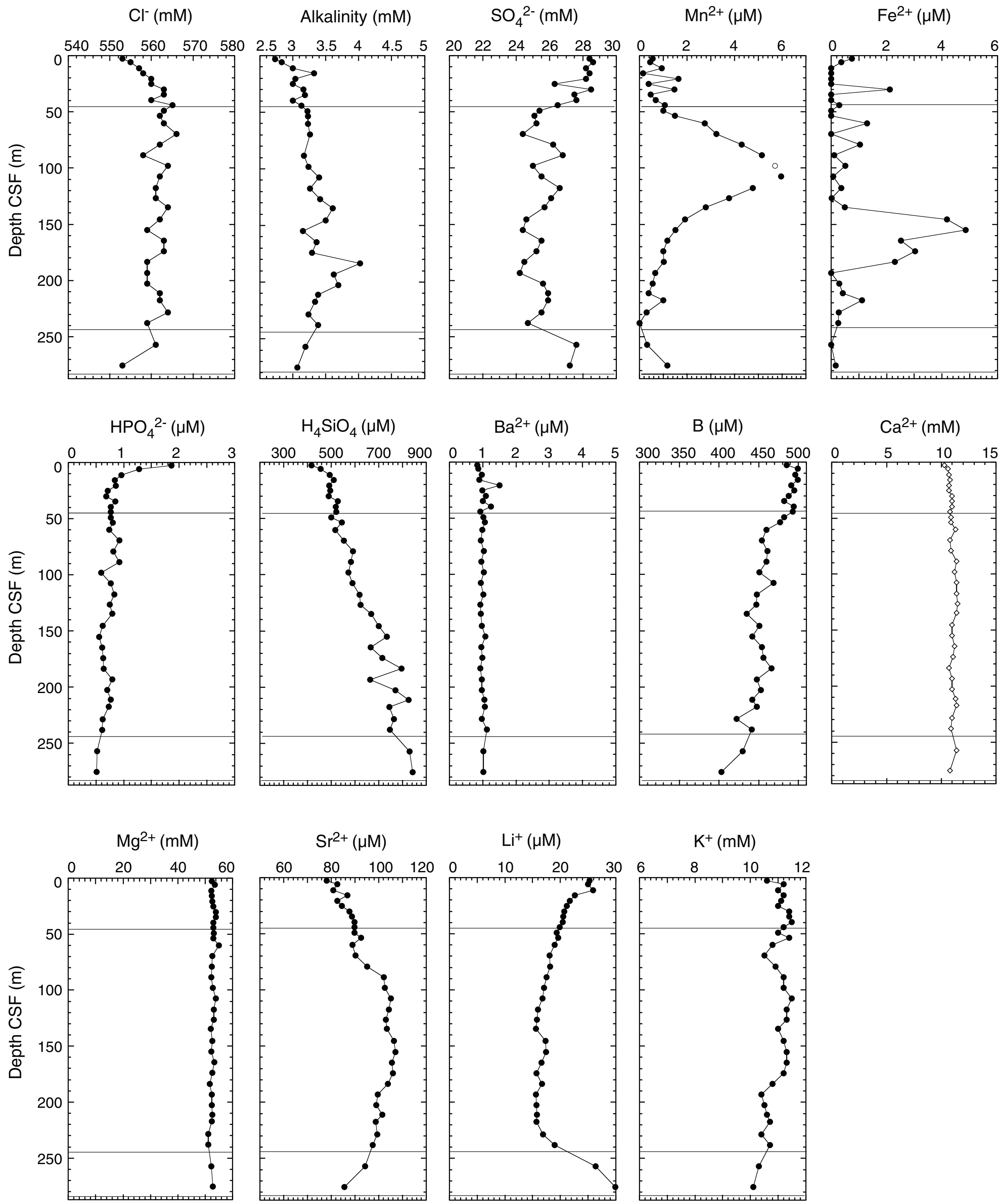

Figure F24. Interstitial water chemistry from Rhizon samples, Holes U1334B and U1334C. Values below the detection limit (see Table T24) are plotted as zero.

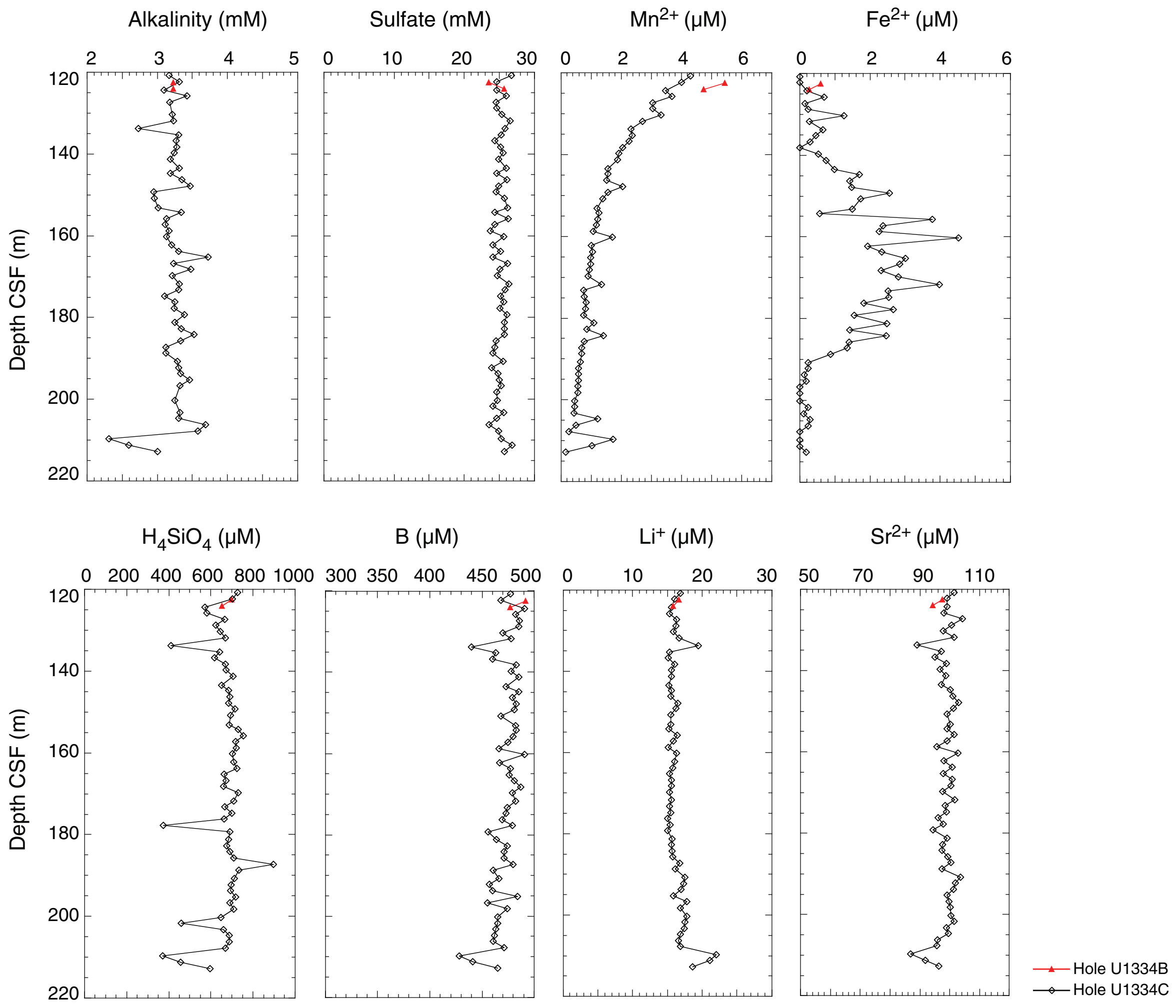

Figure F25. Interstitial water chemistry, Site U1334, comparing Rhizon and squeezed samples. Values below the detection limit (Tables T23, T24) are plotted as zero. Hole U1334C samples are Rhizon samples; other samples are whole-round samples. DD = drilling disturbance, XCB = extended core barrel.

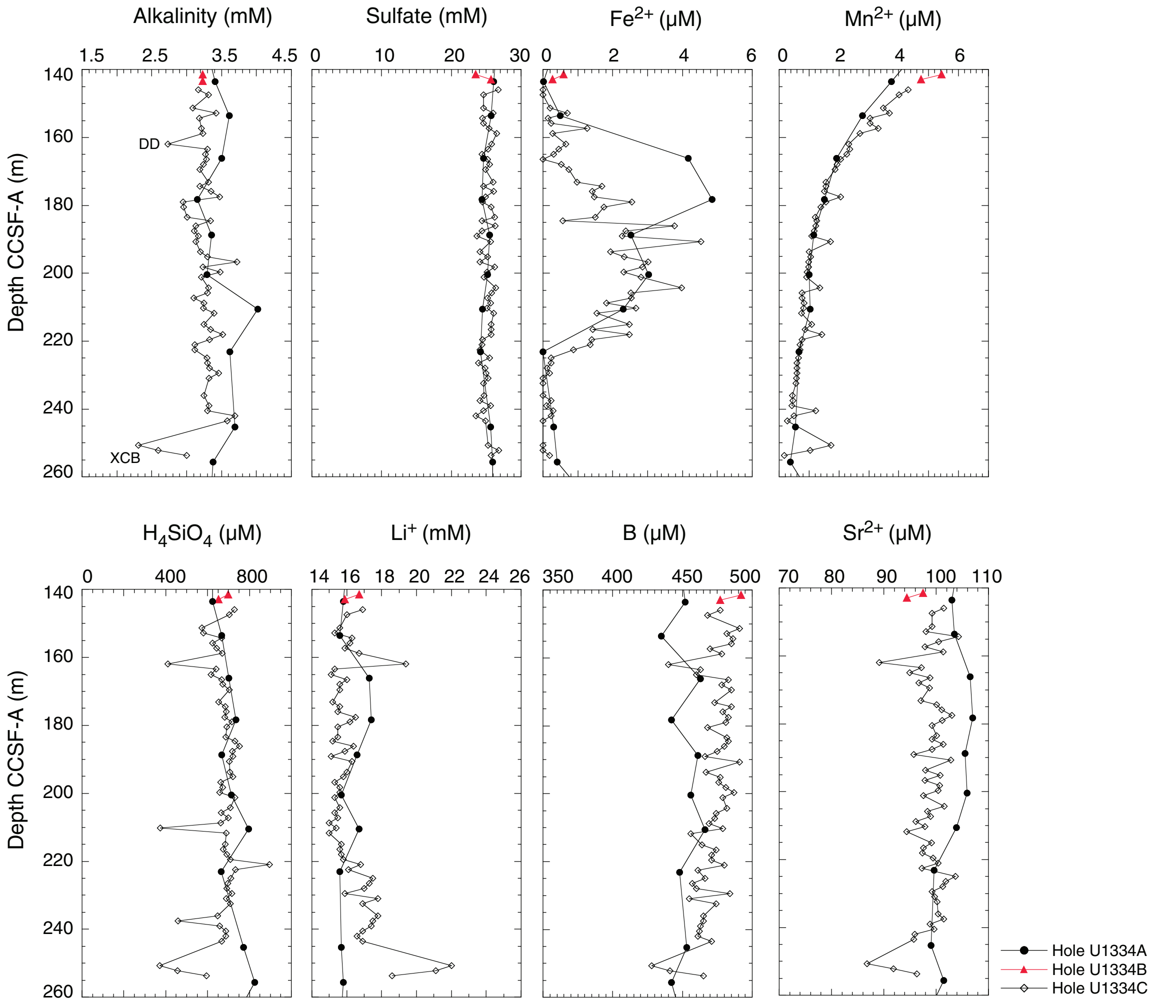

Figure F26. Whole-Round Multisensor Logger (WRMSL) and natural gamma radiation (NGR) data, Holes U1334A–U1334C. Hole U1334B and U1334C data are plotted using offsets (0.5 and 1.0 g/cm³ for gamma ray attenuation [GRA] bulk density; 10 × 10^{-5} and 20 × 10^{-5} SI for magnetic susceptibility; 100 and 200 m/s for *P*-wave velocity; 10 and 20 cps for NGR).

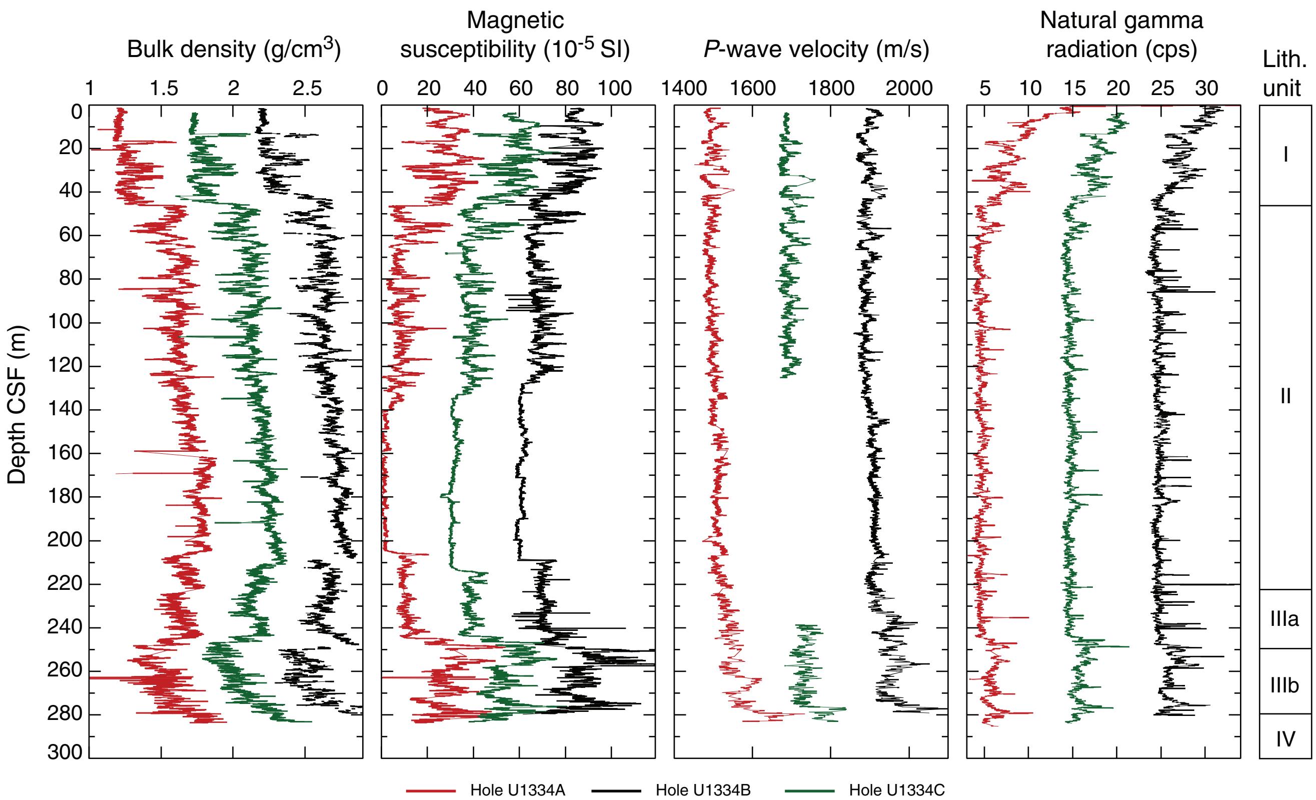

Figure F27. Moisture and density measurements, Hole U1334A. **A.** Porosity and water content. **B.** MAD and GRA bulk density. **C.** Grain density.

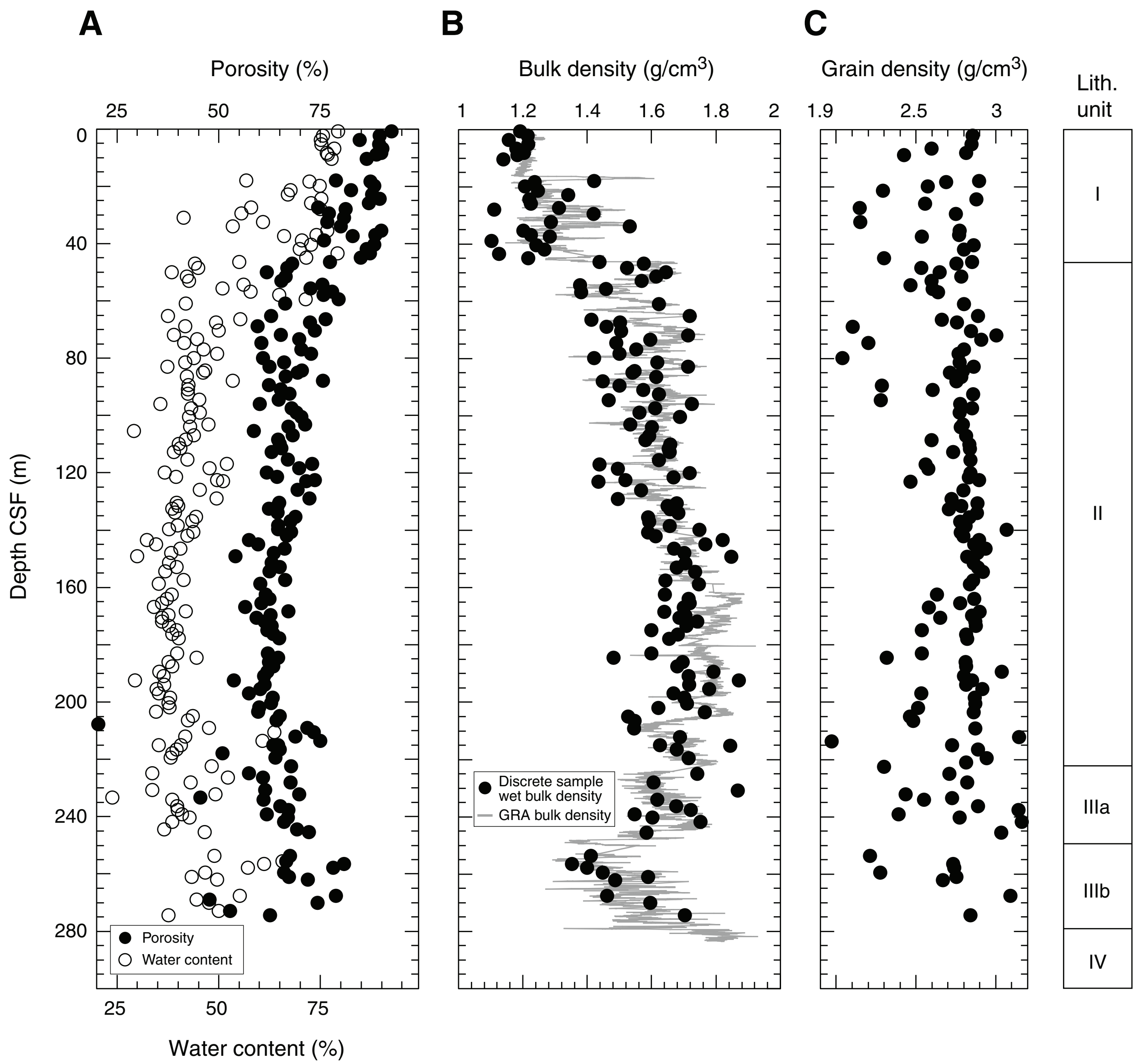

Figure F28. Moisture and density (MAD) analysis of discrete samples, Hole U1334A. Gamma ray attenuation (GRA) density interpolated with a 20 cm wide Gaussian window.

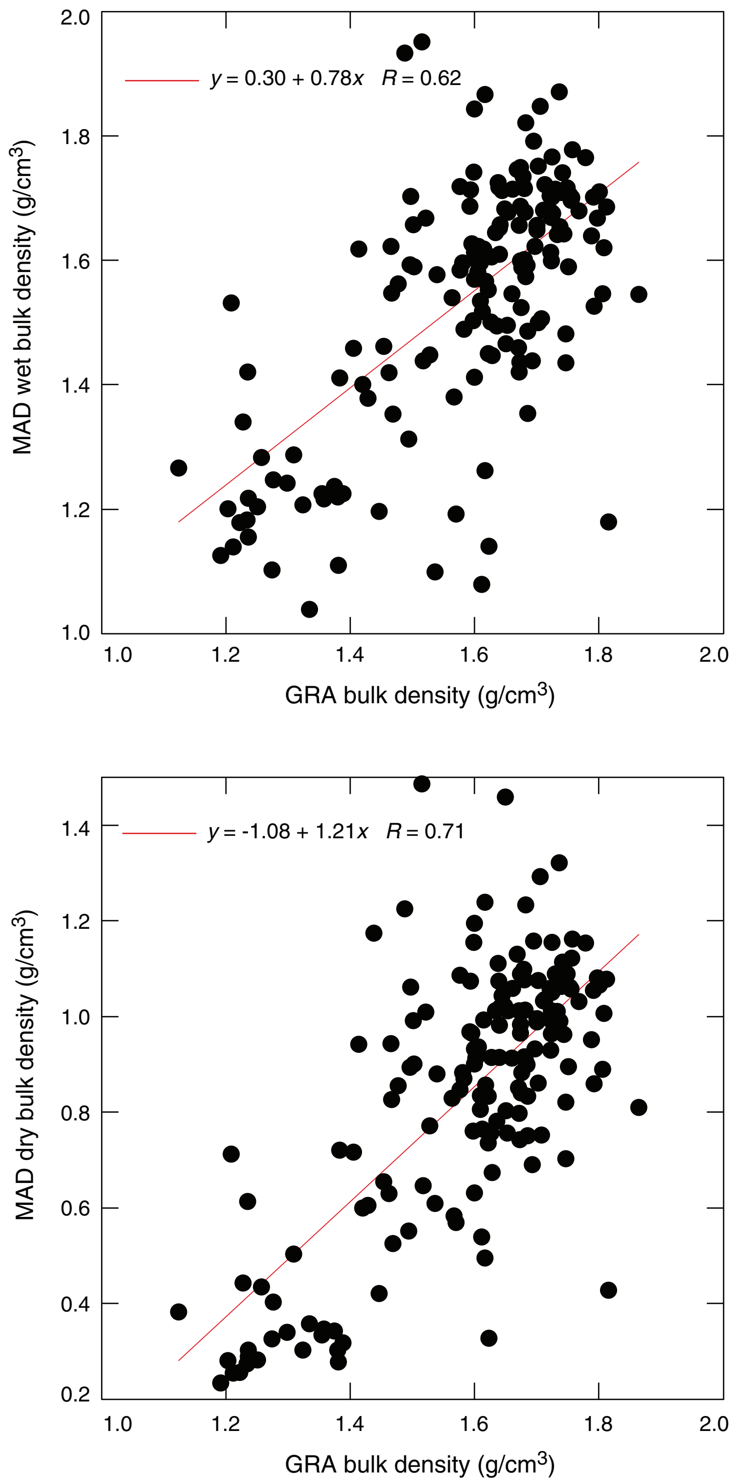

Figure F29. Compressional wave velocity from the *P*-wave logger (PWL) and discrete velocity measurements on split core from Hole U1334A, using the contact probe for *x*-axis measurements and insertion probes for *y*- and *z*-axis measurements. (see **"Compressional wave velocity"** for note on postcruise velocity correction.)

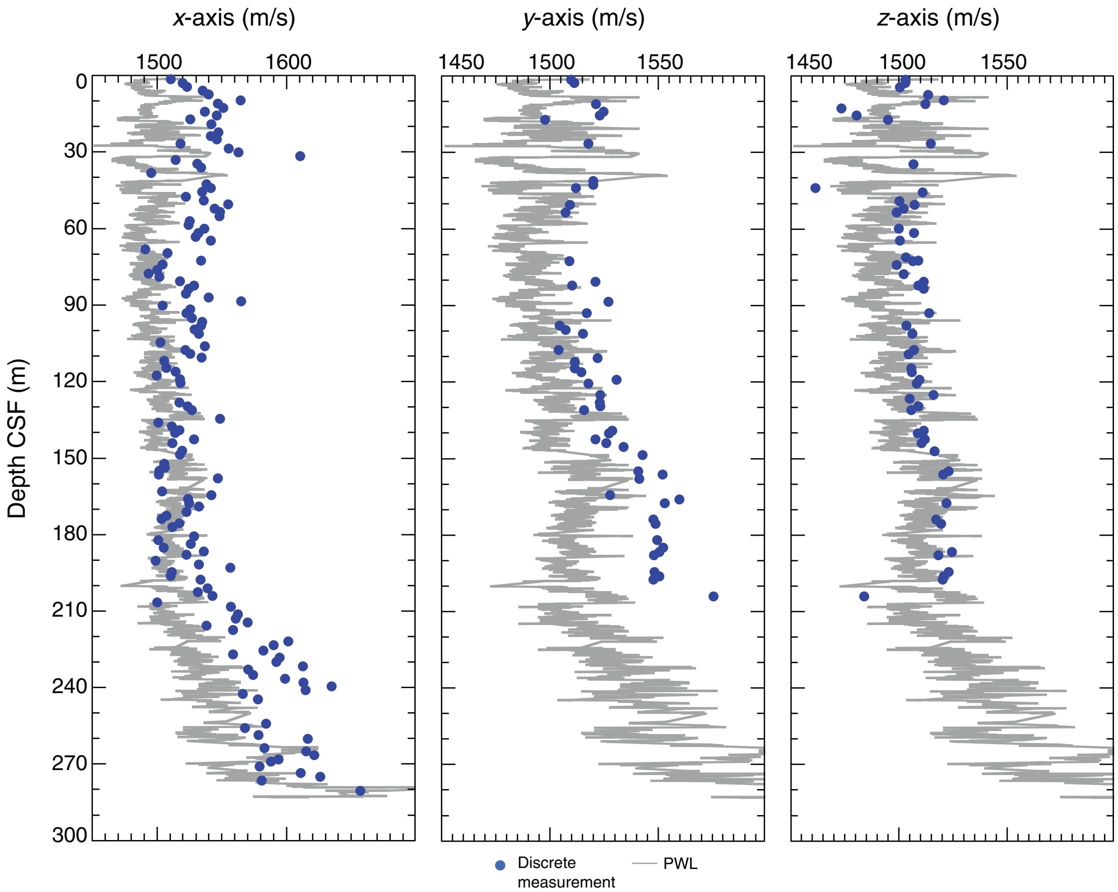

Figure F30. Porosity and thermal conductivity measurements, Hole U1334A.

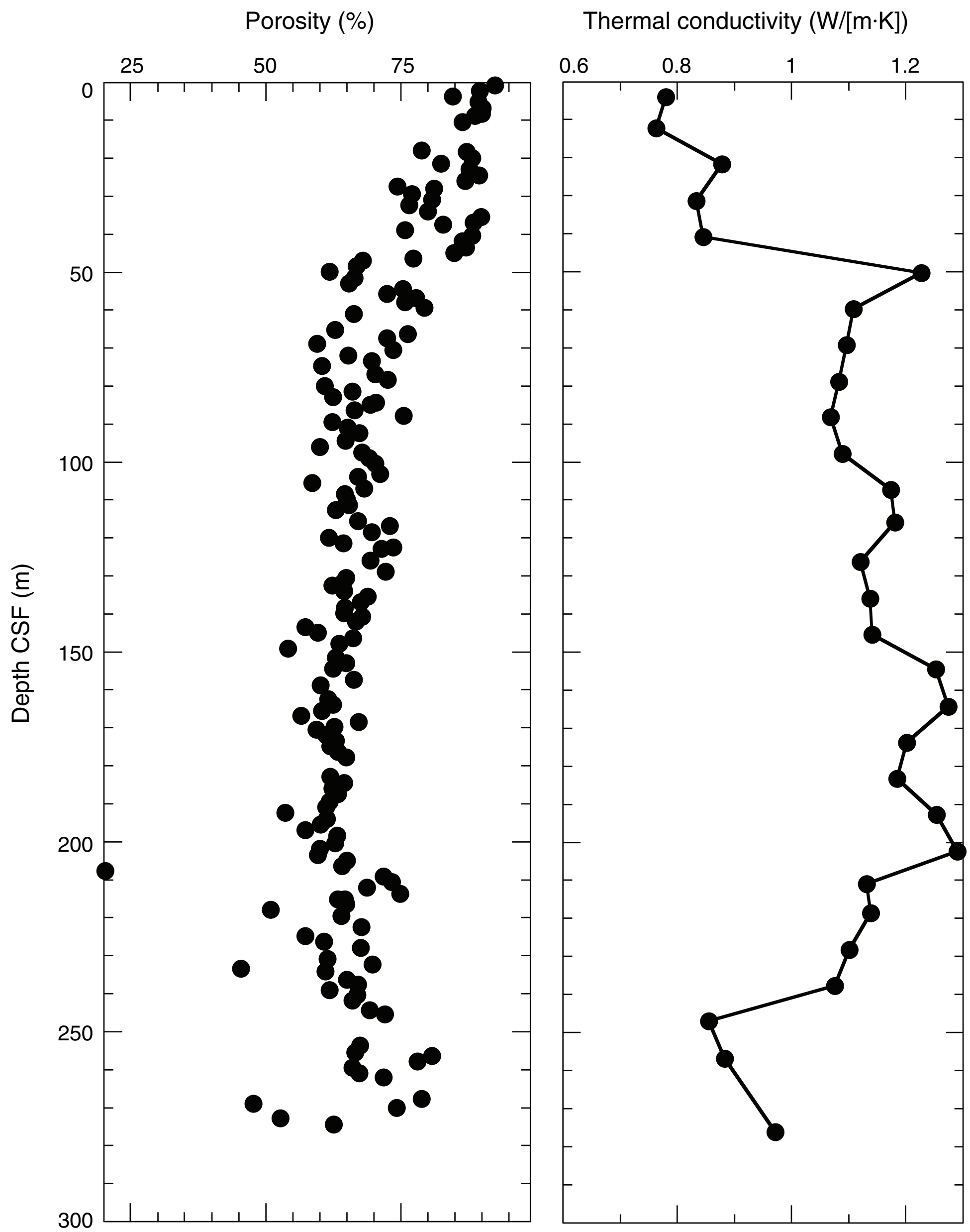

Figure F31. Thermal conductivity vs. porosity, from moisture and density analysis of discrete samples.

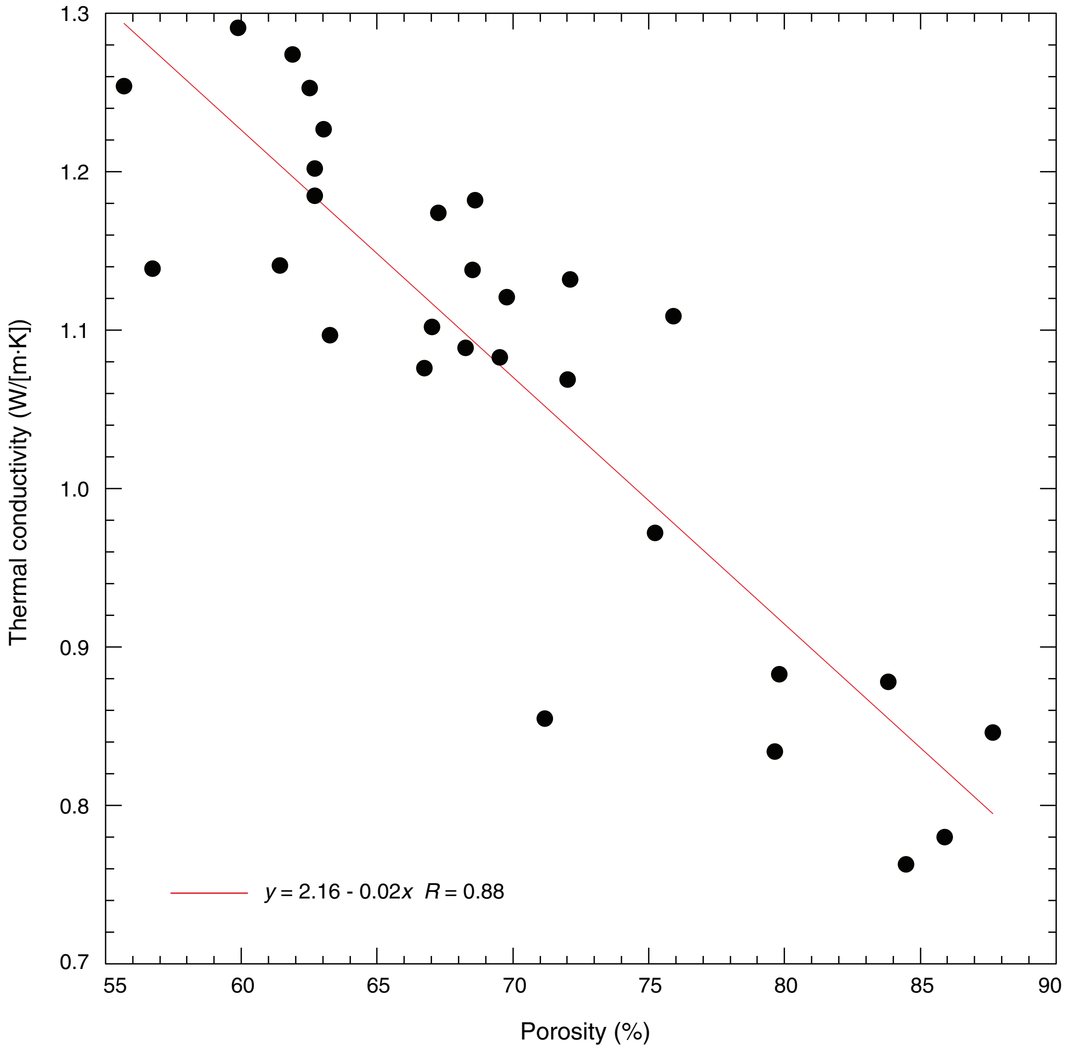

Figure F32. Reflectance spectrophotometer (RSC) data, Holes U1334A–U1334C. RSC for Holes U1334B and U1334C have been offset (20 and 40 for L*; 4 and 5 for a*; 8 and 10 for b*) for core to core comparison. L*, a*, b* = reflectance value of sediment as defined in the LAB color model.

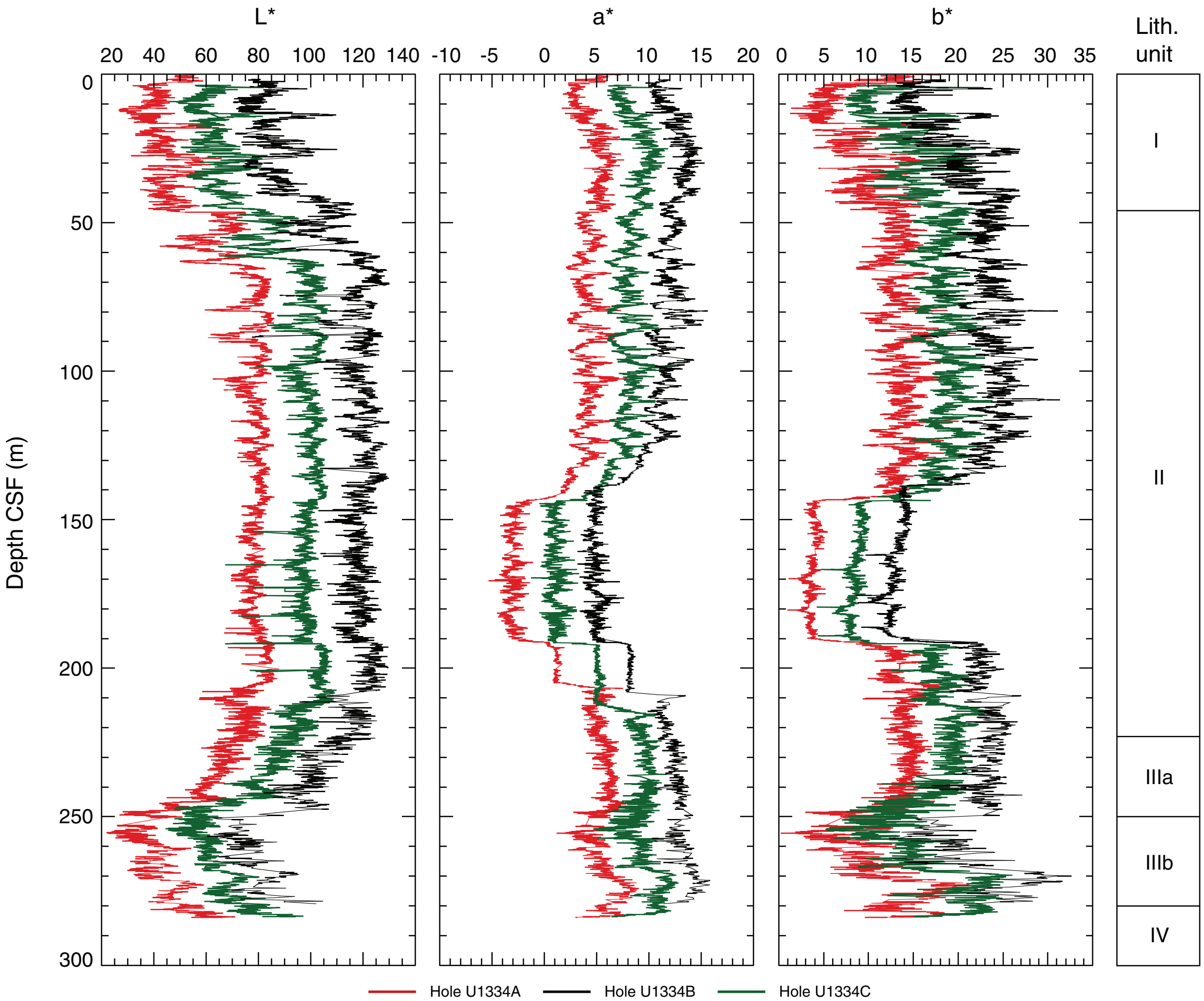

Figure F33. Magnetic susceptibility data, Site U1334. Top panel = spliced section with core breaks (triangles) and hole designations, bottom panel = Holes U1334A (red), U1334B (blue), and U1334C (green), offset from each other by a constant (200 × 10^{-6} SI). **A.** 0–50 m CCSF-A. (**Continued on next six pages.**)

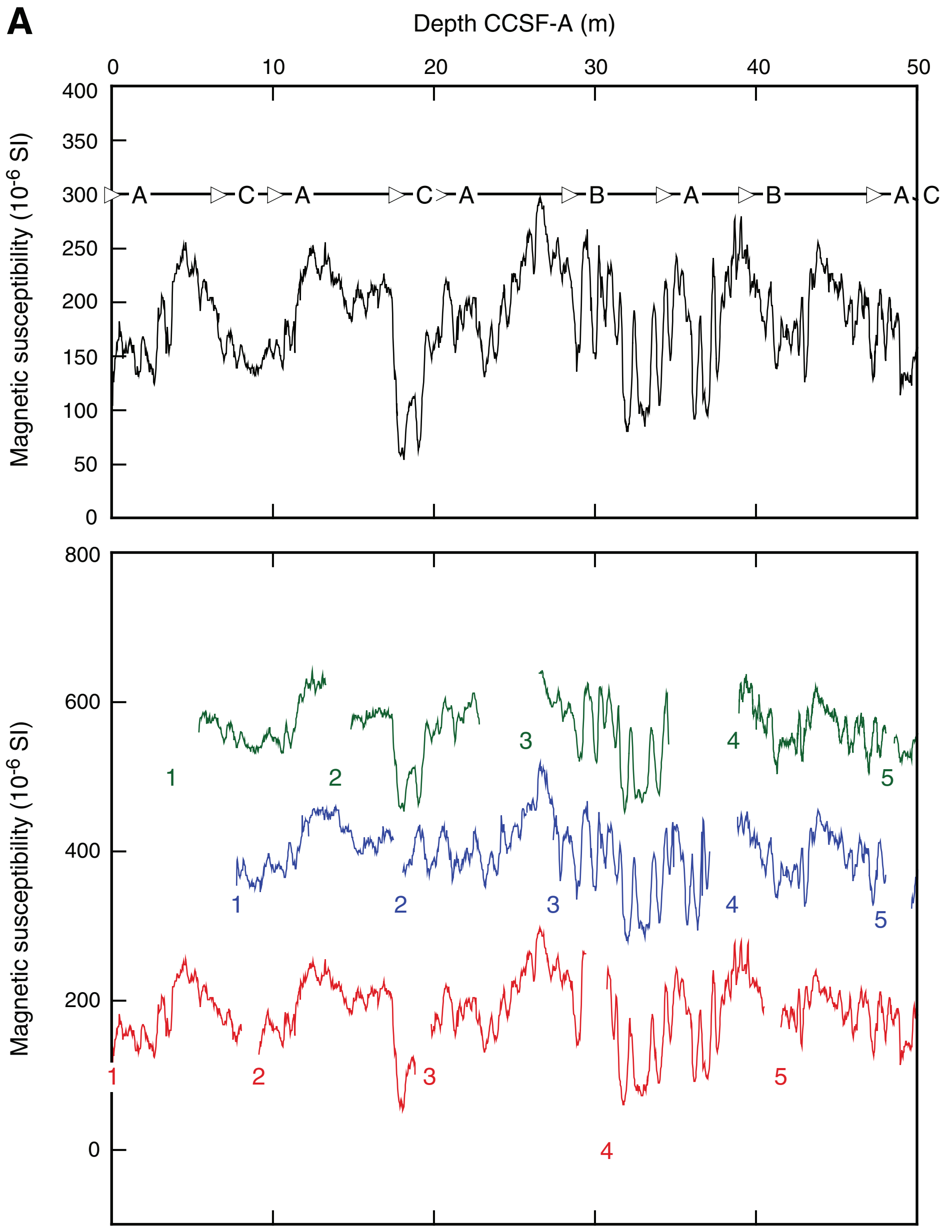

Figure F33 (continued). B. 50–100 m CCSF-A. (**Continued on next page.**)

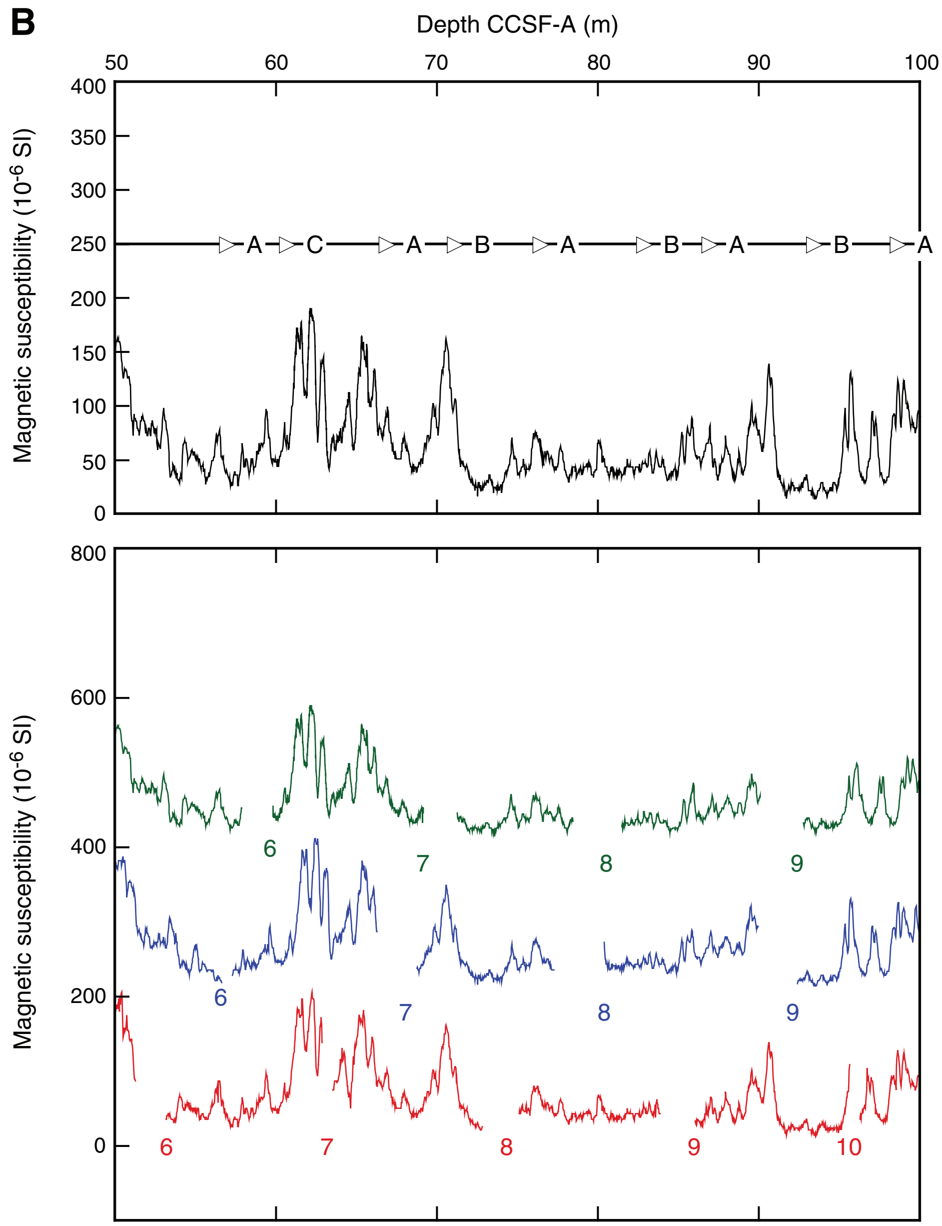

Figure F33 (continued). C. 100–150 m CCSF-A. (**Continued on next page.**)

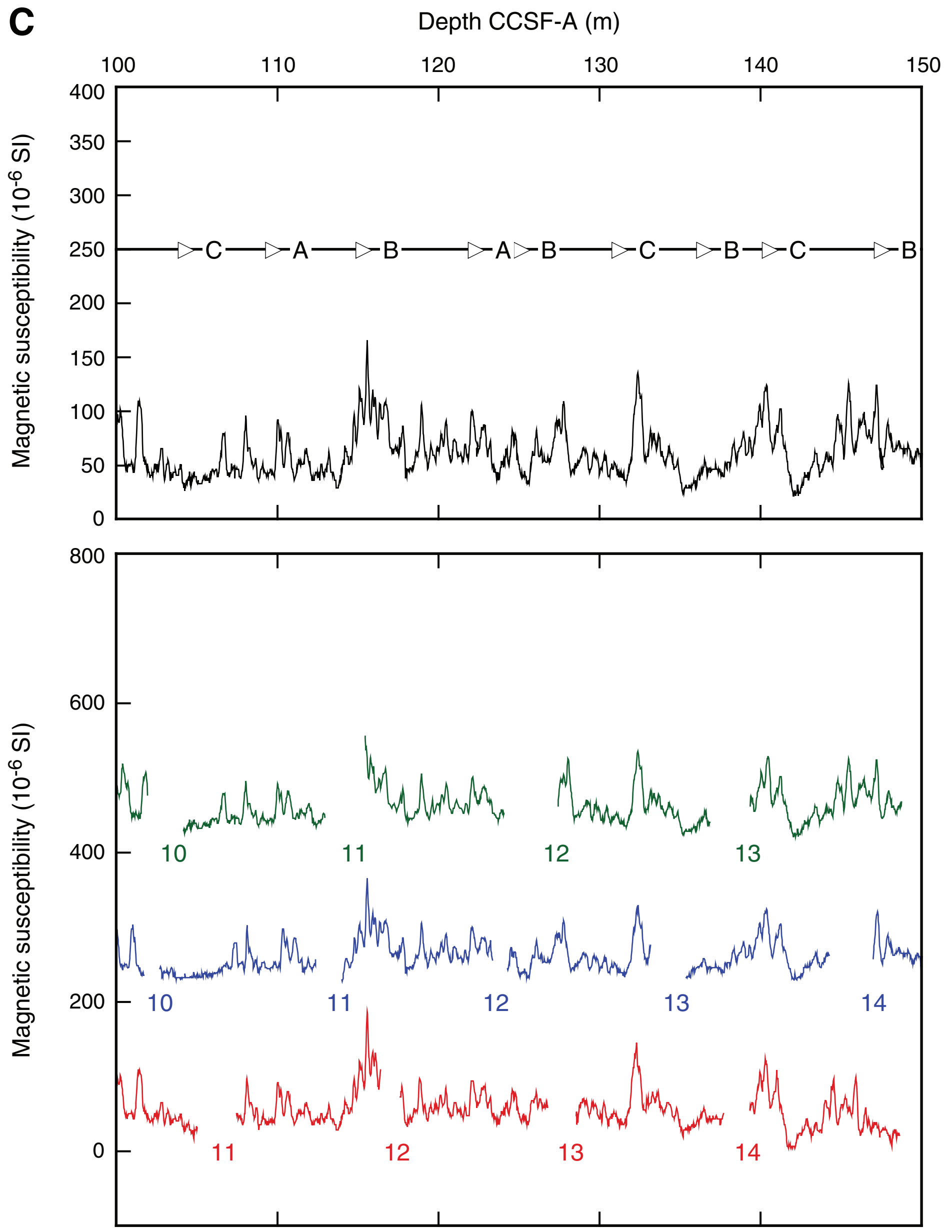

Figure F33 (continued). D. 150–200 m CCSF-A. (**Continued on next page.**)

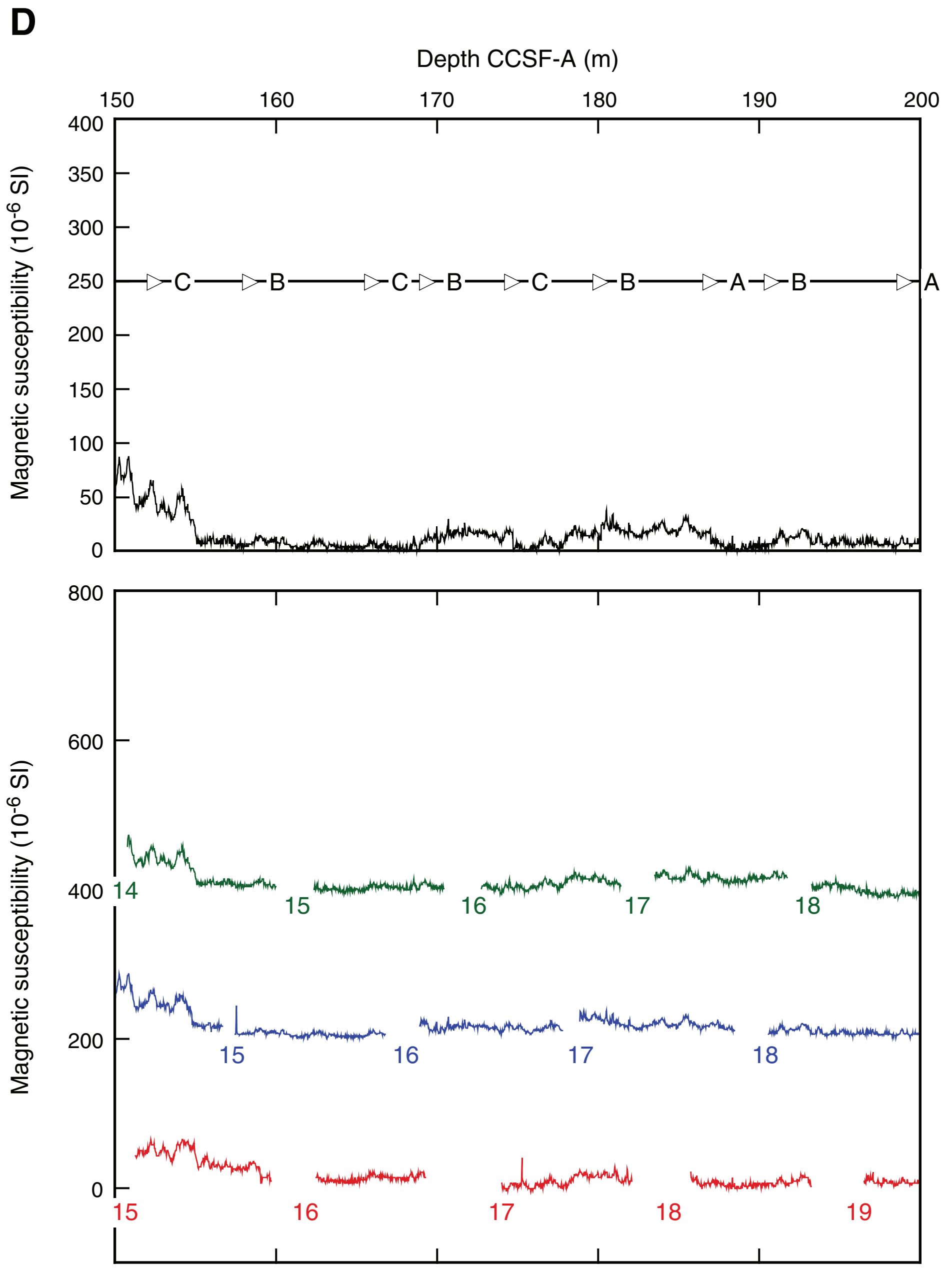

Figure F33 (continued). E. 200–250 m CCSF-A. (Continued on next page.)

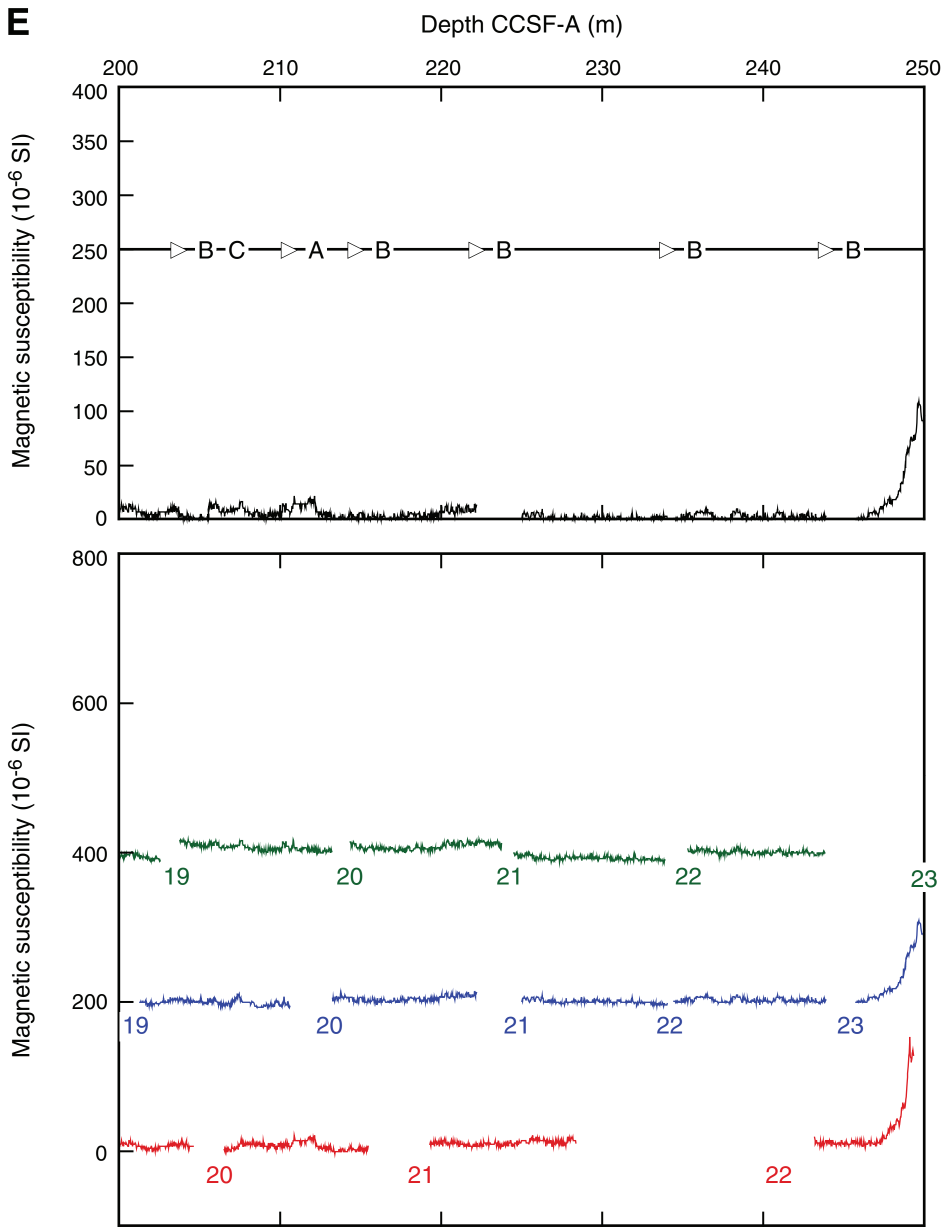

Figure F33 (continued). **F.** 250–300 m CCSF-A. (**Continued on next page.**)

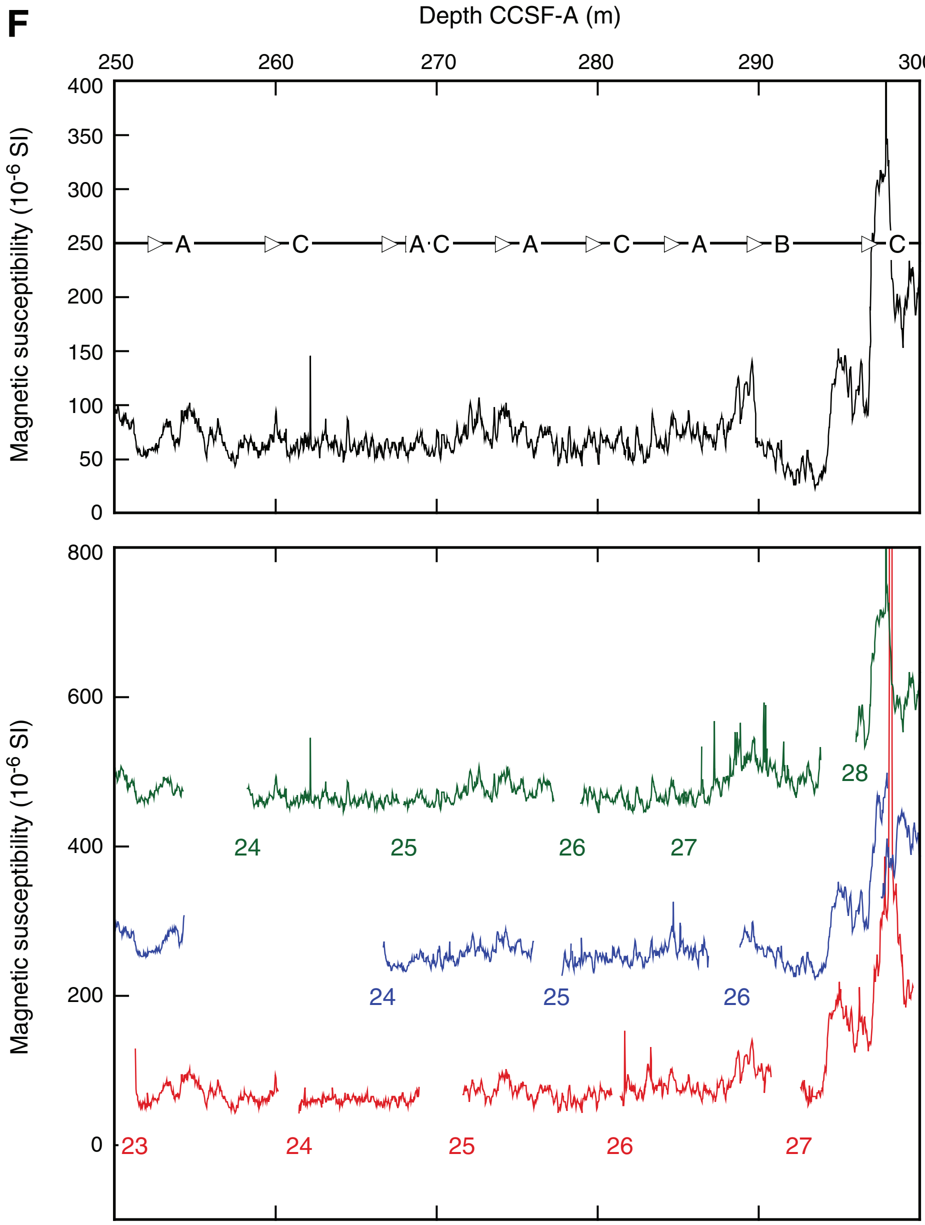

Figure F33 (continued). **G.** 300–350 m CCSF-A.

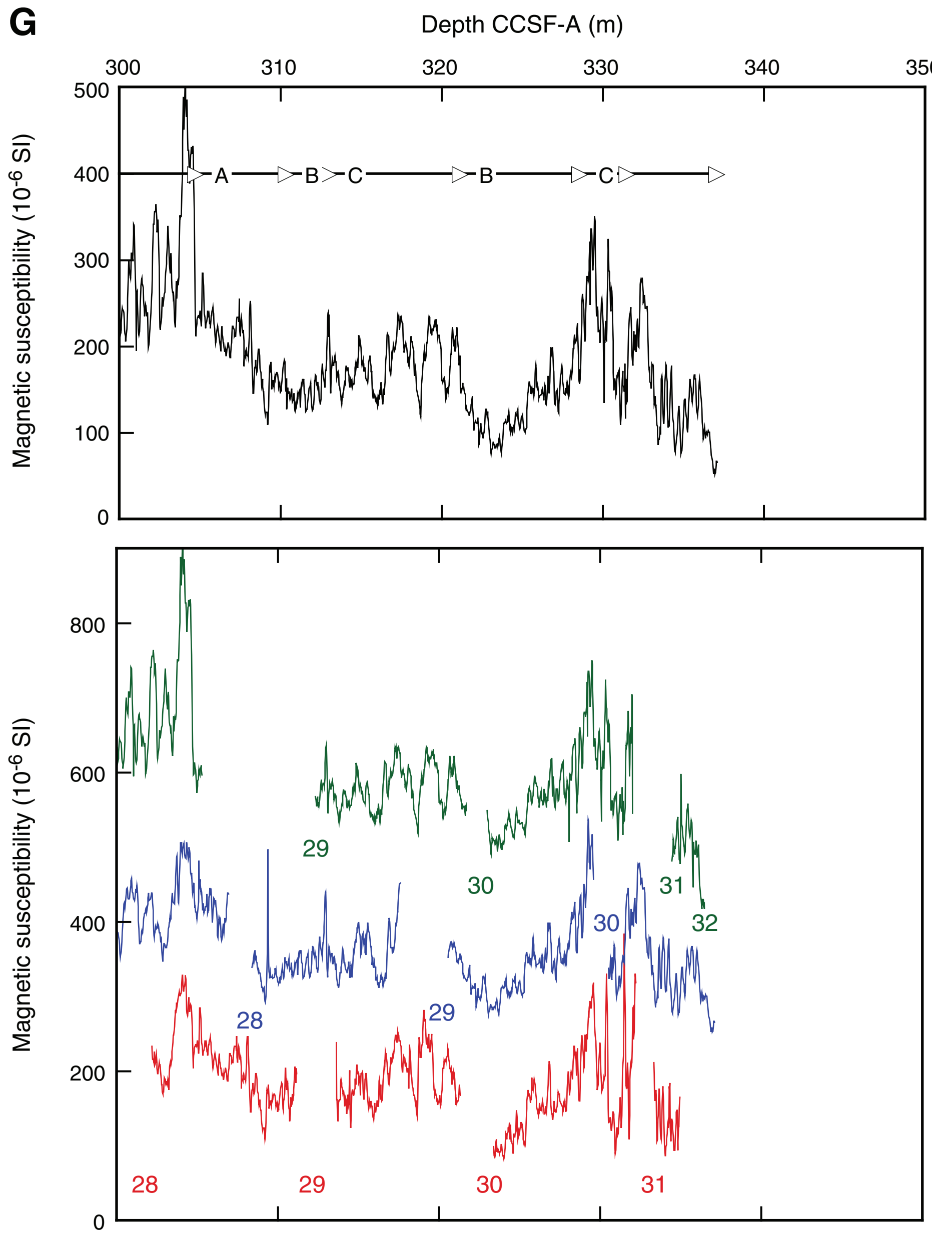

Figure F34. Gamma ray attenuation (GRA) density data, Site U1334. Top panel = spliced section with core breaks (triangles) and hole designations, bottom panel = Holes U1334A (red), U1334B (blue), and U1334C (green), offset from each other by a constant (0.5 g/cm³). **A.** 0–50 m CCSF-A. (**Continued on next six pages.**)

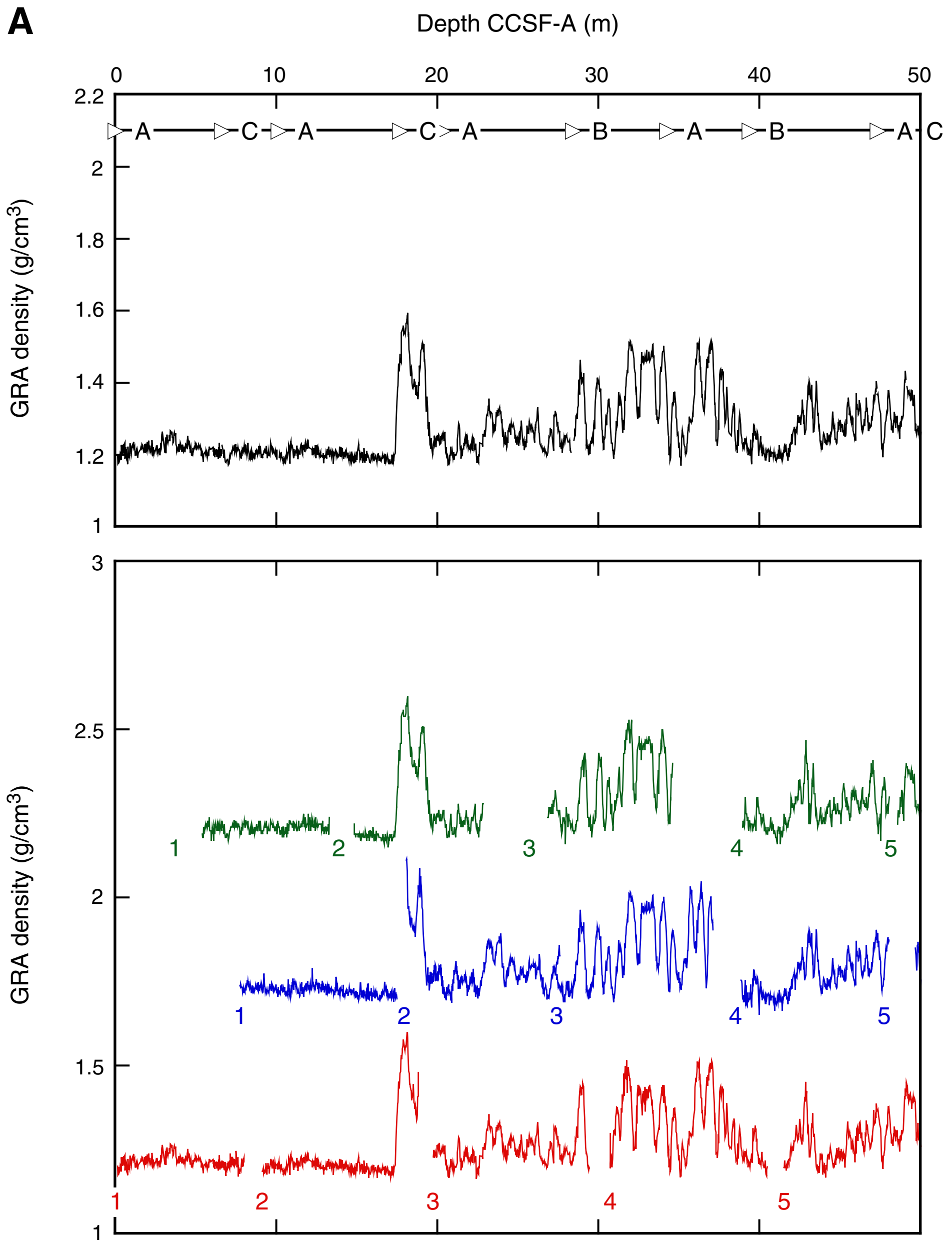

Figure F34 (continued). B. 50–100 m CCSF-A. (Continued on next page.)

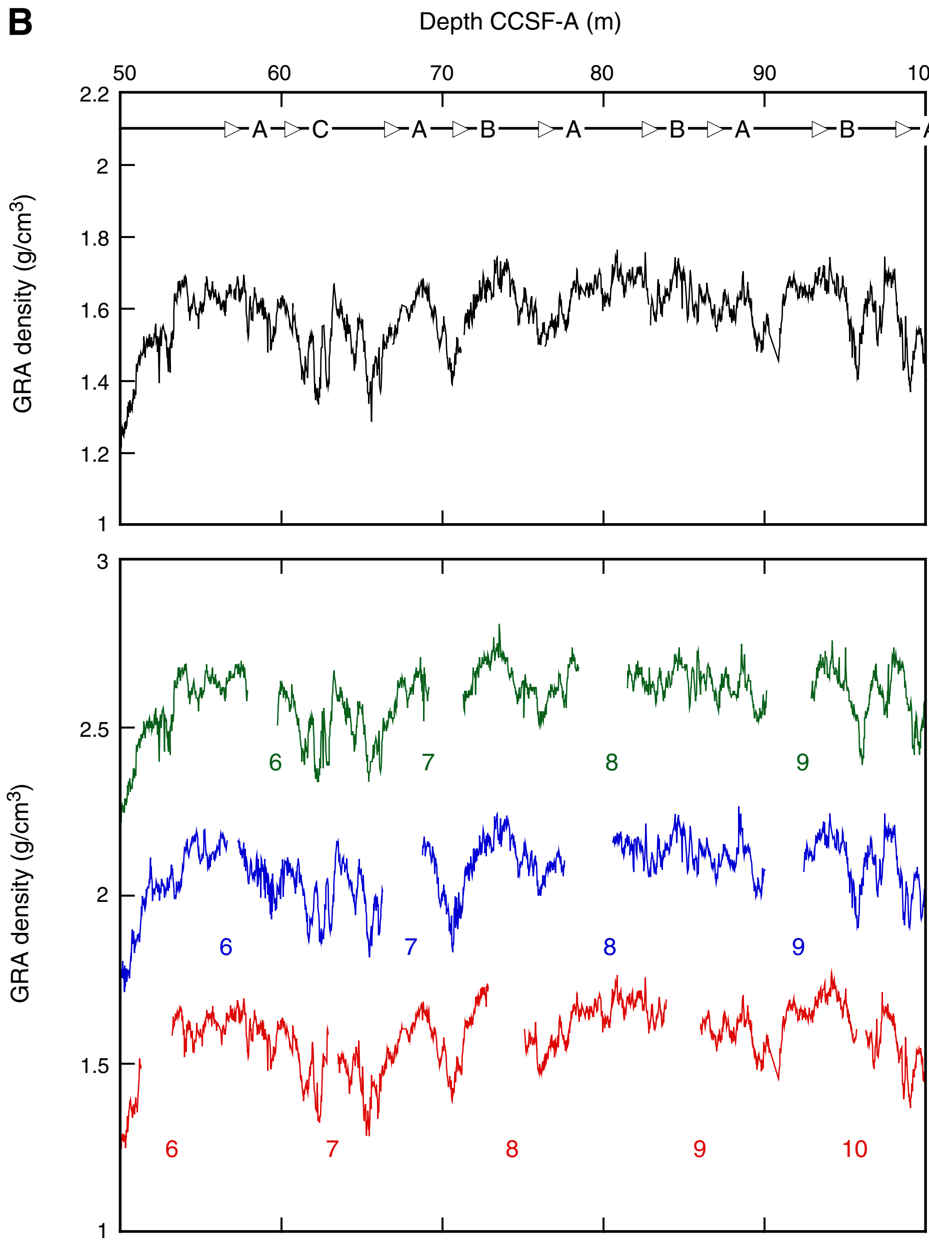

Figure F34 (continued). C. 100–150 m CCSF-A. (**Continued on next page.**)

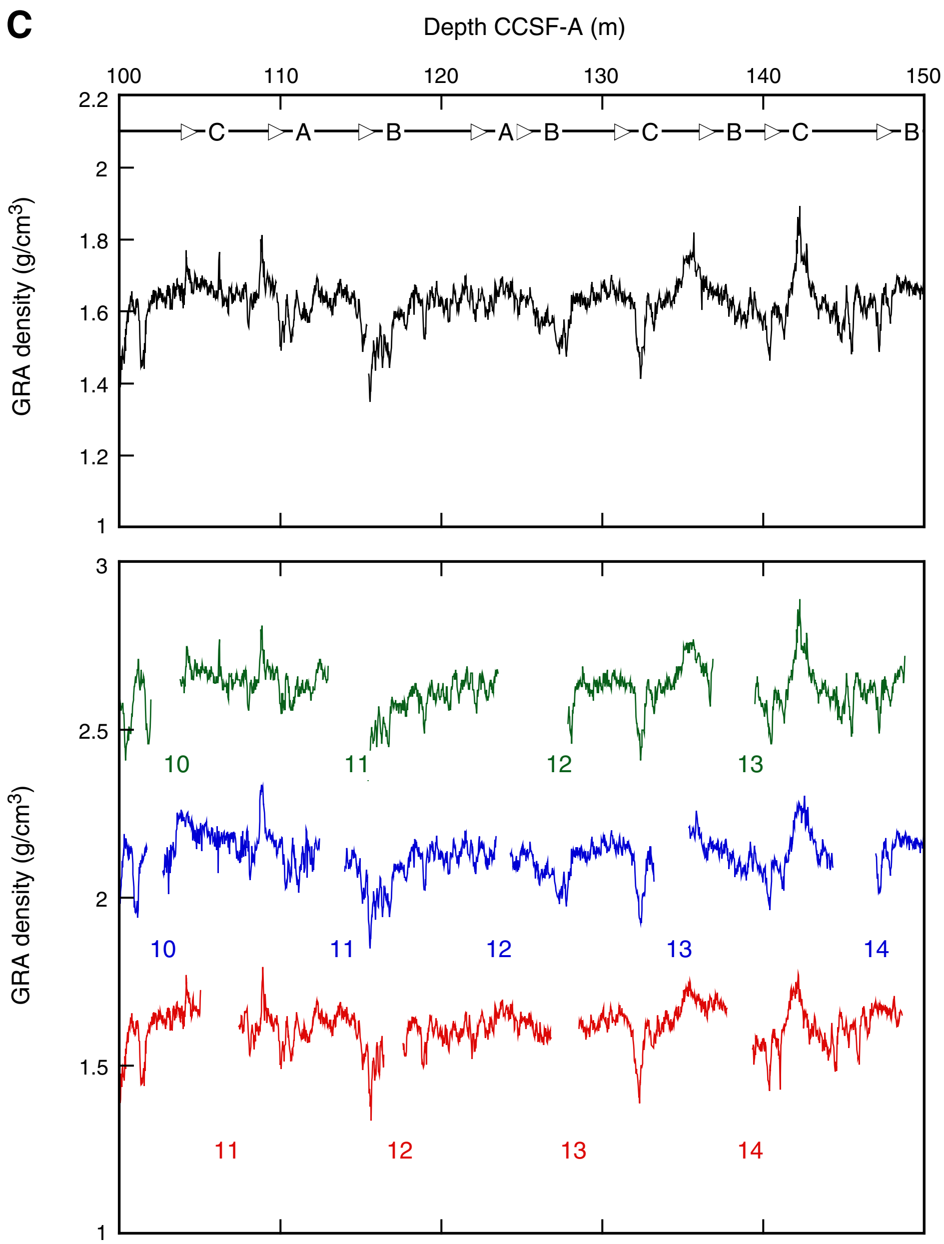

Figure F34 (continued). D. 150–200 m CCSF-A. (Continued on next page.)

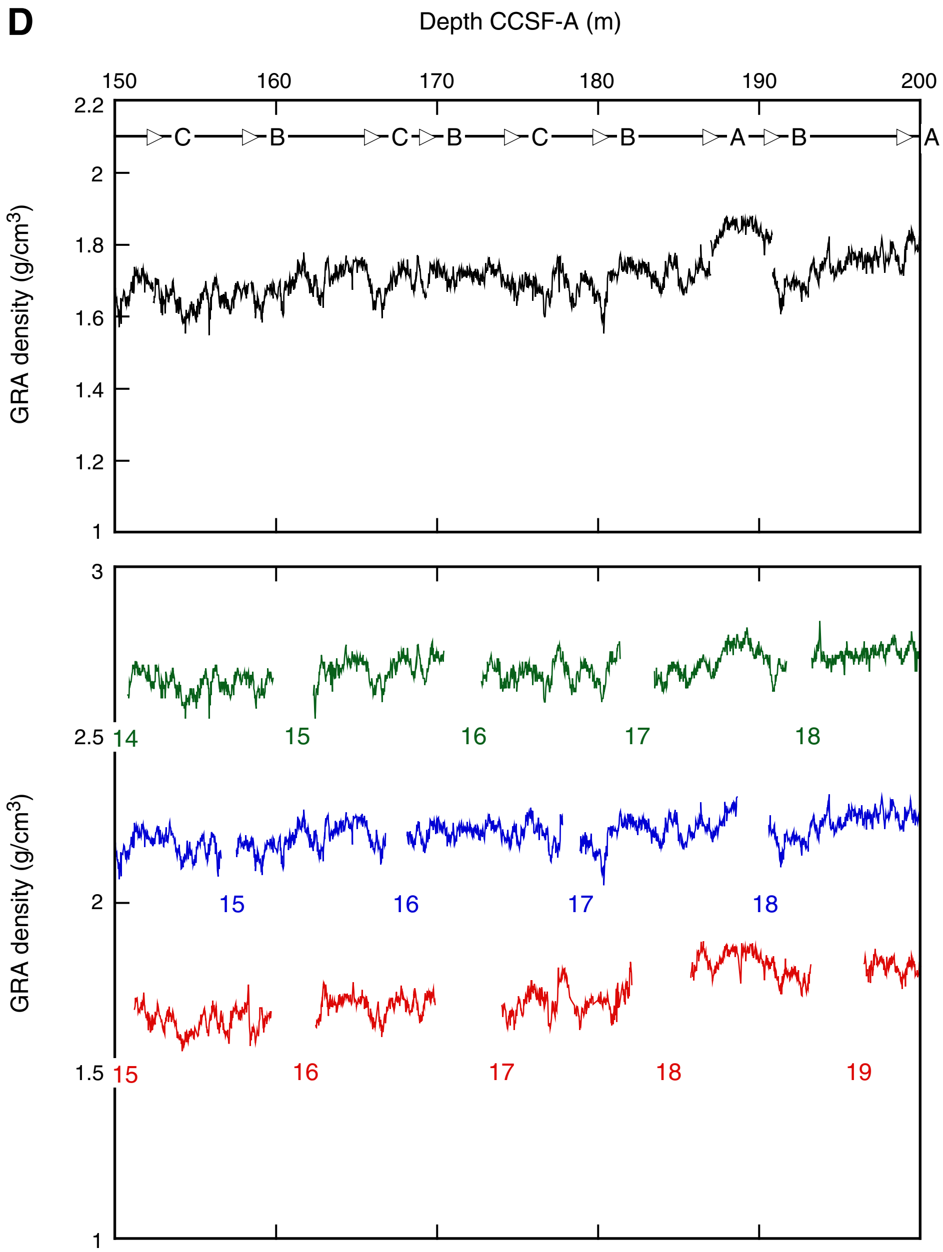

Figure F34 (continued). **E.** 200–250 m CCSF-A. (**Continued on next page.**)

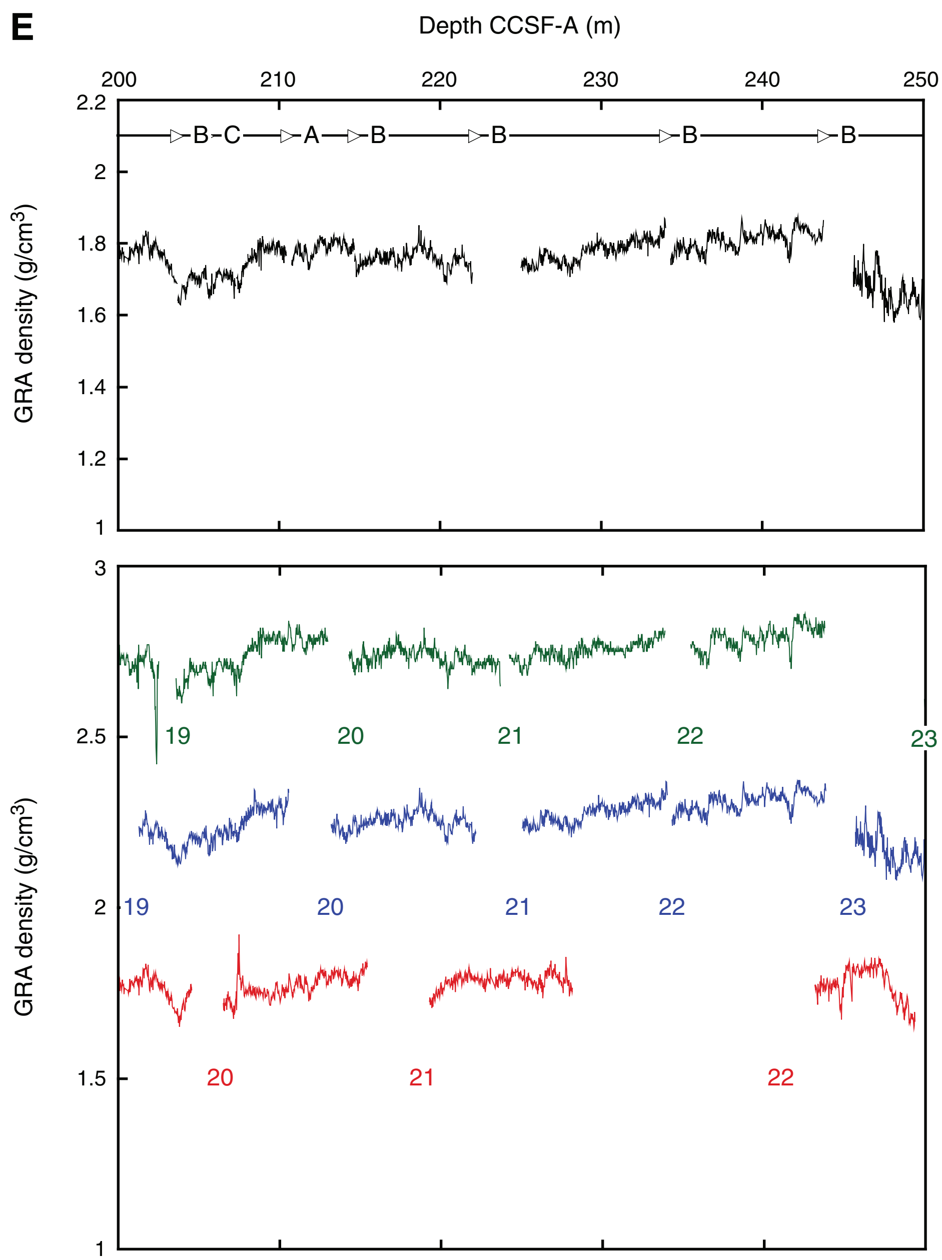

Figure F34 (continued). **F.** 250–300 m CCSF-A. (**Continued on next page.**)

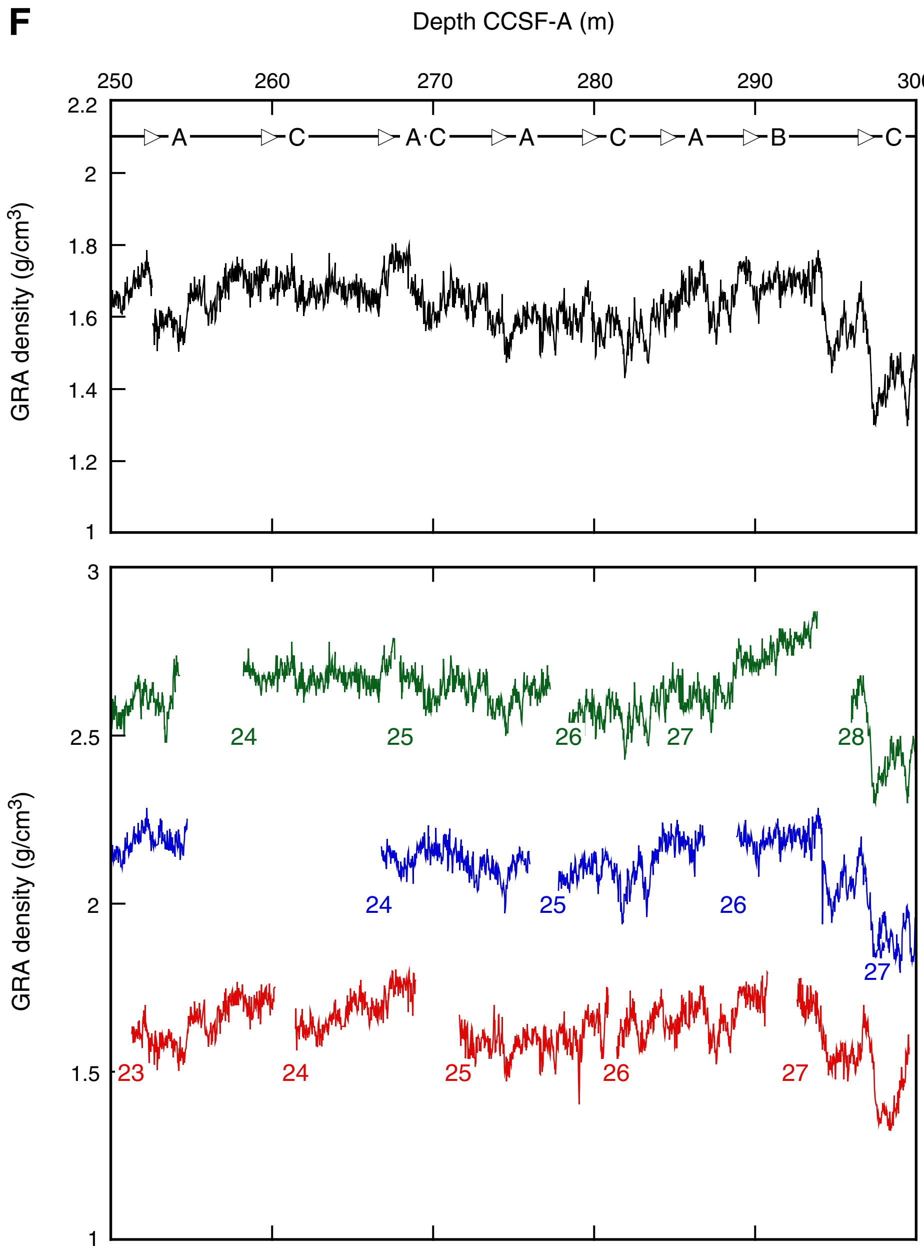

Figure F34 (continued). **G.** 300–350 m CCSF-A.

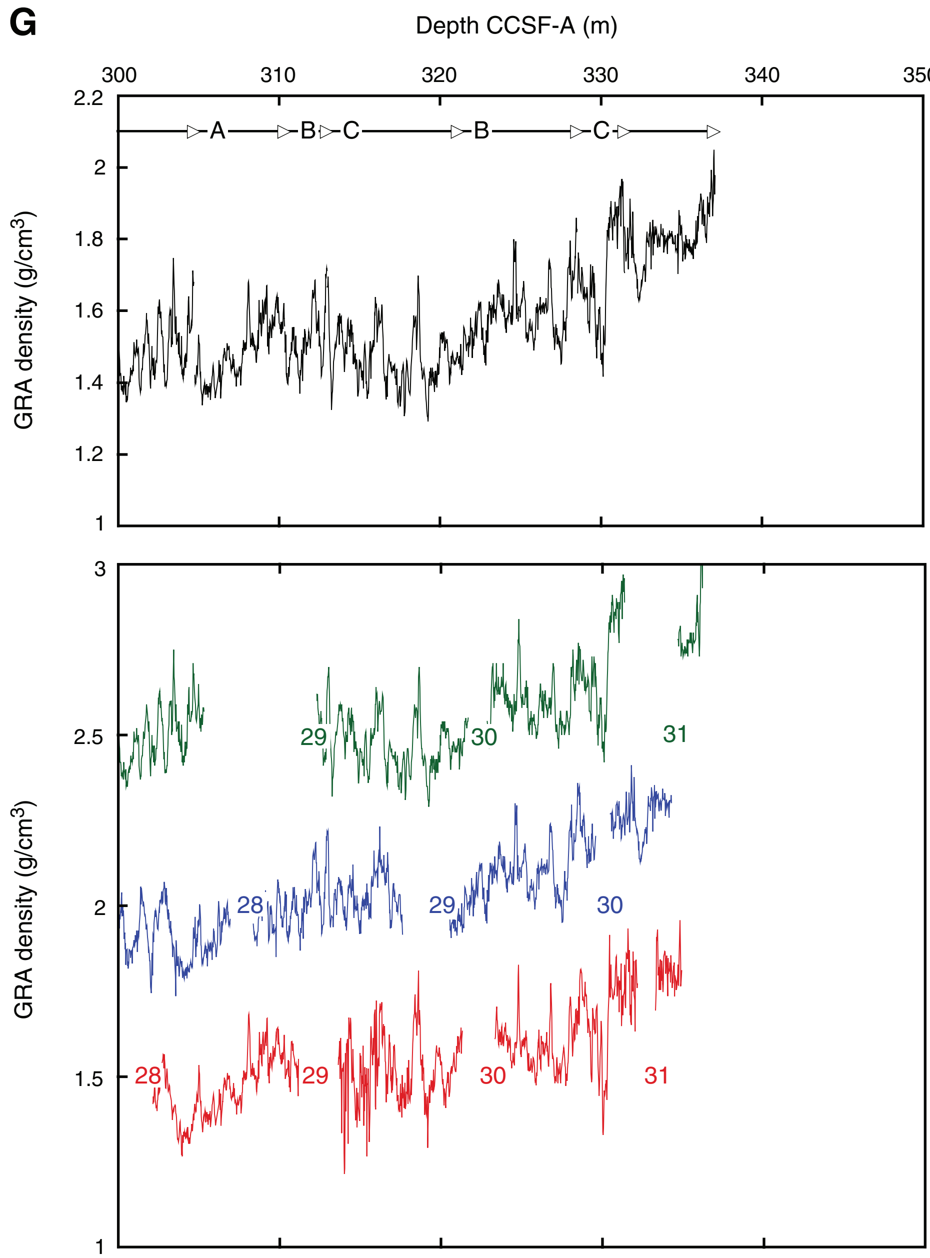

Figure F35. CSF depth vs. CCSF-A depth for tops of cores, Site U1334. Growth factor = slope of the regression line. On average, CCSF-A depth of spliced section is 16% greater than CSF depth.

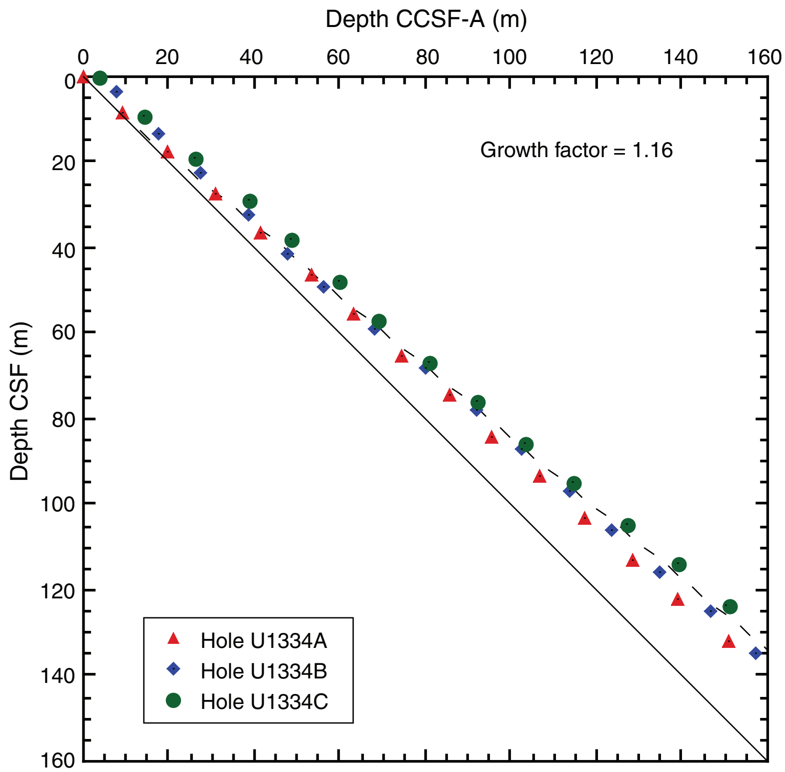

Figure F36. Heat flow calculation, Site U1334. **A.** Sediment temperatures, Hole U1334B. **B.** Thermal resistance based on laboratory thermal conductivity data, Hole U1334A. **C.** Bullard plot where heat flow is calculated from a linear fit of the temperature data. APCT-3 = advanced piston corer temperature tool.

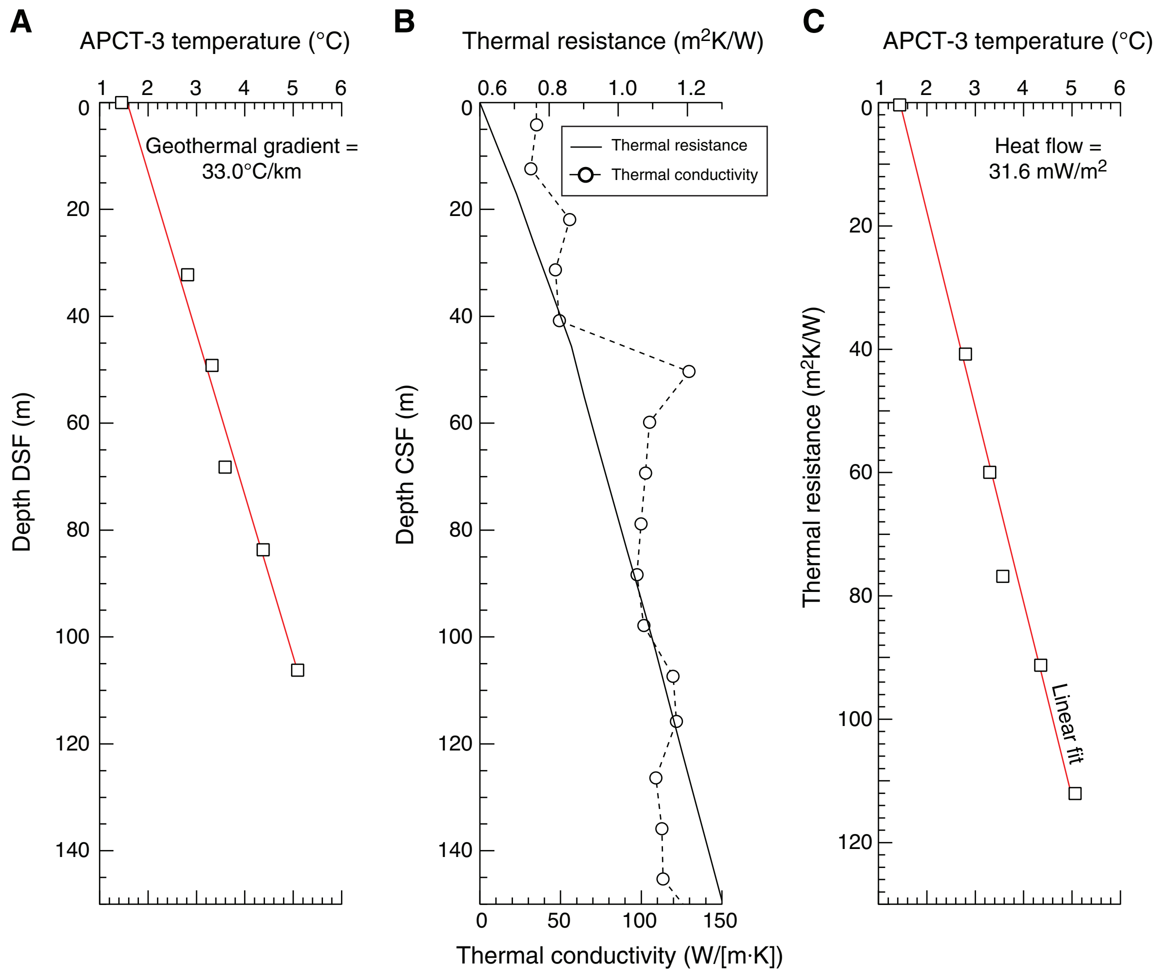

Table T1. Coring summary, Site U1334. (See table notes.) (Continued on next two pages.)

Site U1334
Time on site (h): 177.6 (1222 h, 6 April–2200 h, 13 April 2009)

Hole U1334A
Latitude: 7°59.998′N
Longitude: 131°58.394′W
Time on hole (h): 57.6 (1222 h, 6 April–2150 h, 8 April 2009)
Seafloor (drill pipe measurement below rig floor, m DRF): 4799.3
Distance between rig floor and sea level (m): 11.4
Water depth (drill pipe measurement from sea level, mbsl): 4789.9
Total depth (drill pipe measurement from rig floor, m DRF): 5084.8
Total penetration (drilling depth below seafloor, m DSF): 285.5
Total length of cored section (m): 285.5
Total core recovered (m): 288.8
Core recovery (%): 102
Total number of cores: 32

Hole U1334B
Latitude: 7°59.998′N
Longitude: 131°58.407′W
Time on hole (h): 44.8 (2150 h, 8 April –1840 h, 10 April 2009)
Seafloor (drill pipe measurement below rig floor, m DRF): 4799.3
Distance between rig floor and sea level: 11.4 m
Water depth (drill pipe measurement from sea level, mbsl): 4787.9
Total depth (drill pipe measurement from rig floor, m DRF): 5084.7
Total penetration (drilling depth below seafloor, m DSF): 285.4
Total length of cored section (m): 281.7
Total core recovered (m): 294.6
Core recovery (%): 105
Total number of cores: 31

Hole U1334C
Latitude: 7°59.998′N
Longitude: 131°58.422′W
Time on hole (h): 75.3 (1840 h, 10 April–2200 h, 13 April 2009)
Seafloor (drill pipe measurement below rig floor, m DRF): 4801.0
Distance between rig floor and sea level: 11.4 m
Water depth (drill pipe measurement from sea level, mbsl): 4789.6
Total depth (drill pipe measurement from rig floor, m DRF): 5081.7
Total penetration (drilling depth below seafloor, m DSF): 280.7
Total length of cored section (m): 280.7
Total core recovered (m): 285.8
Core recovery (%): 102
Total number of cores: 32

			Depth DSF (m)			Depth CSF (m)			
Core	Date (2009)	Local time (h)	Top of cored interval	Bottom of cored interval	Interval advanced (m)	Top of cored interval	Bottom of cored interval	Length of core recovered (m)	Recovery (%)
320-U1334A-									
1H	7 Apr	0110	0.0	8.2	8.2	0.00	8.24	8.24	100
2H	7 Apr	0215	8.2	17.7	9.5	8.20	18.16	9.96	105
3H	7 Apr	0345	17.7	27.2	9.5	17.70	27.70	10.00	105
4H	7 Apr	0450	27.2	36.7	9.5	27.20	37.23	10.03	106
5H	7 Apr	0550	36.7	46.2	9.5	36.70	46.83	10.13	107
6H	7 Apr	0740	46.2	55.7	9.5	46.20	56.25	10.05	106
7H	7 Apr	0845	55.7	65.2	9.5	55.70	65.71	10.01	105
8H	7 Apr	0945	65.2	74.7	9.5	65.20	75.11	9.91	104
9H	7 Apr	1050	74.7	84.2	9.5	74.70	84.79	10.09	106
10H	7 Apr	1155	84.2	93.7	9.5	84.20	94.00	9.80	103
11H	7 Apr	1300	93.7	103.2	9.5	93.70	103.80	10.10	106
12H	7 Apr	1410	103.2	112.7	9.5	103.20	112.66	9.65	100
13H	7 Apr	1530	112.7	122.2	9.5	112.70	122.60	9.90	104
14H	7 Apr	1620	122.2	131.7	9.5	122.20	132.01	9.81	103
15H	7 Apr	1720	131.7	141.2	9.5	131.70	141.25	9.55	101
16H	7 Apr	1830	141.2	150.7	9.5	141.20	149.62	8.42	89
17H	7 Apr	1945	150.7	160.2	9.5	150.70	160.75	8.31	106
18H	7 Apr	2200	160.2	169.7	9.5	160.20	170.22	10.02	105
19H	7 Apr	2310	169.7	179.2	9.5	169.70	178.54	8.84	93
20H	8 Apr	0050	179.2	188.7	9.5	179.20	188.68	9.48	100
21H	8 Apr	0245	188.7	198.2	9.5	188.70	198.53	9.83	103
22H	8 Apr	0445	198.2	206.9	8.7	198.20	206.91	8.71	100

Table T1 (continued). (Continued on next page.)

Core	Date (2009)	Local time (h)	Depth DSF (m) Top of cored interval	Depth DSF (m) Bottom of cored interval	Interval advanced (m)	Depth CSF (m) Top of cored interval	Depth CSF (m) Bottom of cored interval	Length of core recovered (m)	Recovery (%)
23X	8 Apr	0630	206.9	214.5	7.6	206.90	216.22	9.32	123
24X	8 Apr	0745	214.5	224.1	9.6	214.50	224.27	9.77	102
25X	8 Apr	0905	224.1	233.6	9.5	224.10	233.84	9.74	103
26X	8 Apr	1030	233.6	243.2	9.6	233.60	243.41	9.81	102
27X	8 Apr	1200	243.2	252.8	9.6	243.20	250.79	7.59	79
28X	8 Apr	1330	252.8	262.4	9.6	252.80	262.76	9.96	104
29X	8 Apr	1455	262.4	272.1	9.7	262.40	272.05	9.65	99
30X	8 Apr	1615	272.1	281.8	9.7	272.10	281.75	9.65	99
31X	8 Apr	1800	281.8	285.0	3.2	281.80	283.94	2.14	67
32X	8 Apr	2005	285.0	285.5	0.5	285.00	285.36	0.36	72
				Advanced total:	285.5			288.83	101
				Total interval cored:	285.5				
320-U1334B-									
1H	8 Apr	2350	3.7	13.2	9.5	3.70	13.72	10.02	105
2H	9 Apr	0100	13.2	22.7	9.5	13.20	23.08	9.88	104
3H	9 Apr	0225	22.7	32.2	9.5	22.70	32.87	10.17	107
4H	9 Apr	0330	32.2	41.7	9.5	32.20	41.96	9.76	103
5H	9 Apr	0450	41.7	49.2	7.5	41.70	50.96	9.26	123
6H	9 Apr	0600	49.2	58.7	9.5	49.20	59.23	10.03	106
7H	9 Apr	0715	58.7	68.2	9.5	58.70	68.91	10.21	107
8H	9 Apr	0820	68.2	77.7	9.5	68.20	78.07	9.87	104
9H	9 Apr	0935	77.7	87.2	9.5	77.70	87.73	10.03	106
10H	9 Apr	1040	87.2	96.7	9.5	87.20	97.25	10.05	106
11H	9 Apr	1200	96.7	106.2	9.5	96.70	106.74	10.04	106
12H	9 Apr	1305	106.2	115.7	9.5	106.20	116.19	9.99	105
13H	9 Apr	1425	115.7	125.2	9.5	115.70	125.64	9.94	105
14H	9 Apr	1530	125.2	134.7	9.5	125.20	135.35	10.15	107
15H	9 Apr	1645	134.7	144.2	9.5	134.70	144.64	9.94	105
16H	9 Apr	1755	144.2	153.7	9.5	144.20	154.27	10.07	106
17H	9 Apr	1905	153.7	163.2	9.5	153.70	163.73	10.03	106
18H	9 Apr	2030	163.2	172.7	9.5	163.20	173.28	10.08	106
19H	9 Apr	2220	172.7	182.2	9.5	172.70	182.69	9.99	105
20H	10 Apr	0010	182.2	191.7	9.5	182.20	191.58	9.38	99
21H	10 Apr	0145	191.7	201.2	9.5	191.70	201.31	9.61	101
22H	10 Apr	0335	201.2	210.7	9.5	201.20	211.13	9.93	105
23X	10 Apr	0515	210.7	219.0	8.3	210.70	220.48	9.78	118
24X	10 Apr	0720	219.0	228.6	9.6	219.00	228.73	9.73	101
25X	10 Apr	0825	228.6	238.2	9.6	228.60	239.10	9.82	102
26X	10 Apr	0935	238.2	247.8	9.6	238.20	247.90	9.70	101
27X	10 Apr	1045	247.8	257.4	9.6	247.80	257.61	9.81	102
28X	10 Apr	1200	257.4	267.0	9.6	257.40	267.34	9.94	104
29X	10 Apr	1325	267.0	276.6	9.6	267.00	277.03	10.03	104
30X	10 Apr	1510	276.6	283.9	7.3	276.60	283.83	7.23	99
31X	10 Apr	1640	283.9	285.4	1.5	283.90	284.02	0.12	8
				Advanced total:	281.7			294.59	105
				Total interval cored:	281.7				
320-U1334C-									
1H	10 Apr	2020	0.0	9.5	9.5	0.00	9.83	9.83	103
2H	10 Apr	2220	9.5	19.0	9.5	9.50	18.72	9.22	97
3H	10 Apr	2330	19.0	28.5	9.5	19.00	28.12	9.12	96
4H	11 Apr	0035	28.5	38.0	9.5	28.50	38.31	9.81	103
5H	11 Apr	0140	38.0	47.5	9.5	38.00	48.03	10.03	106
6H	11 Apr	0240	47.5	57.0	9.5	47.50	57.28	9.78	103
7H	11 Apr	0340	57.0	66.5	9.5	57.00	66.64	9.64	101
8H	11 Apr	0440	66.5	76.0	9.5	66.50	76.36	9.86	104
9H	11 Apr	0540	76.0	85.5	9.5	76.00	85.82	9.82	103
10H	11 Apr	0655	85.5	95.0	9.5	85.50	95.17	9.67	102
11H	11 Apr	0800	95.0	104.5	9.5	95.00	104.62	9.62	101
12H	11 Apr	0910	104.5	114.0	9.5	104.50	114.28	9.78	103
13H	11 Apr	1005	114.0	123.5	9.5	114.00	123.85	9.85	104
14H	11 Apr	1105	123.5	133.0	9.5	123.50	133.03	9.53	100
15H	11 Apr	1210	133.0	142.5	9.5	133.00	142.59	9.50	100
16H	11 Apr	1315	142.5	152.0	9.5	142.50	151.94	9.44	99
17H	11 Apr	1420	152.0	161.5	9.5	152.00	161.52	9.52	100
18H	11 Apr	1525	161.5	171.0	9.5	161.50	171.19	9.69	102
19H	11 Apr	1650	171.0	180.5	9.5	171.00	180.76	9.76	103

Table T1 (continued).

Core	Date (2009)	Local time (h)	Depth DSF (m) Top of cored interval	Depth DSF (m) Bottom of cored interval	Interval advanced (m)	Depth CSF (m) Top of cored interval	Depth CSF (m) Bottom of cored interval	Length of core recovered (m)	Recovery (%)
20H	11 Apr	1800	180.5	190.0	9.5	180.50	190.02	9.52	100
21H	11 Apr	2010	190.0	199.5	9.5	190.00	199.97	9.97	105
22H	11 Apr	2150	199.5	209.0	9.5	199.50	209.41	9.91	104
23X	11 Apr	2315	209.0	214.0	5.0	209.00	213.61	4.61	92
24X	12 Apr	0040	214.0	223.6	9.6	214.00	223.89	9.89	103
25X	12 Apr	0200	223.6	233.2	9.6	223.60	233.35	9.75	102
26X	12 Apr	0315	233.2	239.2	6.0	233.20	240.54	7.34	122
27X	12 Apr	0440	239.2	248.8	9.6	239.20	248.16	8.96	93
28X	12 Apr	0610	248.8	258.4	9.6	248.80	258.62	9.82	102
29X	12 Apr	0730	258.4	268.0	9.6	258.40	268.10	9.70	101
30X	12 Apr	0855	268.0	277.7	9.7	268.00	277.96	9.96	103
31X	12 Apr	1115	277.7	279.7	2.0	277.70	280.11	2.41	121
32X	12 Apr	1310	279.7	280.2	0.5	279.70	280.17	0.47	94
33X	12 Apr	1505	280.2	280.7	0.5	280.20	280.20	0.00	0
				Advanced total:	280.7			285.78	102
				Total interval cored:	280.7				

Notes: DRF = drilling depth below rig floor, DSF = drilling depth below seafloor, CSF = core depth below seafloor. H = APC core, X = XCB core. Local time = UTC – 10 h.

Table T2. Lithologic unit boundaries, Site U1334. (See table notes.)

Unit	Core, section, interval (cm)	Depth CSF (m)	Core, section, interval (cm)	Depth CSF (m)	Core, section, interval (cm)	Depth CSF (m)
	320-U1331A-		320-U1331B-		320-U1331C-	
I	5H-CC,25	46.76	5H-3, 55	45.25	5H-1, 65	38.7
II	27X-2, 26	244.96	26X-4, 124	243.94	27X-6, 96	247.66
III	31X-2, 25*	283.55	31X-5, 30*	282.9	31X-2, 40	279.41
IV	32X-CC, 43*	285.43	31X-CC, 9*	283.99	32X-CC, 43*	280.13
V	32X-CC, 40*	285.4	31X-CC, 11*	284.01	32X-CC, 49*	280.19

Notes: Interval/depth are given for basal boundary of each unit. * = unit extends through at least given interval and depth, but boundary was not cored.

Table T3. Calcareous nannofossil datums, Site U1334. (See table notes.)

Core, section, interval (cm)		Marker species	Age (Ma)	Depth CSF (m)			
Top	Bottom			Top	Bottom	Midpoint	±
320-U1334A-	320-U1334A-						
	2H-6, 120	*Coronocyclus nitescens* present	>12.12		16.90*		
	2H-6, 120	*Calcidiscus premacintyrei* present	>12.45		16.90*		
3H-2, 15	3H-3, 50	Tc *Cyclicargolithus floridanus*	13.33	19.35	21.20	20.28	0.92
3H-4, 50	3H-5, 50	T *Sphenolithus heteromorphus*	13.53	22.7	24.20	23.45	0.75
3H-CC	4H-2, 70	Tc *Discoaster deflandrei*	15.66	27.65	29.40	28.53	0.88
3H-CC	4H-2, 70	B *Discoaster petaliformis*	15.70	27.65	29.40	28.53	0.88
4H-6, 20	4H-7, 15	B *Sphenolithus heteromorphus*	17.71	34.90	36.35	35.63	0.73
5H-3, 100	5H-4, 120	T *Triquetrorhabdulus carinatus*	18.28	40.70	42.40	41.55	0.85
9H-3, 20	9H-4, 100	Tc *Triquetrorhabdulus carinatus*	22.1	77.90	80.20	79.05	1.15
9H-7, 30	9H-CC	B *Sphenolithus disbelemnos*	22.8	84.00	84.74	84.37	0.37
10H-7, 30	10H-CC	T *Sphenolithus delphix*	23.1	93.50	93.95	93.73	0.23
11H-1, 20	11H-2, 20	B *Sphenolithus delphix*	23.2	94.70	96.20	95.45	0.75
12H-7, 30	12H-CC	T *Sphenolithus ciperoensis*	24.4	112.27	112.58	112.43	0.16
12H-CC	13H-1, 45	X *T. longus/T. carinatus*	24.7	112.58	113.15	112.87	0.29
12H-CC	13H-1, 45	Tc *Cyclicargolithus abisectus*	24.7	112.58	113.15	112.87	0.29
16H-6, 40	16H-CC	T *Sphenolithus distentus*	26.8	149.10	149.57	149.34	0.23
16H-6, 40	16H-CC	T *Sphenolithus predistentus*	26.9	149.10	149.57	149.34	0.23
18H-CC	19H-CC	B *Sphenolithus ciperoensis*	27.1	170.17	178.49	174.33	4.16
19H-CC	20H-CC	T *Sphenolithus pseudoradians*	28.8	178.49	188.63	183.56	5.07
21H-CC	22H-2, 70	B *Sphenolithus distentus*	30.0	198.48	200.40	199.44	0.96
24X-CC	25X-1, 80	T *Reticulofenestra umbilicus*	32.0	224.22	224.90	224.56	0.34
26X-CC	27X-2, 11	T *Isthmolithus recurvus*	32.5	243.36	244.81	244.09	0.72
26X-2, 100	26X-3, 100	T *Coccolithus formosus*	32.9	236.10	237.60	236.85	0.75
27X-5, 150	27X-CC	T *Discoaster saipanensis*	34.4	249.70	250.76	250.23	0.53
28X-2, 123	28X-CC	T *Reticulofenestra reticulata*	35.2	255.53	262.62	259.08	3.55
29X-CC	30X-1, 66	B *Isthmolithus recurvus*	36.6	272.00	272.76	272.38	0.38
30X-1, 66	30X-2, 74	T *Chiasmolithus oamaruensis*	37.0	272.76	274.34	273.55	0.79
30X-1, 66	30X-2, 74	T *Chiasmolithus grandis*	37.1	272.76	274.34	273.55	0.79
	32X-CC	*Dictyococcites bisectus* present	<38.0		285.21†		

Notes: Tc = top common, T = top, B = bottom, X = abundance crossover. * = occurrence of taxa in the uppermost nannofossiliferous sample provides a maximum estimate of bioevent depth only, † = occurrence of taxa in the lowest sample provides a maximum estimate of the age.

Table T4. Radiolarian datums, Site U1334. (**See table note.**) (**Continued on next page.**)

Geologic age	Zone	Marker species	Age (Ma)	Core, section, interval (cm) Top	Bottom	Depth CSF (m) Top	Bottom	Midpoint	±
				320-U1334A-	320-U1334A-				
	RN7	T *D. petterssoni*	8.63	1H-4, 105–107	1H-CC	5.56	8.19	6.88	1.32
		D. petterssoni > *D. hughesi*	8.76						
	RN6	B *S. berminghami*	8.76	1H-CC	2H-2, 105–107	8.19	10.76	9.48	1.29
		B *D. hughesi*	8.99	1H-CC	2H-2, 105–107	8.19	10.76	9.48	1.29
		B *D. petterssoni*	12.11	2H-4, 105–107	2H-CC	13.76	18.11	15.94	2.18
		B *L. neotera*	12.95	2H-CC	3H-2, 105–107	18.11	20.25	19.18	1.07
	RN5	T *S. armata*	13.50	3H-2, 105–107	3H-4, 105–107	20.25	23.25	21.75	1.50
		T *A. octopylus*	13.88	3H-2, 105–107	3H-4, 105–107	20.25	23.25	21.75	1.50
		D. dentata > *D. alata*	14.78	3H-4, 105–107	3H-CC	23.25	27.65	25.45	2.20
		B *D. alata*	15.08	3H-CC	4H-2, 105–107	27.65	29.76	28.71	1.06
		B *L. parkerae*	15.03	4H-2, 105–107	4H-4, 105–107	29.76	32.76	31.26	1.50
	RN4	T *C. cingulata*	15.13	4H-2, 105–107	4H-4, 105–107	29.76	32.76	31.26	1.50
		T *L. elongata*	15.15	4H-4, 105–107	4H-CC	32.76	37.18	34.97	2.21
		B *L. renzae*	16.77	4H-CC	5H-2, 104–106	37.18	39.24	38.21	1.03
		B *C. costata*	17.49	5H-2, 104–106	5H-4, 104–106	39.24	42.24	40.74	1.50
	RN3	B *D. dentata*	17.72	5H-2, 104–106	5H-4, 104–106	39.24	42.24	40.74	1.50
		B *L. stauropora*	17.72	5H-4, 104–106	5H-CC	42.24	46.78	44.51	2.27
lower Miocene		B *S. wolffii*	18.57	5H-4, 104–106	5H-CC	42.24	46.78	44.51	2.27
		B *D. forcipata*	18.61	5H-4, 104–106	5H-CC	42.24	46.78	44.51	2.27
		T *D. simplex*	18.69	5H-4, 104–106	5H-CC	42.24	46.78	44.51	2.27
	RN2	T *D. praeforcipata*	19.77	6H-4, 104–106	6H-CC	51.74	56.20	53.97	2.23
		B *D. simplex*	20.34	7H-2, 105–107	7H-4, 105–107	58.25	61.25	59.75	1.50
		B *S. delmontensis*	20.68	7H-2, 105–107	7H-4, 105–107	58.25	61.25	59.75	1.50
		T *L. pegetrum*	20.89	7H-4, 105–107	7H-CC	61.25	65.66	63.46	2.20
		T *T. annosa*	21.38	8H-4, 105–107	8H-CC	70.75	75.06	72.91	2.16
		B *C. virginis*	21.39	7H-CC	8H-2, 105–107	65.66	67.76	66.71	1.05
		B *L. leptetrum*	21.42	7H-CC	8H-2, 105–107	65.66	67.76	66.71	1.05
	RN1	T *E. mitodes*	21.95	9H-2, 105–107	9H-4, 105–107	77.25	80.25	78.75	1.50
		B *C. serrata*	22.04	9H-2, 105–107	9H-4, 105–107	77.25	80.25	78.75	1.50
		B *C. cornuta*	22.26	10H-2, 105–107	10H-4, 105–107	86.75	89.75	88.25	1.50
		B *C. tetrapera*	22.35	10H-2, 105–107	10H-4, 105107	86.75	89.75	88.25	1.50
		T *A. gracilis*	22.62	10H-2, 105–107	10H-4, 105–107	86.75	89.75	88.25	1.50
		B *D. bassanii*	22.93	10H-2, 105–107	10H-4, 105–107	86.75	89.75	88.25	1.50
		B *E. diaphanes*	22.95	10H-4, 105–107	10H-CC	89.75	93.95	91.85	2.10
		T *D. cyclacantha*	22.98	10H-CC	11H-2, 105–107	93.95	96.25	95.10	1.15
	RP22	T *D. riedeli*	23.01	10H-CC	11H-2, 105–107	93.95	96.25	95.10	1.15
		B *D. cyclacantha*	23.29	11H-2, 105–107	11H-4, 105–107	96.25	99.25	97.75	1.50
		T *D. papilio*	23.31	10H-CC	11H-2, 105–107	93.95	96.25	95.10	1.15
		T *L. longicornuta*	24.12	11H-4, 105–107	11H-CC	99.25	103.75	101.50	2.25
		T *A. octopylus*	24.38	13H-2, 105–107	13H-4, 105–107	114.25	117.25	115.75	1.50
		T *L. apodora*	24.50	13H-2, 105–107	13H-4, 105–107	114.25	117.25	115.75	1.50
		B *L. elongata*	25.05	13H-4, 105–107	13H-CC	117.25	122.55	119.90	2.65
		B *A. octopylus*	25.09						
		B *D. praeforcipata*	25.27	13H-CC	14H-2, 105–107	122.55	124.75	123.65	1.10
upper Oligocene		B *C. robusta*	25.27	14H-4, 105–107	14H-CC	127.75	131.96	129.86	2.11
		B *D. tubaria*	25.27	13H-CC	14H-2, 105–107	122.55	124.75	123.65	1.10
		B *L. longicornuta*	25.29	14H-4, 105–107	14H-CC	127.25	131.96	129.61	2.36
		B *D. scambos*	25.33						
	RP21	B *L. apodora*	25.55	15H-4, 105–107	15H-CC	137.25	141.20	139.23	1.97
		T *D. circulus*	26.17	16H-2, 104–106	16H-4, 104–106	143.74	146.74	145.24	1.50
		B *D. riedeli*	26.20	16H-2, 104–106	16H-4, 104–106	143.74	146.74	145.24	1.50
		T *E. plesiodiaphanes*	26.40	16H-2, 104–106	16H-4, 104–106	143.74	146.74	145.24	1.50
		T *L. angusta*	27.68	17H-CC	18H-2, 105–107	159.97	162.70	161.34	1.36
		T *T. setanios*	28.21	19H-2, 105–107	19H-4, 105–107	171.51	174.51	173.01	1.50
		B *T. annosa*	28.33	20H-CC	21H-2, 105–107	188.63	191.25	189.94	1.31
lower Oligocene		B *D. ateuchus*							
		T. triceros > *D. ateuchus*	28.60	20H-CC	21H-2, 105–107	188.63	191.25	189.94	1.31

Table T4 (continued).

Geologic age	Zone	Marker species	Age (Ma)	Core, section, interval (cm)		Depth CSF (m)			
				Top	Bottom	Top	Bottom	Midpoint	±
lower Oligocene	RP20	B *E. mitodes*	29.41	21H-4, 105–107	21H-CC	194.25	198.48	196.37	2.11
		B *T. setanios*	29.51	21H-CC	22H-2, 105–107	198.48	200.75	199.62	1.14
		B *D. circulus*	29.96	21H-4, 105–107	21H-CC	194.25	198.48	196.37	2.11
		T *T. tuberosa*	30.13	22H-CC	23H-2, 98–100	206.86	209.38	208.12	1.26
		T *L. crux*	30.13	23H-2, 98–100	23H-4, 98–100	209.38	212.38	210.88	1.50
		B *E. plesiodiaphanes*	30.37	23H-4, 98–100	23H-CC	212.38	216.17	214.28	1.89
		T *L. oberhaensliae*	30.74	23H-CC	24H-2, 105–107	216.17	217.05	216.61	0.44
		B *D. spinosa*	30.84	24H-4, 105–107	24H-CC	220.05	224.22	222.14	2.08
		T *D. pseudopaplilio*	30.84	24H-CC	25H-2, 105–107	224.22	226.65	225.44	1.22
		T *C. gravida*	30.89	25H-2, 105–107	25H-4, 105–107	226.65	229.65	228.15	1.50
		B *L. crux*	31.00						
		B *T. tuberosa*	31.00	26H-2, 104–106	26H-4, 104–106	236.14	239.14	237.64	1.50
		B *D. pseudopaplilio*	31.00	26H-4, 104–106	26H-CC	239.14	243.36	241.25	2.11
		B *C. gravida*	31.01	26H-4, 104–106	26H-CC	239.14	243.36	241.25	2.11
		T *T. triacantha*	33.34						
		T *L. aristotelis* gr.	33.51	26H-CC	27H-CC	243.36	250.76	247.06	3.70
		T *C. hispida*	33.62	26H-CC	27H-CC	243.36	250.76	247.06	3.70
		T *C. ornatum*	33.62	26H-CC	27H-CC	243.36	250.76	247.06	3.70
		T *L. hadra*	33.75	26H-CC	27H-CC	243.36	250.76	247.06	3.70
		T *L. amphitrite*	33.75	26H-CC	27H-CC	243.36	250.76	247.06	3.70
		T *L. babylonis*	33.75	26H-CC	27H-CC	243.36	250.76	247.06	3.70
		L. aristotelis > *L. angusta*	33.82	26H-CC	27H-CC	243.36	250.76	247.06	3.70
upper Eocene	RP19	T *D. copetata*	33.84	26H-4, 104–106	26H-CC	239.14	243.36	241.25	2.11
		B *L. angusta*	34.13	26H-CC	27H-CC	243.36	250.76	247.06	3.70
		T *C. bandyca*	34.62	28H-2, 126–127	28H-3, 105–107	255.56	256.85	256.21	0.65
		T *C. turris*	34.83	28H-2, 126–127	28H-3, 105–107	255.56	256.85	256.21	0.65
		T *E. fistuligerum*	34.93						
		T *T. bromia*	33.94	28H-2, 126–127	28H-3, 105–107	255.56	256.85	256.21	0.65
		T *T. lochites*	34.13	28H-2, 126–127	28H-3, 105–107	255.56	256.85	256.21	0.65
		T *C. azyx*	35.07	28H-2, 126–127	28H-3, 105–107	255.56	256.85	256.21	0.65
		T *T. tetracantha*	35.30	28H-2, 126–127	28H-3, 105–107	255.56	256.85	256.21	0.65
	RP18	B *L. hadra*	35.34	28H-CC	29X-2, 50–52	262.62	263.85	263.24	0.62
		B *C. bandyca*	36.74	29X-4, 104–106	29X-CC	266.45	272.00	269.23	2.78

Note: T = top, B = bottom.

Table T5. Preservation and relative abundance of radiolarians, Hole U1334A. This table is available in an **oversized format.**

Table T6. Preservation and relative abundance of radiolarians, Hole U1334B. (See table notes.) (Continued on next page.)

Core, section	Radiolarian zone	Abundance	Preservation	Mixing	*Anthocyrtidium marieae*	*Artophormis barbadensis*	*Artophormis gracilis*	*Calocyclas bandyca*	*Calocyclas turris*	*Calocycletta anekathen*	*Calocycletta caepa*	*Calocycletta robusta*	*Calocycletta serrata*	*Calocycletta virginis*	*Carpocanopsis bramlettei*	*Carpocanopsis cingulata*	*Cryptocarpium azyx*	*Cryptocarpium ornatum*	*Cyrtocapsella cornuta*	*Cyrtocapsella tetrapera*	*Dictyoprora armadillo*	*Dictyoprora mongolfieri*	*Didymocyrtis bassanii*	*Didymocyrtis prismatica*
320-U1334B-																								
1H-CC																			R	R				
1H-CC		B									R			F					R	R				
2H-CC	RN5	C	P	2										C	R	R			R	R				
3H-CC	RN4	C	P											C	R	R			F	R				
4H-CC	RN3	C	P									R		R	R	R			F	R				
5H-CC		C	M									F		R	R	R			F	F			R	R
6H-CC	RN2	C	M									F	R	R	R	R			F	F			R	R
7H-CC		C	M									F	R	R	R	R			F	F			R	R
8H-CC	RN1	C	M									F	R			R			F	F			R	R
9H-CC		A	G		R		F					F				R								R
10H-CC	RP22	A	G				R					F				R								R
11H-CC		A	G				R					F				VR?								R
12H-CC		A	G				R					F												R
13H-CC		A	G				R					—												R
14H-CC		A	G				R																	R
15H-CC	RP21	C	P				R																	R
16H-CC		C	P				R																	R
17H-CC		C	P				R																	R
18H-CC		A	G	1			R																	R
19H-CC		A	G	1			R																	R
20H-CC							R																	R
21H-CC		A	G				R																	R
22H-CC	RP20	A	G				R																	
23H-CC		A	G				F																	
24H-CC		A	G				F				R													
25H-CC		A	G				F																	
26H-CC	RP19	A	G			R	R			C								C			R	R		
27H-CC	RP18	F	M					R	R	R							R	R			R	R		
28H-CC	RP17	F	P						R								R	R			R	R		
29H-CC		B																						

Core, section	*Didymocyrtis tubaria*	*Didymocyrtis violina*	*Dorcadospyris ateuchus*	*Dorcadospyris circulus*	*Dorcadospyris copelata*	*Dorcadospyris forcipata*	*Dorcadospyris papilio*	*Dorcadospyris praeforcipata*	*Dorcadospyris pseudopapilio*	*Dorcadospyris quadripes*	*Dorcadospyris scambos*	*Dorcadospyris simplex* s.s.	*Dorcadospyris spinosa*	*Eucyrtidium diaphanes*	*Eucyrtidium mitodes*	*Eucyrtidium plesiodiaphanes*	*Liriospyris longicornuta*	*Lithocyclia angusta*	*Lithocyclia aristotelis* gr.	*Lithocyclia crux*	*Lophocyrtis hadra*	*Lophocyrtis jacchia*	*Lophocyrtis milowi*	*Lophocyrtis oberhaensliae*	*Lophocyrtis pegetrum*
320-U1334B-																									
1H-CC																									
1H-CC																									
2H-CC														R											
3H-CC	R	R				R								R											
4H-CC	R	R				R					R			R											
5H-CC	R	R	VR			R		R			R	R		F											R
6H-CC		R	VR					R			R	R		F											R
7H-CC			R					R			R			F											R
8H-CC			R					R			R			F	R										R
9H-CC	R		R					R			R			R	R										R
10H-CC	R		R				—	R			R			—	R										R
11H-CC	R		R				R	R			R			—	R										R
12H-CC	R		R				R	R			R				R										R
13H-CC			R					—			R				R		R								R
14H-CC			R				—				—				R		—								R
15H-CC			R												R	—									R
16H-CC			R												R	R									R
17H-CC			R	R											R	R									R
18H-CC			R	R											R	R		R							R
19H-CC				R											—	R		R							R
20H-CC			R	R												F		F					R		R
21H-CC				F											R	F		R					R		R
22H-CC																R		R		R			R		
23H-CC										R			R					R		R			R	R	
24H-CC					R				R	R								R		R			R	R	
25H-CC					R													R		R			R		
26H-CC					R														R		R	R			
27H-CC					R														R		R	R			
28H-CC					R														R						
29H-CC																									

Notes: Abundance: A = abundant, C = common, F = frequent, R = rare, VR = very rare, B = barren, — = undetermined. Preservation: G = good, M = moderate, P = poor. Mixing: blank = no mixing of older specimens detected, 1 = 1–3 reworked specimens detected, 2 = 3–10 reworked specimens detected.

Table T6 (continued).

Core, section	Radiolarian zone	Abundance	Preservation	Mixing	*Lychnocanoma amphitrite*	*Lychnocanoma apodora*	*Lychnocanoma babylonis*	*Lychnocanoma elongata*	*Lychnocanoma turgidum*	*Theocorys puriri*	*Theocyrtis annosa*	*Theocyrtis careotuberosa*	*Theocyrtis perysinos*	*Theocyrtis setanios*	*Theocyrtis tuberosa*	*Thyrsocyrtis bromia*	*Thyrsocyrtis krooni*	*Thyrsocyrtis lochites*	*Thyrsocyrtis tetracantha*	*Thyrsocyrtis triacantha*	*Tristylospyris triceros*	*Zealithapium mitra*
320-U1334B-																						
1H-CC																						
1H-CC		B																				
2H-CC	RN5	C	P	2																		
3H-CC	RN4	C	P																			
4H-CC	RN3	C	P					R														
5H-CC		C	M					F														
6H-CC	RN2	C	M					F														
7H-CC		C	M					F														
8H-CC	RN1	C	M					F			R											
9H-CC		A	G			R		F			R											
10H-CC	RP22	A	G					R														
11H-CC		A	G					R														
12H-CC		A	G					R														
13H-CC		A	G			R		—														
14H-CC		A	G			—																
15H-CC		C	P																			
16H-CC	RP21	C	P																			
17H-CC		C	P																			
18H-CC		A	G	1							R		R	R							R	
19H-CC		A	G	1									R	R							R	
20H-CC										R				R							R	
21H-CC		A	G							R				R							R	
22H-CC	RP20	A	G											R							R	
23H-CC		A	G											R	C						R	
24H-CC		A	G									R		R	C						R	
25H-CC		A	G									F			R						R	
26H-CC	RP19	A	G		R		R					R									R	R
27H-CC	RP18	F	M				R					R				R		F	F		R	
28H-CC	RP17	F	P				R		R			R				R		F	R		R	
29H-CC		B																				

Table T7. Preservation and relative abundance of radiolarians, Hole U1334C. (See table notes.) (Continued on next page.)

Core, section	Radiolarian zone	Abundance	Preservation	Mixing	*Acrocubus octopylus*	*Anthocyrtidium marieae*	*Artophormis barbadensis*	*Artophormis gracilis*	*Calocyclas turris*	*Calocycletta costata*	*Calocycletta robusta*	*Calocycletta virginis*	*Carpocanopsis bramlettei*	*Carpocanopsis cingulata*	*Centrobotrys gravida*	*Centrobotrys petrushevskayae*	*Cryptocarpium azyx*	*Cryptocarpium ornatum*	*Cyrtocapsella cornuta*	*Cyrtocapsella tetrapera*	*Dictyoprora armadillo*	*Dictyoprora mongolfieri*	*Didymocyrtis bassanii*	*Didymocyrtis prismatica*	*Didymocyrtis tubaria*	*Didymocyrtis violina*	*Dorcadospyris alata*	*Dorcadospyris ateuchus*	*Dorcadospyris circulus*	*Dorcadospyris cyclacantha*	*Dorcadospyris dentata*	*Dorcadospyris forcipata*	*Dorcadospyris ombros* (upper)	*Dorcadospyris papilio*	*Dorcadospyris praeforcipata*	*Dorcadospyris pseudopapilio*	*Dorcadospyris quadripes*	*Dorcadospyris riedeli*	*Dorcadospyris scambos*	*Dorcadospyris simplex* s.s.	*Eucyrtidium diaphanes*	*Eucyrtidium mitodes*	*Eucyrtidium plesiodiaphanes*	*Liriospyris longicornuta*	*Lithocyclia angusta*	*Lithocyclia aristotelis* gr.	*Lithocyclia crux*	*Lithopera neotera*	*Lithopera renzae*
320-U1334C-																																																	
1H-CC	RN5	F	P	3						VR																																							
2H-CC		C	M	3	VR	R				VR		—							F	F			R				R													R	—							VR	R
3H-CC	RN4	A	M	2	R	R				R		R	R	R					F	F			R	R		R	—				R	R								R	R								
4H-CC	RN3	A	M		—	R				—	F	R	R	R					F	F			R	R		VR?		—			—	R								R	R								
5H-CC	RN2	A	M			R					F	R	VR	R					F	F			R	R				VR				—									R								
6H-CC		A	M			R					F			R					F	F			R	R				VR							R?				R		R								
7H-CC	RN1	A	M			R					F			R					F	R			R	R				R							R				R		R								
8H-CC		A	M			R					F			R					F	R			R	R				R							R				R		R	—							
9H-CC	RP22	A	M			R		R			C			VR					—	—			R	R	R			R							R			R	R		R	R							
10H-CC		C	M					R			C													R	R			R		R					R			R	R			R							
11H-CC		C	M					R			C													R	R			R						R	R				R			R							
12H-CC		C	M					R			F													R				R						R	R				R			R		R					
13H-CC	RP21	C	M					R			R																	R						R	R				R			R	R	R					
14H-CC		C	M					R			—													R				R							—				—			R	—						
15H-CC		C	M					R																																		R	R						
16H-CC		C	M					R																																		R	R						
17H-CC		A	M					R								R								R				R	R													R	R		R				
18H-CC		A	M					R								R								R				R	R													R	R		R				
19H-CC		A	M					R								R								R				R	R													R	R		R				
20H-CC	RP20	A	M					R								R								R				—	F													—	F		R				
21H-CC		A	M					R								R								R				—	F													—	R		R				
22H-CC		C	M					R								R								—					—														R		R				
23H-CC		C	M					R								R																					R		R						R		R		
24H-CC		C	M					R																													R										R		
25H-CC		C	M					F							F																					R	R								R		R		
26H-CC		C	M					F							R																														R		R		
27H-CC		F	P					R										F																											R				
28H-CC	RP18	C	M	1				R									R	R			R	R											R													R			
29H-CC	RP17	F	M				R		F								R	R			R												VR													R			
30H-CC	B	B																																															

Notes: Abundance: A = abundant, C = common, F = frequent, R = rare, VR = very rare, B = barren, — = undetermined. Preservation: M = moderate, P = poor. Mixing: blank = no mixing of older specimens detected, 1 = 1–3 reworked specimens detected, 2 = 3–10 reworked specimens detected, 3 = >10 reworked specimens detected.

Table T7 (continued).

Core, section	Radiolarian zone	Abundance	Preservation	Mixing	*Lophocyrtis hadra*	*Lophocyrtis jacchia*	*Lophocyrtis leptetrum*	*Lophocyrtis milowi*	*Lophocyrtis oberhaensliae*	*Lophocyrtis pegetrum*	*Lychnocanoma amphitrite*	*Lychnocanoma apodora*	*Lychnocanoma babylonis*	*Lychnocanoma elongata*	*Lychnocanoma turgidum*	*Lychnodictyum audax*	*Stichocorys wolffii*	*Theocyrtis annosa*	*Theocyrtis careotuberosa*	*Theocyrtis perpumila*	*Theocyrtis perysinos*	*Theocyrtis setanios*	*Theocyrtis tuberosa*	*Thyrsocyrtis bromia*	*Thyrsocyrtis krooni*	*Thyrsocyrtis lochites*	*Thyrsocyrtis orthotenes*	*Thyrsocyrtis tetracantha*	*Thyrsocyrtis triacantha*	*Tristylospyris triceros*	*Zealithapium mitra*
320-U1334C-																															
1H-CC	RN5	F	P	3																											
2H-CC		C	M	3										VR	—		R														
3H-CC	RN4	A	M	2			R							R			F														
4H-CC	RN3	A	M				R							R			R														
5H-CC	RN2	A	M				R							R			—														
6H-CC		A	M				R			—				R				—													
7H-CC	RN1	A	M				—			R				R				R													
8H-CC		A	M							R				R				R													
9H-CC	RP22	A	M							R				F				F													
10H-CC		C	M							R				R				F													
11H-CC		C	M							R				R				F													
12H-CC		C	M							R		R		R				R													
13H-CC	RP21	C	M							R		R						F													
14H-CC		C	M							R		—						F													
15H-CC		C	M							R								F													
16H-CC		C	M							R								F													
17H-CC		A	M							R								R			—	—									
18H-CC		A	M							R											R	R									
19H-CC		A	M							R											R	R									
20H-CC	RP20	A	M							R								—			R	R								R	
21H-CC		A	M							R								—			R	R								R	
22H-CC		C	M							R											—	—								R	
23H-CC		C	M																				C							R	
24H-CC		C	M					R											R				C							R	
25H-CC		C	M					R	R										R				C							R	
26H-CC		C	M					R	R										F				R							R	
27H-CC		F	P					R											F											R	
28H-CC	RP18	C	M	1	R	R					R		R		R				R					F		F	VR	VR		R	R
29H-CC	RP17	F	M		R	R							R						R	R				R	R	R		R	R	R	R
30H-CC	B	B																													

Table T8. Planktonic foraminifer datums, Site U1334. (**See table note.**)

Core, section, interval (cm)		Marker species	Age (Ma)	Depth CSF (m)			
Top	Bottom			Top	Bottom	Midpoint	±
320-U1334A-	320-U1334A-						
2H-CC	3H-2, 38–40	B *Globorotalia (Fonsella) fohsi robusta*	13.13	18.11	19.58	18.85	0.73
4H-5, 38–40	5H-CC	B *Praeorbulina sicana*	16.97	33.58	46.78	40.18	6.60
5H-4, 39–40	5H-6, 39–41	T *Paragloborotalia kugleri*	21.12	41.59	44.59	43.09	1.50
5H-4, 39–40	5H-6, 39–41	T *Paragloborotalia pseudokugleri*	21.31	41.59	44.59	43.09	1.50
8H-CC	9H-CC	B *Globoquadrina dehiscens*	22.44	75.06	84.74	79.90	4.84
10H-2, 38–40	10H-5, 38–40	B *Paragloborotalia kugleri*	23.0	86.08	90.58	88.33	2.25
13H-2, 38–40	13H-CC	B *Paragloborotalia pseudokugleri*	25.2	113.58	122.55	118.07	4.49
16X-CC	17X-2, 10–12	T *Paragloborotalia opima*	26.9	149.62	152.58	151.10	1.48
19H-2, 38–40	19H-4, 38–40	B *Globigerina angulisuturalis*	29.2	172.18	175.18	173.68	1.50
20X-CC	21X-2, 38–40	T *Subbotina angiporoides*	29.8	188.63	190.58	189.61	0.98
22X-4, 38–40	22X-CC	B *Paragloborotalia opima*	30.8	203.08	206.86	204.97	1.89
320-U1334B-	320-U1334B-						
6H-CC	7H-CC	T *Paragloborotalia kugleri*	21.1	59.20	68.88	64.04	4.84
6H-CC	7H-CC	T *Paragloborotalia pseudokugleri*	21.3	59.20	68.88	64.04	4.84
9H-CC	10H-CC	B *Paragloborotalia kugleri*	23.0	87.70	97.22	92.46	4.76
12H-CC	13H-CC	B *Paragloborotalia pseudokugleri*	25.2	116.14	125.68	120.91	4.77
15H-CC	16H-CC	T *Paragloborotalia opima*	26.9	144.55	154.18	149.37	4.81
18H-CC	19H-CC	B *Globigerina angulisuturalis*	29.2	173.23	182.52	177.88	4.65
20H-CC	21H-CC	T *Subbotina angiporoides*	29.8	191.55	201.26	196.41	4.85
21H-CC	22H-CC	T *Turborotalia ampliapertura*	30.3	201.26	211.10	206.18	4.92
23H-CC	24H-CC	B *Paragloborotalia opima*	30.8	220.45	228.70	224.58	4.13
320-U1334C-	320-U1334C-						
5H-CC	6H-CC	T *Globoquadrina binaiensis*	19.09	48.00	57.25	52.63	4.63
6H-CC	7H-CC	T *Paragloborotalia kugleri*	21.12	57.25	65.66	61.46	4.20
6H-CC	7H-CC	T *Paragloborotalia pseudokugleri*	21.31	57.25	65.66	61.46	4.20
7H-CC	8H-CC	B *Globoquadrina dehiscens*	22.44	65.66	76.33	71.00	5.34
9H-CC	10H-CC	B *Paragloborotalia kugleri*	23.0	85.79	95.14	90.47	4.67
12H-CC	13H-CC	B *Paragloborotalia pseudokugleri*	25.2	114.25	123.72	118.99	4.74
14H-CC	15H-CC	T *Paragloborotalia opima*	26.9	133.00	143.29	138.15	5.14
20H-CC	21H-CC	T *Subbotina angiporoides*	29.8	189.97	199.92	194.95	4.97
21H-CC	22H-CC	T *Turborotalia ampliapertura*	30.3	199.92	209.36	204.64	4.72
22H-CC	23H-CC	B *Paragloborotalia opima*	30.8	209.36	213.56	211.46	2.10

Note: B = bottom, T = top.

Table T9. Distribution of planktonic foraminifers, Site U1334. This table is available in an **oversized format.**

Table T10. Distribution of benthic foraminifers, Site U1334. This table is available in an **oversized format.**

Table T11. Coring-disturbed intervals and gaps, Site U1334. (See table notes.)

Core, section, interval (cm)	Type of disturbance
320-U1334A-	
1H-1, 0–150	Slightly disturbed or highly bioturbated
1H-5, 145–150	Interstitial water
1H-2, 145–150	Interstitial water
1H-4, 145–150	Interstitial water
2H-2, 145–150	Interstitial water
2H-5, 145–150	Interstitial water
3H-1, 0–9	Top of core
3H-2, 145–150	Interstitial water
3H-5, 145–150	Interstitial water
4H-1, 0–5	Top of core
4H-2, 145–150	Interstitial water
4H-5, 145–150	Interstitial water
5H-1, 0–50	Top of core
5H-2, 145–150	Interstitial water
5H-5, 145–150	Interstitial water
6H-2, 145–150	Interstitial water
6H-5, 145–150	Interstitial water
7H-1, 0–50	Top of core
7H-3, 140–150	Interstitial water
8H-1, 0–80	Top of core
8H-3, 140–150	Interstitial water
9H-1, 0–7	Top of core
9H-3, 140–150	Interstitial water
10H-1, 0–75	Top of core
10H-3, 140–150	Interstitial water
11H-1, 0–78	Top of core
11H-3, 140–150	Interstitial water
12H-1, 0–24	Top of core
12H-3, 140–150	Interstitial water
13H-1, 0–37	Top of core
13H-4, 140–150	Interstitial water
14H-1, 0–17	Top of core
14H-3, 140–150	Interstitial water
15H-1, 0–61	Top of core
16H-1, 0–68	Top of core
16H-3, 140–150	Interstitial water
17H-1, 0–8	Top of core
17H-1, 72–73	Expansion
17H-3, 140–150	Interstitial water
18H-1, 0–140	Top of core
18H-3, 140–150	Interstitial water
19H-1, 0–35	Top of core
19H-3, 140–150	Interstitial water
20H-1, 0–30	Top of core
20H-3, 140–150	Interstitial water
21H-1, 0–57	Top of core
21H-3, 140–150	Interstitial water
22H-1, 0–150	Top of core
22H-2, 0–62	Top of core
22H-3, 140–150	Interstitial water
23X-1, 140–150	Interstitial water
24X-2, 140–150	Interstitial water
25X-3, 140–150	Interstitial water
26X-3, 140–150	Interstitial water
28X-3, 140–150	Interstitial water
23X–31X, all sections	Drilling biscuits
320-U1334B-	
2H-1, 0–4	Top of core
3H-1, 0–5	Top of core
3H-1, 46–58	Soupy
4H-1, 0–35	Top of core
5H-1, 0–150	Top of core
5H-2, 0–43	Top of core
6H-1, 0–76	Top of core
6H-3, 140–150	Whole-round sample
7H-1, 0–74	Top of core
8H-1, 0–3	Top of core
9H-1, 0–32	Top of core
10H-1, 0–3	Top of core
11H-1, 0–17	Top of core
12H-1, 0–76	Top of core
13H-1, 0–63	Top of core
15H-1, 0–26	Top of core
18H-1, 0–24	Top of core
19H-1, 0–31	Top of core
20H-1, 0–14	Top of core
21H-1, 0–22	Top of core
21H-1, 40–44	Void
21H-7, 38–50	Disturbed
22H-1, 0–3	Top of core
23X–31X, all sections	Drilling biscuits
320-U1334C-	
1H-1, 0–150	Top of core
1H-2, 0–21	Top of core
2H-1, 0–80	Top of core
3H-1, 0–81	Top of core
4H-1, 0–38	Top of core
5H-1, 0–45	Top of core
6H-1, 0–13	Top of core
7H-1, 0–150	Top of core
7H-2, 0–25	Top of core
8H-1, 0–100	Top of core
8H-7, 33–55	Top of core
9H-1, 0–44	Top of core
10H-1, 0–24	Top of core
11H-1, 0–71	Top of core
12H-1, 0–14	Top of core
13H-1, 0–7	Top of core
14H-1, 0–25	Top of core
15H-1, 0–107	Top of core
16H-1, 0–52	Top of core
17H-1, 0–110	Top of core
18H-1, 0–12	Top of core
19H-1, 0–4	Top of core
22H-1, 0–3	Top of core
22H-6, 100–150	Flow-in
22H-7, 0–63	Flow-in
23X–30X, all sections	Drilling biscuits

Notes: When interval listed is 0–150 cm, entire section is included even if true section length is <150 cm. Top of core = myriad forms of voids, disturbance, and debris from uphole that affect top portion of most cores. For that reason, probably the top 20 cm or so of all cores should be avoided.

Table T12. Paleomagnetic data from archive-half sections, Hole U1334A, at 0 mT AF demagnetization. (**See table notes.**)

Core, section	Offset (m)	Depth CSF (m)	Declination (°)	Inclination (°)	Intensity (A/m)	Time (s)
320-U1334A-						
1H-1	0.10	0.10	260.9	2.9	1.268E–02	3322008935.71875
1H-1	0.15	0.15	255.4	8.3	1.585E–02	3322008941.04687
1H-1	0.20	0.20	257.6	8.4	1.831E–02	3322008946.37500
1H-1	0.25	0.25	256.1	6.1	1.681E–02	3322008951.70312
1H-1	0.30	0.30	248.4	9.3	1.592E–02	3322008957.03125
1H-1	0.35	0.35	246.2	8.0	1.882E–02	3322008962.34375
1H-1	0.40	0.40	246.2	10.9	1.814E–02	3322008967.67187
1H-1	0.45	0.45	243.9	14.1	1.642E–02	3322008973.00000
1H-1	0.50	0.50	244.2	14.6	1.659E–02	3322008978.32812
1H-1	0.55	0.55	247.1	14.8	1.783E–02	3322008983.65625
1H-1	0.60	0.60	246.4	14.2	1.789E–02	3322008988.98437
1H-1	0.65	0.65	246.4	14.4	1.511E–02	3322008994.31250
1H-1	0.70	0.70	241.2	16.7	1.288E–02	3322008999.65625
1H-1	0.75	0.75	237.4	19.8	6.067E–03	3322009004.98437
1H-1	0.80	0.80	237.6	26.0	4.489E–03	3322009010.31250
1H-1	0.85	0.85	256.1	15.0	5.982E–03	3322009015.64062
1H-1	0.90	0.90	37.7	40.2	9.689E–04	3322009020.95312
1H-1	0.95	0.95	87.0	10.5	2.106E–03	3322009026.28125
1H-1	1.00	1.00	87.8	16.1	1.854E–03	3322009031.60937
1H-1	1.05	1.05	236.2	23.9	2.866E–03	3322009036.93750
1H-1	1.10	1.10	241.2	15.7	4.646E–03	3322009042.26562
1H-1	1.15	1.15	203.1	2.8	8.103E–03	3322009047.59375
1H-1	1.20	1.20	236.4	–15.2	2.305E–02	3322009052.90625
1H-1	1.25	1.25	279.4	–19.1	1.366E–02	3322009058.23437
1H-1	1.30	1.30	75.3	–19.0	2.285E–03	3322009063.56250
1H-1	1.35	1.35	96.2	–9.1	2.510E–03	3322009068.89062
1H-1	1.40	1.40	84.8	–11.7	1.130E–03	3322009074.21875
1H-2	0.10	1.60	180.4	10.1	1.184E–03	3322010145.17187
1H-2	0.15	1.65	27.0	15.6	3.677E–04	3322010150.50000
1H-2	0.20	1.70	109.2	5.8	5.426E–04	3322010155.82812
1H-2	0.25	1.75	140.0	–0.6	8.937E–04	3322010161.14062
1H-2	0.30	1.80	164.3	13.5	1.339E–03	3322010166.46875
1H-2	0.35	1.85	224.1	14.5	6.962E–03	3322010171.79687
1H-2	0.40	1.90	235.9	9.0	1.199E–02	3322010177.12500
1H-2	0.45	1.95	224.8	15.6	9.391E–03	3322010182.45312
1H-2	0.50	2.00	218.1	15.8	7.869E–03	3322010187.76562
1H-2	0.55	2.05	196.1	26.3	1.526E–03	3322010193.09375
1H-2	0.60	2.10	231.8	17.9	1.432E–03	3322010198.42187
1H-2	0.65	2.15	221.4	4.2	1.870E–03	3322010203.75000
1H-2	0.70	2.20	62.7	–15.3	5.316E–04	3322010209.07812
1H-2	0.75	2.25	76.3	–7.3	1.217E–03	3322010214.40625
1H-2	0.80	2.30	156.7	13.4	1.491E–03	3322010219.73437
1H-2	0.85	2.35	226.6	13.4	1.375E–03	3322010225.06250
1H-2	0.90	2.40	158.9	10.2	6.641E–04	3322010230.43750
1H-2	0.95	2.45	185.8	–0.9	7.974E–04	3322010235.81250
1H-2	1.00	2.50	219.0	6.2	4.975E–04	3322010241.17187
1H-2	1.05	2.55	47.4	19.9	1.805E–04	3322010246.50000
1H-2	1.10	2.60	217.0	20.2	6.357E–04	3322010251.81250
1H-2	1.15	2.65	199.7	34.9	1.630E–03	3322010257.34375
1H-2	1.20	2.70	216.8	25.2	4.188E–03	3322010262.71875
1H-2	1.25	2.75	220.2	15.4	7.667E–03	3322010268.04687
1H-2	1.30	2.80	212.6	13.5	9.137E–03	3322010273.37500
1H-2	1.35	2.85	219.4	12.7	1.321E–02	3322010278.71875
1H-2	1.40	2.90	220.5	11.6	1.440E–02	3322010284.04687
1H-3	0.10	3.10	224.9	6.0	1.185E–02	3322011464.93750
1H-3	0.15	3.15	220.2	0.7	7.392E–03	3322011470.25000
1H-3	0.20	3.20	221.2	–2.3	6.201E–03	3322011475.57812
1H-3	0.25	3.25	224.7	1.5	9.092E–03	3322011480.90625
1H-3	0.30	3.30	223.6	4.9	1.044E–02	3322011486.23437
1H-3	0.35	3.35	227.2	2.8	8.726E–03	3322011491.56250
1H-3	0.40	3.40	227.0	0.1	9.358E–03	3322011496.87500
1H-3	0.45	3.45	226.3	1.0	9.764E–03	3322011502.20312
1H-3	0.50	3.50	224.6	1.8	6.852E–03	3322011507.53125

Notes: Time = since 1 January 1904. Only a portion of this table appears here. The complete table is available in **ASCII.**

Table T13. Paleomagnetic data from archive-half sections, Hole U1334A, at 20 mT AF demagnetization. (See table notes.)

Core, section	Offset (m)	Depth CSF (m)	Declination (°)	Inclination (°)	Intensity (A/m)	Time (s)	Declination: Core mean (°)	Declination: Geographical coordinates 0°–360°	Declination: Geographical coordinates −90°–270°	CCSF offset (m)	Depth (m) CCSF-A	Depth (m) CCSF-B	VGP (°) Latitude	VGP (°) Longitude
320-U1334A-														
1H-1	0.100	0.100	258.3	10.1	6.761E–03	3322009362.71875	227.8	30.5	30.5	0.000	0.100	0.086	59.6	321.6
1H-1	0.150	0.150	252.8	15.9	7.343E–03	3322009368.03125	227.8	25.0	25.0	0.000	0.150	0.129	65.3	316.0
1H-1	0.200	0.200	254.9	17.1	7.991E–03	3322009373.35937	227.8	27.1	27.1	0.000	0.200	0.172	63.2	314.5
1H-1	0.250	0.250	252.9	16.7	8.058E–03	3322009378.68750	227.8	25.1	25.1	0.000	0.250	0.216	65.2	315.0
1H-1	0.300	0.300	253.2	15.3	8.186E–03	3322009384.01562	227.8	25.4	25.4	0.000	0.300	0.259	64.8	316.7
1H-1	0.350	0.350	249.5	14.2	8.907E–03	3322009389.34375	227.8	21.7	21.7	0.000	0.350	0.302	68.5	318.7
1H-1	0.400	0.400	248.1	15.6	8.551E–03	3322009394.65625	227.8	20.3	20.3	0.000	0.400	0.345	69.9	316.8
1H-1	0.450	0.450	244.2	21.5	7.775E–03	3322009399.98437	227.8	16.4	16.4	0.000	0.450	0.388	73.5	305.7
1H-1	0.500	0.500	242.5	21.4	7.816E–03	3322009405.31250	227.8	14.7	14.7	0.000	0.500	0.431	75.2	304.9
1H-1	0.550	0.550	245.8	21.0	8.196E–03	3322009410.64062	227.8	18.0	18.0	0.000	0.550	0.474	72.0	307.5
1H-1	0.600	0.600	246.7	20.4	8.794E–03	3322009415.96875	227.8	18.9	18.9	0.000	0.600	0.517	71.2	308.8
1H-1	0.650	0.650	245.5	19.0	8.161E–03	3322009421.28125	227.8	17.7	17.7	0.000	0.650	0.560	72.4	310.9
1H-1	0.700	0.700	241.6	19.5	6.880E–03	3322009426.60937	227.8	13.8	13.8	0.000	0.700	0.603	76.2	308.5
1H-1	0.750	0.750	220.6	60.5	1.372E–03	3322009431.93750	227.8	352.8	–7.2	0.000	0.750	0.647	55.9	218.4
1H-1	0.800	0.800	76.5	31.7	1.546E–03	3322009437.26562	227.8	208.7	208.7	0.000	0.800	0.690	–52.1	179.7
1H-1	0.850	0.850	268.1	69.0	9.427E–04	3322009442.59375	227.8	40.3	40.3	0.000	0.850	0.733	34.8	256.7
1H-1	0.900	0.900	55.5	–2.9	3.569E–03	3322009447.90625	227.8	187.7	187.7	0.000	0.900	0.776	–79.9	178.1
1H-1	0.950	0.950	63.7	–5.3	5.176E–03	3322009453.23437	227.8	195.9	195.9	0.000	0.950	0.819	–73.3	155.8
1H-1	1.000	1.000	65.0	–5.0	5.426E–03	3322009458.56250	227.8	197.2	197.2	0.000	1.000	0.862	–72.0	154.9
1H-1	1.050	1.050	80.8	2.3	2.239E–03	3322009463.89062	227.8	213.0	213.0	0.000	1.050	0.905	–55.9	152.1
1H-1	1.100	1.100	42.9	17.2	5.401E–04	3322009469.21875	227.8	175.1	175.1	0.000	1.100	0.948	–72.5	244.3
1H-1	1.150	1.150	239.1	21.9	8.583E–04	3322009474.53125	227.8	11.3	11.3	0.000	1.150	0.991	78.4	300.3
1H-1	1.200	1.200	123.9	–17.8	4.724E–04	3322009479.85937	227.8	256.1	256.1	0.000	1.200	1.034	–14.9	130.7
1H-1	1.250	1.250	48.6	–14.9	1.801E–03	3322009485.18750	227.8	180.8	180.8	0.000	1.250	1.078	–89.1	166.0
1H-1	1.300	1.300	57.0	–7.8	3.629E–03	3322009490.51562	227.8	189.2	189.2	0.000	1.300	1.121	–80.0	161.5
1H-1	1.350	1.350	59.4	–9.6	4.389E–03	3322009495.82812	227.8	191.6	191.6	0.000	1.350	1.164	–78.1	152.7
1H-1	1.400	1.400	55.1	–11.1	4.200E–03	3322009501.15625	227.8	187.3	187.3	0.000	1.400	1.207	–82.4	155.9
1H-2	0.100	1.600	51.7	–15.8	1.826E–03	3322011005.10937	227.8	183.9	183.9	0.000	1.600	1.379	–86.1	137.0
1H-2	0.150	1.650	37.3	–15.2	2.649E–03	3322011010.43750	227.8	169.5	169.5	0.000	1.650	1.422	–79.6	317.3
1H-2	0.200	1.700	43.7	–11.1	2.713E–03	3322011015.75000	227.8	175.9	175.9	0.000	1.700	1.466	–85.3	287.8
1H-2	0.250	1.750	46.3	–10.8	2.293E–03	3322011021.07812	227.8	178.5	178.5	0.000	1.750	1.509	–87.1	258.4
1H-2	0.300	1.800	49.1	–9.7	2.602E–03	3322011026.40625	227.8	181.3	181.3	0.000	1.800	1.552	–86.6	205.4
1H-2	0.350	1.850	49.7	45.4	8.920E–04	3322011031.73437	227.8	181.9	181.9	0.000	1.850	1.595	–55.1	225.1
1H-2	0.400	1.900	228.1	20.9	4.865E–03	3322011037.06250	227.8	0.3	0.3	0.000	1.900	1.638	87.2	234.0
1H-2	0.450	1.950	231.3	19.5	5.515E–03	3322011042.37500	227.8	3.5	3.5	0.000	1.950	1.681	86.0	287.2
1H-2	0.500	2.000	221.5	18.3	4.169E–03	3322011047.70312	227.8	353.7	–6.3	0.000	2.000	1.724	83.6	151.1
1H-2	0.550	2.050	56.7	–4.7	2.218E–03	3322011053.03125	227.8	188.9	188.9	0.000	2.050	1.767	–79.5	170.1
1H-2	0.600	2.100	44.5	–10.1	2.456E–03	3322011058.35937	227.8	176.7	176.7	0.000	2.100	1.810	–85.6	276.6
1H-2	0.650	2.150	37.1	–13.4	1.700E–03	3322011063.68750	227.8	169.3	169.3	0.000	2.150	1.853	–79.3	312.3
1H-2	0.700	2.200	33.6	–17.2	2.605E–03	3322011069.00000	227.8	165.8	165.8	0.000	2.200	1.897	–75.9	322.3
1H-2	0.750	2.250	36.6	–12.0	3.057E–03	3322011074.32812	227.8	168.8	168.8	0.000	2.250	1.940	–78.7	308.9
1H-2	0.800	2.300	35.8	–14.5	2.577E–03	3322011079.65625	227.8	168.0	168.0	0.000	2.300	1.983	–78.1	315.8
1H-2	0.850	2.350	30.9	–12.7	2.037E–03	3322011084.98437	227.8	163.1	163.1	0.000	2.350	2.026	–73.2	313.8
1H-2	0.900	2.400	12.8	–7.5	1.884E–03	3322011090.31250	227.8	145.0	145.0	0.000	2.400	2.069	–54.9	313.2
1H-2	0.950	2.450	11.2	–10.4	1.711E–03	3322011095.62500	227.8	143.4	143.4	0.000	2.450	2.112	–53.6	316.0

Notes: Time = since 1 January 1904. VGP = virtual geomagnetic pole. Only a portion of this table appears here. The complete table is available in ASCII.

Table T14. Paleomagnetic data from archive-half sections, Hole U1334B, at 0 mT AF demagnetization. (**See table notes.**)

Core, section	Offset (m)	Depth CSF (m)	Declination (°)	Inclination (°)	Intensity (A/m)	Time (s)
320-U1334B-						
1H-1	0.100	3.800	135.2	86.1	2.730E–02	3322292723.68750
1H-1	0.150	3.850	39.5	57.2	1.146E–02	3322292729.00000
1H-1	0.200	3.900	40.3	37.7	8.003E–03	3322292734.32812
1H-1	0.250	3.950	35.0	31.3	6.752E–03	3322292739.65625
1H-1	0.300	4.000	35.9	40.0	5.054E–03	3322292744.98437
1H-1	0.350	4.050	34.2	40.2	5.226E–03	3322292750.31250
1H-1	0.400	4.100	31.2	38.6	5.560E–03	3322292755.62500
1H-1	0.450	4.150	24.0	27.2	8.194E–03	3322292760.95312
1H-1	0.500	4.200	27.7	26.0	9.116E–03	3322292766.28125
1H-1	0.550	4.250	27.4	22.5	9.220E–03	3322292771.60937
1H-1	0.600	4.300	25.0	20.0	8.512E–03	3322292776.93750
1H-1	0.650	4.350	22.1	22.1	8.135E–03	3322292782.25000
1H-1	0.700	4.400	23.5	21.2	8.624E–03	3322292787.57812
1H-1	0.750	4.450	24.0	20.1	8.795E–03	3322292792.90625
1H-1	0.800	4.500	24.0	19.0	8.774E–03	3322292798.23437
1H-1	0.850	4.550	22.5	19.3	8.225E–03	3322292803.56250
1H-1	0.900	4.600	26.9	18.5	5.718E–03	3322292808.87500
1H-1	0.950	4.650	15.5	13.3	5.616E–03	3322292814.20312
1H-1	1.000	4.700	15.1	19.0	7.265E–03	3322292819.53125
1H-1	1.050	4.750	22.5	24.6	5.829E–03	3322292824.85937
1H-1	1.100	4.800	38.4	42.5	3.571E–03	3322292830.18750
1H-1	1.150	4.850	32.6	41.6	3.527E–03	3322292835.50000
1H-1	1.200	4.900	35.3	42.8	3.430E–03	3322292840.82812
1H-1	1.250	4.950	34.2	37.4	3.734E–03	3322292846.15625
1H-1	1.300	5.000	25.2	28.1	4.813E–03	3322292851.48437
1H-1	1.350	5.050	22.9	25.0	5.589E–03	3322292856.79687
1H-1	1.400	5.100	25.4	24.8	5.847E–03	3322292862.12500
1H-2	0.100	5.300	30.6	52.9	2.785E–03	3322294509.65625
1H-2	0.150	5.350	35.2	48.9	2.460E–03	3322294514.96875
1H-2	0.200	5.400	35.6	47.0	2.689E–03	3322294520.29687
1H-2	0.250	5.450	44.8	58.6	2.425E–03	3322294525.62500
1H-2	0.300	5.500	32.3	60.6	2.518E–03	3322294530.93750
1H-2	0.350	5.550	25.8	56.7	2.404E–03	3322294536.26562
1H-2	0.400	5.600	23.1	26.1	2.774E–03	3322294541.59375
1H-2	0.450	5.650	27.0	21.7	3.588E–03	3322294546.92187
1H-2	0.500	5.700	21.6	28.0	3.049E–03	3322294552.25000
1H-2	0.550	5.750	333.2	67.9	1.495E–03	3322294557.57812
1H-2	0.600	5.800	227.5	72.7	1.317E–03	3322294562.89062
1H-2	0.650	5.850	259.5	79.3	1.005E–03	3322294568.21875
1H-2	0.700	5.900	120.1	50.4	5.614E–04	3322294573.54687
1H-2	0.750	5.950	196.1	11.4	1.473E–03	3322294578.87500
1H-2	0.800	6.000	5.0	37.3	1.583E–03	3322294584.20312
1H-2	0.850	6.050	20.4	20.4	3.471E–03	3322294589.51562
1H-2	0.900	6.100	17.7	16.9	4.213E–03	3322294594.84375
1H-2	0.950	6.150	32.8	17.2	4.003E–03	3322294600.17187
1H-2	1.000	6.200	25.1	20.8	4.243E–03	3322294605.50000
1H-2	1.050	6.250	18.3	25.4	4.800E–03	3322294610.82812
1H-2	1.100	6.300	23.7	22.6	5.608E–03	3322294616.14062
1H-2	1.150	6.350	22.4	16.9	7.345E–03	3322294621.46875
1H-2	1.200	6.400	20.8	18.1	7.481E–03	3322294626.79687
1H-2	1.250	6.450	20.3	20.4	7.591E–03	3322294632.12500
1H-2	1.300	6.500	17.8	18.2	8.302E–03	3322294637.45312
1H-2	1.350	6.550	18.3	18.7	8.183E–03	3322294642.78125
1H-2	1.400	6.600	18.4	15.8	9.200E–03	3322294648.09375
1H-3	0.100	6.800	25.8	17.6	8.699E–03	3322295318.12500
1H-3	0.150	6.850	25.6	18.0	9.581E–03	3322295323.45312
1H-3	0.200	6.900	26.8	18.7	9.863E–03	3322295328.78125
1H-3	0.250	6.950	26.8	16.3	1.058E–02	3322295334.10937
1H-3	0.300	7.000	26.8	15.2	1.074E–02	3322295339.43750
1H-3	0.350	7.050	26.6	15.1	1.041E–02	3322295344.75000
1H-3	0.400	7.100	25.2	20.5	7.832E–03	3322295350.07812
1H-3	0.450	7.150	27.5	25.0	4.984E–03	3322295355.40625

Notes: Time = since 1 January 1904. Only a portion of this table appears here. The complete table is available in **ASCII.**

Table T15. Paleomagnetic data from archive-half sections, Hole U1334B, at 20 mT AF demagnetization. (**See table notes.**)

Core, section	Offset (m)	Depth CSF (m)	Declination (°)	Inclination (°)	Intensity (A/m)	Time (s)	Declination: Core mean (°)	Declination: Geographical coordinates 0°–360°	Declination: Geographical coordinates –90°–270°	CCSF offset (m)	Depth (m) CCSF-A	Depth (m) CCSF-B	VGP (°) Latitude	VGP (°) Longitude
320-U1334B-														
1H-1	0.100	3.800	212.6	38.3	3.388E–03	3322294098.31250	23.8	188.8	188.8	4.000	7.800	6.724	–59.2	211.9
1H-1	0.150	3.850	232.4	58.1	1.446E–03	3322294103.64062	23.8	208.6	208.6	4.000	7.850	6.767	–36.2	200.5
1H-1	0.200	3.900	44.9	51.6	1.235E–03	3322294108.95312	23.8	21.1	21.1	4.000	7.900	6.810	58.8	264.1
1H-1	0.250	3.950	42.0	40.9	1.127E–03	3322294114.28125	23.8	18.2	18.2	4.000	7.950	6.853	66.7	274.5
1H-1	0.300	4.000	187.1	78.5	8.713E–04	3322294119.60937	23.8	163.3	163.3	4.000	8.000	6.897	–13.2	234.4
1H-1	0.350	4.050	197.9	59.5	1.136E–03	3322294124.93750	23.8	174.1	174.1	4.000	8.050	6.940	–41.4	234.0
1H-1	0.400	4.100	178.6	84.5	1.253E–03	3322294130.26562	23.8	154.8	154.8	4.000	8.100	6.983	–1.9	232.7
1H-1	0.450	4.150	17.6	44.2	1.785E–03	3322294135.59375	23.8	353.8	–6.2	4.000	8.150	7.026	71.1	210.6
1H-1	0.500	4.200	25.9	30.3	3.069E–03	3322294140.90625	23.8	2.1	2.1	4.000	8.200	7.069	81.5	241.7
1H-1	0.550	4.250	26.7	34.6	2.745E–03	3322294146.23437	23.8	2.9	2.9	4.000	8.250	7.112	78.6	242.1
1H-1	0.600	4.300	25.4	31.2	2.568E–03	3322294151.56250	23.8	1.6	1.6	4.000	8.300	7.155	81.0	237.9
1H-1	0.650	4.350	21.2	31.6	2.371E–03	3322294156.89062	23.8	357.4	–2.6	4.000	8.350	7.198	80.6	212.7
1H-1	0.700	4.400	22.3	28.9	2.565E–03	3322294162.21875	23.8	358.5	–1.5	4.000	8.400	7.241	82.4	217.0
1H-1	0.750	4.450	20.7	25.3	2.716E–03	3322294167.54687	23.8	356.9	–3.1	4.000	8.450	7.284	83.9	198.4
1H-1	0.800	4.500	21.1	23.0	2.742E–03	3322294172.85937	23.8	357.3	–2.7	4.000	8.500	7.328	85.2	194.5
1H-1	0.850	4.550	21.3	23.3	2.378E–03	3322294178.18750	23.8	357.5	–2.5	4.000	8.550	7.371	85.2	197.6
1H-1	0.900	4.600	63.3	10.1	9.396E–04	3322294183.51562	23.8	39.5	39.5	4.000	8.600	7.414	50.7	319.8
1H-1	0.950	4.650	336.7	–21.8	8.475E–04	3322294188.82812	23.8	312.9	–47.1	4.000	8.650	7.457	39.3	116.2
1H-1	1.000	4.700	358.1	14.3	1.863E–03	3322294194.15625	23.8	334.3	–25.7	4.000	8.700	7.500	64.5	138.1
1H-1	1.050	4.750	21.1	55.2	8.019E–04	3322294199.48437	23.8	357.3	–2.7	4.000	8.750	7.543	62.2	223.3
1H-1	1.100	4.800	189.7	24.5	1.387E–03	3322294204.81250	23.8	165.9	165.9	4.000	8.800	7.586	–64.9	262.1
1H-1	1.150	4.850	196.6	27.4	1.136E–03	3322294210.12500	23.8	172.8	172.8	4.000	8.850	7.629	–66.4	245.6
1H-1	1.200	4.900	192.2	30.2	1.044E–03	3322294215.45312	23.8	168.4	168.4	4.000	8.900	7.672	–63.2	253.4
1H-1	1.250	4.950	188.5	45.2	7.963E–04	3322294220.78125	23.8	164.7	164.7	4.000	8.950	7.716	–52.2	250.7
1H-1	1.300	5.000	186.3	65.2	7.143E–04	3322294226.10937	23.8	162.5	162.5	4.000	9.000	7.759	–32.6	242.1
1H-1	1.350	5.050	19.3	68.9	8.078E–04	3322294231.43750	23.8	355.5	–4.5	4.000	9.050	7.802	45.5	224.1
1H-1	1.400	5.100	39.0	65.0	9.995E–04	3322294236.75000	23.8	15.2	15.2	4.000	9.100	7.845	48.9	243.8
1H-2	0.100	5.300	198.0	15.2	2.371E–03	3322294926.01562	23.8	174.2	174.2	4.000	9.300	8.017	–73.2	248.3
1H-2	0.150	5.350	195.7	11.4	2.510E–03	3322294931.32812	23.8	171.9	171.9	4.000	9.350	8.060	–74.1	258.7
1H-2	0.200	5.400	192.9	9.9	2.381E–03	3322294936.65625	23.8	169.1	169.1	4.000	9.400	8.103	–73.1	268.3
1H-2	0.250	5.450	190.6	7.4	3.013E–03	3322294941.98437	23.8	166.8	166.8	4.000	9.450	8.147	–72.4	276.8
1H-2	0.300	5.500	192.3	8.8	2.882E–03	3322294947.31250	23.8	168.5	168.5	4.000	9.500	8.190	–73.1	271.1
1H-2	0.350	5.550	194.8	8.1	2.781E–03	3322294952.62500	23.8	171.0	171.0	4.000	9.550	8.233	–75.0	265.0
1H-2	0.400	5.600	188.4	–1.9	2.393E–03	3322294957.95312	23.8	164.6	164.6	4.000	9.600	8.276	–73.1	294.1
1H-2	0.450	5.650	181.3	–4.2	1.800E–03	3322294963.28125	23.8	157.5	157.5	4.000	9.650	8.319	–66.8	304.5
1H-2	0.500	5.700	181.8	–4.2	2.079E–03	3322294968.60937	23.8	158.0	158.0	4.000	9.700	8.362	–67.3	304.1
1H-2	0.550	5.750	192.0	–3.0	2.973E–03	3322294973.93750	23.8	168.2	168.2	4.000	9.750	8.405	–76.6	289.7
1H-2	0.600	5.800	191.8	–1.6	3.858E–03	3322294979.25000	23.8	168.0	168.0	4.000	9.800	8.448	–76.0	287.6
1H-2	0.650	5.850	190.8	–1.3	3.614E–03	3322294984.57812	23.8	167.0	167.0	4.000	9.850	8.491	–75.1	289.1
1H-2	0.700	5.900	190.5	–0.9	3.247E–03	3322294989.90625	23.8	166.7	166.7	4.000	9.900	8.534	–74.8	289.0
1H-2	0.750	5.950	190.4	–0.5	3.407E–03	3322294995.23437	23.8	166.6	166.6	4.000	9.950	8.578	–74.6	288.5
1H-2	0.800	6.000	187.1	1.0	3.040E–03	3322295000.56250	23.8	163.3	163.3	4.000	10.000	8.621	–71.3	291.7

Notes: Time = since 1 January 1904. VGP = virtual geomagnetic pole. Only a portion of this table appears here. The complete table is available in **ASCII.**

Table T16. Paleomagnetic data from archive-half sections, Hole U1334C, at 0 mT AF demagnetization. (**See table notes.**)

Core, section	Offset (m)	Depth CSF (m)	Declination (°)	Inclination (°)	Intensity (A/m)	Time (s)
320-U1334C-						
1H-2	0.250	1.750	95.4	63.4	4.202E–04	3322540468.07812
1H-2	0.300	1.800	328.2	3.8	2.277E–03	3322540473.40625
1H-2	0.350	1.850	331.7	1.6	4.024E–03	3322540478.73437
1H-2	0.400	1.900	320.3	4.5	4.494E–03	3322540484.04687
1H-2	0.450	1.950	326.3	10.4	5.453E–03	3322540489.37500
1H-2	0.500	2.000	332.3	15.2	5.017E–03	3322540494.70312
1H-2	0.550	2.050	349.1	31.9	2.358E–03	3322540500.03125
1H-2	0.600	2.100	343.7	31.0	2.179E–03	3322540505.34375
1H-2	0.650	2.150	337.6	32.0	2.855E–03	3322540510.67187
1H-2	0.700	2.200	335.3	20.4	5.289E–03	3322540516.00000
1H-2	0.750	2.250	333.9	14.6	7.151E–03	3322540521.32812
1H-2	0.800	2.300	328.5	12.2	7.804E–03	3322540526.64062
1H-2	0.850	2.350	328.1	12.2	8.734E–03	3322540531.96875
1H-2	0.900	2.400	326.7	12.0	9.942E–03	3322540537.29687
1H-2	0.950	2.450	331.9	13.6	8.526E–03	3322540542.62500
1H-2	1.000	2.500	334.8	15.1	7.170E–03	3322540547.95312
1H-2	1.050	2.550	329.2	14.7	6.425E–03	3322540553.26562
1H-2	1.100	2.600	329.6	21.3	4.559E–03	3322540558.59375
1H-2	1.150	2.650	328.8	35.0	2.842E–03	3322540563.92187
1H-2	1.200	2.700	320.4	44.5	2.380E–03	3322540569.25000
1H-2	1.250	2.750	319.2	37.9	3.013E–03	3322540574.57812
1H-2	1.300	2.800	320.7	40.2	2.928E–03	3322540579.90625
1H-2	1.350	2.850	330.5	43.1	2.661E–03	3322540585.21875
1H-2	1.400	2.900	345.1	46.0	2.331E–03	3322540590.54687
1H-3	0.100	3.100	20.6	47.7	2.546E–03	3322541712.14062
1H-3	0.150	3.150	24.3	52.9	2.335E–03	3322541717.46875
1H-3	0.200	3.200	351.5	45.2	2.931E–03	3322541722.78125
1H-3	0.250	3.250	344.3	28.4	4.581E–03	3322541728.10937
1H-3	0.300	3.300	348.2	22.9	6.033E–03	3322541733.43750
1H-3	0.350	3.350	347.7	23.4	6.066E–03	3322541738.76562
1H-3	0.400	3.400	345.6	24.5	5.998E–03	3322541744.09375
1H-3	0.450	3.450	344.6	21.0	7.275E–03	3322541749.40625
1H-3	0.500	3.500	348.3	22.1	7.037E–03	3322541754.73437
1H-3	0.550	3.550	354.0	32.5	4.657E–03	3322541760.06250
1H-3	0.600	3.600	350.8	26.6	5.256E–03	3322541765.39062
1H-3	0.650	3.650	347.0	24.8	5.821E–03	3322541770.71875
1H-3	0.700	3.700	347.4	32.5	4.733E–03	3322541776.03125
1H-3	0.750	3.750	348.5	42.2	3.769E–03	3322541781.35937
1H-3	0.800	3.800	349.8	38.8	3.944E–03	3322541786.68750
1H-3	0.850	3.850	354.0	44.3	3.094E–03	3322541792.01562
1H-3	0.900	3.900	355.1	40.1	3.420E–03	3322541797.34375
1H-3	0.950	3.950	349.5	29.4	4.503E–03	3322541802.65625
1H-3	1.000	4.000	348.4	20.5	5.137E–03	3322541807.98437
1H-3	1.050	4.050	350.1	18.5	5.795E–03	3322541813.31250
1H-3	1.100	4.100	352.2	17.9	5.958E–03	3322541818.64062
1H-3	1.150	4.150	352.9	19.6	5.881E–03	3322541823.96875
1H-3	1.200	4.200	352.3	20.6	5.759E–03	3322541829.29687
1H-3	1.250	4.250	357.3	27.6	4.494E–03	3322541834.62500
1H-3	1.300	4.300	0.6	29.7	4.762E–03	3322541839.93750
1H-3	1.350	4.350	357.6	23.0	5.871E–03	3322541845.26562
1H-3	1.400	4.400	355.2	17.2	7.639E–03	3322541850.59375
1H-4	0.100	4.600	349.3	19.2	8.808E–03	3322542789.34375
1H-4	0.150	4.650	350.4	20.6	7.873E–03	3322542794.67187
1H-4	0.200	4.700	351.5	20.9	7.733E–03	3322542800.00000
1H-4	0.250	4.750	352.9	21.4	7.869E–03	3322542805.32812
1H-4	0.300	4.800	351.8	21.2	8.126E–03	3322542810.65625
1H-4	0.350	4.850	353.8	20.7	8.339E–03	3322542815.96875
1H-4	0.400	4.900	355.7	20.8	8.314E–03	3322542821.29687
1H-4	0.450	4.950	353.5	21.6	7.974E–03	3322542826.62500
1H-4	0.500	5.000	352.7	27.5	6.083E–03	3322542831.95312
1H-4	0.550	5.050	355.2	35.8	4.523E–03	3322542837.26562
1H-4	0.600	5.100	359.4	31.7	4.384E–03	3322542842.59375

Notes: Time = since 1 January 1904. Only a portion of this table appears here. The complete table is available in **ASCII.**

Table T17. Paleomagnetic data from archive-half sections, Hole U1334C, at 20 mT AF demagnetization. (See table notes.)

Core, section	Offset (m)	Depth CSF (m)	Declination (°)	Inclination (°)	Intensity (A/m)	Time (s)	Declination			CCSF offset (m)	Depth (m)		VGP (°)	
							Core mean (°)	Geographical coordinates 0°–360°	Geographical coordinates –90°–270°		CCSF-A	CCSF-B	Latitude	Longitude
320-U1334C-														
1H-2	0.225	1.725	152.4	–32.7	1.954E–03	3322541142.42187	351.60	160.8	160.8	3.650	5.375	4.634	–68.9	347.6
1H-2	0.250	1.750	133.0	–29.5	2.056E–03	3322541147.35937	351.60	141.4	141.4	3.650	5.400	4.655	–51.5	333.4
1H-2	0.275	1.775	138.5	–32.1	1.644E–03	3322541152.28125	351.60	146.9	146.9	3.650	5.425	4.677	–56.4	337.6
1H-2	0.300	1.800	135.2	–43.2	1.143E–03	3322541157.21875	351.60	143.6	143.6	3.650	5.450	4.698	–51.3	348.8
1H-2	0.325	1.825	305.6	–66.8	8.219E–04	3322541162.15625	351.60	314.0	–46.0	3.650	5.475	4.720	20.0	77.9
1H-2	0.350	1.850	345.7	–34.9	1.353E–03	3322541167.07812	351.60	354.1	–5.9	3.650	5.500	4.741	62.2	60.0
1H-2	0.375	1.875	306.6	–24.7	1.860E–03	3322541172.01562	351.60	315.0	–45.0	3.650	5.525	4.763	40.6	113.3
1H-2	0.400	1.900	321.0	–29.5	1.576E–03	3322541176.93750	351.60	329.4	–30.6	3.650	5.550	4.784	51.5	99.9
1H-2	0.425	1.925	319.7	–26.9	1.708E–03	3322541181.87500	351.60	328.1	–31.9	3.650	5.575	4.806	51.3	103.1
1H-2	0.450	1.950	321.4	–25.3	1.758E–03	3322541186.79687	351.60	329.8	–30.2	3.650	5.600	4.828	53.2	102.9
1H-2	0.475	1.975	325.5	–24.0	1.722E–03	3322541191.73437	351.60	333.9	–26.1	3.650	5.625	4.849	56.9	99.9
1H-2	0.500	2.000	329.2	–29.1	1.346E–03	3322541196.65625	351.60	337.6	–22.4	3.650	5.650	4.871	57.6	91.3
1H-2	0.525	2.025	327.6	–56.8	7.402E–04	3322541201.59375	351.60	336.0	–24.0	3.650	5.675	4.892	39.4	72.7
1H-2	0.550	2.050	141.2	–34.1	1.030E–03	3322541206.53125	351.60	149.6	149.6	3.650	5.700	4.914	–58.6	341.1
1H-2	0.575	2.075	154.8	–15.3	1.689E–03	3322541211.45312	351.60	163.2	163.2	3.650	5.725	4.935	–73.4	318.5
1H-2	0.600	2.100	146.5	–20.2	1.683E–03	3322541216.39062	351.60	154.9	154.9	3.650	5.750	4.957	–65.1	325.6
1H-2	0.625	2.125	147.0	–19.6	1.784E–03	3322541221.31250	351.60	155.4	155.4	3.650	5.775	4.978	–65.6	324.8
1H-2	0.650	2.150	145.8	–19.7	1.740E–03	3322541226.25000	351.60	154.2	154.2	3.650	5.800	5.000	–64.4	324.8
1H-2	0.675	2.175	142.7	–21.0	1.442E–03	3322541231.18750	351.60	151.1	151.1	3.650	5.825	5.022	–61.4	326.1
1H-2	0.700	2.200	68.7	–40.8	6.218E–04	3322541236.10937	351.60	77.1	77.1	3.650	5.850	5.043	8.5	343.2
1H-2	0.725	2.225	357.0	–17.0	1.097E–03	3322541241.04687	351.60	5.4	5.4	3.650	5.875	5.065	72.5	30.0
1H-2	0.750	2.250	317.3	–4.6	1.703E–03	3322541245.98437	351.60	325.7	–34.3	3.650	5.900	5.086	54.3	122.7
1H-2	0.775	2.275	331.0	–7.4	1.999E–03	3322541250.90625	351.60	339.4	–20.6	3.650	5.925	5.108	66.4	109.1
1H-2	0.800	2.300	331.5	–5.2	2.302E–03	3322541255.84375	351.60	339.9	–20.1	3.650	5.950	5.129	67.3	110.9
1H-2	0.825	2.325	329.8	–3.8	2.335E–03	3322541260.78125	351.60	338.2	–21.8	3.650	5.975	5.151	66.1	114.4
1H-2	0.850	2.350	328.7	–2.9	2.463E–03	3322541265.70312	351.60	337.1	–22.9	3.650	6.000	5.172	65.3	116.5
1H-2	0.875	2.375	326.2	–1.7	3.517E–03	3322541270.64062	351.60	334.6	–25.4	3.650	6.025	5.194	63.2	119.9
1H-2	0.900	2.400	326.3	–1.1	3.122E–03	3322541275.56250	351.60	334.7	–25.3	3.650	6.050	5.216	63.4	120.5
1H-2	0.925	2.425	328.0	–0.4	2.965E–03	3322541280.50000	351.60	336.4	–23.6	3.650	6.075	5.237	65.1	119.9
1H-2	0.950	2.450	329.2	–0.3	2.492E–03	3322541285.42187	351.60	337.6	–22.4	3.650	6.100	5.259	66.2	119.0
1H-2	0.975	2.475	332.3	–0.9	2.148E–03	3322541290.35937	351.60	340.7	–19.3	3.650	6.125	5.280	69.0	115.2
1H-2	1.000	2.500	333.3	–2.9	1.916E–03	3322541295.28125	351.60	341.7	–18.3	3.650	6.150	5.302	69.5	111.4
1H-2	1.025	2.525	342.0	–8.1	1.293E–03	3322541300.21875	351.60	350.4	–9.6	3.650	6.175	5.323	74.6	86.8
1H-2	1.050	2.550	331.8	–10.2	1.425E–03	3322541305.15625	351.60	340.2	–19.8	3.650	6.200	5.345	66.3	105.0
1H-2	1.075	2.575	293.6	–21.9	6.752E–04	3322541310.07812	351.60	302.0	–58.0	3.650	6.225	5.366	29.2	120.2
1H-2	1.100	2.600	135.0	–12.7	9.612E–04	3322541315.01562	351.60	143.4	143.4	3.650	6.250	5.388	–53.7	318.0
1H-2	1.125	2.625	144.3	–11.1	9.040E–04	3322541319.93750	351.60	152.7	152.7	3.650	6.275	5.409	–62.8	314.7
1H-2	1.150	2.650	135.1	–4.6	2.085E–03	3322541324.87500	351.60	143.5	143.5	3.650	6.300	5.431	–53.2	311.1
1H-2	1.175	2.675	156.2	–3.7	2.899E–03	3322541329.79687	351.60	164.6	164.6	3.650	6.325	5.453	–73.5	297.0
1H-2	1.200	2.700	149.5	–4.6	2.412E–03	3322541334.73437	351.60	157.9	157.9	3.650	6.350	5.474	–67.3	304.7
1H-2	1.225	2.725	151.1	–3.7	2.477E–03	3322541339.65625	351.60	159.5	159.5	3.650	6.375	5.496	–68.7	302.3
1H-2	1.250	2.750	152.0	–3.4	2.300E–03	3322541344.59375	351.60	160.4	160.4	3.650	6.400	5.517	–69.5	301.2
1H-2	1.275	2.775	152.8	–4.6	2.145E–03	3322541349.53125	351.60	161.2	161.2	3.650	6.425	5.539	–70.4	302.1
1H-2	1.300	2.800	151.8	–5.5	2.289E–03	3322541354.45312	351.60	160.2	160.2	3.650	6.450	5.560	–69.6	304.2
1H-2	1.325	2.825	149.4	–6.2	2.549E–03	3322541359.39062	351.60	157.8	157.8	3.650	6.475	5.582	–67.4	306.8

Notes: Time = since 1 January 1904. VGP = virtual geomagnetic pole. Only a portion of this table appears here. The complete table is available in ASCII.

Table T18. Mean paleomagnetic direction for each core from Site U1334. (See table notes.)

Core	Inclination (°)	Declination (°)	*N*	*R*	*k*	α95 (°)
320-U1334A-						
1H	11.7	227.8	120	112.623	16.1	3.3
2H	7.2	134.2	134	120.206	9.6	4.1
3H	8.6	58.0	147	135.995	13.3	3.3
4H	2.9	298.4	186	178.691	25.3	2.1
5H	9.2	65.4	156	148.936	21.9	2.5
6H	8.5	92.8	166	159.091	23.9	2.3
7H	1.8	79.1	146	137.247	16.6	3.0
8H	–13.2	329.7	132	123.986	16.3	3.1
9H	18.7	221.3	153	146.716	24.2	2.4
10H	–6.9	330.0	135	128.361	20.2	2.8
11H	–10.9	260.8	150	142.763	20.6	2.6
12H	4.8	274.1	149	143.049	24.9	2.4
13H	–8.2	6.2	148	140.124	18.7	2.8
14H	5.5	104.0	165	162.648	69.7	1.3
15H	–21.1	323.3	135	128.225	19.8	2.8
16H	2.0	66.2	114	106.717	15.5	3.5
17H	0.4	261.9	79	73.061	13.1	4.6
18H	27.1	353.6	99	91.602	13.2	4.1
19H	–27.6	106.2	118	108.072	11.8	4.0
20H	55.9	89.6	101	92.111	11.3	4.4
21H	31.4	246.6	58	51.331	8.5	6.8
22H	*	*				
320-U1334B-						
1H	10.3	23.8	122	112.636	12.9	3.7
2H	15.2	277.2	126	114.806	11.2	3.9
3H	–1.5	174.3	138	126.630	12.0	3.6
4H	7.8	217.1	161	153.013	20.0	2.5
5H	18.5	95.2	122	119.798	55.0	1.7
6H	–0.1	342.7	150	142.110	18.9	2.7
7H	–11.7	235.6	131	124.508	20.0	2.8
8H	–1.7	315.6	151	141.200	15.3	3.0
9H	–3.6	326.0	137	124.714	11.1	3.8
10H	–11.4	305.6	120	111.938	14.8	3.5
11H	–0.2	142.0	152	138.740	11.4	3.5
12H	–10.5	10.3	150	143.804	24.0	2.4
13H	2.9	286.0	145	139.793	27.7	2.3
14H	–5.4	253.9	132	121.035	11.9	3.7
15H	–0.2	261.6	132	122.897	14.4	3.4
16H	3.9	295.8	62	53.998	7.6	7.0
17H	0.7	200.1	52	44.784	7.1	8.0
18H	–29.0	293.7	120	108.173	10.1	4.3
19H	–53.6	253.4	118	108.178	11.9	3.9
20H	32.0	288.6	112	99.711	9.0	4.7
21H	30.4	321.0	149	134.251	10.0	3.8
22H	–12.1	173.3	159	138.893	7.9	4.3
320-U1334C-						
1H	5.3	351.6	261	247.926	19.9	2.0
2H	9.5	302.0	130	122.553	17.3	3.1
3H	10.4	107.3	137	132.448	29.9	2.2
4H	9.0	164.8	163	154.399	18.8	2.6
5H	3.0	258.0	166	162.917	53.5	1.5
6H	2.4	355.7	324	311.366	25.6	1.6
7H	4.9	107.3	267	254.358	21.0	1.9
8H	–3.2	64.4	431	413.746	24.9	1.4
9H	7.6	217.4	403	385.526	23.0	1.5
10H	–3.3	264.5	449	412.650	12.3	2.0
11H	–0.5	340.1	369	358.227	34.2	1.3
12H	–1.8	221.5	309	290.940	17.1	2.0
13H	8.0	359.9	330	303.895	12.6	2.3
14H	–18.0	37.2	221	210.733	21.4	2.1
15H	14.4	254.6	114	104.431	11.8	4.0
16H	–2.2	323.8	92	81.728	8.9	5.3
17H	7.0	57.6	86	75.741	8.3	5.7
18H	–38.9	156.6	132	122.317	13.5	3.5
19H	–50.0	9.4	117	105.676	10.2	4.3
20H	33.0	69.3	99	89.836	10.7	4.6
21H	18.8	162.5	195	174.843	9.6	3.4
22H	*	*				

Notes: Mean paleomagnetic directions and statistics calculated using Fisher statistics for each core. We used data from stable polarity intervals. Reversed polarity intervals were inverted prior to computing mean directions and statistics. Inclination = mean paleomagnetic inclination from stable polarity intervals in core, declination = mean paleomagnetic declination from stable polarity intervals in core. By subtracting this value from observed paleomagnetic declinations measured along core, core can be approximately reoriented back into geographic coordinates. After reorientation, normal polarity intervals will have ~0° declination and reversed polarity intervals will have ~180° declination. *N* = number of paleomagnetic observations used in calculating mean, *R* = resultant vector length from summing N vectors (directions or poles), *k* = precision parameter from Fisher statistical calculations, α95 = 95% confidence angle for mean direction. * = mean direction in determinate.

Table T19. Paleomagnetic results for discrete samples, Hole U1334A. (See table notes.)

Core, section, interval (cm)	Depth CSF (m)	Demag (mT)	Declination			Inclination (°)	Intensity (A/m)
			Azimuthally unoriented (°)	Geographical coordinates 0°–360°	Geographical coordinates –90°–270°		
320-U1334A-							
1H-2, 85	2.35	0	80.6	212.8	212.8	51.3	3.50E–04
1H-2, 85	2.35	5	44.1	176.3	176.3	–5.5	1.18E–03
1H-2, 85	2.35	10	55.9	188.1	188.1	–9.1	1.14E–03
1H-2, 85	2.35	15	63.8	196.0	196.0	–7.8	1.09E–03
1H-2, 85	2.35	20	70.5	202.7	202.7	–4.5	9.11E–04
1H-2, 85	2.35	25	68.4	200.6	200.6	1.8	8.08E–04
1H-2, 85	2.35	30	66.9	199.1	199.1	6.6	5.98E–04
1H-2, 85	2.35	35	61.3	193.5	193.5	16.9	5.66E–04
1H-2, 85	2.35	40	75.9	208.1	208.1	19.2	4.66E–04
1H-2, 85	2.35	50	25.6	157.8	157.8	37.1	6.68E–04
1H-2, 85	2.35	60	12.7	144.9	144.9	74.2	5.62E–04
1H-3, 85	3.85	0	–143.2	–11.0	–11.0	31.4	3.78E–03
1H-3, 85	3.85	5	–163.3	–31.1	–31.1	40.6	1.27E–03
1H-3, 85	3.85	10	46.6	178.8	178.8	13.9	1.26E–03
1H-3, 85	3.85	15	46.5	178.7	178.7	18.2	1.34E–03
1H-3, 85	3.85	20	45.6	177.8	177.8	24.9	1.29E–03
1H-3, 85	3.85	25	50.8	183.0	183.0	44.4	1.13E–03
1H-3, 85	3.85	30	77.6	209.8	209.8	63.7	1.03E–03
1H-3, 85	3.85	35	31.3	163.5	163.5	62.4	1.51E–03
1H-3, 85	3.85	40	116.9	249.1	249.1	78.6	1.24E–03
1H-3, 85	3.85	50	–122.7	9.5	9.5	85.5	1.27E–03
1H-3, 85	3.85	60	–165.7	–33.5	–33.5	77.7	1.70E–03
1H-5, 85	6.85	0	–49.1	83.1	83.1	65.3	3.17E–03
1H-5, 85	6.85	5	41.9	174.1	174.1	30.7	1.35E–03
1H-5, 85	6.85	10	50.8	183.0	183.0	3.4	2.19E–03
1H-5, 85	6.85	15	43.0	175.2	175.2	4.0	2.65E–03
1H-5, 85	6.85	20	49.2	181.4	181.4	7.1	2.13E–03
1H-5, 85	6.85	25	49.2	181.4	181.4	11.9	1.88E–03
1H-5, 85	6.85	30	59.5	191.7	191.7	23.8	1.24E–03
1H-5, 85	6.85	35	42.1	174.3	174.3	33.4	1.14E–03
1H-5, 85	6.85	40	47.9	180.1	180.1	49.9	1.04E–03
1H-5, 85	6.85	50	78.6	210.8	210.8	75.9	9.94E–04
1H-5, 85	6.85	60	43.7	175.9	175.9	81.0	1.02E–03
2H-2, 85	10.55	0	54.2	280.0	–80.0	81.5	3.00E–03
2H-2, 85	10.55	5	113.1	338.9	–21.1	19.1	2.97E–03
2H-2, 85	10.55	10	128.9	354.7	–5.3	16.4	1.68E–03
2H-2, 85	10.55	15	125.6	351.4	–8.6	24.2	1.19E–03
2H-2, 85	10.55	20	128.8	354.6	–5.4	30.5	1.11E–03
2H-2, 85	10.55	25	128.3	354.1	–5.9	45.1	1.01E–03
2H-2, 85	10.55	30	130.3	356.1	–3.9	51.8	1.08E–03
2H-2, 85	10.55	35	133.4	359.2	–0.8	66.4	9.88E–04
2H-2, 85	10.55	40	131.4	357.2	–2.8	70.6	1.05E–03
2H-2, 85	10.55	50	76.6	302.4	–57.6	80.4	1.32E–03
2H-2, 85	10.55	60	–134.7	91.1	91.1	88.2	1.34E–03
2H-3, 85	12.05	0	107.6	333.4	–26.6	65.8	2.20E–03
2H-3, 85	12.05	5	119.1	344.9	–15.1	19.5	4.14E–03
2H-3, 85	12.05	10	113.6	339.4	–20.6	21.4	2.58E–03
2H-3, 85	12.05	15	115.7	341.5	–18.5	27.5	2.11E–03
2H-3, 85	12.05	20	107.5	333.3	–26.7	34.0	1.81E–03
2H-3, 85	12.05	25	124.9	350.7	–9.3	37.1	1.76E–03
2H-3, 85	12.05	30	136.8	2.6	2.6	41.6	1.56E–03
2H-3, 85	12.05	35	92.0	317.8	–42.2	64.6	1.48E–03
2H-3, 85	12.05	40	99.4	325.2	–34.8	67.6	1.52E–03
2H-3, 85	12.05	50	149.1	14.9	14.9	66.2	1.34E–03
2H-3, 85	12.05	60	63.3	289.1	–70.9	83.0	1.42E–03
2H-5, 85	15.05	0	113.3	339.1	–20.9	26.4	2.70E–03
2H-5, 85	15.05	5	155.4	21.2	21.2	63.8	6.35E–04
2H-5, 85	15.05	10	–91.1	134.7	134.7	0.9	7.06E–04
2H-5, 85	15.05	15	–52.9	172.9	172.9	7.9	6.94E–04
2H-5, 85	15.05	20	–55.6	170.2	170.2	15.3	7.97E–04
2H-5, 85	15.05	25	–39.7	186.1	186.1	26.3	7.03E–04

Notes: Only a portion of this table appears here. The complete table is available in ASCII.

Table T20. Principal component analysis (PCA) results for paleomagnetic data, Hole U1334A. (See table notes). (Continued on next page.)

Core, section, interval (cm)	Depth CSF (m)	PCA: Declination: Azimuthally unoriented (°)	PCA: Declination: Geographical coordinates (0°–360°)	PCA: Inclination (°)	PCA: MAD (°)	PCA: Range (mT)	NRM 20 mT (A/m)	Archive-half section at 20 mT AF demagnetization: Declination (°)	Archive-half section at 20 mT AF demagnetization: Inclination (°)	Archive-half section at 20 mT AF demagnetization: NRM (A/m)
320-U1334A-										
1H-2, 85	2.35	63.4	134.6	–26.3	12.0	15–40	9.11E–04	163.1	–12.7	2.037E–03
1H-3, 85	3.85	NA		NA	NA	NA	1.29E–03	2.5	45.2	8.673E–04
1H-5, 85	6.85	33.4	139.1	–13.1	10.4	10–30	2.13E–03	185.3	13.9	1.516E–03
2H-2, 85	10.55	107.1	236.4	9.8	13.0	5–25	1.11E–03	353.6	23.2	2.072E–03
2H-3, 85	12.05	120.6	237.9	8.0	11.2	5–25	1.81E–03	345.2	30.0	2.178E–03
2H-5, 85	15.05	33.4	240.9	35.7	24.9	10–30	7.97E–04	152.2	57.6	6.175E–04
3H-2, 85	20.05	43.2	322.1	11.6	6.4	5–25	9.38E–04	6.6	28.0	1.415E–03
3H-3, 85	21.55	63.6	323.6	3.3	10.7	5–25	1.90E–03	358.6	19.9	2.777E–03
3H-5, 85	24.55	57.8	326.6	4.5	12.1	5–25	3.07E–03	357.3	20.1	3.021E–03
4H-2, 85	29.55	106.3	91.2	–20.0	15.4	15–40	1.01E–03	171.7	–12.2	1.193E–03
4H-3, 85	31.05	126.3	92.7	–12.6	19.8	10–50	2.18E–03	186.1	2.2	1.808E–03
4H-5, 85	34.05	295.2	95.7	–3.6	22.2	5–35	1.51E–03	4.2	10.1	1.624E–03
5H-2, 85	39.05	239.6	333.7	–12.8	9.9	15–35	3.25E–03	179.1	3.2	3.418E–03
5H-3, 85	40.55	88.2	335.2	33.2	16.3	5–60	2.39E–03	14.0	35.6	2.621E–03
5H-5, 85	43.55	80.2	338.2	–13.6	15.2	5–60	2.22E–03	6.3	23.5	1.169E–03
6H-2, 85	48.55	NA		NA	NA	NA	3.55E–04	359.2	13.1	2.336E–04
6H-3, 85	50.05	168.6	317.3	13.9	7.0	5–25	5.49E–04	334.0	36.9	4.760E–04
6H-5, 85	53.05	265.2	320.3	–16.0	38.0	10–60	7.25E–04	181.6	–8.8	8.246E–04
7H-2, 85	58.05	85.7	339.0	–2.8	28.6	5–30	9.65E–04	359.8	8.5	1.002E–03
7H-3, 85	59.55	81.2	340.5	40.8	28.4	0–25	4.63E–04	356.2	47.5	4.271E–04
7H-5, 85	61.05	NA		NA	NA	NA	4.07E–04	184.9	7.4	7.120E–04
8H-2, 85	67.55	214.7	97.9	15.7	18.1	5–25	2.78E–04	186.1	–0.4	3.744E–04
8H-3, 85	69.05	176.1	99.4	–2.0	6.0	5–25	4.95E–04	168.6	–4.7	5.342E–04
8H-5, 85	72.05	340.2	102.4	5.2	10.2	15–35	4.06E–04	354.5	11.7	5.936E–04
9H-2, 85	77.05	202.6	215.8	13.2	11.9	5–50	6.15E–04	359.6	15.4	8.004E–04
9H-3, 85	78.55	199.6	217.3	0.4	4.4	5–25	5.09E–04	316.9	53.6	5.149E–04
9H-5, 85	81.55	193.4	220.3	–4.5	14.4	5–60	4.45E–04	7.1	14.4	5.940E–04
10H-2, 85	86.55	150.9	116.6	–18.4	19.9	15–40	4.08E–04	179.6	0.7	4.721E–04
10H-3, 85	88.05	63.9	118.1	20.6	43.3	5–60	6.95E–04	356.4	2.9	8.175E–04
10H-5, 85	91.05	NA		NA	NA	NA	2.87E–04	200.4	68.9	1.220E–04
11H-2, 85	96.05	209.8	195.3	24.9	17.9	5–25	3.15E–04	217.1	36.4	4.563E–04
11H-3, 85	97.55	NA		NA	NA	NA	4.48E–04	185.6	48.1	2.319E–04
11H-5, 85	100.55	65.9	199.8	–2.2	5.9	15–35	1.12E–03	176.2	6.4	1.112E–03
12H-2, 85	105.55	201.9	191.5	–10.4	33.2	5–25	2.24E–04	174.2	3.6	1.071E–03
12H-3, 85	107.05	262.2	193.0	–5.1	25.1	5–30	9.90E–04	352.4	9.4	1.036E–03
12H-5, 85	110.05	286.2	196.0	–0.1	17.6	5–50	1.28E–03	13.7	6.3	1.687E–03
13H-2, 85	114.05	197.7	107.9	–11.1	4.9	10–30	6.80E–04	180.3	16.3	1.104E–03
13H-3, 85	115.55	0.5	109.4	–8.2	11.4	5–35	3.40E–04	3.5	2.7	3.676E–04
13H-5, 85	118.55	176.1	112.4	–15.5	10.7	5–35	7.65E–04	165.8	8.5	6.259E–04
14H-2, 85	124.55	314.2	20.6	–4.8	28.4	5–25	5.66E–04	354.6	19.7	4.050E–04
14H-3, 85	126.05	90.4	22.1	–30.8	14.7	10–35	9.63E–04	356.7	–2.8	1.117E–03
14H-5, 85	129.05	94.9	25.0	20.1	16.8	0–50	1.97E–03	357.9	–4.2	1.951E–03
15H-2, 85	134.05	147.2	170.8	–4.3	6.5	20–40	8.32E–04	175.3	16.3	1.090E–03
15H-3, 85	135.55	195.6	172.3	8.8	31.7	5–35	4.58E–04	158.1	25.7	7.771E–04
15H-5, 85	138.55	NA		NA	NA	NA	3.04E–04	212.1	22.3	5.127E–05
16H-2, 85	143.55	NA		NA	NA	NA	4.98E–05	357.0	–11.9	3.198E–05
16H-3, 85	145.05	NA		NA	NA	NA	7.91E–04	5.5	5.6	3.864E–05
16H-5, 85	148.05	NA		NA	NA	NA	2.81E–04	23.7	–4.8	1.554E–05
17H-2, 85	153.05	NA		NA	NA	NA	1.04E–04	340.0	66.2	8.091E–05
17H-3, 85	154.55	NA		NA	NA	NA	6.67E–04	15.9	2.5	1.323E–03
17H-5, 85	157.55	NA		NA	NA	NA	1.35E–04	210.4	–5.8	6.524E–04
18H-2, 85	162.55	NA		NA	NA	NA	2.44E–04	1.5	13.8	1.521E–04
18H-3, 85	164.05	NA		NA	NA	NA	6.11E–04	32.8	28.6	1.554E–04
18H-5, 85	167.05	NA		NA	NA	NA	4.96E–04	173.8	42.0	1.173E–04
19H-2, 85	171.97	NA		NA	NA	NA	3.22E–04	242.5	16.0	3.725E–05
19H-3, 85	173.47	NA		NA	NA	NA	8.89E–04	178.1	32.4	7.918E–05
19H-5, 85	176.47	NA		NA	NA	NA	6.21E–04	174.4	52.6	3.106E–05
20H-2, 85	181.55	NA		NA	NA	NA	3.95E–04	275.9	69.3	4.033E–05
20H-3, 85	183.05	NA		NA	NA	NA	4.57E–04	359.0	39.6	3.632E–05
21H-2, 85	191.05	NA		NA	NA	NA	4.24E–04	85.4	50.5	8.364E–05
21H-3, 85	192.55	NA		NA	NA	NA	1.43E–04	298.0	76.2	1.192E–04
22H-2, 85	200.55	NA		NA	NA	NA	3.28E–04	52.0	38.7	3.990E–05
22H-3, 85	202.05	NA		NA	NA	NA	2.28E–04	167.6	5.5	1.956E–05

Table T20 (continued).

Core, section, interval (cm)	Depth CSF (m)	PCA					NRM 20 mT (A/m)	Archive-half section at 20 mT AF demagnetization		
		Declination		Inclination (°)	MAD (°)	Range (mT)		Declination (°)	Inclination (°)	NRM (A/m)
		Azimuthally unoriented (°)	Geographical coordinates (0°–360°)							
23X-2, 105	209.45	209.2	209.2	9.8	17.9	5–60	1.29E–03			
23X-3, 90	210.80	144.2	144.2	50.9	17.3	0–25	7.32E–04			
23X-5, 90	213.80	24.7	24.7	10.6	13.2	10–30	5.46E–04			
24X-2, 77	216.77	94.0	94.0	13.0	29.9	0–35	1.26E–03			
24X-3, 83	218.33	25.8	25.8	1.2	14.4	5–30	6.91E–04			
24X-5, 98	221.48	NA		NA	NA	NA	7.23E–04			
24X-7, 30	223.80	214.3	214.3	3.2	17.7	30–60	4.48E–04			
25X-1, 95	225.05	164.0	164.0	–2.1	13.6	20–50	1.06E–03			
25X-3, 101	228.11	328.4	328.4	–12.2	14.9	5–25	1.38E–03			
25X-5, 85	230.95	56.7	56.7	–5.9	32.1	0–60	5.81E–04			
26X-1, 73	234.33	178.3	178.3	–12.1	7.4	20–40	1.67E–03			
26X-3, 113	237.73	200.7	200.7	–4.1	9.1	30–60	1.14E–03			
26X-5, 91	240.51	357.1	357.1	5.7	11.4	10–30	4.16E–04			
28X-1, 130	254.10	264.8	264.8	–17.9	24.1	10–50	1.65E–03			
28X-3, 78	256.58	301.2	301.2	–8.3	10.3	20–40	2.32E–03			
28X-5, 76	259.56	280.2	280.2	–17.6	20.7	10–60	1.51E–03			
29X-1, 95	263.35	131.9	131.9	–58.3	19.9	10–60	1.42E–03			
29X-3, 106	264.97	NA		NA	NA	NA	1.62E–03			
29X-5, 104	267.95	193.7	193.7	–7.4	8.7	10–30	2.07E–03			
29X-7, 124	270.81	349.2	349.2	–12.5	12.5	10–40	1.61E–03			
30X-1, 114	273.24	47.3	47.3	–4.6	13.2	10–30	1.60E–03			
30X-3, 95	276.05	2.4	2.4	–10.9	8.6	10–30	8.75E–04			
30X-5, 90	279.00	236.7	236.7	–13.1	4.6	10–35	2.50E–03			
30X-7, 55	281.15	NA		NA	NA	NA	9.89E–04			

Notes: MAD = maximum angular deviation, NRM = natural remanent magnetization. NA = not applicable.

Table T21. Magnetic susceptibility of discrete samples, Hole U1334A. (See table notes.) (Continued on next two pages.)

Core, section, interval (cm)	Depth CSF (m)	LIMS ID	Susceptibility Raw (10^{-6})	Susceptibility Corrected (10^{-6})	Total mass (g)	Bulk density (g/cm³)	Volume (cm³)	Susceptibility Volume normalized (10^{-5})	Susceptibility Mass normalized (m³/kg)	Susceptibility Whole core (raw values)	Scale factor
320-U1334A-											
1H-1, 84–86	0.85	CUBE653331	127.1	132.0	10.43	1.19	4.90	18.86	8.859E–08	23.43	8.05E–01
1H-2, 84–86	2.35	CUBE653351	59.4	64.3	7.84	1.21	2.67	16.83	5.741E–08	23.23	7.24E–01
1H-3, 84–86	3.85	CUBE653361	236.0	240.9	12.38	1.16	6.74	25.02	1.362E–07	31.63	7.91E–01
1H-4, 84–86	5.35	CUBE653371	181.5	186.4	11.10	1.22	5.35	24.41	1.175E–07	33.20	7.35E–01
1H-5, 84–86	6.85	CUBE653381	158.9	163.8	11.36	1.18	5.74	19.97	1.009E–07	27.92	7.15E–01
1H-6, 39–41	7.90	CUBE653341	166.5	171.4	12.30	1.20	6.40	18.73	9.754E–08	23.01	8.14E–01
2H-1, 84–86	9.05	CUBE655331	151.8	156.7	11.82	1.18	6.11	17.94	9.280E–08	24.48	7.33E–01
2H-2, 84–86	10.55	CUBE655341	198.9	203.8	12.16	1.14	6.64	21.47	1.173E–07	29.49	7.28E–01
2H-3, 84–86	12.05	CUBE655351	209.5	214.4	11.59	1.20	5.83	25.74	1.295E–07	35.65	7.22E–01
2H-4, 84–86	13.55	CUBE655361	182.4	187.3	11.78	1.20	5.99	21.89	1.113E–07	30.91	7.08E–01
2H-5, 84–86	15.05	CUBE655371	174.4	179.3	11.51	1.20	5.76	21.77	1.090E–07	31.02	7.02E–01
2H-6, 84–86	16.55	CUBE655381	158.9	163.8	12.03	1.20	6.20	18.50	9.531E–08	24.71	7.48E–01
2H-7, 49–51	17.70	CUBE655391	109.5	114.4	12.75	1.42	5.74	13.95	6.281E–08	17.21	8.10E–01
3H-1, 84–86	18.55	CUBE655901	193.4	198.3	12.32	1.24	6.25	22.21	1.127E–07	28.90	7.68E–01
3H-2, 84–86	20.05	CUBE655911	194.5	199.4	11.63	1.21	5.83	23.93	1.200E–07	28.32	8.45E–01
3H-3, 84–86	21.55	CUBE655921	175.2	180.1	12.50	1.25	6.34	19.88	1.009E–07	24.40	8.15E–01
3H-4, 84–86	23.05	CUBE655931	211.8	216.7	12.08	1.34	5.59	27.16	1.256E–07	32.64	8.32E–01
3H-5, 84–86	24.55	CUBE655941	287.3	292.2	12.04	1.22	6.11	33.48	1.699E–07	39.85	8.40E–01
3H-6, 84–86	26.05	CUBE655951	242.2	247.1	12.42	1.22	6.39	27.06	1.393E–07	35.52	7.62E–01
3H-7, 49–51	27.20	CUBE655961	231.3	236.2	12.17	1.31	5.77	28.63	1.359E–07	28.77	9.95E–01
4H-1, 84–86	28.05	CUBE657671	85.4	90.3	13.25	1.30	6.64	9.52	4.770E–08	18.62	5.11E–01
4H-2, 84–86	29.55	CUBE657681	69.1	74.0	13.35	1.42	6.17	8.40	3.882E–08	16.07	5.22E–01
4H-3, 84–86	31.05	CUBE657691	165.2	170.1	12.40	1.20	6.51	18.30	9.602E–08	26.08	7.02E–01
4H-4, 84–86	32.55	CUBE657701	106.9	111.8	13.49	1.29	6.91	11.32	5.801E–08	24.56	4.61E–01
4H-5, 84–86	34.05	CUBE657711	122.8	127.7	13.39	1.53	5.74	15.56	6.676E–08	25.95	6.00E–01
4H-6, 84–86	35.55	CUBE657721	264.4	269.3	11.80	1.20	6.00	31.40	1.598E–07	36.80	8.53E–01
4H-7, 49–51	36.70	CUBE657731	209.5	214.4	11.95	1.22	6.01	24.97	1.256E–07	31.37	7.96E–01
5H-1, 84–86	37.55	CUBE659081	153.6	158.5	12.36	1.28	6.05	18.33	8.977E–08	27.12	6.76E–01
5H-2, 84–86	39.05	CUBE659091	228.7	233.6	12.47	1.29	6.10	26.81	1.311E–07	32.36	8.28E–01
5H-3, 84–86	40.55	CUBE659101	190.3	195.2	12.62	1.24	6.46	21.14	1.083E–07	28.46	7.43E–01
5H-4, 84–86	42.05	CUBE659111	170.6	175.5	12.05	1.27	5.89	20.86	1.020E–07	26.89	7.76E–01
5H-5, 84–86	43.55	CUBE659121	193.8	198.7	12.89	1.37	6.04	23.04	1.079E–07	26.63	8.65E–01
5H-6, 84–86	45.05	CUBE659131	165.0	169.9	12.91	1.22	6.84	17.40	9.212E–08	24.83	7.01E–01
5H-7, 74–76	46.45	CUBE659141	77.9	82.8	14.09	1.44	6.60	8.78	4.113E–08	15.41	5.69E–01
6H-1, 84–86	47.05	CUBE660361	49.9	54.8	13.12	1.58	5.41	7.09	2.923E–08	8.08	8.77E–01
6H-2, 84–86	48.55	CUBE660381	28.9	33.8	14.84	1.52	6.72	3.52	1.593E–08	7.03	5.00E–01
6H-3, 84–86	50.05	CUBE660391	28.9	33.8	14.83	1.64	6.22	3.81	1.597E–08	7.20	5.29E–01
6H-4, 84–86	51.55	CUBE660401	34.6	39.5	13.56	1.61	5.56	4.98	2.040E–08	7.82	6.36E–01
6H-5, 84–86	53.05	CUBE660411	29.6	34.5	12.70	1.57	5.17	4.67	1.901E–08	9.51	4.91E–01
6H-6, 84–86	54.55	CUBE660421	136.1	141.0	12.25	1.38	5.56	17.76	8.057E–08	21.68	8.19E–01
6H-7, 64–66	55.85	CUBE660371	126.8	131.7	11.86	1.46	4.98	18.51	7.773E–08	19.61	9.44E–01
7H-1, 119–121	56.90	CUBE661671	83.8	88.7	13.07	1.38	6.14	10.11	4.751E–08	14.84	6.81E–01
7H-2, 84–86	58.05	CUBE661681	165.4	170.3	13.05	1.45	5.85	20.39	9.135E–08	21.09	9.67E–01
7H-3, 84–86	59.55	CUBE661701	82.4	87.3	14.09	1.53	6.22	9.83	4.338E–08	11.13	8.83E–01
7H-4, 84–86	61.05	CUBE661711	29.4	34.3	14.88	1.62	6.34	3.79	1.614E–08	7.87	4.81E–01
7H-5, 84–86	62.55	CUBE661721	67.7	72.6	13.82	1.31	7.03	7.23	3.678E–08	15.69	4.61E–01
7H-6, 84–86	64.05	CUBE661731	38.4	43.3	14.45	1.57	6.27	4.83	2.095E–08	10.75	4.49E–01
7H-7, 59–61	65.30	CUBE661691	9.7	14.6	14.55	1.72	5.80	1.76	7.007E–09	4.59	3.83E–01
8H-1, 129–131	66.50	CUBE662461	32.4	37.3	13.79	1.41	6.51	4.01	1.893E–08	8.07	4.96E–01
8H-2, 84–86	67.55	CUBE662471	38.8	43.7	13.84	1.50	6.16	4.97	2.209E–08	8.79	5.65E–01
8H-3, 84–86	69.05	CUBE662481	18.8	23.7	14.71	1.46	6.93	2.40	1.129E–08	6.55	3.66E–01
8H-4, 84–86	70.55	CUBE662491	23.7	28.6	15.20	1.51	7.05	2.84	1.316E–08	7.12	3.99E–01
8H-5, 84–86	72.05	CUBE662501	26.7	31.6	14.83	1.71	5.98	3.70	1.493E–08	6.04	6.13E–01
8H-6, 84–86	73.55	CUBE662511	29.0	33.9	14.75	1.60	6.37	3.73	1.610E–08	6.80	5.48E–01
8H-7, 54–56	74.75	CUBE662521	29.0	33.9	14.45	1.49	6.62	3.58	1.642E–08	6.49	5.52E–01
9H-1, 84–86	75.55	CUBE663541	49.8	54.7	14.71	1.54	6.55	5.84	2.602E–08	6.63	8.81E–01
9H-2, 84–86	77.05	CUBE663551	41.7	46.6	13.66	1.55	5.84	5.59	2.390E–08	7.18	7.79E–01
9H-3, 84–86	78.55	CUBE663561	87.9	92.8	13.82	1.50	6.15	10.56	4.698E–08	11.37	9.29E–01
9H-4, 84–86	80.05	CUBE663571	26.8	31.7	13.33	1.42	6.15	3.61	1.665E–08	8.44	4.28E–01
9H-5, 84–86	81.55	CUBE663581	31.5	36.4	13.98	1.62	5.80	4.39	1.823E–08	3.75	1.17E+00
9H-6, 84–86	83.05	CUBE663591	23.5	28.4	13.96	1.71	5.47	3.63	1.422E–08	3.68	9.87E–01
9H-7, 74–76	84.45	CUBE663601	97.3	102.2	13.72	1.55	5.90	12.13	5.214E–08	9.41	1.29E+00
10H-1, 89–91	85.10	CUBE664681	35.8	40.7	13.45	1.54	5.75	4.95	2.119E–08	9.79	5.06E–01
10H-2, 84–86	86.55	CUBE664691	26.3	31.2	13.15	1.61	5.30	4.12	1.662E–08	9.02	4.57E–01
10H-3, 84–86	88.05	CUBE664701	80.9	85.8	13.23	1.45	5.97	10.06	4.538E–08	14.37	7.00E–01

Table T21 (continued). (Continued on next page.)

Core, section, interval (cm)	Depth CSF (m)	LIMS ID	Susceptibility Raw (10^{-6})	Susceptibility Corrected (10^{-6})	Total mass (g)	Bulk density (g/cm^3)	Volume (cm^3)	Susceptibility Volume normalized (10^{-5})	Susceptibility Mass normalized (m^3/kg)	Susceptibility Whole core (raw values)	Scale factor
10H-4, 84–86	89.55	CUBE664711	44.3	49.2	14.14	1.50	6.37	5.40	2.433E–08	10.77	5.02E–01
10H-5, 84–86	91.05	CUBE664721	40.5	45.4	14.17	1.57	6.09	5.22	2.241E–08	7.44	7.01E–01
10H-6, 84–86	92.55	CUBE664731	32.7	37.6	13.61	1.62	5.56	4.73	1.933E–08	6.25	7.57E–01
10H-7, 39–41	93.60	CUBE664741	25.9	30.8	13.67	1.65	5.52	3.91	1.577E–08	4.87	8.02E–01
11H-1, 89–91	94.60	CUBE665311	42.8	47.7	14.76	1.47	6.93	4.82	2.263E–08	8.04	5.99E–01
11H-2, 84–86	96.05	CUBE665321	30.5	35.4	14.85	1.73	5.95	4.17	1.671E–08	6.87	6.07E–01
11H-3, 84–86	97.55	CUBE665331	56.4	61.3	14.33	1.61	6.05	7.10	2.996E–08	9.20	7.71E–01
11H-4, 84–86	99.05	CUBE665341	47.3	52.2	13.82	1.56	5.90	6.19	2.645E–08	7.35	8.43E–01
11H-5, 84–86	100.55	CUBE665351	38.6	43.5	14.62	1.68	5.97	5.10	2.080E–08	6.75	7.55E–01
11H-6, 84–86	102.05	CUBE665361	36.1	41.0	9.08	1.60	2.80	10.25	3.160E–08	13.19	7.77E–01
11H-7, 49–51	103.20	CUBE665371	115.6	120.5	13.53	1.53	5.82	14.48	6.234E–08	16.78	8.63E–01
12H-1, 84–86	104.05	CUBE665781	47.2	52.1	14.62	1.60	6.26	5.83	2.496E–08	8.46	6.89E–01
12H-2, 84–86	105.55	CUBE665791	57.3	62.2	14.65	2.06	4.89	8.91	2.970E–08	9.07	9.82E–01
12H-3, 84–86	107.05	CUBE665801	57.6	62.5	14.27	1.59	6.08	7.20	3.066E–08	8.33	8.64E–01
12H-4, 84–86	108.55	CUBE665811	85.5	90.4	14.46	1.58	6.24	10.13	4.374E–08	10.99	9.22E–01
12H-5, 84–86	110.05	CUBE665821	62.2	67.1	14.04	1.66	5.70	8.24	3.345E–08	8.60	9.58E–01
12H-6, 84–86	111.55	CUBE665831	59.4	64.3	13.77	1.65	5.56	8.10	3.267E–08	8.04	1.01E+00
12H-7, 39–41	112.37	CUBE665841	61.8	66.7	14.23	1.55	6.22	7.50	3.279E–08	8.76	8.56E–01
13H-2, 84–86	114.05	CUBE666811	57.5	62.4	13.85	1.64	5.64	7.75	3.153E–08	8.77	8.84E–01
13H-3, 84–86	115.55	CUBE666821	47.3	52.2	13.56	1.62	5.53	6.61	2.694E–08	6.79	9.74E–01
13H-4, 84–86	117.05	CUBE666831	107.4	112.3	13.92	1.44	6.48	12.12	5.647E–08	12.77	9.49E–01
13H-5, 84–86	118.55	CUBE666841	49.5	54.4	13.40	1.37	6.45	5.91	2.842E–08	9.29	6.36E–01
13H-6, 84–86	120.05	CUBE666851	33.6	38.5	14.97	1.72	6.04	4.47	1.802E–08	5.37	8.31E–01
13H-7, 84–86	121.55	CUBE666861	43.1	48.0	14.38	1.67	5.87	5.73	2.336E–08	7.03	8.15E–01
13H-8, 49–51	122.20	CUBE666871	44.1	49.0	13.87	1.52	6.11	5.61	2.474E–08	7.74	7.25E–01
14H-1, 84–86	123.05	CUBE667411	85.7	90.6	12.18	1.58	4.81	13.19	5.205E–08	12.93	1.02E+00
14H-2, 84–86	124.55	CUBE667421	50.9	55.8	15.07	1.60	6.54	5.96	2.590E–08	6.13	9.74E–01
14H-3, 84–86	126.05	CUBE667431	55.2	60.1	13.92	1.57	5.95	7.07	3.024E–08	4.44	1.59E+00
14H-4, 84–86	127.55	CUBE667441	94.7	99.6	13.29	1.50	5.81	11.99	5.244E–08	8.94	1.34E+00
14H-5, 84–86	129.05	CUBE667451	100.6	105.5	14.31	1.68	5.79	12.75	5.161E–08	8.00	1.59E+00
14H-6, 84–86	130.55	CUBE667461	54.4	59.3	14.12	1.65	5.78	7.19	2.941E–08	4.14	1.73E+00
15H-1, 94–96	132.65	CUBE668491	34.9	39.8	14.44	1.66	5.94	4.69	1.929E–08	6.32	7.42E–01
15H-2, 84–86	134.05	CUBE668501	28.5	33.4	12.79	1.64	4.99	4.69	1.830E–08	7.33	6.40E–01
15H-3, 84–86	135.55	CUBE668511	44.1	49.0	15.03	1.59	6.57	5.22	2.283E–08	8.23	6.35E–01
15H-4, 84–86	137.05	CUBE668521	7.2	12.1	14.18	1.59	6.02	1.41	5.967E–09	4.90	2.86E–01
15H-5, 84–86	138.55	CUBE668531	3.2	8.1	15.46	1.66	6.56	0.87	3.674E–09	4.19	2.06E–01
15H-6, 64–66	139.85	CUBE668541	9.3	14.2	14.24	1.75	5.52	1.81	6.993E–09	3.35	5.39E–01
16H-1, 94–96	142.15	CUBE669761	2.1	7.0	14.29	1.61	6.01	0.81	3.416E–09	1.86	4.37E–01
16H-2, 84–86	143.55	CUBE669771	–3.7	1.2	13.33	1.82	4.80	0.17	6.128E–10	1.49	1.14E–01
16H-3, 84–86	145.05	CUBE669781	–1.0	3.9	14.59	1.77	5.66	0.48	1.860E–09	2.19	2.19E–01
16H-4, 84–86	146.55	CUBE669791	–0.9	4.0	14.83	1.67	6.13	0.46	1.907E–09	2.19	2.10E–01
16H-5, 84–86	148.05	CUBE669801	–2.4	2.5	14.66	1.70	5.92	0.29	1.177E–09	2.46	1.19E–01
16H-6, 54–56	149.25	CUBE669811	–0.7	4.2	14.60	1.85	5.42	0.54	2.010E–09	1.76	3.08E–01
17H-1, 84–86	151.55	CUBE670691	0.3	5.2	14.94	1.70	6.07	0.60	2.428E–09	0.82	7.33E–01
17H-2, 84–86	153.05	CUBE670701	3.1	8.0	14.63	1.68	5.98	0.94	3.831E–09	0.64	1.46E+00
17H-3, 84–86	154.55	CUBE670711	–0.6	4.3	14.77	1.73	5.87	0.52	2.060E–09	1.07	4.85E–01
17H-4, 84–86	156.05	CUBE670721	5.5	10.4	11.85	1.68	4.32	1.69	6.152E–09	2.71	6.22E–01
17H-5, 84–86	157.55	CUBE670731	5.4	10.3	13.30	1.64	5.30	1.36	5.414E–09	2.55	5.32E–01
17H-6, 64–66	158.85	CUBE670741	3.2	8.1	14.89	1.75	5.90	0.96	3.789E–09	2.02	4.72E–01
18H-2, 84–86	162.55	CUBE671281	1.1	6.0	15.91	1.64	6.89	0.61	2.635E–09	1.90	3.21E–01
18H-3, 84–86	164.05	CUBE671291	–3.6	1.3	12.92	1.72	4.85	0.19	6.962E–10	0.56	3.32E–01
18H-4, 84–86	165.55	CUBE671301	2.6	7.5	14.25	1.72	5.62	0.93	3.677E–09	0.69	1.36E+00
18H-5, 84–86	167.05	CUBE671311	8.0	12.9	14.12	1.70	5.60	1.61	6.391E–09	1.12	1.44E+00
18H-6, 84–86	168.55	CUBE671321	13.4	18.3	14.23	1.64	5.88	2.18	8.997E–09	1.73	1.26E+00
18H-7, 69–71	169.80	CUBE671331	2.8	7.7	14.21	1.70	5.64	0.95	3.779E–09	1.06	8.98E–01
19H-1, 94–96	170.65	CUBE672211	4.6	9.5	14.62	1.69	5.95	1.12	4.537E–09	1.54	7.25E–01
19H-2, 84–86	171.97	CUBE672221	–5.1	–0.2	12.25	1.74	4.40	–0.03	–9.029E–11	1.24	–2.02E–02
19H-3, 84–86	173.47	CUBE672231	0.4	5.3	15.21	1.71	6.21	0.59	2.418E–09	1.35	4.40E–01
19H-4, 84–86	174.97	CUBE672241	–2.6	2.3	13.12	1.60	5.33	0.30	1.223E–09	1.01	2.97E–01
19H-5, 84–86	176.47	CUBE672251	–2.2	2.7	14.51	1.68	5.90	0.32	1.290E–09	1.13	2.80E–01
19H-6, 84–86	177.97	CUBE672261	–1.5	3.4	13.81	1.65	5.57	0.43	1.717E–09	1.14	3.75E–01
20H-1, 84–86	180.05	CUBE673001	–0.1	4.8	14.72	1.70	5.95	0.56	2.272E–09	0.77	7.34E–01
20H-2, 84–86	181.55	CUBE673011	3.6	8.5	12.88	1.58	5.23	1.13	4.592E–09	1.43	7.93E–01
20H-3, 84–86	183.05	CUBE673021	3.8	8.7	13.64	1.60	5.66	1.07	4.460E–09	1.27	8.46E–01
20H-4, 84–86	184.55	CUBE673031	0.2	5.1	14.55	1.48	6.72	0.53	2.455E–09	2.25	2.36E–01
20H-5, 84–86	186.05	CUBE673041	–1.1	3.8	12.59	1.70	4.72	0.56	2.113E–09	0.48	1.17E+00
20H-6, 84–86	187.55	CUBE673051	–1.1	3.8	14.45	1.68	5.87	0.46	1.853E–09	0.39	1.17E+00
20H-7, 39–41	188.40	CUBE673061	–2.0	2.9	15.06	1.73	6.05	0.34	1.364E–09	0.86	3.96E–01

Table T21 (continued).

Core, section, interval (cm)	Depth CSF (m)	LIMS ID	Susceptibility		Total mass (g)	Bulk density (g/cm³)	Volume (cm³)	Susceptibility			Scale factor
			Raw (10^{-6})	Corrected (10^{-6})				Volume normalized (10^{-5})	Mass normalized (m^3/kg)	Whole core (raw values)	
21H-1, 84–86	189.55	CUBE673801	–2.6	2.3	14.52	1.79	5.54	0.28	1.085E–09	1.70	1.67E–01
21H-2, 84–86	191.05	CUBE673811	–2.7	2.2	14.60	1.71	5.84	0.27	1.064E–09	1.58	1.69E–01
21H-3, 84–86	192.55	CUBE673821	–4.1	0.8	14.70	1.87	5.40	0.10	3.843E–10	1.44	7.26E–02
21H-4, 84–86	194.05	CUBE673831	–1.1	3.8	13.15	1.72	4.99	0.53	2.016E–09	1.55	3.43E–01
21H-5, 84–86	195.55	CUBE673841	3.3	8.2	13.81	1.78	5.19	1.11	4.174E–09	2.26	4.91E–01
21H-6, 84–86	197.05	CUBE673851	–3.0	1.9	14.42	1.67	5.89	0.22	9.102E–10	1.89	1.18E–01
21H-7, 29–31	198.00	CUBE673861	2.3	7.2	13.82	1.70	5.43	0.93	3.656E–09	2.11	4.41E–01
22H-2, 84–86	200.55	CUBE674691	–1.6	3.3	13.29	1.71	5.09	0.46	1.742E–09	2.26	2.01E–01
22H-3, 84–86	202.05	CUBE674701	–2.3	2.6	11.70	1.62	4.39	0.42	1.559E–09	1.71	2.44E–01
22H-4, 84–86	203.55	CUBE674711	–5.8	–0.9	13.90	1.77	5.27	–0.12	–4.558E–10	1.71	–7.01E–02
22H-5, 84–86	205.05	CUBE674721	10.8	15.7	14.14	1.72	5.54	1.98	7.777E–09	3.98	4.98E–01
22H-6, 84–86	206.55	CUBE674731	85.6	90.5	11.87	1.55	4.71	13.46	5.337E–08	15.14	8.89E–01
23X-1, 84–86	207.75	CUBE675301	47.0	51.9	13.63	1.55	5.85	6.21	2.665E–08	8.92	6.96E–01
23X-2, 104–106	209.45	CUBE675311	61.9	66.8	13.82	1.53	6.03	7.76	3.384E–08	11.76	6.59E–01
23X-3, 89–91	210.80	CUBE675321	67.0	71.9	13.61	1.69	5.34	9.42	3.699E–08	12.09	7.79E–01
23X-4, 109–111	212.50	CUBE675331	45.5	50.4	12.60	1.26	6.35	5.56	2.801E–08	9.78	5.69E–01
23X-5, 89–91	213.80	CUBE675341	54.6	59.5	13.50	1.63	5.48	7.60	3.085E–08	9.32	8.16E–01
23X-6, 89–91	215.30	CUBE675351	51.1	56.0	14.66	1.84	5.46	7.18	2.673E–08	8.92	8.04E–01
24X-1, 87–89	215.38	CUBE675891	44.9	49.8	14.12	1.68	5.68	6.13	2.466E–08	9.85	6.23E–01
24X-2, 76–78	216.77	CUBE675901	46.1	51.0	13.60	1.35	6.65	5.37	2.624E–08	9.30	5.77E–01
24X-3, 82–84	218.33	CUBE675911	47.5	52.4	14.10	1.71	5.55	6.62	2.603E–08	9.45	7.00E–01
24X-4, 92–94	219.93	CUBE675921	47.0	51.9	13.78	1.60	5.74	6.33	2.638E–08	8.77	7.22E–01
24X-5, 97–99	221.48	CUBE675931	42.1	47.0	14.49	1.44	6.89	4.77	2.268E–08	9.72	4.91E–01
24X-6, 84–86	222.85	CUBE675941	46.3	51.2	14.75	1.60	6.35	5.64	2.428E–08	11.23	5.03E–01
24X-7, 29–31	223.80	CUBE675951	52.7	57.6	14.60	1.74	5.74	7.02	2.760E–08	10.68	6.57E–01
25X-1, 94–96	225.05	CUBE677081	50.8	55.7	11.57	1.19	5.85	6.66	3.369E–08	11.06	6.02E–01
25X-2, 100–102	226.61	CUBE677091	64.8	69.7	12.19	1.61	4.73	10.30	4.000E–08	12.14	8.49E–01
25X-3, 100–102	228.11	CUBE677101	62.8	67.7	12.29	1.36	5.67	8.36	3.854E–08	10.59	7.90E–01
25X-4, 86–88	229.47	CUBE677111	54.9	59.8	12.40	1.87	4.18	10.00	3.374E–08	10.51	9.52E–01
25X-5, 84–86	230.95	CUBE677121	17.2	22.1	8.68	1.45	2.82	5.48	1.779E–08	8.86	6.18E–01
25X-6, 69–71	232.30	CUBE677131	35.0	39.9	9.99	1.95	2.77	10.09	2.794E–08	10.23	9.86E–01
26X-1, 72–74	234.33	CUBE678031	46.9	51.8	12.23	1.62	4.72	7.68	2.966E–08	11.21	6.86E–01
26X-2, 134–136	236.45	CUBE678041	40.2	45.1	10.84	1.68	3.73	8.47	2.915E–08	12.96	6.54E–01
26X-3, 112–114	237.73	CUBE678051	49.6	54.5	11.84	1.72	4.21	9.06	3.220E–08	11.58	7.82E–01
26X-4, 117–119	239.28	CUBE678061	41.8	46.7	11.72	1.55	4.61	7.09	2.787E–08	10.74	6.60E–01
26X-5, 90–92	240.51	CUBE678071	44.0	48.9	10.36	1.60	3.60	9.50	3.302E–08	13.55	7.01E–01
26X-6, 82–84	241.93	CUBE678021	82.5	87.4	12.51	1.75	4.52	13.54	4.892E–08	18.98	7.13E–01
28X-1, 129–131	254.10	CUBE679881	168.8	173.7	12.05	1.41	5.29	23.00	1.009E–07	36.62	6.28E–01
28X-3, 77–79	256.58	CUBE679891	240.1	245.0	11.80	1.35	5.33	32.19	1.453E–07	36.87	8.73E–01
28X-4, 68–70	257.99	CUBE679901	129.7	134.6	9.60	1.40	3.58	26.34	9.815E–08	31.87	8.26E–01
28X-5, 75–77	259.56	CUBE679911	158.0	162.9	12.00	1.45	5.11	22.30	9.502E–08	26.46	8.43E–01
28X-6, 65–67	260.96	CUBE679931	146.8	151.7	13.39	1.59	5.53	19.19	7.931E–08	24.79	7.74E–01
29X-1, 94–96	263.35	CUBE680611	247.2	252.1	13.85	1.50	6.17	28.59	1.274E–07	31.62	9.04E–01
29X-3, 105–107	264.97	CUBE680621	163.1	168.0	11.86	1.50	4.85	24.27	9.916E–08	26.43	9.18E–01
29X-4, 109–111	266.51	CUBE680631	122.6	127.5	12.36	1.50	5.18	17.23	7.221E–08	26.00	6.63E–01
29X-5, 103–105	267.95	CUBE680641	121.3	126.2	9.39	1.46	3.28	26.92	9.408E–08	33.45	8.05E–01
29X-6, 71–73	269.13	CUBE680651	200.6	205.5	12.48	1.10	7.18	20.04	1.153E–07	32.64	6.14E–01
29X-7, 123–125	270.81	CUBE680661	210.4	215.3	12.19	1.60	4.76	31.65	1.236E–07	26.85	1.18E+00
30X-1, 113–115	273.24	CUBE681581	107.2	112.1	12.59	1.08	7.41	10.59	6.233E–08	16.24	6.52E–01
30X-2, 106–108	274.67	CUBE681591	92.2	97.1	9.41	1.70	2.83	24.01	7.219E–08	22.44	1.07E+00
30X-3, 94–96	276.05	CUBE681601	156.0	160.9	13.63	1.68	5.37	20.98	8.263E–08	23.97	8.76E–01
30X-4, 92–94	277.53	CUBE681611	207.7	212.6	13.89	1.67	5.56	26.77	1.071E–07	30.95	8.65E–01
30X-5, 89–91	279.00	CUBE681621	257.5	262.4	13.85	1.60	5.79	31.74	1.326E–07	33.56	9.46E–01
30X-6, 89–91	280.50	CUBE681631	195.3	200.2	12.70	1.79	4.54	30.86	1.103E–07	24.73	1.25E+00
30X-7, 54–56	281.15	CUBE681641	241.9	246.8	12.26	1.37	5.58	30.94	1.409E–07	40.20	7.70E–01
									Mean scale factor:		7.06E–01

Notes: Depth = depth to middle of discrete sample measured in meters using the core depth below seafloor, method A (CSF), depth scale. LIMS ID = sample identification within the Laboratory Information Management System (LIMS) database. Susceptibility raw = volume magnetic susceptibility (in SI units) of the discrete sample measured in the Kappabridge with the volume of the cube assumed to be 7 cm^3. Susceptibility corrected = the susceptibility of the plastic cube with a label was determined to be -4.9×10^{-6} (SI) with a standard error of $\pm 0.19 \times 10^{-6}$. Mass = mass of sample including mass of plastic cube, which has a mean of 4.5921 g. Bulk density = density from moisture and density (MAD) measurements. When these were not available or were obviously anomalous, we used a density of 1.2 m^3/kg. Volume = volume of sediments, calculated by subtracting mass of plastic cube from total mass and then dividing by bulk density. Volume normalized susceptibility = susceptibility of discrete samples normalized by true sample volume. These are unitless in the SI unit system. Mass normalized susceptibility = susceptibility of discrete samples normalized by mass of sediments in each sample cube. Scale factor = factor whole-core raw susceptibility values would need to be multiplied by to convert them to SI volume normalized susceptibilities.

Table T22. Magnetostratigraphy, Site U1334. This table is available in an **oversized format.**

Table T23. Interstitial water data from squeezed whole-round samples, Site U1334. (**See table notes.**)

Core, section, interval (cm)	Depth (m)		pH	Alkalinity (mM)	Cl^- (mM)	SO_4^{2-} (mM)	HPO_4^{2-} (µM)	H_4SiO_4 (µM)	Mn^{2+} (µM)	Fe^{2+} (µM)	Ca^{2+} (mM)	Mg^{2+} (mM)	B (µM)	Sr^{2+} (µM)	Ba^{2+} (µM)	Li^+ (µM)	K^+ (mM)
	CSF	CCSF-A															
320-U1334A-																	
1H-2, 145–150	2.95	2.95	7.58	2.73	553	28.4	1.86	417	0.56	0.74	10.3	52.4	485	78.0	0.83	25.3	10.6
1H-4, 145–150	5.95	5.95	7.62	2.83	555	28.6	1.28	456	0.44	0.36	10.6	53.5	499	82.6	0.86	25.0	11.2
2H-2, 145–150	11.15	12.02	7.66	3.00	557	28.2	0.96	494	0.93	BDL	10.7	52.3	496	80.8	0.97	25.9	11.0
2H-5, 145–150	15.65	16.52	7.65	3.32	558	28.4	0.84	511	BDL	BDL	10.8	52.5	499	86.7	0.89	22.6	11.2
3H-2, 145–150	20.65	22.62	7.62	3.04	560	28.2	0.86	492	1.63	BDL	10.7	52.7	491	82.6	1.50	21.7	11.1
3H-5, 145–150	25.15	27.12	7.62	3.00	560	26.3	0.71	495	0.39	BDL	10.7	53.0	495	84.5	0.99	21.2	11.0
4H-2, 145–150	30.15	33.63	7.61	3.16	563	28.5	0.68	489	1.46	2.11	11.0	54.0	488	87.6	1.09	20.7	11.4
4H-5, 145–150	34.65	38.13	7.60	3.18	563	27.5	0.85	528	0.47	BDL	11.0	53.9	482	88.8	1.00	20.5	11.4
5H-2, 145–150	39.65	44.42	7.52	3.00	560	27.6	0.77	519	0.69	BDL	11.0	53.1	494	89.7	1.24	20.4	11.5
5H-5, 145–150	44.15	48.92	7.52	3.13	565	26.5	0.77	521	1.06	0.29	10.8	53.1	493	89.7	0.92	19.9	11.2
6H-2, 145–150	49.15	56.08	7.58	3.22	563	25.4	0.77	501	1.01	BDL	10.9	53.2	482	89.7	1.01	19.3	11.0
6H-5, 145–150	53.65	60.58	7.54	3.23	562	25.1	0.80	544	1.49	BDL	10.9	53.1	477	92.6	1.07	19.6	11.4
7H-3, 140–150	60.10	67.52	7.48	3.23	563	25.2	0.74	516	2.75	1.29	11.3	55.0	460	88.9	0.99	19.0	10.8
8H-3, 140–150	69.60	78.66	7.48	3.26	566	24.4	0.92	554	3.23	BDL	10.8	52.7	454	90.3	0.95	18.1	10.5
9H-3, 140–150	79.10	90.32	—	—	562	26.2	0.81	592	4.31	1.04	10.9	52.5	466	95.2	1.04	18.2	10.9
10H-3, 140–150	88.60	99.91	7.45	3.17	558	26.8	0.92	583	5.15	BDL	11.4	52.2	469	102.2	0.96	17.5	11.2
11H-3, 140–150	98.10	111.02	7.26	3.24	564	25.0	0.59	573	5.70	0.51	11.2	52.8	451	102.5	1.04	17.1	11.2
12H-3, 140–150	107.60	121.75	7.51	3.33	562	25.5	0.77	589	5.97	BDL	11.4	53.9	476	105.1	0.95	16.8	11.5
13H-4, 140–150	117.60	133.04	7.63	3.26	561	26.6	0.83	620	4.77	0.37	11.4	53.3	448	104.2	1.02	16.0	11.3
14H-3, 140–150	126.60	143.53	7.51	3.41	561	26.1	0.75	623	3.76	BDL	11.5	53.2	452	103.0	0.92	15.8	11.3
15H-3, 140–150	134.70	153.56	7.41	3.61	564	25.7	0.79	668	2.79	0.49	11.4	52.0	435	103.5	0.94	15.6	11.0
16H-3, 140–150	145.60	166.16	7.57	3.50	562	24.6	0.62	701	1.92	4.17	11.0	52.6	463	106.5	0.97	17.3	11.2
17H-3, 140–150	155.10	178.32	7.89	3.15	559	24.4	0.56	735	1.52	4.85	11.0	52.2	442	107.0	1.08	17.4	11.3
18H-3, 140–150	164.60	188.70	7.81	3.36	563	25.5	0.61	667	1.16	2.52	11.2	53.4	461	105.5	0.96	16.6	11.3
19H-3, 140–150	174.02	200.44	7.42	3.29	563	25.2	0.63	714	1.00	3.03	11.1	52.6	456	105.9	0.99	15.7	11.2
20H-3, 140–150	183.60	210.58	7.47	4.02	559	24.5	0.64	795	1.03	2.30	10.7	51.8	466	103.9	0.93	16.7	10.8
21H-3, 140–150	193.10	223.10	7.42	3.62	559	24.2	0.79	664	0.67	BDL	11.0	52.4	448	99.6	0.97	15.6	10.4
22H-3, 140–150	202.60	245.30	7.52	3.69	559	25.6	0.70	771	0.55	0.30	11.0	52.4	453	99.0	0.98	15.7	10.5
23X-3, 140–150	211.30	255.60	7.60	3.38	562	25.9	0.77	826	0.38	0.41	11.3	52.6	442	101.5	1.05	15.8	10.6
24X-2, 140–150	217.40	264.30	7.53	3.34	562	25.9	0.73	745	1.01	1.12	11.4	52.4	448	98.7	1.07	15.7	10.7
25X-3, 140–150	228.50	275.90	7.51	3.24	564	25.5	0.62	764	0.30	0.28	11.0	51.2	422	99.3	0.98	16.9	10.4
26X-3, 140–150	238.00	285.71	7.51	3.38	559	24.7	0.61	746	BDL	0.26	10.9	51.2	441	97.4	1.13	19.0	10.7
28X-3, 140–150	257.20	306.11	7.48	3.19	561	27.6	0.52	830	0.32	BDL	11.4	52.2	430	94.3	1.01	26.4	10.3
30X-3, 140–150	275.37	326.34	7.57	3.07	553	27.2	0.51	842	1.16	BDL	10.8	52.9	403	85.6	1.02	29.9	10.1

Notes: — = no data. BDL = below detection limit (Mn^{2+} = 0.3 µM, Fe^{2+} = 0.2 µM). H_4SiO_4 values measured by different techniques during Expeditions 320 and 321 disagree significantly, especially for low values. Therefore, caution should be used concerning the H_4SiO_4 data and comparison between the different expeditions.

Table T24. Interstitial water data from rhizon samples, Site U1334. (See table notes.)

Core, section, interval (cm)	Depth (m) CSF	Depth (m) CCSF-A	pH	Alkalinity (mM)	SO_4^{2-} (mM)	H_4SiO_4 (µM)	Mn^{2+} (µM)	Fe^{2+} (µM)	B (µM)	Sr^{2+} (µM)	Ba^{2+} (µM)	Li^+ (µM)
320-U1334B-												
13H-5, 75	122.45	141.44	7.5	3.23	23.5	700	5.44	0.60	492	97.5	BDL	16.7
13H-6, 75	123.95	142.94	7.4	3.23	25.7	653	4.74	0.27	477	94.4	BDL	15.9
320-U1334C-												
13H-5, 75	120.75	145.88	7.5	3.17	26.7	728	4.31	BDL	477	101.5	BDL	16.9
13H-6, 75	122.25	147.38	7.6	3.31	24.6	703	4.01	BDL	468	99.2	BDL	16.0
14H-1, 79	124.29	151.35	7.6	3.09	24.6	572	3.48	0.20	491	99.2	0.85	15.6
14H-2, 79	125.79	152.85	7.4	3.42	26.0	580	3.69	0.70	482	98.1	0.66	15.3
14H-3, 79	127.29	154.35	7.4	3.18	24.5	667	3.05	0.14	486	104.3	BDL	16.3
14H-4, 79	128.79	155.85	—	—	24.6	623	3.04	0.23	485	100.5	BDL	16.2
14H-5, 79	130.29	157.35	7.6	3.21	25.4	643	3.32	1.26	470	97.9	BDL	15.9
14H-6, 79	131.79	158.85	7.5	3.23	26.5	669	2.70	0.27	478	101.4	BDL	16.7
15H-1, 75	133.75	161.98	7.5	2.73	25.8	410	2.33	0.66	440	89.1	BDL	19.4
15H-2, 75	135.25	163.48	7.5	3.30	25.3	640	2.36	0.45	463	97.2	BDL	15.3
15H-3, 75	136.75	164.98	7.4	3.27	24.4	617	2.26	0.30	460	94.9	0.62	15.1
15H-4, 75	138.25	166.48	7.5	3.28	25.2	668	2.05	BDL	483	98.8	BDL	16.0
15H-5, 75	139.75	167.98	7.6	3.24	25.5	673	1.93	0.53	478	96.7	BDL	15.6
15H-6, 75	141.25	169.48	7.5	3.19	24.9	705	1.87	0.75	485	98.7	BDL	15.6
16H-1, 100	143.50	173.19	7.5	3.31	26.0	652	1.57	0.98	473	97.1	BDL	15.2
16H-2, 75	144.75	174.44	7.6	3.19	24.6	684	1.56	1.69	485	100.1	BDL	15.6
16H-3, 75	146.25	175.94	7.6	3.35	26.1	690	1.52	1.42	479	101.1	BDL	15.5
16H-4, 75	147.85	177.54	7.7	3.47	24.9	683	2.05	1.47	483	103.0	0.60	16.5
16H-5, 75	149.25	178.94	7.6	2.95	24.5	715	1.56	2.55	481	101.2	BDL	16.2
16H-6, 75	150.75	180.44	7.6	2.96	25.7	693	1.39	1.74	468	99.2	BDL	15.5
17H-1, 115	153.15	183.50	7.7	3.01	26.2	686	1.21	1.50	482	100.1	BDL	15.5
17H-2, 75	154.25	184.60	7.6	3.34	24.4	731	1.26	0.57	483	99.2	BDL	15.2
17H-3, 75	155.75	186.10	7.7	3.13	26.3	753	1.22	3.77	480	101.4	BDL	16.4
17H-4, 75	157.25	187.60	7.6	3.11	24.4	719	1.17	2.37	475	99.2	0.46	15.9
17H-5, 75	158.75	189.10	7.6	3.17	23.7	720	1.08	2.27	466	95.7	BDL	15.1
17H-6, 75	160.25	190.60	7.5	3.13	25.6	703	1.71	4.53	491	102.8	BDL	16.3
18H-1, 75	162.25	193.69	7.7	3.20	24.1	707	1.00	1.93	467	98.0	BDL	16.0
18H-2, 75	163.75	195.19	—	3.30	25.2	722	1.05	2.33	477	100.8	BDL	15.8
18H-3, 75	165.25	196.69	7.9	3.72	24.1	662	0.99	3.01	476	97.9	BDL	15.3
18H-4, 75	166.75	198.19	7.6	3.23	26.2	672	0.98	2.85	481	100.7	BDL	15.6
18H-5, 75	168.25	199.69	7.6	3.48	25.1	659	0.94	2.31	487	100.4	BDL	15.6
18H-6, 75	169.75	201.19	7.5	3.21	24.7	731	0.91	2.81	479	97.6	BDL	15.3
19H-1, 75	171.75	204.27	7.5	3.31	26.4	710	1.36	3.97	482	101.6	BDL	15.6
19H-2, 75	173.25	205.77	7.6	3.30	25.8	665	0.76	2.52	474	98.4	BDL	15.3
19H-3, 75	174.75	207.27	7.6	3.10	25.2	698	0.77	2.54	473	98.9	BDL	15.5
19H-4, 75	176.25	208.77	7.6	3.25	25.6	663	0.84	1.82	469	96.1	BDL	15.0
19H-5, 75	177.75	210.27	7.5	3.24	25.1	375	0.81	2.66	479	97.9	BDL	15.4
19H-6, 75	179.25	211.77	7.5	3.39	26.1	690	0.75	1.55	456	94.4	BDL	15.0
20H-1, 75	181.25	215.02	7.5	3.25	25.7	685	1.09	2.48	464	99.1	BDL	15.7
20H-2, 75	182.75	216.52	7.4	3.34	25.7	675	0.87	1.43	474	97.6	BDL	15.6
20H-3, 75	184.25	218.02	7.5	3.52	25.7	691	1.42	2.47	471	97.4	BDL	15.7
20H-4, 75	185.75	219.52	7.4	3.33	24.5	709	0.77	1.40	471	99.4	BDL	15.8
20H-5, 75	187.25	221.02	7.6	3.12	24.4	897	0.69	1.35	480	100.4	BDL	16.8
20H-6, 75	188.75	222.52	7.6	3.12	24.1	733	0.70	0.87	461	97.3	BDL	16.1
21H-1, 75	190.75	224.95	7.6	3.29	25.5	712	0.65	0.24	466	103.7	BDL	17.5
21H-2, 75	192.25	226.45	7.6	3.30	23.9	697	0.59	0.23	457	101.8	BDL	17.3
21H-3, 75	193.75	227.95	7.6	3.33	24.8	692	0.59	0.12	460	101.3	BDL	17.0
21H-4, 75	195.25	229.45	7.6	3.46	25.0	716	0.59	0.19	484	99.2	BDL	15.9
21H-5, 75	196.75	230.95	7.6	3.32	25.3	690	0.57	BDL	455	99.7	BDL	17.8
21H-6, 75	198.25	232.45	—	—	24.6	708	0.56	BDL	474	100.2	BDL	16.9
22H-1, 75	200.25	236.05	7.6	3.25	24.7	649	0.45	BDL	465	100.4	BDL	17.8
22H-2, 75	201.75	237.55	—	—	24.1	459	0.46	0.23	465	101.5	BDL	17.5
22H-3, 75	203.25	239.05	7.7	3.32	25.6	659	0.43	0.10	463	98.8	BDL	17.4
22H-4, 75	204.75	240.55	7.7	3.30	24.6	687	1.22	0.29	462	99.6	BDL	16.9
22H-5, 75	206.25	242.05	7.7	3.69	23.5	686	0.49	0.24	461	95.9	BDL	16.6
22H-6, 75	207.75	243.55	7.6	3.58	24.9	668	0.27	BDL	471	95.7	BDL	16.9
23X-1, 75	209.75	250.68	7.7	2.31	25.3	371	1.74	BDL	428	86.8	BDL	22.0
23X-2, 75	211.25	252.18	7.6	2.59	26.8	457	1.03	BDL	441	91.9	BDL	21.1
23X-3, 75	212.75	253.68	7.6	3.00	25.7	595	0.17	0.19	465	96.3	BDL	18.6

Notes: — = no data. BDL = below detection limit (Mn^{2+} = 0.03 µM, Fe^{2+} = 0.1 µM, Ba^{2+} = 0.4 µM) calculated as three times the standard deviation of multiple measures of a blank. H_4SiO_4 values measured by different techniques during Expeditions 320 and 321 disagree significantly, especially for low values. Therefore, caution should be used concerning the H_4SiO_4 data and comparison between the different expeditions.

Table T25. Inorganic geochemistry of solid samples, Hole U1334A. (**See table notes.**)

Core, section, interval (cm)	Depth CSF (m)	Major element oxide (wt%)										Trace element (ppm)							
		SiO_2	Al_2O_3	Fe_2O_3T	MnO	MgO	CaO	Na_2O	K_2O	TiO_2	P_2O_5	Ba	Cr	Cu	Sc	Sr	V	Y	Zr
320-U1334A-																			
1H-3, 65–66	3.65	52.11	12.10	6.87	2.81	3.78	1.27	4.47	2.21	0.57	0.79	9832	46.0	1606	39.2	376.9	115.4	269.9	234.5
2H-3, 64-65	11.84	53.66	9.68	8.17	3.90	3.72	1.58	5.20	1.83	0.45	0.96	7706	31.6	1937	38.0	344.6	89.3	359.8	239.8
3H-3, 65–66	21.35	23.35	3.07	3.05	0.73	1.52	30.93	3.05	0.74	0.14	0.43	2921	14.5	427	9.4	1326	22.4	83.7	81.9
5H-3, 65–66	40.35	41.71	4.77	5.99	1.26	2.40	16.97	4.18	1.10	0.20	0.42	8156	24.4	748	11.3	1045	61.7	79.5	103.3
6H-3, 65–66	49.85	7.42	0.21	0.56	0.12	0.43	39.65	1.24	0.12	0.01	0.22	1418	BDL	89	0.6	1824	BDL	17.6	18.1
11H-3, 65–66	97.35	12.21	0.68	1.20	0.13	0.62	38.21	1.58	0.25	0.03	0.16	2221	6.3	160	2.1	2144	BDL	21.9	27.8
14H-3, 65–66	125.85	11.43	0.54	1.01	0.17	0.52	42.34	1.45	0.21	0.02	0.29	1973	5.9	109	1.4	2212	BDL	18.1	22.0
17H-3, 65–66	154.35	7.45	0.24	0.54	0.11	0.38	41.20	1.09	0.14	0.01	0.16	1494	19.4	46	0.5	2051	BDL	15.1	18.1
20H-3, 65–66	182.85	8.42	0.29	0.68	0.07	0.42	39.07	1.16	0.18	0.01	BDL	1535	BDL	82	0.9	2010	BDL	13.9	22.0
24X-2, 45–46	216.45	13.35	0.28	0.96	0.20	0.46	40.70	1.20	0.15	0.01	0.21	1668	BDL	100	1.4	1681	BDL	12.8	23.8
25X-6, 52–53	232.12	22.56	0.30	1.17	0.31	0.58	36.01	1.62	0.18	0.01	0.26	1652	BDL	111	1.0	1357	BDL	17.3	20.1
27X-1, 119–120	244.39	8.79	0.21	0.99	0.19	0.45	40.55	1.01	0.10	0.01	0.20	1403	5.3	87	1.2	1805	BDL	15.6	22.4
27X-3, 90–91	247.10	23.63	1.76	3.62	1.21	1.20	34.18	1.61	0.61	0.06	0.28	3332	9.3	269	3.7	1776	28.7	38.9	44.0
27X-6, 9–10	249.79	33.14	1.26	4.55	1.42	1.56	29.75	2.02	0.47	0.06	0.31	3916	10.1	290	4.6	1334	39.0	38.2	42.5
28X-1, 80–81	253.60	24.91	1.15	4.83	1.43	1.67	31.16	2.04	0.45	0.06	0.34	2922	11.5	314	3.8	1322	39.4	42.7	44.5
28X-3, 56–57	256.36	52.24	2.27	9.75	5.14	3.08	13.61	3.52	0.81	0.11	0.54	6861	16.1	723	8.0	695.7	106.1	78.2	78.5
29X-3, 54–55	264.45	23.10	0.83	4.17	1.71	1.52	33.75	1.54	0.41	0.04	0.28	4000	8.9	288	3.4	1523	43.2	37.0	39.2
31X-2, 20–21	283.50	7.04	0.34	1.23	0.21	0.66	39.82	0.69	0.21	0.02	0.29	BDL	BDL	107	1.4	1107	BDL	15.1	20.1

Notes: BDL = below detection limit (SiO_2 = 3.5 wt%, Al_2O_3 = 0.04 wt%, Fe_2O_3 T = 0.003 wt%, MnO = 0.0004 wt%, MgO = 0.007 wt%, CaO = 0.1 wt%, Na_2O = 0.02 wt%, K_2O = 0.004 wt%, TiO_2 = 0.001 wt%, P_2O_5 = 0.1 wt%, Ba = 28 wt%, Cr = 5 wt%, Cu = 16 wt%, Sc = 0.4 wt%, Sr = 3 wt%, V = 4 wt%, Y = 1.7 wt%, Zr = 4 wt%). See Table **T9** in the "Methods" chapter for maximum values of calibration.

Table T26. Calcium carbonate and organic carbon data, Site U1334. (See table notes.) (Continued on next page.)

Core, section, interval (cm)	Depth CSF (m)	Carbon (wt%)			
		$CaCO_3$	IC	TC	TOC
320-U1334A-					
1H-1, 65–66	0.65	BDL	BDL	0.20	0.15
1H-2, 65–66	2.15	BDL	BDL	ND	ND
1H-3, 65–66	3.65	BDL	BDL	ND	ND
1H-4, 65–66	5.15	BDL	BDL	ND	ND
1H-5, 65–66	6.65	BDL	BDL	ND	ND
1H-6, 20–21	7.70	BDL	BDL	ND	ND
2H-1, 64–65	8.84	BDL	BDL	ND	ND
2H-2, 64–65	10.34	BDL	BDL	0.19	0.096
2H-3, 64–65	11.84	BDL	BDL	ND	ND
2H-4, 64–65	13.34	BDL	BDL	ND	ND
2H-5, 64–65	14.84	BDL	BDL	ND	ND
2H-6, 64–65	16.34	BDL	BDL	ND	ND
2H-7, 64–65	17.84	59.9	7.20	ND	ND
3H-1, 65–66	18.35	37.6	4.51	4.36	0.06
3H-2, 65–66	19.85	27.6	3.32	ND	ND
3H-3, 65–66	21.35	59.5	7.15	ND	ND
3H-4, 65–66	22.85	30.3	3.64	ND	ND
3H-5, 65–66	24.35	19.4	2.33	ND	ND
3H-6, 65–66	25.85	20.0	2.41	ND	ND
3H-7, 30–31	27.00	72.0	8.65	ND	ND
4H-1, 65–66	27.85	33.7	4.05	4.07	0.05
4H-2, 65–66	29.35	73.8	8.86	ND	ND
4H-3, 65–66	30.85	20.9	2.51	ND	ND
4H-4, 65–66	32.35	51.3	6.15	ND	ND
4H-5, 65–66	33.85	12.7	1.53	ND	ND
4H-6, 65–66	35.35	18.2	2.19	ND	ND
4H-7, 29–30	36.49	BDL	BDL	ND	ND
5H-1, 65–66	37.35	28.2	3.39	ND	ND
5H-2, 65–66	38.85	3.4	0.41	ND	ND
5H-3, 65–66	40.35	26.4	3.17	ND	ND
5H-4, 65–66	41.85	54.9	6.60	6.19	0.05
5H-5, 65–66	43.35	45.5	5.47	ND	ND
5H-6, 65–66	44.85	65.8	7.90	ND	ND
5H-7, 55–56	46.25	58.4	7.01	ND	ND
6H-1, 65–66	46.85	89.1	10.69	ND	ND
6H-2, 65–66	48.35	92.2	11.07	10.52	BDL
6H-3, 65–66	49.85	87.9	10.55	ND	ND
6H-4, 65–66	51.35	85.9	10.32	ND	ND
6H-5, 65–66	52.85	85.4	10.25	ND	ND
6H-6, 65–66	54.35	59.4	7.14	ND	ND
7H-1, 65–66	56.35	78.6	9.43	9.49	BDL
7H-2, 65–66	57.85	37.3	4.48	ND	ND
7H-3, 65–66	59.35	76.7	9.21	ND	ND
7H-4, 65–66	60.85	85.6	10.27	ND	ND
7H-5, 65–66	62.35	74.7	8.96	ND	ND
7H-6, 65–66	63.85	81.1	9.73	ND	ND
7H-7, 39–40	65.09	88.7	10.65	ND	ND
8H-2, 65–66	67.35	77.7	9.33	10.12	BDL
8H-3, 65–66	68.85	91.1	10.93	ND	ND
8H-4, 65–66	70.35	88.3	10.60	ND	ND
8H-5, 65–66	71.85	91.6	10.99	ND	ND
8H-6, 65–66	73.35	87.6	10.51	ND	ND
8H-7, 36–37	74.56	87.9	10.56	ND	ND
9H-1, 75–76	76.10	84.2	10.10	11.00	0.04
9H-2, 65–66	76.85	84.3	10.12	ND	ND
9H-3, 65–66	78.35	73.7	8.85	ND	ND
9H-4, 65–66	79.85	82.4	9.90	ND	ND
9H-5, 65–66	81.35	89.9	10.80	ND	ND
9H-6, 65–66	82.85	88.7	10.65	ND	ND
9H-7, 55–56	84.25	80.0	9.60	ND	ND
10H-1, 100–101	85.20	82.7	9.92	10.71	0.04
10H-2, 65–66	86.35	87.4	10.50	ND	ND
10H-3, 65–66	87.85	68.2	8.18	ND	ND
10H-4, 65–66	89.35	84.4	10.14	ND	ND
10H-5, 65–66	90.85	84.1	10.10	ND	ND
10H-6, 65–66	92.35	91.6	11.00	ND	ND
11H-1, 77–78	94.47	85.8	10.30	11.30	0.04
11H-2, 65–66	95.85	88.5	10.63	ND	ND
11H-3, 65–66	97.35	79.3	9.52	ND	ND
11H-4, 65–66	98.85	79.4	9.53	ND	ND
11H-5, 65–66	100.35	81.9	9.83	ND	ND
11H-6, 65–66	101.85	79.0	9.49	ND	ND
11H-7, 29–30	102.99	61.4	7.37	ND	ND
12H-1, 65–66	103.85	82.8	9.93	10.14	0.03
12H-2, 65–66	105.35	78.9	9.47	ND	ND
12H-3, 65–66	106.85	78.9	9.47	ND	ND
12H-4, 65–66	108.35	82.5	9.90	ND	ND
12H-5, 65–66	109.85	84.2	10.11	ND	ND
12H-6, 65–66	111.35	86.7	10.40	ND	ND
12H-7, 20–21	112.17	79.3	9.52	ND	ND
13H-2, 65–66	113.85	83.7	10.05	ND	ND
13H-3, 65–66	115.35	88.5	10.62	10.15	0.04
13H-4, 65–66	116.85	51.1	6.13	ND	ND
13H-5, 65–66	118.35	82.2	9.87	ND	ND
13H-6, 65–66	119.85	88.2	10.59	ND	ND
13H-7, 65–66	121.35	85.8	10.30	ND	ND
14H-1, 65–66	122.85	77.1	9.26	10.33	0.04
14H-2, 65–66	124.35	79.8	9.58	ND	ND
14H-3, 65–66	125.85	82.2	9.87	ND	ND
14H-4, 65–66	127.35	79.9	9.59	ND	ND
14H-5, 65–66	128.85	75.3	9.04	ND	ND
14H-6, 65–66	130.35	84.8	10.18	ND	ND
14H-7, 25–26	131.45	82.2	9.87	ND	ND
15H-1, 75–76	132.45	92.5	11.10	11.23	0.04
15H-2, 65–66	133.85	86.7	10.41	ND	ND
15H-3, 65–66	135.35	79.2	9.50	ND	ND
15H-4, 65–66	136.85	88.6	10.63	ND	ND
15H-5, 65–66	138.35	89.1	10.70	ND	ND
15H-6, 45–46	139.65	89.8	10.79	ND	ND
15H-7, 40–41	140.60	82.8	9.94	ND	ND
16H-1, 74–75	141.94	82.2	9.87	10.46	0.04
16H-2, 64–65	143.34	92.3	11.08	ND	ND
16H-3, 64–65	144.84	97.8	11.74	ND	ND
16H-4, 64–65	146.34	86.0	10.32	ND	ND
16H-5, 64–65	147.84	94.5	11.35	ND	ND
16H-6, 34–35	149.04	89.0	10.69	ND	ND
17H-1, 65–66	151.35	88.1	10.58	11.06	0.04
17H-2, 65–66	152.85	75.9	9.11	ND	ND
17H-3, 65–66	154.35	90.5	10.86	ND	ND
17H-4, 65–66	155.85	90.5	10.87	ND	ND
17H-5, 65–66	157.35	89.3	10.72	ND	ND
17H-6, 45–46	158.65	93.2	11.19	ND	ND
18H-2, 65–66	162.35	89.7	10.77	11.70	0.04
18H-3, 65–66	163.85	93.9	11.27	ND	ND
18H-4, 65–66	165.35	90.2	10.83	ND	ND
18H-5, 65–66	166.85	87.7	10.53	ND	ND
18H-6, 65–66	168.35	83.3	10.00	ND	ND
18H-7, 50–51	169.60	88.0	10.56	ND	ND
19H-1, 65–66	170.35	88.9	10.67	11.28	0.04
19H-2, 65–67	171.77	87.2	10.46	ND	ND
19H-3, 65–67	173.27	91.5	10.99	ND	ND
19H-4, 65–67	174.77	86.2	10.35	ND	ND
19H-5, 65–67	176.27	88.4	10.61	ND	ND
19H-6, 65–67	177.77	89.0	10.68	ND	ND
20H-1, 65–67	179.85	85.3	10.24	11.05	0.04
20H-2, 65–66	181.35	86.0	10.32	ND	ND
20H-3, 65–66	182.85	85.9	10.31	ND	ND
20H-4, 65–66	184.35	85.1	10.22	ND	ND
20H-5, 65–66	185.85	89.2	10.71	ND	ND
20H-6, 65–66	187.35	90.2	10.82	ND	ND
20H-7, 20–21	188.20	88.5	10.62	ND	ND
21H-1, 64–65	189.34	92.0	11.04	11.13	0.03
21H-2, 64–65	190.84	87.8	10.54	ND	ND

Table T26 (continued).

Core, section, interval (cm)	Depth CSF (m)	Carbon (wt%)			
		$CaCO_3$	IC	TC	TOC
21H-3, 64–65	192.34	89.4	10.73	ND	ND
21H-4, 64–65	193.84	95.4	11.45	ND	ND
21H-5, 64–65	195.34	87.8	10.54	ND	ND
21H-6, 64–65	196.84	88.4	10.61	ND	ND
21H-7, 9–10	197.79	90.9	10.91	ND	ND
22H-2, 70–71	200.40	89.1	10.69	11.71	0.04
22H-3, 65–66	201.85	88.2	10.58	ND	ND
22H-4, 65–66	203.35	92.1	11.06	ND	ND
22H-5, 65–66	204.85	91.5	10.98	ND	ND
22H-6, 65–66	206.35	75.0	9.00	ND	ND
23X-1, 65–66	207.55	83.7	10.04	ND	ND
23X-2, 65–66	209.05	77.0	9.24	10.15	0.03
23X-3, 65–66	210.55	77.6	9.31	ND	ND
23X-4, 65–66	212.05	79.8	9.57	ND	ND
23X-5, 65–66	213.55	84.9	10.19	ND	ND
24X-1, 54–55	215.04	84.4	10.13	10.42	0.04
23X-6, 65–66	215.05	85.4	10.25	ND	ND
24X-2, 45–46	216.45	80.6	9.68	ND	ND
24X-3, 37–38	217.87	77.1	9.26	ND	ND
24X-4, 40–41	219.40	76.4	9.17	ND	ND
24X-5, 40–41	220.90	83.7	10.04	ND	ND
24X-6, 40–41	222.40	81.8	9.82	ND	ND
24X-7, 20–21	223.70	82.1	9.85	ND	ND
25X-1, 70–71	224.80	61.9	7.43	9.57	0.04
25X-2, 69–70	226.29	69.9	8.39	ND	ND
25X-3, 77–78	227.87	67.2	8.06	ND	ND
25X-4, 67–68	229.27	67.4	8.09	ND	ND
25X-5, 59–60	230.69	71.8	8.62	ND	ND
25X-6, 52–53	232.12	68.9	8.27	ND	ND
25X-7, 21–22	233.31	73.4	8.81	ND	ND
26X-1, 39–40	233.99	65.1	7.81	8.65	BDL
26X-2, 116–117	236.26	78.0	9.36	ND	ND
26X-3, 95–96	237.55	79.6	9.56	ND	ND
26X-4, 89–90	238.99	77.6	9.31	ND	ND
26X-5, 60–61	240.20	73.3	8.80	ND	ND
26X-6, 63–63	241.73	80.1	9.61	ND	ND
27X-1, 119–120	244.39	84.7	10.16	ND	ND
27X-2, 77–78	245.47	64.1	7.70	8.24	0.04
27X-3, 90–91	247.10	62.5	7.50	ND	ND
27X-4, 90–91	248.10	54.1	6.50	ND	ND
27X-5, 90–91	249.10	9.2	1.11	1.91	0.06
27X-6, 9–10	249.79	49.5	5.95	ND	ND
27X-CC, 41–42	250.73	50.0	6.00	ND	ND
28X-1, 80–81	253.60	55.6	6.68	ND	ND
28X-2, 123–124	255.53	BDL	BDL	0.68	0.09
28X-3, 56–57	256.36	17.2	2.06	ND	ND
28X-4, 41–42	257.71	39.6	4.75	ND	ND
28X-5, 65–66	259.45	50.8	6.10	6.75	BDL
28X-6, 55–56	260.85	55.4	6.66	ND	ND
28X-7, 19–20	261.99	54.2	6.51	ND	ND
29X-1, 53–55	262.93	62.5	7.50	7.86	0.03
29X-3, 54–55	264.45	61.1	7.33	ND	ND
29X-4, 84–86	266.25	69.3	8.32	ND	ND
29X-5, 76–78	267.67	37.1	4.45	ND	ND
29X-6, 47–49	268.88	69.9	8.39	ND	ND
29X-7, 70–72	270.27	54.2	6.51	ND	ND
29X-8, 42–44	271.50	64.5	7.75	ND	ND
30X-1, 78–79	272.88	72.7	8.73	9.56	0.03
30X-2, 77–78	274.37	76.3	9.16	ND	ND
30X-3, 83–84	275.93	71.7	8.61	ND	ND
30X-4, 83–84	277.43	66.5	7.99	ND	ND
30X-5, 103–104	279.13	52.1	6.25	ND	ND
30X-6, 46–47	280.06	79.2	9.50	ND	ND
30X-7, 41–42	281.01	73.5	8.82	ND	ND
31X-1, 65–66	282.45	84.4	10.13	10.64	0.04
31X-2, 20–21	283.50	86.2	10.34	ND	ND

Notes: IC = inorganic carbon, TC = total carbon, TOC = total organic carbon determined by acidification method. BDL = below detection limit ($CaCO_3$ = <1 wt%, TOC = <0.03 wt%) as determined by three times the standard deviation of replicate measures of a low concentration sample. ND = not determined.

Table T27. Moisture and density measurements, Hole U1334A. (**Continued on next page.**)

Core, section, interval (cm)	Depth CSF (m)	Water content (%)	Density (g/cm³)			Porosity (%)
			Wet bulk	Dry bulk	Grain	
320-U1334A-						
1H-1, 75–76	0.75	79.4	1.19	0.25	3.23	92.4
1H-2, 75–76	2.25	75.5	1.21	0.30	2.85	89.6
1H-4, 75–76	5.25	75.2	1.22	0.30	2.85	89.4
1H-5, 75–76	6.75	78.3	1.18	0.26	2.60	90.2
1H-6, 75–76	8.25	76.6	1.20	0.28	2.81	90.0
2H-1, 75–76	8.95	76.8	1.18	0.27	2.43	88.7
2H-7, 75–76	17.95	56.8	1.42	0.61	2.89	78.8
3H-1, 75–76	18.45	72.3	1.24	0.34	2.69	87.2
3H-2, 75–76	19.95	74.9	1.21	0.30	2.57	88.2
3H-3, 75–76	21.45	67.7	1.25	0.40	2.29	82.4
3H-4, 75–76	22.95	66.9	1.34	0.44	3.59	87.6
3H-5, 75–76	24.45	75.2	1.22	0.30	2.88	89.5
3H-6, 75–76	25.95	72.7	1.22	0.33	2.56	86.9
3H-7, 75–76	27.45	58.0	1.31	0.55	2.15	74.3
4H-2, 75–76	29.45	55.6	1.42	0.63	2.75	77.1
4H-3, 75–76	30.95	41.3	2.00	1.17	6.10	80.8
4H-4, 75–76	32.45	60.9	1.29	0.50	2.15	76.6
4H-5, 75–76	33.95	53.5	1.53	0.71	3.56	80.0
4H-6, 75–76	35.45	76.7	1.20	0.28	2.77	89.9
4H-7, 75–76	36.95	74.0	1.22	0.32	2.77	88.5
5H-1, 75–76	37.45	66.1	1.28	0.44	2.54	82.8
5H-3, 75–76	40.45	72.7	1.24	0.34	2.86	88.1
5H-4, 75–76	41.95	69.8	1.27	0.38	2.80	86.4
5H-6, 75–76	44.95	71.5	1.22	0.35	2.30	84.9
5H-7, 65–66	46.35	55.0	1.44	0.65	2.85	77.3
6H-1, 75–76	46.95	44.2	1.58	0.88	2.75	68.0
6H-2, 75–76	48.45	44.9	1.52	0.84	2.53	66.8
6H-3, 75–76	49.95	38.5	1.64	1.01	2.65	61.8
6H-4, 75–76	51.45	42.2	1.61	0.93	2.78	66.5
6H-5, 75–76	52.95	42.6	1.57	0.90	2.60	65.4
6H-6, 75–76	54.45	56.1	1.38	0.61	2.47	75.4
6H-7, 55–56	55.75	50.9	1.46	0.72	2.61	72.5
7H-1, 110–111	56.80	57.8	1.38	0.58	2.64	77.9
7H-4, 75–76	60.95	41.8	1.62	0.94	2.80	66.3
7H-7, 50–51	65.20	37.5	1.72	1.07	2.89	62.8
8H-1, 120–121	66.40	55.3	1.41	0.63	2.66	76.3
8H-2, 75–76	67.45	49.3	1.50	0.76	2.76	72.4
8H-3, 75–76	68.95	41.7	1.46	0.85	2.10	59.5
8H-4, 75–76	70.45	50.0	1.51	0.75	2.85	73.6
8H-5, 75–76	71.95	39.0	1.71	1.04	3.00	65.3
8H-6, 75–76	73.45	44.7	1.60	0.88	2.91	69.7
8H-7, 45–46	74.65	41.5	1.49	0.87	2.20	60.4
9H-2, 75–76	76.95	46.3	1.55	0.83	2.80	70.2
9H-3, 75–76	78.45	49.6	1.50	0.76	2.76	72.6
9H-4, 75–76	79.95	43.9	1.42	0.80	2.04	60.9
9H-5, 75–76	81.45	41.8	1.62	0.94	2.77	66.0
9H-6, 75–76	82.95	37.3	1.71	1.07	2.86	62.5
9H-7, 65–75	84.35	46.6	1.55	0.83	2.80	70.4
10H-1, 80–81	85.00	46.2	1.54	0.83	2.71	69.4
10H-2, 75–76	86.45	42.2	1.61	0.93	2.78	66.5
10H-3, 75–76	87.95	53.4	1.45	0.67	2.75	75.5
10H-4, 75–76	89.45	42.6	1.50	0.86	2.29	62.3
10H-5, 75–76	90.95	42.4	1.57	0.91	2.60	65.2
10H-6, 75–76	92.45	42.5	1.62	0.93	2.86	67.3
11H-1, 80–81	94.50	45.2	1.47	0.80	2.28	64.8
11H-2, 75–76	95.95	35.6	1.73	1.11	2.78	60.0
11H-3, 75–76	97.45	43.2	1.61	0.91	2.85	67.9
11H-4, 75–76	98.95	45.3	1.56	0.85	2.77	69.2
11H-5, 75–76	100.45	42.6	1.69	0.97	3.25	70.2
11H-7, 40–41	103.10	47.5	1.53	0.81	2.79	71.2
12H-1, 75–76	103.95	42.9	1.60	0.91	2.78	67.1
12H-2, 75–76	105.45	29.2	2.06	1.46	3.53	58.6
12H-3, 75–76	106.95	43.9	1.59	0.89	2.81	68.2
12H-4, 75–76	108.45	41.8	1.58	0.92	2.60	64.6
12H-5, 75–76	109.95	40.2	1.66	0.99	2.83	65.0
12H-6, 75–76	111.45	40.5	1.65	0.98	2.84	65.4
12H-7, 75–76	112.72	38.9	1.66	1.01	2.73	63.0
13H-3, 75–76	115.45	42.3	1.62	0.94	2.84	67.0
13H-4, 75–76	116.95	52.0	1.44	0.69	2.56	73.0
13H-5, 75–76	118.45	47.7	1.50	0.78	2.58	69.7
13H-6, 75–76	119.95	36.8	1.72	1.09	2.84	61.7
13H-7, 75–76	121.45	39.5	1.67	1.01	2.83	64.3
13H-8, 75–76	122.45	49.6	1.52	0.76	2.90	73.6
14H-1, 75–76	122.95	51.0	1.44	0.70	2.47	71.5
14H-3, 75–76	125.95	45.4	1.57	0.86	2.80	69.4
14H-5, 75–76	128.95	49.4	1.50	0.76	2.72	72.2
14H-6, 75–76	130.45	39.6	1.68	1.01	2.88	64.9
14H-7, 35–36	131.55	40.0	1.65	0.99	2.78	64.5
15H-1, 85–86	132.55	38.5	1.66	1.02	2.71	62.4
15H-2, 75–76	133.95	39.3	1.68	1.02	2.88	64.5
15H-3, 75–76	135.45	44.4	1.59	0.88	2.84	68.9
15H-4, 75–76	136.95	43.5	1.59	0.90	2.78	67.6
15H-5, 75–76	138.45	39.9	1.66	1.00	2.81	64.6
15H-6, 55–56	139.75	37.8	1.75	1.09	3.07	64.5
15H-7, 50–51	140.70	43.7	1.59	0.89	2.78	67.8
16H-1, 85–86	142.05	42.4	1.61	0.93	2.80	66.8
16H-2, 75–76	143.45	32.3	1.82	1.23	2.90	57.4
16H-3, 75–76	144.95	34.6	1.77	1.16	2.86	59.7
16H-4, 75–76	146.45	40.6	1.67	0.99	2.93	66.2
16H-5, 75–76	147.95	38.3	1.70	1.05	2.88	63.6
16H-6, 45–46	149.15	30.0	1.85	1.29	2.82	54.1
17H-1, 75–76	151.45	37.8	1.70	1.06	2.86	62.9
17H-2, 75–76	152.95	39.7	1.68	1.01	2.89	65.0
17H-3, 75–76	154.45	36.9	1.73	1.10	2.92	62.5
17H-5, 75–76	157.45	41.4	1.64	0.96	2.86	66.3
17H-6, 55–56	158.75	35.3	1.75	1.13	2.84	60.2
18H-2, 75–76	162.45	38.4	1.64	1.01	2.63	61.6
18H-3, 75–76	163.95	37.3	1.72	1.08	2.86	62.4
18H-4, 75–76	165.45	36.0	1.72	1.10	2.78	60.4
18H-5, 75–76	166.95	34.0	1.70	1.12	2.58	56.5
18H-6, 75–76	168.45	42.0	1.64	0.95	2.90	67.2
18H-7, 60–61	169.70	37.7	1.70	1.06	2.85	62.8
19H-1, 80–81	170.50	36.0	1.69	1.08	2.65	59.3
19H-2, 75–76	171.87	36.0	1.74	1.11	2.87	61.2
19H-3, 75–76	173.37	37.8	1.71	1.06	2.87	63.0
19H-4, 75–76	174.87	39.7	1.60	0.96	2.53	61.9
19H-5, 75–76	176.37	38.6	1.68	1.03	2.82	63.3
19H-6, 75–76	177.87	40.2	1.65	0.99	2.82	64.9
20H-3, 75–76	182.95	39.7	1.60	0.96	2.54	62.0
20H-4, 75–76	184.45	44.6	1.48	0.82	2.32	64.6
20H-5, 75–76	185.95	37.6	1.70	1.06	2.81	62.3
20H-6, 75–76	187.45	38.6	1.68	1.03	2.81	63.4
21H-1, 75–76	189.45	35.4	1.79	1.16	3.04	61.9
21H-2, 75–76	190.95	36.5	1.71	1.09	2.80	61.1
21H-3, 75–76	192.45	29.4	1.87	1.32	2.85	53.7
21H-4, 75–76	193.95	36.6	1.72	1.09	2.81	61.3
21H-5, 75–76	195.45	34.6	1.78	1.16	2.92	60.2
21H-6, 75–76	196.95	35.2	1.67	1.08	2.53	57.3
21H-7, 75–76	198.45	38.1	1.70	1.05	2.87	63.3
22H-2, 75–76	200.45	37.6	1.71	1.07	2.87	62.9
22H-3, 75–76	201.95	37.9	1.62	1.01	2.51	60.0
22H-4, 75–76	203.45	34.6	1.77	1.15	2.86	59.7
22H-5, 75–76	204.95	43.6	1.53	0.86	2.46	65.0
22H-6, 75–76	206.45	42.5	1.55	0.89	2.48	64.1
23X-2, 75–76	209.15	47.6	1.55	0.81	2.87	71.8
23X-4, 75–76	212.15	41.7	1.69	0.98	3.15	68.8
23X-5, 75–76	213.65	60.8	1.26	0.50	1.97	74.9
23X-6, 70–71	215.10	40.7	1.63	0.96	2.73	64.6
24X-1, 64–65	215.14	35.2	1.84	1.19	3.26	63.4
24X-2, 54–55	216.54	39.7	1.68	1.01	2.89	65.0
24X-4, 50–51	219.50	38.2	1.71	1.06	2.94	64.0
24X-5, 50–51	221.00	1.7	2.73	2.69	2.81	4.5
24X-6, 50–51	222.50	48.3	1.44	0.74	2.30	67.7
25X-1, 80–81	224.90	33.7	1.74	1.15	2.71	57.4
25X-3, 90–91	228.00	43.1	1.61	0.91	2.82	67.6

Table T27 (continued).

Core, section, interval (cm)	Depth CSF (m)	Water content (%)	Density (g/cm^3)			Porosity (%)
			Wet bulk	Dry bulk	Grain	
25X-5, 69–70	230.79	33.7	1.87	1.24	3.21	61.4
25X-6, 61–62	232.21	49.3	1.45	0.74	2.43	69.8
25X-7, 29–30	233.39	23.9	1.95	1.49	2.73	45.5
26X-1, 50–51	234.10	38.6	1.62	0.99	2.55	61.0
26X-2, 127–128	236.37	39.8	1.68	1.01	2.89	65.1
26X-3, 106–107	237.66	39.9	1.72	1.04	3.14	67.1
26X-4, 98–99	239.08	40.9	1.55	0.91	2.39	61.8
26X-5, 69–70	240.29	42.8	1.60	0.92	2.77	67.0
26X-6, 70–71	241.80	38.6	1.75	1.08	3.16	66.0
27X-1, 119–120	244.39	36.7	1.93	1.22	3.98	69.2
27X-2, 77–78	245.47	46.6	1.58	0.85	3.03	72.1
28X-1, 91–92	253.71	48.9	1.41	0.72	2.21	67.4
28X-3, 67–68	256.47	61.1	1.35	0.53	2.73	80.8
28X-4, 52–53	257.82	57.1	1.40	0.60	2.74	78.1
28X-5, 74–75	259.54	46.7	1.45	0.77	2.28	66.1
28X-6, 65–66	260.95	43.4	1.59	0.90	2.75	67.3
28X-7, 29–30	262.09	49.5	1.49	0.75	2.67	71.9
29X-5, 70–71	267.61	55.2	1.46	0.65	3.09	78.8
29X-7, 52–53	270.09	47.7	1.60	0.84	3.24	74.3
30X-2, 76–77	274.36	37.7	1.70	1.06	2.84	62.6

Table T28. Split-core *P*-wave velocity measurements, Hole U1334A. (**Continued on next page.**)

Core, section	Depth CSF (m)	Velocity (m/s)		
		x-axis	*y*-axis	*z*-axis
320-U1334A-				
1H-1	1.38		1510	1503
1H-1	1.46	1551		
1H-2	2.82		1511	1503
1H-2	2.90	1559		
1H-3	4.35			1500
1H-3	4.45	1563		
1H-4	5.91	1574		
1H-5	7.37			1513
1H-5	7.45	1579		
2H-1	9.55			1521
2H-1	9.65	1601		
2H-2	11.04		1521	1512
2H-2	11.11	1586		
2H-3	12.59			1473
2H-3	12.65	1590		
2H-4	14.08		1525	1446
2H-4	14.15	1577		
2H-5	15.52		1523	1480
2H-5	15.60	1585		
2H-6	17.08		1498	1495
2H-6	17.15	1565		
3H-1	19.15	1580		
3H-2	20.60	1444		
3H-3	22.07		1414	1424
3H-3	22.15	1585		
3H-4	23.65	1583		
3H-5	24.91		1436	
3H-5	25.10	1583		
3H-6	26.56		1518	1515
3H-6	26.67	1557		
4H-1	28.65	1592		
4H-2	30.10	1599		
4H-3	31.58		1447	1445
4H-3	31.65	1646		
4H-4	33.15	1554		
4H-5	34.53			1507
4H-5	34.61	1571		
4H-6	35.95		1435	
4H-6	36.11	1574		
5H-1	38.16	1537		
5H-4	41.20		1520	
5H-4	42.58		1520	
5H-4	42.67	1575		
5H-5	44.02		1512	1461
5H-5	44.10	1579		
5H-6	45.55			1511
5H-6	45.65	1573		
6H-1	47.55			
6H-1	47.65	1562		
6H-2	49.02			1500
6H-2	49.10	1575		
6H-3	50.54		1509	1507
6H-3	50.63	1594		
6H-4	52.05			1502
6H-4	52.15	1580		
6H-5	53.47		1507	1499
6H-5	53.59	1585		
6H-6	55.07			1457
6H-6	55.15	1585		
7H-1	57.06		2347	
7H-1	57.15	1563		
7H-2	58.56		1419	
7H-2	58.65	1563		
7H-3	59.96		1400	1500
7H-3	60.05	1574		
7H-4	61.55		1405	1507
7H-4	61.65	1569		
7H-5	63.04		1433	
7H-5	63.15	1566		
7H-6	64.54			1501
7H-6	64.65	1579		
8H-2	68.04			
8H-2	68.15	1532		
8H-3	69.54	1547		
8H-4	71.05		1405	1503
8H-4	71.15	2773		
8H-5	72.41		2361	1509
8H-5	72.55		1509	1507
8H-5	72.65	1570		
8H-6	74.15	1545		
9H-1	76.15	1540		
9H-2	77.57			1502
9H-2	77.65	1536		
9H-3	79.05	1542		
9H-4	80.56		1521	1511
9H-4	80.65	1557		
9H-5	82.05		1510	1509
9H-5	82.29	1567		
9H-6	83.55			1511
9H-6	83.65	1563		
10H-1	85.65	1563		
10H-2	87.15	1577		
10H-3	88.48		1527	1426
10H-4	88.56	1601		
10H-4	90.15	1544		
10H-5	91.65	1564		
10H-6	93.08		1517	1514
10H-6	93.15	1563		
11H-1	95.14	1564		
11H-2	96.65	1573		
11H-3	97.97		1504	1503
11H-3	98.04	1572		
11H-4	99.58		1507	1771
11H-4	99.65	1568		
11H-5	101.05		1515	1506
11H-5	101.15	1570		
12H-1	104.57			1453
12H-1	104.65	1544		
12H-2	106.06		1403	
12H-2	106.15	1575		
12H-3	107.45		1504	1507
12H-3	107.55	1565		
12H-4	109.07		1410	1504
12H-4	109.14	1565		
12H-5	110.54		1522	1449
12H-5	110.65	1572		
12H-6	111.93	1546		
12H-6	112.06		1511	
13H-2	114.57		1511	1506
13H-2	114.64	1550		
13H-3	116.06		1515	1506
13H-3	116.14	1557		
13H-4	117.46			
13H-4	117.54	1541		
13H-5	119.06		1531	1509
13H-5	119.15	1557		
13H-6	120.55		1518	1508
13H-6	120.65	1559		
14H-2	125.05		1523	1516
14H-3	126.43			1505
14H-3	126.54	2655		
14H-4	128.04		1523	1459
14H-4	128.14	1559		
14H-5	129.55		1523	1509
14H-5	129.65	1562		

Table T28 (continued).

Core, section	Depth CSF (m)	Velocity (m/s) *x*-axis	*y*-axis	*z*-axis
14H-6	131.03		1516	1506
14H-6	131.12	1566		
15H-2	134.65	1587		
15H-3	136.04	1543		
15H-4	137.55		1434	
15H-4	137.65	1553		
15H-5	139.04		1529	1511
15H-5	139.15	1560		
15H-6	140.06		1527	1509
15H-6	140.14	1557		
16H-1	142.55		1521	1512
16H-1	142.65	1570		
16H-2	144.05		1526	1510
16H-2	144.14	1554		
16H-3	145.46		1534	
16H-3	145.56	2687		
16H-4	147.07			1517
16H-4	147.15	1561		
16H-5	148.56		1543	1465
16H-5	148.65	1560		
17H-1	152.07		1441	
17H-1	152.15	1546		
17H-2	153.55		1440	1465
17H-2	153.64	1549		
17H-3	154.98		1541	1523
17H-3	155.04	1546		
17H-4	156.35		1552	1520
17H-4	156.44	1544		
17H-5	157.96		1541	
17H-5	158.04	1589		
18H-2	163.05		1408	
18H-2	163.14	1546		
18H-3	164.46		1528	
18H-3	164.54	1579		
18H-4	166.05		1560	1471
18H-4	166.14	1566		
18H-5	167.56		1553	1522
18H-5	167.65	1563		
18H-6	168.97			1471
18H-6	169.05	1572		
19H-1	171.08	1565		
19H-2	172.71	1550		
19H-3	173.91		1548	1517
19H-3	173.98	1545		
19H-4	175.51		1549	1519
19H-4	175.58	1558		
19H-5	176.99		1436	
19H-5	177.08	1553		
20H-1	180.67	1569		
20H-2	182.07		1549	1473
20H-2	182.15	1542		
20H-3	183.48		1427	
20H-3	183.57	1564		
20H-4	185.07		1552	
20H-4	185.16	1545		
20H-5	186.59		1551	1524
20H-5	186.66	1575		
20H-6	187.93		1548	1518
20H-6	187.97	1569		
21H-1	190.16	1540		
21H-2	191.58		1459	
21H-2	191.66	1570		
21H-3	193.04	1595		
21H-4	194.57		1548	1523
21H-4	194.65	1553		
21H-5	196.10		1551	1521
21H-5	196.16	1552		
21H-6	197.57		1548	1520
21H-6	197.65	1575		
22H-2	201.15	1580		
22H-3	202.57	1572		
22H-4	204.09		1575	1484
22H-4	204.17	1583		
22H-6	206.62	1542		
23X-1	208.35	1598		
23X-3	211.24	1600		
23X-4	212.77		1432	
23X-4	213.01	1597		
23X-5	214.49	1606		
23X-6	215.83	1578		
23X-6	215.83		1433	
24X-2	217.34	1600		
24X-5	221.93	1639		
24X-6	223.44	1623		
25X-1	225.49	1627		
25X-2	226.96		1635	
25X-2	227.04	1602		
25X-3	228.35	1638		
25X-4	230.06	1633		
25X-5	231.55	1654		
25X-6	232.97	1614		
26X-1	235.05	1613		
26X-2	236.57	1638		
26X-3	237.94	1652		
26X-4	239.56	1675		
26X-5	241.06	1656		
26X-6	242.55	1607		
27X-1	244.61	1618		
28X-1	254.23	1623		
28X-2	255.76	1609		
28X-3	257.14	3281		
28X-4	258.76	1617		
28X-5	260.15	1656		
29X-2	263.75	1628		
29X-3	265.02	1660		
29X-4	266.51	1659		
29X-5	268.25	1633		
29X-6	269.14	1628		
29X-7	270.92	1619		
30X-1	273.40	1649		
30X-2	275.04	1664		
30X-3	276.45	1622		
30X-6	280.55	1695		

Table T29. Thermal conductivity, Hole U1334A.

Core, section, interval (cm)	Depth CSF (m)	Thermal conductivity (W/[m·K])
320-U1334A-		
1H-3, 115	4.15	0.780
2H-3, 115	12.35	0.763
3H-3, 115	21.85	0.878
4H-3, 115	31.35	0.834
5H-3, 115	40.85	0.846
6H-3, 115	50.35	1.227
7H-3, 115	59.85	1.109
8H-3, 115	69.35	1.097
9H-3, 115	78.85	1.083
10H-3, 115	88.35	1.069
11H-3, 115	97.85	1.089
12H-3, 115	107.35	1.174
13H-3, 115	115.85	1.182
14H-3, 115	126.35	1.121
15H-3, 115	135.85	1.138
16H-3, 115	145.35	1.141
17H-3, 80	154.50	1.253
18H-3, 115	164.35	1.274
19H-3, 115	173.77	1.202
20H-3, 115	183.35	1.185
21H-3, 115	192.85	1.254
22H-3, 115	202.35	1.291
23X-3, 115	211.05	1.132
24X-3, 115	218.65	1.139
25X-3, 115	228.25	1.102
26X-3, 115	237.75	1.076
27X-3, 90	247.10	0.855
28X-3, 115	256.95	0.883
30X-3, 115	276.25	0.972

Table T30. Shipboard core top, composite, and corrected composite depths, Site U1334.

Core	Depth CSF (m)	Offset (m)	Top depth (m) CCSF-A	Top depth (m) CCSF-B
320-U1334A-				
1H	0.00	0.00	0.00	0.00
2H	8.20	0.87	9.07	7.82
3H	17.70	1.97	19.67	16.96
4H	27.20	3.48	30.68	26.45
5H	36.70	4.77	41.47	35.75
6H	46.20	6.93	53.13	45.80
7H	55.70	7.42	63.12	54.41
8H	65.20	9.06	74.26	64.02
9H	74.70	11.22	85.92	74.07
10H	84.20	11.31	95.51	82.33
11H	93.70	12.92	106.62	91.92
12H	103.20	14.15	117.35	101.16
13H	112.70	15.44	128.14	110.47
14H	122.20	16.93	139.13	119.94
15H	131.70	18.86	150.56	129.80
16H	141.20	20.56	161.76	139.45
17H	150.70	23.22	173.92	149.93
18H	160.20	24.10	184.30	158.88
19H	169.70	26.42	196.12	169.07
20H	179.20	26.98	206.18	177.74
21H	188.70	30.00	218.70	188.53
22H	198.20	42.70	240.90	207.67
23X	206.90	44.30	251.20	216.55
24X	214.50	46.90	261.40	225.34
25X	224.10	47.40	271.50	234.05
26X	233.60	47.71	281.31	242.51
27X	243.20	49.24	292.44	252.10
28X	252.80	48.91	301.71	260.09
29X	262.40	49.68	312.08	269.04
30X	272.10	50.97	323.07	278.51
31X	281.80	51.48	333.28	287.31
32X	285.00	51.48	336.48	290.07
320-U1334B-				
1H	3.70	4.00	7.70	6.64
2H	13.20	4.69	17.89	15.42
3H	22.70	4.64	27.34	23.57
4H	32.20	6.27	38.47	33.16
5H	41.70	5.99	47.69	41.11
6H	49.20	7.31	56.51	48.71
7H	58.70	9.29	67.99	58.61
8H	68.20	12.14	80.34	69.26
9H	77.70	14.35	92.05	79.36
10H	87.20	15.44	102.64	88.48
11H	96.70	17.09	113.79	98.10
12H	106.20	17.28	123.48	106.45
13H	115.70	18.99	134.69	116.12
14H	125.20	21.74	146.94	126.67
15H	134.70	22.49	157.19	135.51
16H	144.20	23.79	167.99	144.82
17H	153.70	25.14	178.84	154.17
18H	163.20	27.10	190.30	164.05
19H	172.70	28.25	200.95	173.23
20H	182.20	30.80	213.00	183.62
21H	191.70	32.95	224.65	193.66
22H	201.20	32.95	234.15	201.85
23X	210.70	34.66	245.36	211.52
24X	219.00	47.60	266.60	229.83
25X	228.60	48.79	277.39	239.13
26X	238.20	50.39	288.59	248.78
27X	247.80	49.72	297.52	256.48
28X	257.40	50.80	308.20	265.69
29X	267.00	53.11	320.11	275.96
30X	276.60	53.72	330.32	284.76
31X	283.90	53.72	337.62	291.05
320-U1334C-				
1H	0	3.65	3.65	3.15
2H	9.5	4.33	13.83	11.93
3H	19	6.65	25.65	22.11
4H	28.5	10.04	38.54	33.22
5H	38	10.11	48.11	41.47
6H	47.5	12.06	59.56	51.34
7H	57	12.06	69.06	59.53
8H	66.5	13.96	80.46	69.36
9H	76	16.30	92.30	79.57
10H	85.5	17.98	103.48	89.20
11H	95	19.69	114.69	98.87
12H	104.5	22.75	127.25	109.69
13H	114	25.13	139.13	119.94
14H	123.5	27.06	150.56	129.79
15H	133	28.23	161.23	138.99
16H	142.5	29.69	172.19	148.44
17H	152	30.35	182.35	157.20
18H	161.5	31.44	192.94	166.32
19H	171	32.52	203.52	175.45
20H	180.5	33.77	214.27	184.72
21H	190	34.20	224.20	193.27
22H	199.5	35.80	235.30	202.84
23X	209	40.93	249.93	215.46
24X	214	44.20	258.20	222.59
25X	223.6	44.30	267.90	230.95
26X	233.2	45.17	278.37	239.97
27X	239.2	46.08	285.28	245.93
28X	248.8	47.12	295.92	255.11
29X	258.4	53.90	312.30	269.23
30X	268	54.52	322.52	278.04
31X	277.7	56.73	334.43	288.30
32X	279.7	56.73	336.43	290.02
33X	280.2	56.73	336.93	290.45

Table T31. Splice tie points, Site U1334. (See table notes.)

Hole, core, section, interval (cm)	Depth (m)			Hole, core, section, interval (cm)	Depth (m)	
	CSF	CCSF-A			CSF	CCSF-A
320-				320-		
U1334A-1H-5, 80	6.80	6.80	Tie to	U1334C-1H-3, 15	3.15	6.80
U1334C-1H-5, 69	6.69	10.35	Tie to	U1334A-2H-1, 128	9.48	10.35
U1334A-2H-6, 132	17.02	17.89	Tie to	U1334C-2H-4, 10	13.56	17.89
U1334C-2H-5, 108	16.04	20.37	Tie to	U1334A-3H-1, 70	18.40	20.37
U1334A-3H-6, 145	26.65	28.62	Tie to	U1334B-3H-1, 128	23.98	28.62
U1334B-3H-5, 114	29.84	34.48	Tie to	U1334A-4H-3, 80	31.00	34.48
U1334A-4H-6, 139	36.09	39.57	Tie to	U1334B-4H-1, 110	33.30	39.57
U1334B-4H-6, 145	41.15	47.42	Tie to	U1334A-5H-4, 144	42.64	47.42
U1334A-5H-6, 30	44.50	49.27	Tie to	U1334C-5H-1, 116	39.16	49.27
U1334C-5H-7, 5	47.05	57.16	Tie to	U1334A-6H-3, 103	50.23	57.16
U1334A-6H-6, 23	53.93	60.86	Tie to	U1334C-6H-1, 130	48.80	60.86
U1334C-6H-5, 149	54.99	67.05	Tie to	U1334A-7H-3, 93	59.63	67.05
U1334A-7H-6, 68	63.88	71.30	Tie to	U1334B-7H-3, 31	62.01	71.30
U1334B-7H-6, 102	67.22	76.51	Tie to	U1334A-8H-2, 76	67.46	76.51
U1334A-8H-6, 128	73.98	83.04	Tie to	U1334B-8H-2, 119	70.89	83.04
U1334B-8H-5, 75	74.95	87.10	Tie to	U1334A-9H-1, 118	75.88	87.10
U1334A-9H-6, 20	82.40	93.61	Tie to	U1334B-9H-2, 6	79.26	93.61
U1334B-9H-5, 74	84.44	98.80	Tie to	U1334A-10H-3, 29	87.49	98.80
U1334A-10H-6, 142	93.12	104.43	Tie to	U1334C-10H-1, 95	86.45	104.43
U1334C-10H-5, 37	91.87	109.84	Tie to	U1334A-11H-3, 22	96.92	109.84
U1334A-11H-6, 132	102.52	115.44	Tie to	U1334B-11H-2, 14	98.34	115.44
U1334B-11H-6, 100	105.20	122.30	Tie to	U1334A-12H-4, 45	108.15	122.30
U1334A-12H-6, 43	111.13	125.27	Tie to	U1334B-12H-2, 29	107.99	125.27
U1334B-12H-6, 39	114.09	131.37	Tie to	U1334C-12H-3, 113	108.63	131.37
U1334C-12H-7, 36	113.86	136.61	Tie to	U1334B-13H-2, 41	117.61	136.61
U1334B-13H-5, 5	121.75	140.75	Tie to	U1334C-13H-2, 12	115.62	140.75
U1334C-13H-6, 86	122.36	147.49	Tie to	U1334B-14H-1, 55	125.75	147.49
U1334B-14H-4, 101	130.71	152.45	Tie to	U1334C-14H-2, 39	125.39	152.45
U1334C-14H-6, 44	131.44	158.49	Tie to	U1334B-15H-1, 130	136.00	158.49
U1334B-15H-6, 129	143.49	165.99	Tie to	U1334C-15H-4, 26	137.76	165.99
U1334C-15H-6, 74	141.24	169.47	Tie to	U1334B-16H-1, 148	145.68	169.47
U1334B-16H-5, 75	150.95	174.74	Tie to	U1334C-16H-2, 105	145.05	174.74
U1334C-16H-6, 53	150.53	180.22	Tie to	U1334B-17H-1, 138	155.08	180.22
U1334B-17H-6, 67	161.87	187.01	Tie to	U1334A-18H-2, 122	162.92	187.01
U1334A-18H-5, 53	166.73	190.83	Tie to	U1334B-18H-1, 53	163.73	190.83
U1334B-18H-6, 126	171.96	199.06	Tie to	U1334A-19H-3, 2	172.64	199.06
U1334A-19H-6, 19	177.31	203.72	Tie to	U1334B-19H-2, 127	175.47	203.72
U1334B-19H-4, 12	177.32	205.57	Tie to	U1334C-19H-2, 55	173.05	205.57
U1334C-19H-5, 105	178.05	210.57	Tie to	U1334A-20H-3, 139	183.59	210.57
U1334A-20H-6, 98	187.68	214.67	Tie to	U1334B-20H-2, 16	183.86	214.67
U1334B-20H-7, 34	191.34	222.15	Append to	U1334B-21H-1, 38	192.08	225.03
U1334B-21H-7, 36	201.06	234.01	Append to	U1334B-22H-1, 15	201.35	234.30
U1334B-22H-7, 67	210.87	243.82	Append to	U1334B-23X-1, 30	211.00	245.66
U1334B-23 X-5, 118	217.88	252.54	Tie to	U1334A-23X-1, 134	208.24	252.54
U1334A-23 X-6, 110	215.50	259.80	Tie to	U1334C-24X-2, 10	215.60	259.80
U1334C-24 X-6, 137	222.87	267.07	Tie to	U1334A-24X-4, 117	220.17	267.07
U1334A-24 X-5, 116	221.66	268.56	Tie to	U1334C-25X-1, 66	224.26	268.56
U1334C-25 X-5, 22	229.82	274.12	Tie to	U1334A-25X-2, 112	226.72	274.12
U1334A-25 X-6, 75	232.35	279.75	Tie to	U1334C-26X-1, 138	234.58	279.75
U1334C-26 X-5, 25	239.45	284.62	Tie to	U1334A-26X-3, 31	236.91	284.62
U1334A-26 X-6, 91	242.01	289.72	Tie to	U1334B-26X-1, 113	239.33	289.72
U1334B-26 X-6, 77	246.47	296.86	Tie to	U1334C-28X-1, 93	249.73	296.86
U1334C-28 X-6, 127	257.57	304.69	Tie to	U1334A-28X-2, 149	255.79	304.69
U1334A-28 X-6, 113	261.43	310.33	Tie to	U1334B-28X-2, 63	259.53	310.33
U1334B-28 X-4, 26	262.16	312.96	Tie to	U1334C-29X-1, 66	259.06	312.96
U1334C-29 X-6, 129	267.19	321.10	Tie to	U1334B-29X-1, 99	267.99	321.10
U1334B-29 X-6, 90	275.40	328.51	Tie to	U1334C-30X-4, 149	273.99	328.51
U1334C-30 X-6, 135	276.85	331.38	Tie to	U1334B-30-1, 105	277.65	331.38

Notes: Spliced section is interrupted between 222 and 245.7 m CCSF-A because of coring gaps and lack of correlation. Sampling in this depth interval will not recover a complete stratigraphic sequence.

Table T32. Magnetostratigraphic and biostratigraphic datums, Site U1334. (See table note.)

Event	Age (Ma)	Depth CCSF-A (m)	Error (m)
C1n–C1r.1r	0.781	0.60	
C5n.1r–C5n.2n	9.987	12.22	
C5n.2n–C5r.1r	11.040	14.29	
C5r.1r–C5r.1n	11.118	14.39	
C5r.1n–C5r.2r	11.154	14.57	
C5r.2r–C5r.2n	11.554	15.54	
C5r.2n–C5r.3r	11.614	15.72	
C5r.3r–C5An.1n	12.014	16.79	
C5An.1n–C5An.1r	12.116	17.09	
C5An.1r–C5An.2n	12.207	17.39	
C5An.2n–C5Ar.1r	12.415	18.32	
C5Ar.1r–C5Ar.1n	12.730	20.27	
C5Ar.1n–C5Ar.2r	12.765	20.37	
C5Ar.2r–C5Ar.2n	12.820	20.82	
C5Ar.2n–C5Ar.3r	12.878	20.92	
C5Ar.3r–C5AAn	13.015	21.67	
C5AAn–C5AAr	13.183	22.29	
C5AAr–C5ABn	13.369	23.07	
C5ABn–C5ABr	13.605	24.67	
C5ABr–C5ACn	13.734	25.37	
C5ACn–C5ACr	14.095	26.72	
C5ACr–C5ADn	14.194	26.97	
C5ADn–C5ADr	14.581	28.69	
C5Bn.2n–C5Br	15.160	31.28	
C5Br–C5Cn.1n	15.974	36.66	
C5Cn.1n–C5Cn.1r	16.268	33.18	
C5Cn.1r–C5Cn.2n	16.303	38.56	
C5Cn.2n–C5Cn.2r	16.472	38.86	
C5Cn.2r–C5Cn.3n	16.543	39.28	
C5Cn.3n–C5Cr	16.721	39.66	
C5Dn–C5Dr	17.533	42.65	
C5Dr–C5En	18.056	44.70	
C5En–C5Er	18.524	47.00	
C5Er–C6n	18.748	48.22	
C6n–C6r	19.722	57.98	
C6r–C6An.1n	20.040	61.83	
C6An.1n–C6An.1r	20.213	65.25	
C6An.1r–C6An.2n	20.439	68.52	
C6Ar–C6AAn	21.083	79.88	
C6AAn–C6AAr.1r	21.159	81.58	
C6AAr.3r–C6Bn.1n	21.767	86.97	
C6Bn.1n–C6Bn.1r	21.936	89.14	
C6Bn.1r–C6Bn.2n	21.992	89.74	
C6Br–C6Cn.1n	22.564	98.21	
C6Cn.1n–C6Cn.1r	22.754	99.96	
C6Cn.1r–C6Cn.2n	22.902	102.16	
C6Cn.2n–C6Cn.2r	23.030	104.01	
C6Cn.2r–C6Cn.3n	23.278	107.55	
C6Cn.3n–C6Cr	23.340	108.70	
C6Cr–C7n.1n	24.022	118.97	
C7n.1n–C7n.1r	24.062	119.57	
C7n.1r–C7n.2n	24.147	120.92	
C7n.2n–C7r	24.459	125.67	
C7An–C7Ar	24.984	130.42	
C7Ar–C8n.1n	25.110	132.37	
C8n.1n–C8n.1r	25.248	135.29	
C8n.2n–C8r	26.032	158.51	
C9n–C9r	27.412	178.42	
C10n.1n–C10n.1r	28.126	190.25	
C10n.1r–C10n.2n	28.164	191.32	
C10n.2n–C10r	28.318	197.58	
Nannofossils			
T *Coronocyclus nitescens*	12.12	17.77	
T *Calcidiscus premacintyrei*	12.45	17.77	
Tc *Cyclicargolithus floridanus*	13.33	22.24	0.92
T *Sphenolithus heteromorphus*	13.53	25.42	0.75
Tc *Discoaster deflandrei*	15.66	32.01	0.88
B *Discoaster petaliformis*	15.70	32.01	0.88
B *Sphenolithus heteromorphus*	17.71	39.11	0.73
T *Triquetrorhabdulus carinatus*	18.28	46.32	0.85
Tac *Triquetrorhabdulus carinatus*	22.09	90.27	1.15
B *Sphenolithus disbelemnos*	22.8	95.59	0.37
T *Sphenolithus delphix*	23.1	105.03	0.23
B *Sphenolithus delphix*	23.2	108.37	0.75
T *Sphenolithus ciperoensis*	24.4	126.57	0.16
X *T. longus/T. carinatus*	24.7	128.31	0.29
Tc *Cyclicargolithus abisectus*	24.7	128.31	0.29
T *Sphenolithus distentus*	26.8	169.89	0.23
T *Sphenolithus predistentus*	26.9	169.89	0.23
B *Sphenolithus ciperoensis*	27.1	200.75	4.16
T *Sphenolithus pseudoradians*	28.8	210.54	5.07
B *Sphenolithus distentus*	30.0	242.14	0.96
T *Reticulofenestra umbilicus*	32.0	271.96	0.34
T *Isthmolithus recurvus*	32.5	293.33	0.72
T *Coccolithus formosus*	32.9	284.56	0.75
T *Discoaster saipanensis*	34.4	299.47	0.53
T *Reticulofenestra reticulata*	35.2	307.98	3.55
B *Isthmolithus recurvus*	36.6	323.35	0.38
T *Chiasmolithus oamaruensis*	37.0	324.52	0.79
T *Chiasmolithus grandis*	37.1	324.52	0.79
B *Dictyococcites bisectus*	38.0	336.69	
Radiolarians			
T *Diartus petterssoni*	8.63	6.88	1.32
B *Diartus hughesi*	8.99	10.34	1.29
B *Diartus petterssoni*	11.71	16.80	2.18
B *Lithopera neotera*	12.95	21.15	1.07
T *Stichocorys armata*	13.50	23.72	1.50
Dorcadospyris dentata > *Dorcadospyris alata*	14.78	27.42	2.20
B *Dorcadospyris alata*	15.08	32.19	1.06
B *Lithopera renzae*	16.77	41.69	1.03
B Dorcadospyris *dentata*	17.72	45.51	1.50
B *Dorcadospyris forcipata*	18.61	49.28	2.27
T *Dorcadospyris praeforcipata*	19.77	60.90	2.23
T *Lophocyrtis pegetrum*	20.89	70.88	2.21
B *Calocycletta virginis*	21.39	75.77	1.05
T *Eucyrtidium mitodes*	21.95	89.97	1.50
T *Artophormis gracilis*	22.62	99.56	1.50
B *Dorcadospyris cyclacantha*	23.29	110.67	1.50
T *Lychnocanoma apodora*	24.50	131.19	1.50
B *Calocycletta robusta*	25.27	146.78	2.11
T *Eucyrtidium plesiodiaphanes*	26.40	165.80	1.50
T *Lithocyclia angusta*	27.68	185.43	1.36
T *Theocyrtis setanios*	28.21	199.43	1.50
B *Eucyrtidium mitodes*	29.41	226.37	2.11
T *Theocyrtis tuberosa*	30.13	252.42	1.26
T *Lophocyrtis oberhaensliae*	30.74	263.51	0.44
T *Lithocyclia aristotelis* gr.	33.51	296.30	3.70
B *Lithocyclia angusta*	34.13	296.30	3.70
T *Calocyclas turris*	34.83	305.11	0.65
B *Calocyclas bandyca*	36.74	318.91	2.78
Foraminifers			
B *Globorotalia (Fohsella) foshi robusta*	13.13	20.81	0.73
T *Globoquadrina binaiensis*	19.09	62.70	4.66
T *Paragloborotalia kugleri*	21.12	73.42	4.84
T *Paragloborotalia pseudokugleri*	21.31	73.42	4.84
B *Globoquadrina dehiscens*	22.44	87.08	4.84
B *Paragloborotalia kugleri*	23.0	105.33	4.68
B *Paragloborotalia pseudokugleri*	25.2	139.17	4.49
T *Paragloborotalia opima*	26.9	171.28	1.48
B *Globigerina angulisuturalis*	29.2	203.11	1.50
T *Subbotina angiporoides*	29.8	229.25	4.85
T *Turborotalia ampliapertura*	30.3	239.79	4.92
B *Paragloborotalia opima*	30.8	257.41	1.89

Note: T = top, Tc = top common, B = bottom, X = abundance crossover.

Table T33. Results from APCT-3 temperature profiles, Hole U1334B. (See table notes.)

Core	Temperature (°C) Average at mudline	Minimum above mudline	Depth DSF (m)	In situ temperature (°C)	Thermal resistance (m^2K/m)
320-U1334B-					
3H	1.522	1.450	32.2	2.82	40.6
5H	1.514	1.451	49.2	3.32	59.8
7H	1.527	1.457	68.2	3.59	76.7
9H	1.507	1.463	83.7	4.38	91.2
11H	1.510	1.466	106.2	5.09	112.1
Average:	1.516	1.457			

Notes: In situ temperatures were determined using the TP-Fit software by Martin Heesemann. Thermal resistance was calculated from thermal conductivity data (see **"Physical properties"**) corrected for in situ conditions (see **"Downhole measurements"** in the "Methods" chapter).